Antiapoptotic survival strategies of human neurons

Dissertation

zur

Erlangung des Doktorgrades (Dr. rer. nat.)

der

Mathematisch-Naturwissenschaftlichen Fakultät

der

Rheinischen Friedrich-Wilhelms-Universität Bonn

vorgelegt von

Ruven Wilkens

aus

Frankfurt am Main

Bonn, 2021

Angefertigt mit Genehmigung der Mathematisch-Naturwissenschaftlichen Fakultät der

Rheinischen Friedrich-Wilhelms-Universität Bonn

1. Gutachter: Prof. Dr. Philipp Koch

2. Gutachter: Prof. Dr. Jörg Höhfeld

Tag der Promotion: 16.06.2021

Erscheinungsjahr: 2021

Our minds are all we have.

They are all we have ever had.

And they are all we can offer others.

- Sam Harris -

Table of contents

List of Figures

List of Tables

1 Abstract

Neurons of the central and peripheral nervous system are the key information processing and relay units within the human body. Since neurons are post-mitotic cells and neurogenesis in the adult human brain is very limited, neurons lost to injury or cellular stress cannot be replaced. Thus, neurons within mature neuronal networks of the brain have to be guarded by protective strategies to remain functional over the lifespan of an individual. Using human induced pluripotent stem cell (hiPSC)-derived forebrain neurons, this study aimed to analyze transcriptional changes during neuronal maturation and to identify possible regulatory differences between immature and mature neurons regarding their potential for long-term survival. In particular, neuronal maturation was accompanied by an increasing threshold for mitochondrial outer membrane permeabilization, the initial step of the intrinsic apoptosis pathway. In addition, mature neurons displayed a downregulation of the apoptotic proteins APAF-1 and Caspases-3, -7 and -9. We also observed an increased ubiquitination of the mitochondrial inhibitor of apoptosis protein (IAP) antagonist SMAC/DIABLO. Conversely, protein levels of XIAP, the major IAP, were strongly upregulated during the time course of neuronal maturation. These beneficial adaptations synergized to suppress the intrinsic apoptosis pathway endowing mature neurons with significantly higher survival competency than immature neurons when challenged with a wide range of different cellular insults.

Approaches to further improve neuronal survival capabilities are highly desirable for the prevention of age-related neurodegeneration. Recently, genetic or pharmacological activation of the hexosamine biosynthetic pathway (HBP) have been reported to protect *C. elegans* and murine cells from tunicamycin (TM)-induced protein folding stress and toxic protein aggregation. The HBP integrates several metabolic pathways to synthesize the aminosugar uridine diphosphate N-acetylglucosamine (UDP-GlcNAc) which is a substrate for glycosylation reactions. Increased UDP-GlcNAc levels have been linked to a protective activation of the PERK branch of the integrated stress response (ISR). HBP activity can be increased by gain-of-function (gof) point mutations in the rate limiting enzyme GFAT-1 or by supplementation of N-acetylglucosamine (GlcNAc). Using CRISPR-Cas9 gene editing, we generated hiPSCs harboring the GFAT-1 G451E gof mutation to assess the related effects in human neural cells. We found genetic GFAT-1 gof to confer protection against TM-induced stress in NPCs and immature neurons but not in mature neurons which were inherently resistant. GlcNAc supplementation was only effective in NPCs but not in neurons. Corresponding Western blot experiments did not confirm an involvement of the PERK branch of the ISR and thus call into question the relevance of the previously proposed mechanism in human neural cells. Consequently, the protective potential of HBP activation beyond TM-resistance and the underlying mechanism warrant further investigation.

2 Zusammenfassung

Als Teil des zentralen und peripheren Nervensystems sind Neurone von fundamentaler Bedeutung für die Integration und Weiterleitung von Informationen innerhalb des menschlichen Körpers. Da Neurone post-mitotische Zellen sind und das Ausmaß an Neurogenese im adulten Gehirn sehr limitiert ist, können durch Verletzungen oder Stress beschädigte Neurone nicht ersetzt werden. Um für die gesamte Lebensdauer eines Individuums ihre Funktion erfüllen zu können, müssen Neurone in reifen neuronalen Netzwerken des Gehirns daher präventiv besonders geschützt werden. Das Ziel dieser Arbeit war es, mit Hilfe von humanen Neuronen des Vorderhirns, die aus induzierten pluripotenten Stammzellen generiert wurden, transkriptionelle Veränderungen während der neuronalen Reifung zu analysieren, um mögliche Unterschiede zwischen unreifen und reifen Neuronen hinsichtlich ihrer Überlebensstrategien zu identifizieren. Dabei wurde festgestellt, dass sich im Rahmen des neuronalen Reifungsprozesses die Schwelle für die Permeabilisierung der äußeren Mitochondrienmembran erhöht, welche die Initiierung des intrinsischen Apoptosesignalwegs ist. Des Weiteren wurden die apoptosefördernden Proteine APAF-1 und die Caspasen-3, -7 und -9 in reifen Neuronen herunterreguliert. Es wurde weiterhin eine zunehmende Ubiquitinierung des mitochondrialen Proteins SMAC/DIABLO beobachtet, welches üblicherweise durch die Inhibition von überlebensfördernden Proteinen die Apoptose begünstigt. Im Gegenzug stieg die zelluläre Verfügbarkeit des Proteins XIAP, einem zentralen Antagonisten vieler proapoptotischer Faktoren, im Laufe der neuronalen Reifung an. Gemeinsam führten diese positiven Anpassungen dazu, dass die Überlebensfähigkeit von reifen im Vergleich zu unreifen Neuronen bei Exposition mit einem breiten Spektrum an molekularen Stressoren signifikant besser ausfiel.

Obwohl reife Neurone durch die genannten Anpassungen eine erhöhte inhärente Widerstandsfähigkeit gegen zytotoxischen Stress besitzen, stellen altersbedingte neurodegenerative Erkrankungen ein großes Risiko für die menschliche Gesundheit dar. Daher wird weiterhin nach Ansätzen gesucht, mit denen die Überlebensfähigkeit von Neuronen verbessert werden kann. In Studien mit *C. elegans* und murinen Zelllinien wurde eine protektive Wirkung durch die genetische und pharmakologische Aktivierung des Hexosaminbiosynthesesignalwegs (HBS) gegenüber Tunikamycin-induziertem Zellstress und toxischer Proteinaggregation entdeckt. Der HBS integriert verschiedene metabolische Signalwege und katalysiert die Synthese des Aminozuckers Uridindiphosphat N-acetylglucosamin (UDP-GlcNAc), dem zentralen Substrat für Glykosilierungsreaktionen. Eine erhöhte intrazelluläre Konzentration von UDP-GlcNAc soll demnach eine Aktivierung der Proteinkinase PERK und somit der integrierten Stressantwort bewirken. Eine Induktion des HBS kann durch aktivitätsfördernde Punktmutationen des geschwindigkeitsbestimmenden Enzyms GFAT-1 oder durch Zugabe von N-acetylglucosamin (GlcNAc) erreicht werden. Mittels CRISPR-Cas9 Genomeditierung

wurden im Rahmen dieser Arbeit humane induzierte pluripotente Stammzellen mit der aktivierenden GFAT-1 G451E Punktmutation generiert, um die beschriebenen Effekte in menschlichen neuralen Zellen zu untersuchen. Diese GFAT-1 Variante verbesserte die Überlebensfähigkeit von neuralen Vorläuferzellen und unreifen Neuronen in Gegenwart von Tunikamycin. Eine Behandlung mit GlcNAc hatte eine protektive Wirkung bei Vorläuferzellen, jedoch nicht bei Neuronen. In Western Blot Experimenten wurde keine Aktivierung von PERK und der integrierten Stressantwort beobachtet, sodass der zuvor veröffentlichte Mechanismus in humanen neuralen Zellen nicht relevant zu sein scheint. Der mögliche protektive Effekt einer HBS-Aktivierung in humanen neuralen Zellen über den Schutz vor Tunikamycin hinaus und der zugrundeliegende Wirkmechanismus bedürfen daher weiterer Untersuchungen.

3 Introduction

3.1 Neurogenesis of the neocortex

The human brain is estimated to contain about 86 billion neurons and a similar number of supporting cells like astrocytes, oligodendrocytes and microglia (Azevedo *et al.*, 2009). Together, these cells establish and maintain vast, interconnected neural networks that are the basis for human movement, emotion and thought. Neurons are the central hubs for integrating and relaying electrochemical information throughout the central and peripheral nervous system. The brain develops from neuroepithelial cells (NECs) at the rostral end of the neural tube. The most rostral part of the early developing brain gives rise to the telencephalon, or cerebrum, which constitutes the largest portion of the human brain. The ventral region of the telencephalon forms the basal ganglia whereas the dorsal region becomes the cerebral cortex (Stiles & Jernigan, 2010; Dennis *et al.*, 2017; Mukhtar & Taylor, 2018). Both regions have their own proliferative zones that are the origin of progenitor cells and distinct types of neurons. Embryonic neurogenesis of glutamatergic cortical projection neurons starts at the margin of the dorsal ventricular system in an area called ventricular zone (VZ) (Molyneaux *et al.*, 2007; Lodato & Arlotta, 2015). At an early stage, the number of NECs in the VZ is strongly expanded by rapid rounds of symmetric cell divisions (Fig. 1). This proliferative phase provides the pool of cells that is necessary to generate the large numbers of neurons within the brain. NECs give rise to radial glial cells (RGCs) which can differentiate into cortical neurons, astrocytes and oligodendrocytes or generate intermediate progenitors (IPs) (Florio & Huttner, 2014; Paridaen & Huttner, 2014). As the number of IPs increases, they form the subventricular zone (SVZ) adjacent to the VZ. RGCs and IPs can differentiate into immature projection neurons that subsequently migrate outward to form the six-layered structure of the neocortex. Radial neuronal migration is guided by a scaffold of fibers from RGCs that are attached to the pial basement membrane (Fig. 1). The earliest born neurons form the preplate (PP) which is subsequently split into the marginal zone (MZ) and the subplate (SP) by the arrival of the following wave of neurons (Marín-Padilla, 1992; Nichols & Olson, 2010). These later arriving neurons lay the foundation of the cortical plate (CP) and constitute the deepest layer (layer VI) of the mature neocortex. Subsequently migrating neurons expand the CP by traversing the existing layers and forming more superficial layers below the MZ. This “inside-out” process of arrangement relies on Cajal-Retzius cells within the MZ that use reelin signaling to stop migration and initiate settlement of newly arriving neurons (D’Arcangelo *et al.*, 1995; Martínez-Cerdeño & Noctor, 2014; Marín-Padilla, 2015). The mature brain contains six cortical layers but no more SP and MZ. The initial pool of RGCs and IPs is depleted at later stages as their symmetric divisions proceed to predominantly produce daughter cells which both differentiate into neurons.

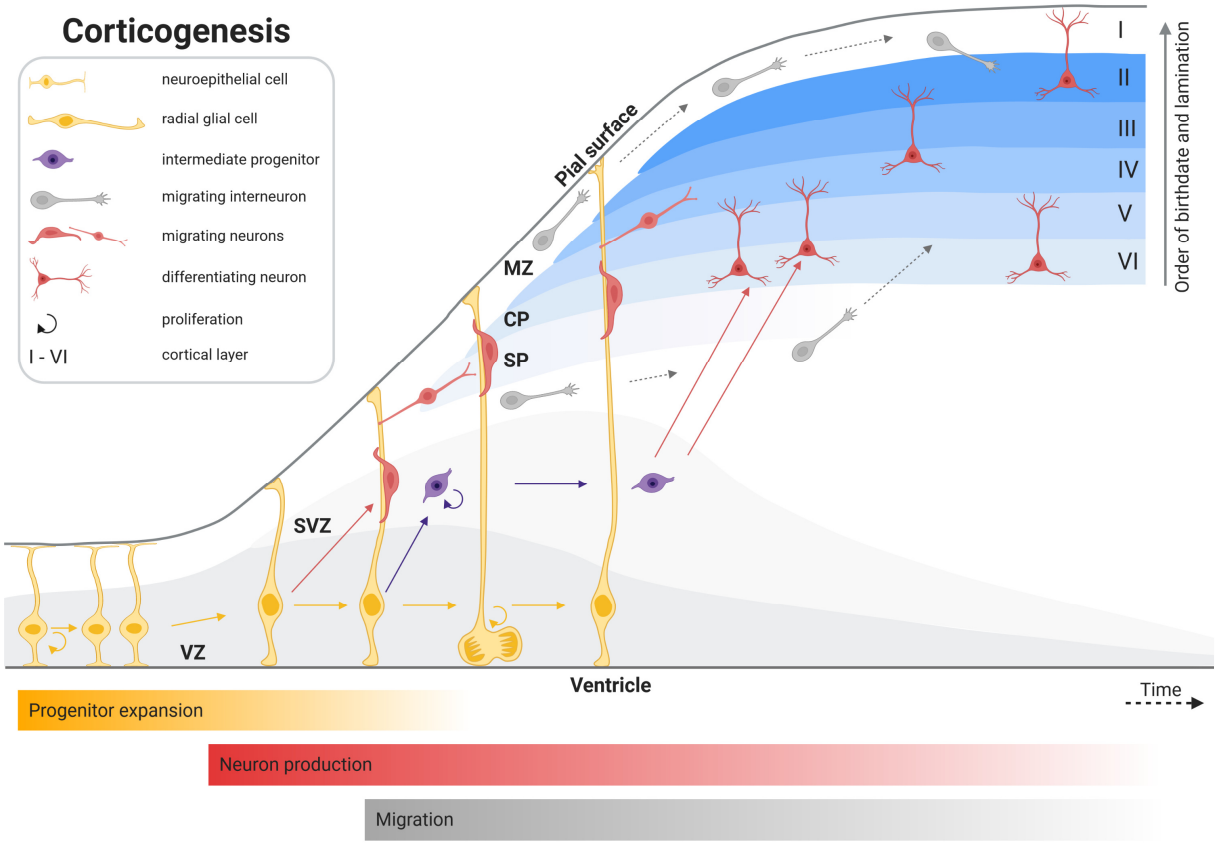

Fig. 1: Generation of the cerebral cortex during embryonic development.

The cellular basis of the cortex is formed by an expanding pool of neuroepithelial cells in the ventricular zone which subsequently differentiate into radial glial cells. Radial glial cells proliferate and can give rise to cortical neurons or intermediate progenitors. Additionally, they serve as a scaffold for the migration of neurons towards the emerging cortical plate. Intermediate progenitors proliferate in the subventricular zone and can differentiate into neurons. The deeper cortical layers are formed first (V and VI) and are subsequently traversed by later born neurons that form the upper cortical layers. VZ: ventricular zone, SVZ: subventricular zone, SP: subplate, CP: cortical plate, MZ: marginal zone (illustration created with BioRender.com).

Aside from the glutamatergic projection neurons that originate from RGCs and IPs and then migrate radially outward into the different cortical layers, the completed neocortex also contains GABAergic inhibitory interneurons derived from the ventral proliferative zone of the ganglionic eminence (GE). The adult neocortex contains 70-80% glutamatergic excitatory projection neurons and 20-30% GABAergic inhibitory interneurons (Hornung & De Tribolet, 1994; Wonders & Anderson, 2006; Sahara *et al.*, 2012). This distribution of the neuronal population provides the necessary balance of inhibitory and excitatory inputs within neuronal networks. GABAergic interneurons arise from RGCs and progenitors within the VZ and SVZ of the GE (Hansen *et al.*, 2013; Ma *et al.*, 2013b). Subsequently, they are guided by chemoattractants from the developing cortex and repulsive signals from the GE. They migrate tangentially, perpendicular to the RGC scaffold, either superficially along the MZ or follow a deeper route along the SVZ and finally integrate into the different cortical layers. As they arrive at their

destination, they begin to establish synaptic connections with glutamatergic projection neurons to form intricate neuronal networks. The initial number of generated neurons far exceeds the number of neurons in the completed cortex as functionally superfluous cells are eliminated by programmed cell death (PCD) during refinement of neuronal interconnectivity (Oppenheim, 1991).

3.2 Adult neurogenesis

The vast majority of neurogenesis is concluded during the prenatal period and the adult human brain was long thought to be incapable of generating young neurons. The idea that the neuronal composition of the human brain was set in stone at birth was questioned after neural stem cells were discovered in the dentate gyrus of the hippocampus (Eriksson *et al.*, 1998; Gage, 2000; Ehninger & Kempermann, 2008). The seminal study by Eriksson and colleagues detected dividing cells in postmortem tissue of cancer patients that had been injected with bromodeoxyuridine (BrdU) for diagnostic detection of tumors. Three decades earlier, in the 1960s, neurogenesis had been reported in the hippocampus and the cortex of adult rats and cats (Altman, 1962, 1963; Altman & Das, 1965). A few years later, neurogenesis was observed in the visual cortex of rats (Kaplan, 1981) and for the first time in primates (Kaplan, 1983). These reports were augmented by findings of widespread neurogenesis in the brains of songbirds (Goldman & Nottebohm, 1983; Alvarez-Buylla *et al.*, 1988). In 1999, neurogenesis was discovered in the dentate gyrus of the hippocampus and the neocortex of adult monkeys (Gould *et al.*, 1999; Kornack & Rakic, 1999). Together, these findings overturned the old dogma of a fixed adult brain.

Research on neurogenesis within the adult human brain has mostly focused on the hippocampus where it has been reported to persist up into the ninth decade of life. Adult neurogenesis seems to be influenced by an individual's behavior and environmental influences. It can be stimulated by physical exercise but deteriorates under conditions of stress and disease. For example, Alzheimer's disease (AD) has been reported to cause a progressive decline in hippocampal neurogenesis (Moreno-Jiménez *et al.*, 2019).

As post-mitotic cells, neurons are unable to self-renew by cell division and thus brain injuries like stroke and neurodegenerative diseases that destroy specific parts of the neuron incur irreversible damage. Consequently, high hopes are placed on therapeutic approaches that aim at stimulating local adult neurogenesis or injecting appropriate neural progenitor cells (NPCs) directly into the affected region of the brain to replenish the neuron population. NPCs for regenerative medicine are pre-patterned to differentiate into the desired type of neuron which then integrate into the existing local brain circuitry. Cell replacement therapy is already being tested in early clinical trials for the treatment of Parkinson's disease (PD). For this trial, seven PD patients were selected to be implanted with NPCs primed to

differentiate into dopaminergic neurons to reverse the damage done within the substantia nigra (Barker *et al.*, 2017). This procedure was previously tested in rats and monkey models of PD in which the treatment significantly improved motor functions (Doi *et al.*, 2014; Kikuchi *et al.*, 2017).

Even though advances have been made in the study of adult human neurogenesis the topic remains disputed. Recently, two independent papers published briefly one after the other made opposing claims about absence or presence of adult neurogenesis in the hippocampus (Boldrini *et al.*, 2018; Sorrells *et al.*, 2018). However, the majority of research data is still in favor of neurogenesis in the human adult hippocampus. Much of the current controversy regarding extent and location of adult neurogenesis arises from the fact that the field is hampered by technical difficulty concerning the preservation and handling of postmortem tissue samples. In the future, it will be interesting to see whether methodological advances and more standardized procedures for tissue preservation and handling will help to dissolve the current uncertainties and allow clearer statements about the functional relevance of adult neurogenesis in the human brain.

3.3 Hallmarks of neuronal maturation

After reaching their final destination in the orderly assembled structures of the brain, neurons mature by undergoing transcriptional, morphological and functional changes that equip them to perform as long-lasting, highly specialized information processing and relay units within complex networks.

A hallmark of neuronal maturation is the establishment of cellular polarity resulting from the formation of the dendritic arbor and the axon. This spatial separation is largely driven by differential organization of cytoskeletal components which gives rise to two morphologically and functionally distinct compartments. Whereas dendrites are specialized to receive synaptic input, the axon has to propagate the integrated signal to the downstream synapse. This organization is the basis for the unidirectional signal transmission by neurons. Microtubules form the structural basis of neuronal morphology. They consist of α- and β-Tubulin heterodimers that oligomerize end-to-end to form long filaments which then associate laterally to form a higher order tubular structure (Weisenberg, 1972). This arrangement causes microtubules to have an intrinsic polarity depending on the Tubulin subunit exposed at the respective end. An end of α-Tubulin subunits is referred to as the (-) end whereas β-Tubulin subunits constitute the (+) end. Of note, microtubule extension is significantly faster at the (+) end (Walker *et al.*, 1988). The orientation of microtubules also plays a role in the directionality of transport of organelles and vesicles which is mediated by kinesin and dynein motor proteins. Microtubules in dendrites have a mixed orientation of (-) and (+) ends and are enriched for microtubule-associated protein 2 (MAP2) as a stabilizing protein. In axons, microtubules are uniformly oriented with the

(+) end pointing outward to the axonal growth cone and they are mainly supported by associated Tau protein. As neurons mature, the expression of Tau, which is encoded by the *MAPT* gene, increases to provide the building material for the elongation of the growing axon (Fiock *et al.*, 2020). Maintenance of polarity is central for proper neuronal function. Disruption of orderly Tau distribution has been described as a hallmark of neurodegenerative tauopathies (Iqbal *et al.*, 2009; Gao *et al.*, 2018).

After the initial phase of polarization during which one neurite is determined to become the future axon, another important structural domain of mature neurons called the axon initial segment (AIS) is established. The AIS is located at the proximal axon where it constitutes the border between somatodendritic and axonal compartment (Leterrier, 2016; Huang & Rasband, 2018). It serves as a selective barrier for cellular constituents coming to and from the axon and also is the site for the initiation of action potentials (APs). Central constituents of the AIS are the scaffold proteins Ankyrin G and β4-Spectrin as well as voltage-gated Na^+ (Nav) and K^+ (Kv) ion channels. Ankyrin G is a high molecular weight protein with multiple protein interaction modules including spectrin-binding domains and a membrane-binding domain (Bennett & Lorenzo, 2013). During development, Ankyrin G acts as a nucleation core for the recruitment of the other AIS components. It connects to a scaffold of β4-Spectrin (Komada & Soriano, 2002; Dzhashiashvili *et al.*, 2007; Yang *et al.*, 2007) and evenly spaced actin rings (Leterrier *et al.*, 2011; Xu *et al.*, 2013; D'Este *et al.*, 2015). Furthermore, Ankyrin G tethers cell adhesion molecules (CAMs), Nav and Kv channels to the AIS membrane (Fache *et al.*, 2004; Wang *et al.*, 2014a) and hooks them onto microtubules by interaction with microtubule-associated proteins (Leterrier *et al.*, 2011; Kuijpers *et al.*, 2016). Compared to the distal axon or dendrites, Nav channels are enriched about 30-fold in the AIS (Kole *et al.*, 2008; Lorincz & Nusser, 2010) where they are responsible for initiation of APs (Clark *et al.*, 2009; Kole & Stuart, 2012). Since ion channels and CAMs are highly enriched in the AIS membrane domain and simultaneously tightly anchored to the cytoskeleton, they form a diffusion barrier for membrane proteins and lipids and thus contribute to neuronal polarity (Kobayashi *et al.*, 1992; Nakada *et al.*, 2003). In the cytoplasm the AIS acts as a sorting station for the intracellular trafficking of vesicles by excluding somatodendritic cargoes and forwarding axonal components. Even though the exact mechanism of how this is achieved has not yet been elucidated but it is likely to rely on differential roles of dynein and kinesin motor proteins (Farías *et al.*, 2015; Nirschl *et al.*, 2017).

The AIS is a highly plastic domain that can vary its size and shift its physical location closer to or further away from the axon hillock. This fine-tunes the excitability of a given neuron by decreasing or increasing the current threshold for generation of APs (Fried *et al.*, 2009; Grubb & Burrone, 2010; Kuba, 2010). Integrity of the AIS is essential for the maintenance of neuronal polarity and function. Knockdown of Ankyrin G disrupts the normal molecular organization by causing a redistribution of

somatodendritic proteins like MAP2 into the axon and promoting the formation of postsynaptic densities within the former axonal compartment (Hedstrom *et al.*, 2008; Sobotzik *et al.*, 2009; Leterrier *et al.*, 2011). Aberrations in the *ANK3* gene coding for Ankyrin G have been implicated in bipolar disorder, epilepsy, intellectual disability, schizophrenia and autism spectrum disorder (Huang & Rasband, 2018).

Splicing of transcripts encoding cytoskeletal components like Ankyrin G within the AIS and synaptic proteins relies on a protein called neuronal nuclei (NeuN) (Wang *et al.*, 2015; Lin *et al.*, 2016; Jacko *et al.*, 2018). NeuN is a nuclear protein that was discovered in an antibody screen on tissue of the central and peripheral nervous system of adult mice (Mullen *et al.*, 1992; Weyer & Schilling, 2003) and has since become a canonical marker protein to distinguish immature and mature neurons. It was later identified as RBFOX3, a member of the RNA-binding protein FOX (RBFOX) family of alternative splicing factors (Kim *et al.*, 2009). RBFOX proteins promote neuron-specific exon inclusion and are increasingly expressed as neuronal maturation proceeds. The importance of NeuN/RBFOX3 is highlighted by reports implicating its dysfunction to be involved in delayed neurodevelopment (Utami *et al.*, 2014) and epilepsy (Lal *et al.*, 2013).

An essential part of the maturation process of every neuron is its integration into complex neuronal circuits within the developing brain. Transmission of electrochemical signals between two neurons requires precise synaptic connections. Synapses are highly asymmetric structures that rely on a well-coordinated assembly of membrane domains and protein complexes at the axonal presynaptic terminal and the dendritic postsynaptic density (PSD) (Südhof, 2018; Edge *et al.*, 2020). Mature synapses contain hundreds of distinct proteins that maintain its structure and functionality (Collins *et al.*, 2006). Pre- and postsynaptic proteins are produced and packaged in transport vesicles already before acute synaptogenesis (Fletcher *et al.*, 1991; Rao *et al.*, 1998). Presynaptic transport vesicles are loaded with scaffold proteins like Piccolo and Bassoon, proteins involved in vesicle fusion like SNAP-25 and synapsins as well as neurotransmitters. In contrast, postsynaptic transport vesicles contain a different set of scaffold proteins specific for the PSD like PSD-95 and Shank, neurotransmitter receptors and voltage gated ion channels. These vesicles are rapidly recruited to nascent synapses after initial contact between filopodia of the axonal growth cone and dendrites. It has been proposed that presynaptic vesicles continually cycle between neurotransmitter release and reuptake at predefined sites of the axonal growth cone to probe the extracellular space for a fitting dendritic counterpart. On the dendritic site, vesicles containing the matching neurotransmitter receptors follow the same pattern. Once an initial contact has been made, the nascent connection is reinforced by a large variety of trans-synaptic cell adhesion molecules including neural cell adhesion molecule (NCAM), SynCAM, neuroligins, neurexins, synaptic adhesion-like molecules (SALMs), nectins, integrins and

cadherins. This diverse set of cell adhesion molecules stabilizes the nascent synapse until larger scaffolding proteins like PSD-95 are recruited to support the synaptic architecture (Han & Kim, 2008; Lie *et al.*, 2018; Liu, 2019). PSD-95 and other scaffolding proteins link neurotransmitter receptors, ion channels and trans-synaptic cell adhesion molecules via PDZ protein interaction domains. Additionally, synaptic maturation is enhanced by secreted factors of and direct contact with astrocytes in the proximity (Allen & Barres, 2005). With maturation, the postsynaptic compartment undergoes cytoarchitectural changes and develops into a dendritic spine.

As neurons start to express higher numbers and a more diverse set of ion channels and integrate them into their plasma membrane, their electrophysiological properties begin to change (Bardy *et al.*, 2016; Burke *et al.*, 2020). The presence of more ion conducting channels in the membrane leads to a decreased membrane resistance and a higher excitability. During development, neuronal networks go through different phases of network activity. At first, firing of neurons is sporadic and uncoordinated but then advances to a period of synchronized oscillations. This process has been described *in vivo* (Leinekugel *et al.*, 2002; Khazipov *et al.*, 2004; Kilb *et al.*, 2011), in primary cortical cultures (Corlew *et al.*, 2004) and cortical organoids (Trujillo *et al.*, 2019). Synchronized firing finally transitions into more complex activity patterns within specialized circuits (Kirwan *et al.*, 2015; Luhmann *et al.*, 2016).

3.4 Stem cell technology and direct conversion for the generation of human neurons

The generation of induced-pluripotent stem cells (iPSCs) by reprogramming of terminally differentiated somatic cells has provided the scientific community with an unprecedented potential to generate and investigate any type of human tissue. IPSCs can be obtained from almost any cell type including fibroblasts, keratinocytes, peripheral blood cells or renal tubular and renal epithelial cells from urine (Liu *et al.*, 2020). Initially, reprogramming employed retroviral or lentiviral expression systems of the four transcription factors OCT4, KLF4, SOX2 and c-MYC (Takahashi & Yamanaka, 2006; Takahashi *et al.*, 2007). These approaches entailed stable integration of the viral transgenes into the host genome which is especially problematic for therapeutic approaches as it raises the tumorigenic potential of the resulting cell lines. Today, transient expression of the aforementioned reprogramming factors can be achieved more elegantly by nonintegrative delivery systems such as sendai virus vectors (Chen *et al.*, 2013).

PSCs are defined by their ability to self-renew via extensive proliferation and their potency to differentiate into all cell types of the three primary germ layers (Wobus & Boheler, 2005).

As differentiation protocols have become more refined, increasingly complex human cell types can be generated including distinct neuronal subtypes, cardiomyocytes and insulin secreting pancreatic β cells. IPSCs also cleared the way for the generation of standardized 3D organoids which are miniature models of whole tissue niches that facilitate insights into developmental processes. IPSC technology removed ethical concerns associated with the use of embryonic stem cells (ESCs) and may reduce the need for animal research. Disease modeling and drug screening with iPSC-derived cultures and organoids may better recapitulate the actual efficacy of lead drug candidates in the human system for which standard immortalized cell lines and animal models are less suitable (Kola & Landis, 2004; Lin, 2008; Rubin, 2008; Mertens *et al.*, 2013b). Additionally, autologous transplantation of iPSC-derived grafts within the scope of cell replacement therapy eliminates the risk of immune rejection without the need to administer immunosuppressive drugs.

More recently, iPSC technology has been amended by a surge of studies on cell fate instruction via direct conversion through transdifferentiation (Fig. 2). The latter also uses terminally differentiated somatic cells like fibroblasts or peripheral blood cells to generate cells of choice but skips the pluripotent intermediary (Ladewig *et al.*, 2013). Whereas genomic and epigenetic traits of aging are removed during the generation of iPSCs, direct conversion retains the molecular aging signature of the respective donor individual. Therefore, direct conversion opened up new possibilities to study age-related degenerative diseases which can be challenging to model with iPSC-based systems. Direct generation of the desired target cells can be achieved by overexpression of distinct transcription factors or by using a set of small molecule compounds to chemically steer the fate of cells (Vierbuchen *et al.*, 2010; Biswas & Jiang, 2016; Takeda *et al.*, 2018). As a transgene-free approach, chemical reprogramming is of great interest for clinical applications. Aside from *in vitro* generated grafts, direct cell fate conversion is also tested *in vivo* at the site of interest. For example, astrocytes have successfully been converted into distinct neuronal subtypes directly in different regions of the mouse brain (Guo *et al.*, 2014; Liu *et al.*, 2015; Janowska *et al.*, 2019).

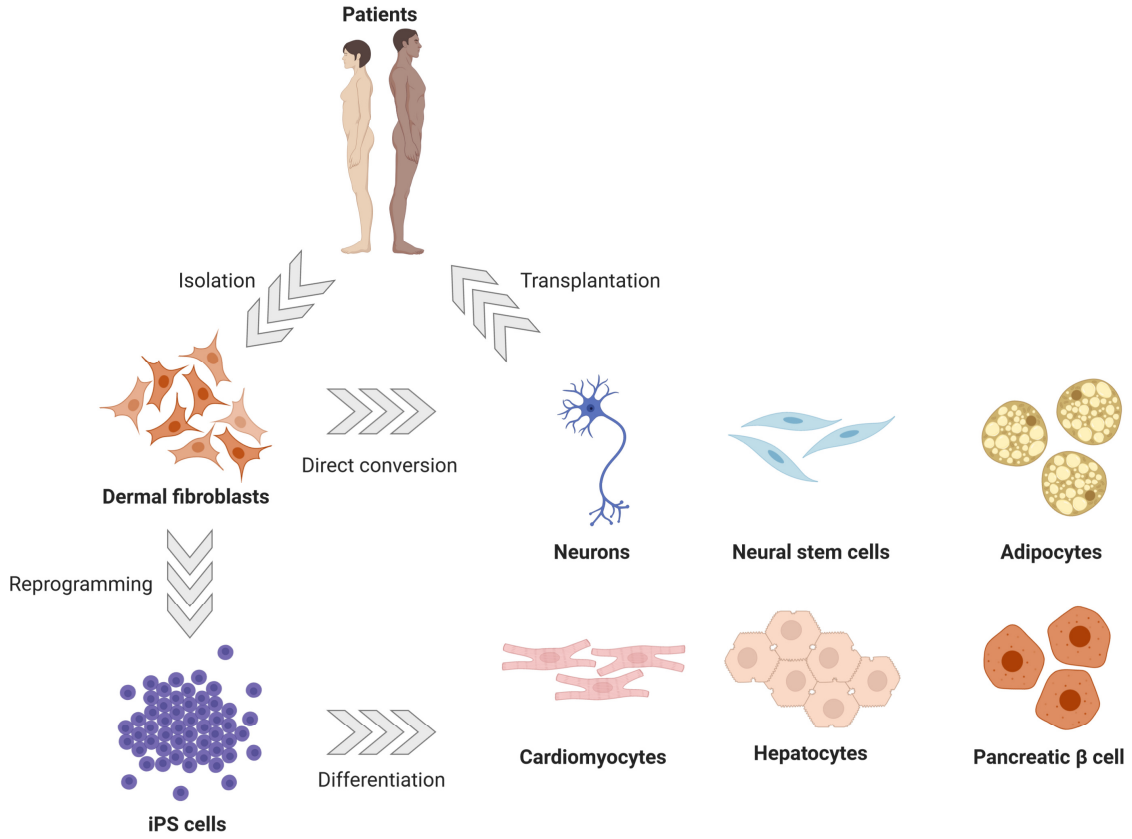

Fig. 2: IPSC and direct conversion technology.

Dermal fibroblasts isolated from a skin biopsy can be directly converted into desired cell types via transdifferentiation. This is achievable either chemically by application of specific small molecule cocktails or genetically by expression of transcription factors specific for the desired cell type. Alternatively, dermal fibroblasts can be reprogrammed to iPS cells by forced expression of the transcription factors OCT4, KLF4, SOX2 and c-MYC. In a second step, iPSCs can then be differentiated to a variety of cell types via specific differentiation procedures. The obtained patient-specific cells may be transplanted back into the patient within the scope of cell replacement therapy (illustration created with BioRender.com).

IPSCs and direct conversion provide two avenues to obtain functionally active human neurons *in vitro*. Fate instruction of iPSCs into distinct neuronal subtypes requires fine-tuning of engrained developmental morphogen signaling pathways by small molecules. This allows generation of region-specific neuroepithelial cells (NECs) with the inherent tendency to differentiate into related types of neurons (Fasano *et al.*, 2010; Kriks *et al.*, 2011; Paşca *et al.*, 2011; Tao & Zhang, 2016). Forebrain NECs can be induced from iPSCs via inhibition of SMAD-mediated BMP and TGF-β signaling and the WNT pathway using noggin/LDN193189, SB431542/A83-01 and XAV939 (Chambers *et al.*, 2009; Li *et al.*, 2009; Shi *et al.*, 2012). In the absence of further guiding cues neural induction defaults to NPCs with a forebrain fate. For the generation of NPCs with midbrain or hindbrain identity, the degree of caudalization can in large part be titrated by increasing activation of WNT signaling via CHIR99021 (Kirkeby *et al.*, 2012; Moya *et al.*, 2014; Lu *et al.*, 2016).

The first directly converted neurons were reported by Vierbuchen *et al*. in 2010. They coined the term induced neurons (iNs) for the neurons they generated from mouse fibroblasts via overexpression of the three neurogenic transcription factors Ascl1, Brn2 and Mytl1 (Vierbuchen *et al.*, 2010). Shortly thereafter, human fibroblasts were successfully converted into iNs by adding NEUROD1 to the three transcription factors used before (Pang *et al.*, 2011). Subsequent studies showed that similar results are obtained by overexpression of ASCL1 and NGN2 (Son *et al.*, 2011; Liu *et al.*, 2013). Since then iNs have also been generated in the absence of transcription factors by overexpression of microRNAs (Xue *et al.*, 2013; Victor *et al.*, 2014) and by chemical induction with small molecules (Hu *et al.*, 2015; Li *et al.*, 2015).

Together, iPSC technology and direct conversion enable patient-specific disease modeling and more reliable drug screening thanks to their faithful recapitulation of hereditary and aging effects. In addition, they open the door to individualized cell replacement therapy. Alongside next generation sequencing techniques, these cell-based approaches will become the bedrock of personalized medicine in the future.

3.5 Apoptosis

Cells that have exceeded their lifespan, have become functionally superfluous or were irreversibly damaged by the impact of stress or disease have to be removed from the respective tissue. Depending on tissue and cell type, the natural rate of turnover of senescent cells differs substantially. Many cells are constantly replaced in an effort to renew the respective tissue. Neutrophils are estimated to have an average lifespan of 10 h, enterocytes of the intestinal epithelium 5-7 days and erythrocytes last for about 120 days (Marshman *et al.*, 2002; Spalding *et al.*, 2005; Tak *et al.*, 2013). With the exception of very limited neurogenesis in the hippocampus human neurons are not replaced and thus have to persist for the entire life time of an individual which today almost equates to a whole century. Cell death also functions as an essential tool during developmental processes to cull excess cells as in the removal of cells in the interdigital region or neurons that are not properly integrated into the brain circuitry (Oppenheim, 1991; Buss *et al.*, 2006; Fuchs & Steller, 2011; Ghose & Shaham, 2020).

Mechanisms by which cells may be removed can be distinguished based on whether they trigger a subsequent activation of the immune system or not. Inflammatory modes of cell death like necrosis, necroptosis and pyroptosis result in the uncontrolled release of cellular contents into the surrounding tissue which leads to recruitment and activation of immune cells to the respective site (Elmore, 2007; Nagata, 2018; D'Arcy, 2019). In contrast, non-inflammatory cell death like apoptosis and autophagy proceeds in a more orderly fashion and entails self-digestion, condensation and packaging of

macromolecules and cellular debris. Aside from a resulting involvement of the immune system, causes of cell death may also be distinguished by their mode of activation. Accidental cell death is caused by localized injuries like physical trauma or ischemia. Controlled or programmed cell death (PCD) relies on defined signaling pathways and is essential for the elimination of damaged or infected cells and the clearance of superfluous cells during developmental processes. The two modes of non-inflammatory PCD are apoptosis and autophagy. Pertaining to the death of cells, apoptosis has been studied much more extensively and is often incorrectly used as a synonym for PCD.

Apoptosis is either initiated cell autonomously by signals from intracellular homeostasis control mechanisms or by an extrinsic stimulus resulting from the interaction with natural killer cells or macrophages of the host immune system. Both apoptosis pathways rely on enzymatic cascades driven by members of the family of caspase cysteine-aspartic proteases. As a general principle, the first caspase within a pathway to be activated is referred to as an initiator caspase. The latter activates downstream effector or executioner caspases by proteolytic cleavage of inactive precursor forms. Finally, effector caspases cleave downstream targets which leads to DNA condensation and dismantling of the cell. In apoptosis, Caspases-2, -8, -9 and -10 are the initiator caspases that activate the effector Caspases-3, -6 and -7 (Slee *et al.*, 2001; Chen & Wang, 2002; Parrish *et al.*, 2013).

The extrinsic apoptosis pathway is triggered by activation of transmembrane receptor proteins called death receptors which are a subgroup of the tumor necrosis factor (TNF) receptor superfamily (Fig. 3). The four known death receptors are the receptor for TNFα, the Fas receptor (FasR) and TNF-related apoptosis-inducing ligand receptor 1 and 2 (TRAIL1/2) (Trauth *et al.*, 1989; Itoh & Nagata, 1993; Wajant, 2003). These receptors contain intracellular death domain (DD) protein-protein interaction modules for homo oligomerization or recruitment of proapoptotic adaptor proteins like FAS-associated death domain (FADD) or TNF receptor associated death domain (TRADD). These adaptor proteins facilitate the formation of the death-inducing signal complex (DISC) (Kischkel *et al.*, 1995; Sessler *et al.*, 2013) by recruiting monomers of Procaspases-8 or -10 which dimerize and subsequently activate by intra- and interdimeric cleavage. Subsequently, these two initiator caspases activate Caspases-3 and -7 or cleave BH3 interacting-domain death agonist (BID) to truncated BID (tBID) which is capable of initiating the intrinsic apoptosis pathway at mitochondria.

The intrinsic apoptotic pathway is activated by stress stimuli like nutrient or growth factor deprivation, oxidative stress, ionizing radiation, disruption of protein homeostasis, DNA damage or cross-talk from the extrinsic pathway. Central steps along the intrinsic apoptosis pathway are mitochondrial outer membrane permeabilization (MOMP) (Dewson & Kluck, 2009; Tait & Green, 2010), apoptosome assembly (Riedl & Salvesen, 2007), activation of effector caspases and apoptotic body formation (Fig. 3).

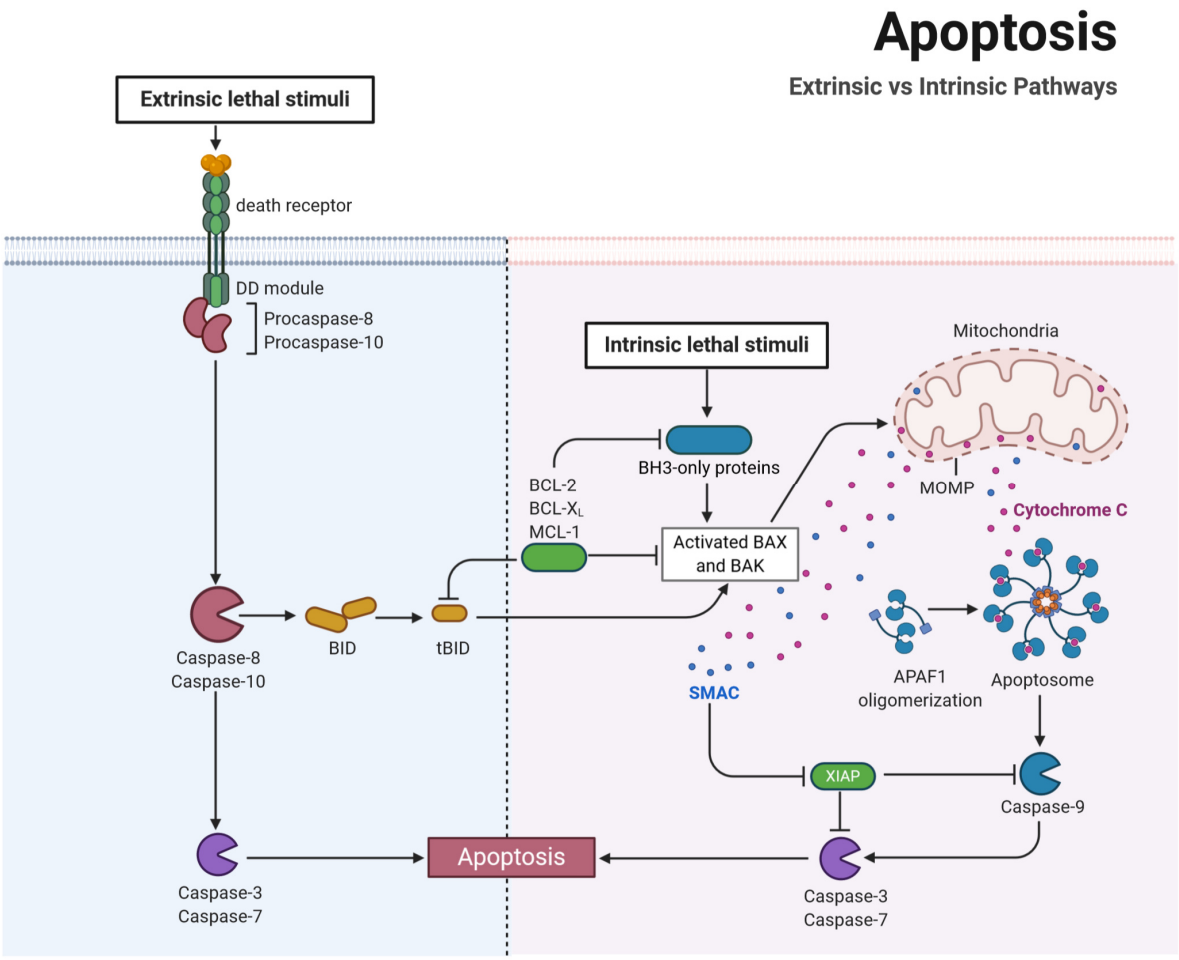

Fig. 3: The extrinsic and intrinsic apoptosis signaling pathways.

Schematic illustration of signaling events of the extrinsic and intrinsic apoptosis pathways. The extrinsic apoptosis pathway is triggered via activation of death receptors which recruit Procaspase-8 and -10 with their intracellular death domain (DD) module. This leads to caspase activation. Caspase-8 and -10 are then able to activate effector Caspases-3 and -7 or cleave BID to its truncated form (tBID) which promotes mitochondrial outer membrane permeabilization (MOMP). A lethal intrinsic stimulus engages the intrinsic apoptosis pathway by affecting the balance of proapoptotic (BH3-only) and antiapoptotic BCL-2 proteins (BCL-2, BCL-X_L, MCL-1). This promotes oligomerization of BAX and BAK resulting in pore-formation within the outer mitochondrial membrane. Once this membrane has been permeabilized, SMAC and Cytochrome c are released into the cytosol. Cytochrome C and APAF-1 form the apoptosome and cause activation of Caspase-9 which subsequently activates the downstream effector Caspases-3 and -7. The inhibitor of apoptosis protein (IAP) XIAP is able to block caspase activity but may itself be inhibited by SMAC. Active effector caspases initiate the execution phase of apoptosis (illustration created with BioRender.com).

Initiation of the intrinsic apoptosis pathway hinges on the balance of proapoptotic and pro-survival members of the BCL-2 family of proteins (Singh *et al.*, 2019a). BCL-2 proteins contain up to four different types of BCL-2 homology domains (BH1-4) that mediate protein-protein interactions. Proapoptotic BCL-2 proteins with several different types of BH domains are BAX and BAK. Other proapoptotic members like BID, BAD, BIM, BMF, Puma, Noxa and HRK only contain BH3 domains.

The pro-survival BCL-2 proteins MCL-1, BCL-2, BFL-1, BCL-xL and BCL-w exert their function by preventing BAX and BAK from oligomerizing and forming pores in the outer mitochondrial membrane for MOMP (Wei *et al.*, 2001; George *et al.*, 2007; Dewson *et al.*, 2008). During apoptosis, BH3-only proteins bind to and neutralize pro-survival BCL-2 members and also bind to and activate BAX and BAK directly thereby allowing MOMP to proceed. Permeabilization of the mitochondrial membrane releases additional proapoptotic proteins such as second mitochondria-derived activator of caspases (SMAC), also called direct inhibitor of apoptosis-binding protein with low pI (DIABLO), high-temperature requirement A2 (HtrA2) and Cytochrome c from the intermembrane space into the cytosol. SMAC and HtrA2 promote apoptosis indirectly by inhibiting caspase-inactivating proteins like X-linked inhibitor of apoptosis protein (XIAP) (Suzuki *et al.*, 2001; Rehm *et al.*, 2003; Saito *et al.*, 2003; Srinivasula *et al.*, 2003; Yang *et al.*, 2003; Creagh *et al.*, 2004). In contrast, Cytochrome c which usually is an integral component of the electron transport chain causes a direct progression of the apoptotic cascade by binding to apoptotic protease-activating factor-1 (APAF-1) (Zou *et al.*, 1997). Together, Cytochrome c and APAF-1 form a protein complex called apoptosome. As the DISC within the extrinsic pathway, the apoptosome offers the structural platform for recruitment and activation of the initiator caspase which within the intrinsic pathway is Caspase-9 (Riedl & Salvesen, 2007; Bratton & Salvesen, 2010; Li *et al.*, 2017b). The caspase activation and recruitment domain (CARD) of APAF-1 allows binding and thus dimerization of inactive Caspase-9 which is subsequently activated by autocatalytic cleavage. Active Caspase-9 enables processing of inactive Caspases-3, -6 and -7 into their active forms (Slee *et al.*, 1999; Guerrero *et al.*, 2008). These effector caspases then cleave hundreds of downstream targets to finalize cellular dismantling characterized by the morphological hallmarks of apoptosis like condensation of cytoplasm and chromatin, nuclear fragmentation and formation of apoptotic bodies. For example, BID is cleaved to enhance MOMP, poly ADP-ribose polymerase-1 (PARP-1) is inactivated to halt DNA repair (Kaufmann *et al.*, 1993; Soldani & Scovassi, 2002), caspase-activated DNase (CAD) is enabled to catalyze DNA fragmentation (Larsen & Sørensen, 2017) and the cytoskeletal regulator rho-associated coiled-coil-containing protein kinase 1 (ROCK1) is cleaved to induce membrane blebbing (Sebbagh *et al.*, 2001). Caspase activity also causes apoptotic cells to display increased levels of phosphatidylserine on the surface of their plasma membrane which serves as a phagocytosis signal for macrophages that proceed to clear the tissue from cellular remnants.

An important class of pro-survival proteins are the members of the inhibitor of apoptosis protein (IAP) family (Hrdinka & Yabal, 2019). IAPs are characterized by the presence of a baculovirus IAP repeat (BIR) domain which mediates protein-protein interaction. The BIR domain was so named because it was the common feature of a group of proteins that protected insect cells from apoptosis induced by baculoviral infection (Crook *et al.*, 1993; Birnbaum *et al.*, 1994). To date, eight BIR containing (BIRC) proteins are known in humans: NLR (nucleotide-binding domain and leucine-rich repeat containing)

family apoptosis inhibitory protein (NAIP), cellular inhibitor of apoptosis 1 (cIAP1), cIAP2, X chromosome-linked IAP (XIAP), Survivin, Bruce, Livin and testis specific IAP (TS-IAP). IAPs contain up to three BIR domains. Additionally, cIAP1, cIAP2, XIAP, Livin and TS-IAP are able to act as E3 ubiquitin ligases by attaching ubiquitin moieties to themselves or target proteins via their carboxy-terminal really interesting new gene (RING) domain. Fittingly, XIAP, cIAP1, cIAP2 and TS-IAP also possess a ubiquitin associated (UBA) domain which enables recognition of polyubiquitin chains (Gyrd-Hansen *et al.*, 2008; Blankenship *et al.*, 2009). As a post-translational modification (PTM), chains of ubiquitin mark proteins for proteasomal degradation and are thus essential in the regulation of protein turnover. XIAP, encoded by the *BIRC4* gene, contains three BIR domains and has the widest scope of antiapoptotic capacity (Schile *et al.*, 2008; Vucic, 2018). Via direct interaction it blocks the catalytic activity of initiator Caspase-9 and the effector Caspases-3 and -7 (Shiozaki *et al.*, 2003; Scott *et al.*, 2005). Additionally, XIAP may act as an E3 ubiquitin ligase to promote the degradation of proapoptotic SMAC/DIABLO (Macfarlane *et al.*, 2002; Qin *et al.*, 2016). Bruce (*BIRC6*) is involved in the degradation of Caspase-9 and SMAC/DIABLO (Hao *et al.*, 2004) which can also be inhibited by Livin and TS-IAP (Vucic *et al.*, 2002; Shin *et al.*, 2005). CIAP1 and 2 block apoptosis by modulating TNF and NF-κB signaling (Estornes & Bertrand, 2015; Lalaoui & Vaux, 2018).

Due to their strong survival promoting functions, IAPs have become promising targets in the treatment of cancers which are notorious for their increased resistance to apoptosis (Hanahan & Weinberg, 2011). Increased levels of IAP expression correlate with poor prognosis in many forms of human cancer including colorectal (Xiang *et al.*, 2009), prostate (Krajewska *et al.*, 2003), blood (Grzybowska-Izydorczyk *et al.*, 2010) and lung cancer (Ferreira *et al.*, 2001). To increase the susceptibility of cancer cells to apoptosis, IAPs are deprived of their capability to bind proapoptotic proteins by saturating their BIR domains with so called SMAC mimetics. The latter are small molecules structurally designed to recapitulate part of the IAP-binding motif (IBM) consisting of the N-terminal Ala-Val-Pro-Ile (AVPI) peptide. So far, eight compounds have entered clinical trials and are being investigated for their potential for combination therapy with chemotherapy, radiation and other approaches (Morrish *et al.*, 2020).

3.6 Regulation of apoptosis in neurons

During development, neurogenesis initially creates a surplus of neurons to provide an abundance of cellular material for formation of the mature brain circuitry. Once the necessary neuronal connections have been established, superfluous neurons are removed by apoptosis. Consequently, neuronal apoptosis is essential in early stages of network formation but becomes undesirable at later stages.

As neurons mature, they acquire an increased survival competency through a variety of adaptations that synergize to prevent their accidental loss (Kole *et al.*, 2013; Hollville *et al.*, 2019). For example, immature neurons are more susceptible to nerve growth factor (NGF) deprivation (Lazarus *et al.*, 1976; Easton *et al.*, 1997) and viral infections (Labrada *et al.*, 2002; Ahn *et al.*, 2008). Mature cortical neurons from rats have been shown to possess reduced expression of APAF-1 and Caspase-3 (Yakovlev *et al.*, 2001). Reduction of APAF-1 protein levels due to chromatin remodeling has also been reported for mouse sympathetic neurons (Wright *et al.*, 2007). Additionally, mouse cortical neurons show a developmental downregulation of the splicing regulator PTBP1 which allows alternative splicing of *BAK1* mRNA leading to loss of BAK protein and a restriction of neuronal apoptosis by impeding MOMP (Lin *et al.*, 2020). Furthermore, the two microRNAs miR-24 and miR-29 are upregulated during neuronal maturation. They are involved in post-transcriptional suppression of BH3-only proteins (Kole *et al.*, 2011; Annis *et al.*, 2016) and offer protection *in vivo* during ischemic stroke (Khanna *et al.*, 2013) and ethanol-induced toxicity (Qi *et al.*, 2014). Apart from developmentally controlled downregulation of proapoptotic factors, cytoprotective effects may also be mediated by neuronal activity. For example, survival of mouse cortical neurons under stress conditions is boosted by synaptic stimulation (Papadia *et al.*, 2008; Léveillé *et al.*, 2010). While mature neurons are highly susceptible to excitotoxic cell death by excessive stimulation, physiological activation of NMDA receptors may also enhance pro-survival signaling via activation of ERK and AKT (Perkinton *et al.*, 2002; Sutton & Chandler, 2002; Hetman & Kharebava, 2006; Papadia *et al.*, 2008). So far, all of these findings have been made in animal models or in cell culture systems using neurons from rodents. However, these examples illustrate the tight control of apoptotic signaling events in mature neurons.

3.7 The hexosamine biosynthetic pathway

The hexosamine biosynthetic pathway (HBP) is a four-step metabolic pathway which results in the production of the amino sugar uridine 5'-diphospho-N-acetyl-D-glucosamine (UDP-GlcNAc). The latter is widely used as a precursor for the synthesis of glycosaminoglycans and glycolipids as well as in the post-translational modification of proteins by N- and O-linked glycosylation and O-GlcNAcylation.

The HBP consumes about 2 to 5% of the total cellular glucose (Marshall *et al.*, 1991) as it is fueled by fructose-6-phosphate generated during glycolysis. In the first reaction of the HBP, fructose-6-phosphate and glutamine are converted into glucosamine-6-phosphate (GlcN-6P) and glutamate (Fig. 4). This rate-limiting reaction is catalyzed by the enzyme glutamine-fructose-6-phosphate aminotransferase-1 (GFAT-1). The second reaction requires acetyl-coenzyme A (Ac-CoA) from fatty acid metabolism. The acetyl group of Ac-CoA is transferred to GlcN-6P by glucosamine-phosphate

N-acetyltransferase (GNA-1) to yield N-acetylglucosamine-6-phosphate (GlcNAc-6P). Subsequently, GlcNAc phosphomutase (PGM-3) isomerizes GlcNAc-6P to GlcNAc-1P which is finally converted together with uridine triphosphate (UTP) to UDP-GlcNAc by UDP-N-acetylglucosamine pyrophosphorylase (UAP-1) (Ghosh *et al.*, 1960; Chiaradonna *et al.*, 2018). This sequence of reactions reveals that the HBP is highly intertwined with all parts of the cellular metabolism as it requires carbohydrate, amino acid, fatty acid and nucleotide input. This interconnectedness positions the HBP as a metabolic hub to gauge the energy status of a cell and to couple it to a wide range of downstream signaling events depending on the availability of UDP-GlcNAc.

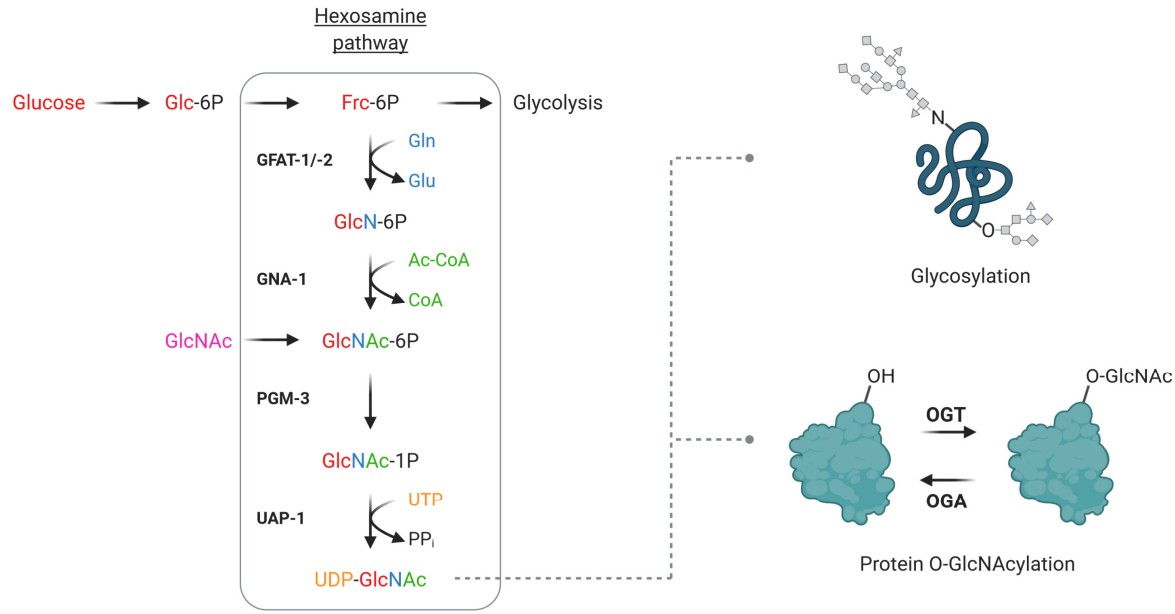

Fig. 4: Hexosamine biosynthetic pathway (HBP).

The HBP is fueled by fructose-6-phosphate (Frc-6P) which is produced during glycolysis. Four consecutive reactions convert Frc-6P into UDP-GlcNAc. The rate-limiting step is the first reaction which is catalyzed by GFAT-1/2. The HBP requires molecules from carbohydrate (red), amino acid (blue), fatty acid (green) and nucleotide (orange) metabolism, making the HBP a metabolic hub. The first two reactions may be skipped by supplementation of GlcNAc (pink). UDP-GlcNAc serves as the essential substrate for glycosylation of proteins and other macromolecules as well as the O-GlcNAcylation of serine/threonine residues within target proteins. Enzymes are indicated in bold type (illustration created with BioRender.com).

The UDP-GlcNAc generated by the HBP can be isomerized into UDP-N-acetylgalactosamine (UDP-GalNAc) by UDP-galactose-4-epimerase (GALE) (Leloir, 1951; Thoden *et al.*, 2001; Holden *et al.*, 2003). These two hexosamines serve as building blocks for complex N- and O-linked glycan modifications of proteins and glycan structures on glycolipids. Therefore, both amino sugars make up a substantial portion of the glycocalyx which is formed by glycan trees on proteins and lipids protruding outward from the cell membrane into the extracellular space. The glycocalyx constitutes the outermost layer of cells and is thus essential for cell-cell interactions. In addition, GlcNAc and GalNAc extensively

contribute to components of the extracellular matrix (ECM) which consists of proteins and glycosaminoglycans secreted by cells of the respective niche (Frantz *et al.*, 2010; Varki, 2011, 2017; Hynes & Naba, 2012; Moremen *et al.*, 2012).

Aside from its presence in glycan structures, single molecules of UDP-GlcNAc also play an important role in the post-translational modification of proteins by O-GlcNAcylation (Ma & Hart, 2014; Yang & Qian, 2017). GlcNAc can be covalently linked to the hydroxyl group of serine or threonine amino acid side chains by the enzyme O-GlcNAc transferase (OGT) (Haltiwanger *et al.*, 1990). The sugar moiety can be removed again by O-GlcNAcase (OGA). O-GlcNAcylation is a dynamic PTM similar to phosphorylation and has been implicated in modulating protein-protein interaction, protein localization and stability as well as enzymatic activity. By these means, it influences circadian rhythm, metabolism, cellular stress response and transcriptional regulation. Via O-GlcNAcylation all these processes are coupled to UDP-GlcNAc levels, HBP flux and thus the metabolic state of the cell. O-GlcNAc cycling relies on only two highly conserved enzymes, OGT and OGA, whereas phosphorylation of proteins is regulated by several hundreds of kinases and phosphatases (Manning *et al.*, 2002). Both PTMs compete for the same functional groups within proteins and the correct dynamics between them is crucial for cellular homeostasis (Hart *et al.*, 2011). Dysregulation of O-GlcNAcylation has been reported in diabetes, cardiovascular disease, malfunction of the immune system, cancer and neurodegenerative disorders (Wani *et al.*, 2017; Akella *et al.*, 2019; Nie & Yi, 2019). The importance of O-GlcNAcylation and its interplay with phosphorylation is well illustrated by its relevance in Alzheimer's disease (Yuzwa & Vocadlo, 2014): Normally, the microtubule-associated protein tau is highly modified by phosphorylation during early brain development and less in the healthy adult brain in which the phosphorylation sites are in large part blocked by O-GlcNAcylation. In AD patients, levels of global O-GlcNAcylation are reduced, allowing tau to be abundantly phosphorylated. The resulting hyperphosphorylated tau is prone to aggregate and form the neurofibrillary tangles that are characteristic for AD (Gong *et al.*, 2016). Studies on mouse models of AD observed decreased aggregation of tau and improved cognitive health when tau was strongly conjugated with O-GlcNAc. Interestingly, O-GlcNAc is also found in the cytosolic domain of the amyloid precursor protein (APP) which possibly modulates its cleavage to Aβ peptides (Griffith *et al.*, 1995).

In addition to its involvement in the direct modification of proteins, UPD-GlcNAc serves as the starting compound for the synthesis of N-acetylneuraminic acid (Neu5Ac), the precursor for the generation of sialic acids. These sugar molecules are usually found in terminal positions of complex glycan branches (Varki, 2008). This glycan capping increases the half-life of proteins in circulation and therefore has clinical significance in the administration of therapeutic glycoproteins (Bork *et al.*, 2009; Flintegaard *et al.*, 2010; Lindhout *et al.*, 2011). In humans, sialic acids are ubiquitously distributed but are most

enriched in the brain where they are 2-4 times more abundant than in the brains of other mammals (Wang *et al.*, 1998; Wang, 2012; Schnaar *et al.*, 2014). In the brain, the bulk of sialic acids are part of gangliosides, a class of glycolipids, which reside in the plasma membrane of neurons and are enriched in lipid rafts (Schnaar, 2016). Gangliosides may either interact laterally with components within the plasma membrane (*cis* mode) or bind to complementary recognition molecules of other cells or the ECM (*trans* mode). *Cis* regulation enhances the activity of the tropomyosin receptor kinase A (TrkA) upon stimulation with nerve growth factor (NGF) (Farooqui *et al.*, 1997) and is involved in the intracellular trafficking of the GluR2 subunit of α-amino-3-hydroxy-5-methyl-4-isoxazolepropionic acid (AMPA) receptors (Prendergast *et al.*, 2014). The *trans* binding of gangliosides to sialic acid-binding immunoglobin-like lectin-4 (siglec-4) stabilizes myelination of axons (Yang *et al.*, 1996; Schnaar, 2010). Additionally, *cis* and *trans* interactions of gangliosides play a role in the regulation of axonal outgrowth (Da Silva *et al.*, 2005; Schnaar & Lopez, 2009).

Aside from their presence in gangliosides, sialic acids are used in the assembly of polysialic acid (polySia), a linear homo polymer of varying length that is attached to proteins as a PTM (Schnaar *et al.*, 2014). The vast majority of polySia modifications in the brain are found on NCAM (PSA-NCAM) and to a lesser extent on SynCAM and other proteins. By influencing the binding capability of NCAM to its interaction partners, polySia facilitates the migration of NPCs, modulates anchoring to ECM components and impacts synaptogenesis. In addition, polySia has been shown to interact with brain-derived neurotrophic factor (BDNF) as well as neurotrophin (NT)-3 and -4. PolySia is believed to scavenge these soluble factors from the extracellular milieu to enhance activation of the related beneficial neuronal downstream signaling pathways (Kanato *et al.*, 2008; Isomura *et al.*, 2011). With its wide-ranging distribution, polySia has an impact on neuronal plasticity, cognition and memory (Gómez-Climent *et al.*, 2011; Guirado *et al.*, 2014).

3.8 Glutamine-fructose 6-phosphate aminotransferase (GFAT)-1 – Pacemaker of the hexosamine pathway

As the first and rate-limiting enzyme of the HBP, GFAT-1 (EC 2.6.1.16) is the major regulator in the generation of UDP-GlcNAc. GFAT-1 catalyzes the transfer of an amino group from L-glutamine to fructose-6-phosphate to produce glucosamine-6-phosphate and L-glutamate. Eukaryotic GFAT-1 forms a homotetramer (Raczynska *et al.*, 2007; Richez *et al.*, 2007). The crystal structure of a full-length monomer of eukaryotic GFAT-1 has only recently been described (Ruegenberg *et al.*, 2020). Structurally, GFAT-1 consists of a glutaminase and a combined isomerase/transferase domain joined by a linker region (Denisot *et al.*, 1991; Mouilleron *et al.*, 2006). Once GFAT-1 binds both of its

substrates, a conformational change leads to formation of a channel between the active sites of the two domains. Ammonia released from L-glutamine at the glutaminase domain traverses this channel to reach the isomerase/transferase domain. The latter isomerizes fructose-6-phosphate to D-glucose-6-phosphate to which it subsequently transfers the incoming ammonia to finalize the reaction. Since the binding pockets and the central catalytic residues are highly conserved, this reaction mechanism is very similar from prokaryotes to humans (Mouilleron *et al.*, 2011). Unique to eukaryotic GFAT-1 is its negative feedback inhibition by UDP-GlcNAc, the end product of the HBP (Kornfeld, 1967; Milewski *et al.*, 1999). UDP-GlcNAc indirectly inhibits the glutaminase activity by its interaction with the interdomain linker and the isomerase domain. Interestingly, substitution of the glycine residue at position 451 within the isomerase domain by glutamate diminishes this negative feedback regulation (Fig. 5) (Ruegenberg *et al.*, 2020).

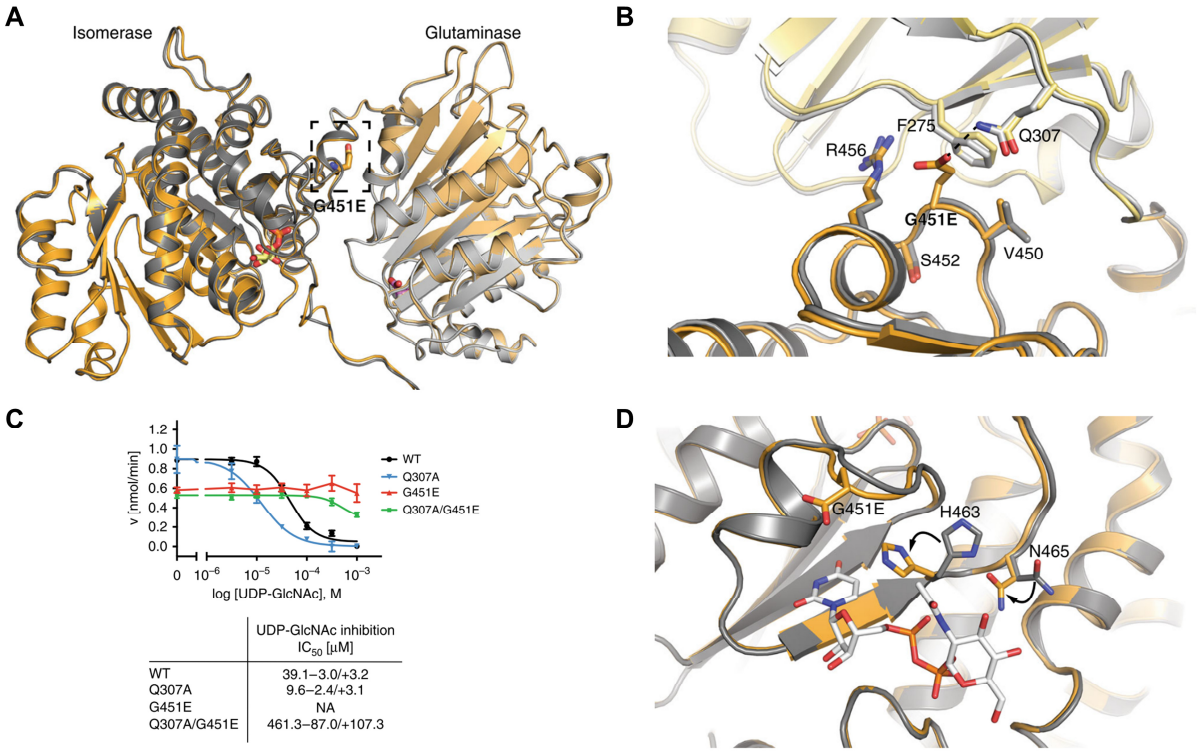

	UDP-GlcNAc inhibition IC_{50} [µM]
WT	39.1–3.0/+3.2
Q307A	9.6–2.4/+3.1
G451E	NA
Q307A/G451E	461.3–87.0/+107.3

Fig. 5: The GFAT-1 G451E gof variant is not affected by UDP-GlcNAc feedback inhibition.

Superposition of the protein structures of wild type GFAT-1 (grey) and the G451E variant (yellow). (**A**) GFAT-1 consists of an isomerase and a glutaminase domain joined by a linker region. The G451E substitution (black box) is located in the isomerase domain but the glutamate side chain protrudes towards the interdomain linker. (**B**) Close-up of amino acids surrounding the site of the G451E exchange. The glutamate side chain takes up considerably more space than the original glycine residue. (**C**) Feedback inhibition of different GFAT-1 variants by the HBP product UDP-GlcNAc with corresponding IC_{50} values. GFAT-1 G451E is resistant to this mode of regulation. (**D**) Side chain movements of amino acid residues within the UDP-GlcNAc-binding pocket of GFAT-1 G451E prevent correct interaction with UDP-GlcNAc (grey sticks). Figures modified from (Ruegenberg *et al.*, 2020).

The G451E gain-of-function (gof) variant of GFAT-1 was previously reported to promote survival in *C. elegans* and mammalian cell lines confronted with tunicamycin-induced endoplasmic reticulum (ER) stress (Denzel *et al.*, 2014; Horn *et al.*, 2020). The stress resistance is conferred by increased intracellular levels of UDP-GlcNAc and a concomitant activation of the integrated stress response (ISR; discussed below) although the mechanistic link between the two is not yet understood.

Alternative splicing yields two isoforms of GFAT-1 that differ slightly in the length of the interdomain linker and their tissue distribution. Apart from the *GFPT1* gene on chromosome 2 which encodes the two GFAT-1 isoforms, a paralog gene named *GFPT2* was found on chromosome 5. *GFPT2* encodes a second GFAT that possesses 75-80% amino acid sequence homology to GFAT-1 in mice and humans (Oki *et al.*, 1999). GFAT-1/2 both catalyze the same reaction within the HBP but differ in their enzyme kinetics. Compared to GFAT-1, expression of GFAT-2 is less ubiquitous and it is claimed to be predominantly expressed in the central nervous system of mice and humans (Oki *et al.*, 1999).

Fine-tuning of GFAT activity and thus UDP-GlcNAc production, may be achieved via post-translational modifications (PTMs). However, data on the regulation of GFAT by PTMs is still scarce. Protein kinase A (PKA) phosphorylates GFAT at Ser205 and Ser235 but the resulting effects on enzymatic activity are still unresolved (Zhou *et al.*, 1998; Chang *et al.*, 2000). Similarly, the significance of phosphorylation on Ser243 by adenosine monophosphate-activated kinase (AMPK) and mechanistic target of rapamycin complex 2 (mTORC2) is unclear as contradicting publications reported opposite effects on GFAT activity (Li *et al.*, 2007; Eguchi *et al.*, 2009; Zibrova *et al.*, 2017; Moloughney *et al.*, 2018).

Of note, an induction of GFAT expression has been reported as a coping mechanism under conditions of nutrient deprivation and as a response to unfolded protein stress. The *GFPT1* promoter region contains recognition sites for the transcriptional inducers ATF4 and XBP1s that are produced during starvation and accumulation of misfolded proteins, respectively (Wang *et al.*, 2014b; Chaveroux *et al.*, 2016). Under both stress conditions, increased GFAT expression boosts HBP flux and consequently O-GlcNAcylation of proteins to stabilize proteostasis. Since the HBP integrates multiple metabolic inputs and aberrant metabolism is a hallmark of cancer cells, changes in GFAT expression have been implicated in tumorigenesis. Dysregulation of GFAT correlates with poor prognosis in breast (Dong *et al.*, 2016), gastric (Duan *et al.*, 2016) and pancreatic cancer (Yang *et al.*, 2016) as well as hepatocellular carcinoma (Li *et al.*, 2017a).

In conclusion, GFAT occupies a key role in cellular homeostasis by providing suitable levels of UDP-GlcNAc for the production of glycan macromolecules and O-GlcNAc modification. These are essential for signal transduction, structure and solubility of proteins.

3.9 The integrated stress response

The integrated stress response (ISR) is a coping mechanism in eukaryotic cells to deal with various kinds of intrinsic and extrinsic stress stimuli as well as pathological conditions to restore cellular homeostasis. The ISR can be triggered by the activation of oncogenes, viral infection, accumulation of unfolded proteins, hypoxia or shortage of glucose and amino acids. These stimuli activate different branches of signaling pathways within the ISR which all converge on the phosphorylation of the alpha subunit of eukaryotic translation initiation factor 2 (eIF2α) (Harding *et al.*, 2000; Pakos-Zebrucka *et al.*, 2016; Costa-Mattioli & Walter, 2020). The most prominent downstream target of eIF2α is activating transcription factor 4 (ATF4) which in turn promotes expression of various target genes. Activation of the ISR leads to an increased expression of chaperones and other protective proteins while reducing global protein synthesis to boost recovery of the affected cell. However, prolonged or too intense activation of the ISR can lead to the activation of programmed cell death.

The ISR revolves around phosphorylation of eIF2α at serine 51 (Ser51). It can be catalyzed by one of the four serine/threonine kinases heme-regulated eIF2α kinase (HRI), double-stranded RNA-dependent protein kinase (PKR), PKR-like ER kinase (PERK) and general control non-derepressible 2 (GCN2) (Wek, 2018) (Fig. 6). When activated by distinct stress stimuli, the four eIF2α kinases dimerize and then undergo autophosphorylation. The modes of activation of these kinases partly overlap providing the possibility for fine-tuning responses to different types of cellular stress. HRI is mostly expressed in erythroid cells where it senses the availability of heme (Zhang *et al.*, 2019b). Activation of GCN2 is triggered by increased concentrations of deacylated transfer RNA (tRNA) which occurs due to amino acid starvation (Wek *et al.*, 1995; Inglis *et al.*, 2019). PKR is a cytosolic protein that is activated by the presence of double-stranded RNA originating mostly from viral infection but has also been shown to induce a response to growth factor deprivation, oxidative or ER stress and caspase activity (García *et al.*, 2007). PERK is a transmembrane protein located in the ER and was named based on its similarity to PKR (Harding *et al.*, 1999, 2003). It can either be activated by an accumulation of unfolded proteins or by glucose deprivation. The luminal domain of PERK displays a high degree of sequence homology to the luminal domain of inositol-requiring enzyme-1 (IRE-1) which is involved in sensing of misfolded proteins within the scope of the unfolded protein response (UPR). In the absence of unfolded proteins, PERK is bound to 78-kDa glucose-regulated protein (GRP78), also called binding immunoglobulin protein (BiP). GRP78 is a chaperon of the 70-kDa heat shock protein (HSP70) family. If unfolded proteins accumulate in the lumen of the ER, GRP78 is recruited away from PERK to assist in protein folding leaving PERK free to dimerize and activate (Bertolotti *et al.*, 2000; Ma *et al.*, 2002). However, an alternative model in which PERK is directly activated by unfolded proteins has also been proposed (Wang *et al.*, 2018).

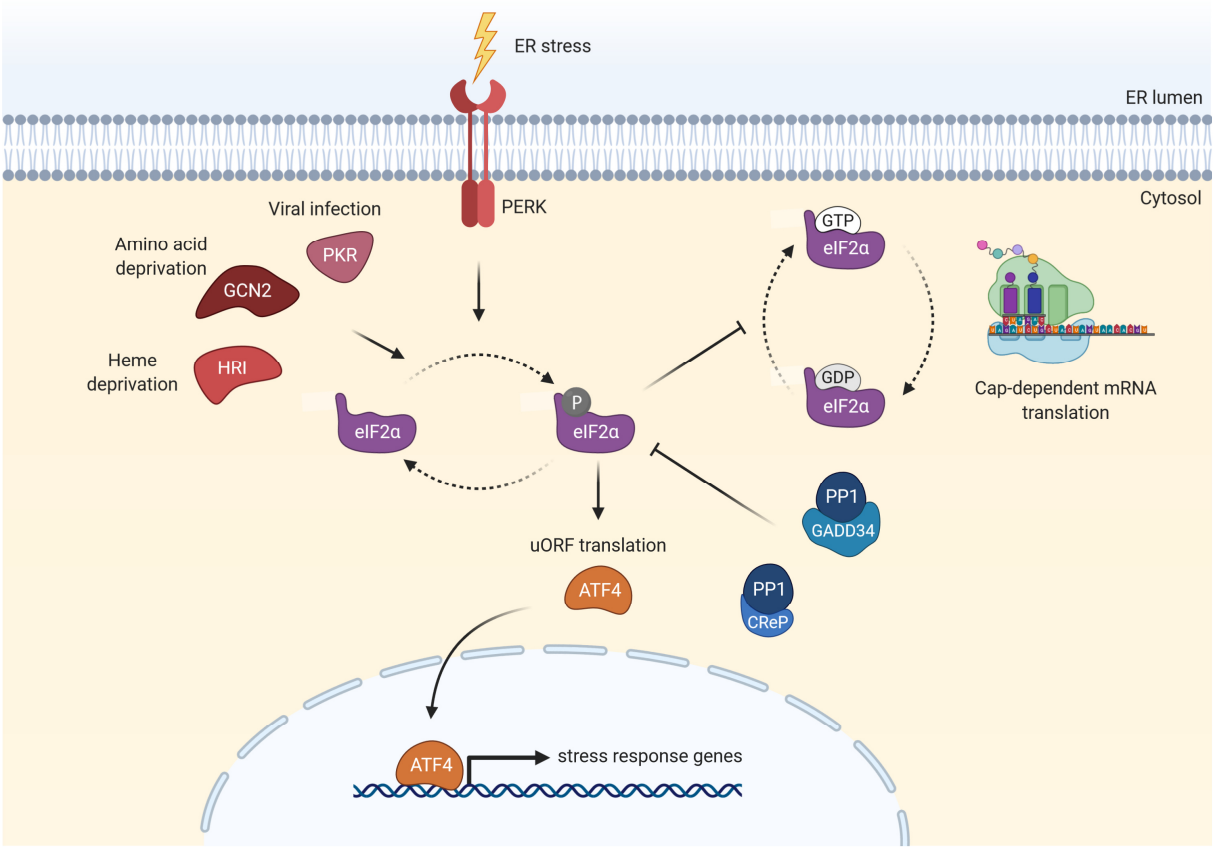

Fig. 6: Integrated stress response (ISR) signaling pathway.

The four protein kinases HRI, GCN2, PKR and PERK serve as stress sensors to detect a variety of events that disturb cellular homeostasis. Stress detection activates these kinases which facilitate phosphorylation of eIF2α, a subunit of the heterotrimeric eukaryotic translation initiation factor 2 (eIF2). Phosphorylation of eIF2α prevents the exchange of GDP with GTP thereby interrupting eIF2α and thus ribosome function during protein translation. Inhibition of cap-dependent mRNA translation enables translation of mRNAs that contain upstream open-reading frames (uORFs), most notably *ATF4*. Once translated, ATF4 protein serves as a transcription factor to induce expression of stress response genes. The ISR is negatively regulated by dephosphorylation of eIF2α via the phosphatase PP1 and its regulatory subunits CreP or GADD34 (illustration created with BioRender.com).

Convergence of ISR on eIF2α Ser51 phosphorylation shuts down global 5'cap-dependent AUG-dependent mRNA translation. Aside from the α subunit the heterotrimeric G protein eIF2 complex also contains a β and a γ subunit. To initiate eukaryotic translation, the eIF2 complex first recruits GTP. The eIF2-GTP complex subsequently binds methionyl-initiator tRNA (Met-tRNA$_i^{Met}$) to form the ternary translation initiation complex. The Met-tRNA$_i^{Met}$ is coupled to the P site of the 40S ribosomal subunit under the expenditure of energy via the hydrolysis of GTP to GDP to constitute the 43S pre-initiation complex. The resulting eIF2-GDP is unable to bind further Met-tRNA$_i^{Met}$ and thus GDP has to be replaced with GTP to enable further Met-tRNA$_i^{Met}$ recruitment and translation initiation. Removal of GDP from the eIF2 complex requires an interaction with the guanine nucleotide exchange factor (GEF) eIF2B (Hinnebusch *et al.*, 2016).

Usually, translation proceeds with recruitment of the 43S pre-initiation complex to the 5' methylguanine cap of mRNAs, scanning of the 5' untranslated region (UTR) for the AUG start codon and finally assembly of the 80S ribosome. However, phosphorylation of eIF2α by ISR kinases causes a conformational change that increases the affinity of eIF2-GDP to eIF2B GEF and simultaneously prevents the exchange of GDP for GTP. Consequently, phosphorylation of eIF2α turns eIF2 into an eIF2B inhibitor and prevents renewal of the pool of ternary complex (Adomavicius *et al.*, 2019; Gordiyenko *et al.*, 2019; Kenner *et al.*, 2019). Hence, re-formation of the 43S pre-initiation complex and consequently protein synthesis is attenuated. Abrogating standard 5'cap-dependent translation in this manner opens the door for an alternative mode of translation that focuses on mRNAs containing short inhibitory upstream open reading frames (uORFs) (Chen & Tarn, 2019). In the absence of stress and ISR activation, translation of these mRNAs is initiated at uORFs but not at the AUG of their canonical coding sequence (CDS). As ribosome re-initiation is delayed due to scarcity of the ternary complex, inhibitory uORFs are skipped and translation of the canonical CDS is enabled. Exemplary proteins regulated by this mode of translation are ATF4 (Vattem & Wek, 2004), CHOP (Palam *et al.*, 2011) and GADD34 (Lee *et al.*, 2009). The main effector of the ISR is the transcription factor ATF4. Depending on the stress stimulus, it may act alone or in conjunction with other transcription factors to initiate a wide range of responses (Pakos-Zebrucka *et al.*, 2016).

To resume normal protein translation, eIF2α Ser51 phosphorylation can be attenuated by the protein phosphatase 1 (PP1) complex. PP1 contains either growth arrest and DNA damage-inducible protein (GADD34) or constitutive repressor of eIF2α phosphorylation (CreP) as a regulatory subunit to modulate activity of the catalytic subunit. Whereas CreP is constitutively expressed (Jousse *et al.*, 2003), GADD34 in particular constitutes a major negative feedback mechanism as its expression requires ATF4 and its translation is favored by uORF skipping (Novoa *et al.*, 2001). Additionally, GADD34 may enhance apoptosis by inhibiting pro-survival signaling via the Akt pathway (Farook *et al.*, 2013).

The ISR plays a role in cancer (Bobrovnikova-Marjon *et al.*, 2010; Hart *et al.*, 2012), diabetes (Zhang *et al.*, 2006; Hart *et al.*, 2012), innate immunity (Cláudio *et al.*, 2013) and long-term memory formation (Chen *et al.*, 2003; Buffington *et al.*, 2014). ISR involvement in memory formation stems from its influence on synaptic plasticity by localized regulation of protein translation in dendrites. Genetic or pharmacological inhibition of the ISR boosts memory formation (Costa-Mattioli *et al.*, 2007; Sharma *et al.*, 2018) whereas mutations causing its overactivation promote cognitive disability (Borck *et al.*, 2012; Kernohan *et al.*, 2015). As a regulator of protein homeostasis, activation of the ISR has also been observed in proteinopathies of the brain like Alzheimer's disease (Chang *et al.*, 2002; Smith & Mallucci, 2016).

4 Aims of this study

This doctoral thesis focused on two major subjects related to survival mechanisms and stress resilience in human iPSC-derived neurons:

Various studies have observed a maturation-dependent increase in the survival competence of different neuronal subtypes of rodents (Kole *et al.*, 2013; Hollville *et al.*, 2019). Widespread apoptosis in the human nervous system plays an important role in the early phases of development but becomes detrimental later in life when it occurs due to aging or neurodegeneration. Understanding neuronal survival mechanisms may provide insight into possible malfunctions involved in the manifestation of neurodegenerative diseases. Here I set out to dissect the maturation process of human iPSC-derived forebrain neurons morphologically, biochemically and on the transcriptional level using bulk and single-cell RNA sequencing. I aimed to characterize early and advanced stages of neuronal maturation and to identify associated changes in the regulation of apoptosis signaling pathways. In addition, I sought to assess the effects of a variety of cellular stressors on the viability of immature and mature neuronal cultures.

A breakdown of the proteostasis network lies at the heart of neurodegenerative proteinopathies like Machado-Joseph, Alzheimer's, Parkinson's or Huntington's disease. Recent work in *C. elegans* and mammalian cell lines suggested an increase in HBP flux by GFAT gain-of-function and a resulting activation of the ISR as an approach to improve proteostasis, increase cellular stress resistance and alleviate toxic protein aggregation (Denzel *et al.*, 2014; Horn *et al.*, 2020). However, these effects have not yet been investigated in human cell lines. Therefore, this study aimed to use CRISPR-Cas9 genome-editing to establish human iPSCs harboring the reported GFAT-1 G451E gof mutation. These hiPSCs and GlcNAc supplementation should then be employed to investigate whether elevated HBP output also confers pro-survival benefits to human NPCs and neurons based on activation of the ISR.

5 Materials

5.1 Cell culture

5.1.1 Cell culture solutions, supplements and base media

Tab. 1: Commercial cell culture stock solutions.

Compound	Concentration	Manufacturer	Catalogue number	Registered office
B-27 supplement	50x	Life Technologies	17504-044	Carlsbad, USA
Bovine albumin fraction V	7.5%	Life Technologies	15260037	Carlsbad, USA
EDTA 0.5M, pH 8.0 UltraPure™	0.5 M	Life Technologies	15575020	Carlsbad, USA
Geltrex™, hESC-qualified	15 mg/ml	Life Technologies	A1413302	Carlsbad, USA
GlutaMAX supplement	100x	Life Technologies	35050038	Carlsbad, USA
MEM-NEAA	100x	Life Technologies	11140035	Carlsbad, USA
PBS	1x	Life Technologies	D8537-500ML	Carlsbad, USA
Penicillin/Streptomycin	100x	Life Technologies	15140122	Carlsbad, USA
Sodium pyruvate	100x	Life Technologies	11360039	Carlsbad, USA
TrypLE™ Express	1x	Life Technologies	12605-028	Carlsbad, USA

Tab. 2: Stock solutions of small molecules, growth factors, stressors and self-made solutions.

Compound	Concentration	Solvent	Final concentration
3-Methyladenine	100 mM	DMEM/F-12	1-2 mM
A83-01	10 mM	DMSO	500 nM
Bafilomycin A1	10 mM	Ethanol	5-15 nM
Borate buffer, pH 8.4	25 mM	ddH_2O	25 mM
Bryostatin 1	27 µM	Ethanol	0.27 nM
$CaCl_2$	60 mM	ddH_2O	1.8 mM
CHIR99021	10 mM	DMSO	3 µM
Cyclopamine	5 mM	Ethanol	1 mM
DAPT	25 mM	DMSO	5 mM
FGF-2 (147)	10 µg/ml	ddH_2O	10 ng/ml
FGF-2 (154)	200 µg/ml	0.1% BSA in ddH_2O	200 ng/ml
Forskolin	25 mM	DMSO	10 µM
GABA	100 mM	ddH_2O	300 µM
Glucose	400 mg/ml	ddH_2O	800 µg/ml
Insulin	5 mg/ml	10 mM NaOH	20 µg/ml
L-Ascorbic acid	500 mM	ddH_2O	200 µM
L-Ascorbic acid 2-phosphate (LAAP)	64 mg/ml	ddH_2O	64 µg/ml
Laminin, murine	1-2 mg/ml	TBS	3.75 µg/ml
LDN193189 hydrochloride	10 mM	DMSO	200 nM
LM22A	1 mM	DMSO	1 µM
LM22B	10 mM	DMSO	1 µM

MG132	10 mM	DMSO	0.5 – 10 µM
Palbociclib (PD-0332991) HCl	2 mM	DMSO	2 µM
Poly-L-lysine hydrobromide (MW 30,000-70,000)	1 mg/ml	ddH_2O	0.1 mg/ml
Progesterone	50 µg/ml	Ethanol	250 ng/ml
Putrescine	915 mM; 80.6 mg/ml	ddH_2O	403 ng/ml
Puromycin	10 mg/ml	ddH_2O	1 µg/ml
ROCK inhibitor (Y-27632)	5 mM	ddH_2O	5 or 10 µM
Rotenone	10 mM	DMSO	0.5 – 2.5 µM
Sodium selenite	70 µg/ml	ddH_2O	0.14 ng/ml
Staurosporine	5 mM	DMSO	50 nM
TGF-β1	20 µg/ml	ddH_2O	2 ng/ml
TGF-β3	10 µg/ml	ddH_2O	10 ng/ml
Thapsigargin	2 mM	DMSO	0.5 – 2 µM
Transferrin	5 mM; 50 mg/ml	ddH_2O	11 µg/ml
Tunicamycin	1 mM	DMSO	0.25 – 1.5 µM
XAV939	10 mM	DMSO	2 µM

Tab. 3: Cell culture base media.
Composition of ready-to-use complete cell culture media are listed in section 5.1.2. All cell culture media were stored at 4°C.

Medium	**Manufacturer**	**Catalogue number**	**Registered office**
DMEM/F-12 with glutamine	Life Technologies	11320-074	Carlsbad, USA
DMEM/F-12 with glutamine and HEPES	Life Technologies	11330-057	Carlsbad, USA
DMEM with GlutaMAX	Life Technologies	61965-059	Carlsbad, USA

Tab. 4: Composition of self-made 100x N2-supplement.
2.5 ml of N2-supplement were used for 500 ml of DMEM/F-12 with glutamine (1:200).

Component	**Volume**	**Final concentration**
DMEM/F-12 with glutamine	3.5 ml	70 % (v/v)
Insulin (5 mg/ml)	500 µl	0.5 mg/ml
Progesterone (50 µg/ml)	63 µl	630 ng/ml
Putrescine (80.6 mg/ml)	100 µl	1.612 mg/ml
Sodium selenite (70 µg/ml)	37 µl	520 ng/ml
Transferrin (50 mg/ml)	1.0 ml	10 mg/ml
Total	5 ml	

5.1.2 Composition of ready-to-use cell culture media

Tab. 5: Final composition of cell culture media.
All media were stored at 4°C.

Medium (base)	Additive / Component	Final concentration
HiPSC medium (DMEM/F-12 with glutamine and HEPES)	Pen/Strep	1%
	L-ascorbic acid 2-phosphate	64 µg/ml
	Sodium selenite	14 ng/ml
	FGF-2 (154)	200 ng/ml
	Insulin	20 µg/ml
	TGF-β1	2 ng/ml
	Transferrin	11 µg/ml
Neural progenitor induction medium (DMEM/F-12 with glutamine)	Pen/Strep	1%
	GlutaMAX	1%
	Glucose	800 µg/ml
	B27-supplement	0.5%
	N2-supplement	0.5%
	A83-01	500 nM
	Cyclopamine	1 mM
	LDN193189	200 nM
	XAV939	2 µM
NPC propagation medium (DMEM/F-12 with glutamine)	As neural progenitor induction medium but without cyclopamine.	
Neuronal differentiation, phase 1 (DMEM/F-12 with glutamine)	Pen/Strep	1%
	GlutaMAX	1%
	Glucose	800 µg/ml
	B27-supplement	0.5%
	N2-supplement	0.5%
	$CaCl_2$	1.8 mM
	Ascorbic acid	200 µM
	LM22A	1 µM
	LM22B	1 µM
	PD-0332991	2 µM
	DAPT	5 µM
Neuronal differentiation, phase 2 (DMEM/F-12 with glutamine)	As for phase 1 with the addition of	
	CHIR99021	3 µM
	Forskolin	10 µM
	GABA	300 µM
Neuronal differentiation, phase 3 (DMEM/F-12 with glutamine)	Pen/Strep	1%
	GlutaMAX	1%
	Glucose	800 µg/ml
	B27-supplement	0.5%
	N2-supplement	0.5%
	$CaCl_2$	1.8 mM
	Ascorbic acid	200 µM
	LM22A	1 µM
	LM22B	1 µM
	PD-0332991	2 µM
	CHIR99021	3 µM
Neuronal differentiation, phase 4 (DMEM/F-12 with glutamine)	As for phase 3 but without CHIR99021	

Wash medium (DMEM with GlutaMAX)	Pen/Strep	1%

5.1.3 Cell lines

The cell lines listed in Tab. 6 were previously reprogrammed and characterized in our group. Their generation was not subject of this thesis.

Tab. 6: HiPSC lines from healthy control subjects used in this study.

Cell line	Clone	Gender / Age	Origin
28	#1	female / 44 years	Dermal fibroblasts reprogrammed using sendai virus
28	#4	female / 44 years	as above
68	#3	female / 25 years	as above

5.2 Molecular biology

5.2.1 Reagents

Tab. 7: Molecular biology reagents.

Compound	Manufacturer	Catalogue number	Registered office
1 kb marker	New England Biolabs	N0468S	Ipswich, USA
100 bp marker, Quick-Load®	New England Biolabs	N0467S	Ipswich, USA
Adult brain total RNA, human	BioCat	R1234035-50-BC	Heidelberg, Germany
dNTPs	Steinbrenner Laborsysteme	SL-Set-L-dNTPs	Wiesenbach, Germany
Fetal brain total RNA, human	Tebu Bio	1F01-50	Le-Perray-en-Yvelines, France
peqGREEN DNA/RNA binding dye	VWR	peql37-5010	Radnor, USA
Protein marker PS 10 plus	GeneON Bioscience	310004	Ludwigshafen, Germany
Rnase AWAY	Thermo Fisher	10666421	Waltham, USA
TriFast™, peqGOLD	VWR	30-2010	Radnor, USA

5.2.2 Enzymes

Tab. 8: Enzymes.

Enzyme	Manufacturer	Catalogue number	Registered office
BbsI	New England Biolabs	R3539	Ipswich, USA
Dnase I, amplification grade	Sigma-Aldrich	AMPD1-1KT	Darmstadt, Germany
Dnase I, cell culture	Sigma-Aldrich	10104159001	Darmstadt, Germany
Proteinase K (20mg/ml)	GeneON Bioscience	405-001	Ludwigshafen, Germany
T4 PNK	New England Biolabs	M02015S	Ipswich, USA
Taq DNA polymerase	Biozym	331610	Hessisch Oldendorf, Germany

5.2.3 Plasmids

The px459 backbone was used to insert a gRNA for targeting the *GFPT1* gene. See methods section 6.5 for more detailed information.

Tab. 9: Plasmid used for CRISPR-Cas9 genome editing.

Plasmid	Relevant ORFs	Source
px459	*Streptococcus pyogenes* Cas9 enzyme Puromycin N-acetyltransferase β-lactamase	Group of Feng Zhang Addgene plasmid #62988

5.2.4 Bacterial cultures

Chemically competent *E. coli* DH5α were obtained from New England Biolabs (#2987H).

Tab. 10: Media and solutions used for cultivation of bacteria.

Medium / Solution	Concentration	Solvent	Final concentration
Ampicillin stock solution	100 mg/ml	ddH_2O	100 µg/ml
LB (Luria/Miller)	25 g/L	ddH_2O	25 g/L
LB – agar	15 g/L	ddH_2O	15 g/L

5.2.5 Primers

All primers were ordered from Integrated DNA Technologies Inc. (Coralville, USA) and reconstituted at 100 µM in nuclease-free H_2O for 30 min at 37°C and 400 rpm in a thermomixer.

Tab. 11: Primers for PCR and qRT-PCR.

Primer name	Sequence (5'->3')
18s rRNA-For	AAACGGCTACCACATCCAAG
18s rRNA-Rev	CCTCCAATGGATCCTCGTTA
APAF1 exon16-For	CAGCTGATGGAACCTTAAAGC

APAF1 exon19-Rev	GTCTGGTCATCAGAAGATGTC
ARC-For	TCAGCTCCAGTGATTCACGC
ARC-Rev	GGGAACCTTGAGACCTGTTGT
BCL11B-For	CAACCCGCAGCACTTGTC
BCL11B-Rev	CCTCGTCTTCTTCGAGGATGG
CASP9 exon2-For	AGACCAGTGGACATTGGTTC
CASP9 exon8-Rev	GGTCCCTCCAGGAAACAAA
DLG4-For	AGCCCCAGGATATGAGTTGC
DLG4-Rev	CCCAGACCTGAGTTACCCCT
FOS-For	CAAGCGGAGACAGACCAACT
FOS-Rev	AGTCAGATCAAGGGAAGCCA
GAD1-For	ATCCTGGTTGACTGCAGAGAC
GAD1-Rev	CCAGTGGAGAGCTGGTTGAA
GFAT1 clones-For	GCCAGAGTCTGTCGTGAACA
GFAT1 clones-Rev	GCAACCACTTGCTGAAGAGC
GFPT1-For	CGGCTGCCTGATTTGATT
GFPT1-Rev	GATAGCCTCGTCCCATTA
GRIA2-For	GGATCCTCATTAAGAACCCCAGT
GRIA2-Rev	TGAGGGCACTGGTCTTTTCC
GRIA4-For	AGGTGAATGTGGACCCAAGG
GRIA4-Rev	AAGGTCAGCTTCATTCTCTTCG
GRIN1-For	GGCAACACCAACATCTGGAA
GRIN1-Rev	CCATCCGCATACTTGGAAGAC
GRIN2B-For	CTCACCCCCTTTCCGCTTT
GRIN2B-Rev	AAGGCATCCAGTTTCCCTGTT
Mycoplasma-For	GGGAGCAAACAGGATTAGATACCCT
Mycoplasma-Rev	TGCACCATCTGTCACTCTGTTAACCTC
NPAS4-For	AACACTACCGCCTGTTGGC
NPAS4-Rev	GCAGTAATGGGTCCCTCTGG
NRXN1-For	GTGTTTTGCCGGTGCTGTTA
NRXN1-Rev	CTTTTACCTTGGTCGCCCATC
RBFOX3-For	GCGCTGAGCCCGTTGAAAT
RBFOX3-Rev	CTCCTTCTGGACCGTCCTTG
SLC17A7-For	AGCTGGGATCCAGAGACTGT
SLC17A7-Rev	CCGAAAACTCTGTTGGCTGC
SLC17A6-For	TCAGATTCCGGGAGGCTACA
SLC17A6-Rev	TGGGTAGGTCACACCCTCAA
SYN-For	CAGCTCAACAAATCCCAGTCTC
SYN-Rev	GGTCTCAGCTTTCACCTCGT
TBR1-For	ACGAACAACAAAGGAGCTTCA
TBR1-Rev	TGGTACTTGTGCAAGGACTGTA

Tab. 12: Primers used for Sanger sequencing.

Primer name	Sequence (5'->3')	Purpose
GFAT-1 clones-For	GCCAGAGTCTGTCGTGAACA	Verify GGC > GAG mutation in *GFPT1* gene
hU6-For	GAGGGCCTATTTCCCATGATT	Verify insertion of GFAT1 gRNA into px459 plasmid

5.2.6 Oligonucleotides

Sequences of the GFAT1-targeting gRNA sense and anti-sense oligonucleotides and the single-stranded oligonucleotide used as a repair template for the CRISPR-Cas9-mediated introduction of the GFAT1 G451E point mutation. The oligonucleotides were ordered from Integrated DNA Technologies Inc. (Coralville, USA).

Tab. 13: Oligonucleotides for CRISPR-Cas9 genome editing.

Name	Sequence (5'->3')
GFAT1 gRNA sense	CACCGGTGGGGATCACAAACACAGT
GFAT1 gRNA anti-sense	AAACACTGTGTTTGTGATCCCCACC
GFAT1 G451E ssOligo	CAGATACTTTGATGGGTCTTCGTTACTGTAAGGAGAGAGGAGCTCTAACTGTGG GGATCACGAATACTGTTGAGAGTTCCATATCACGGGAGACAGATTGTGGAGTTC ATATTAATGCTGGTCCTGAGATTGGTGTGGCCAGTAC

5.3 Biochemistry

5.3.1 Buffers and solutions

Tab. 14: Self-made buffers and solutions.

Buffer / Solution	Component	Concentration
Anode buffer (1x), SDS-PAGE	Tris-HCl, pH 8.8	200 mM
APS stock solution	APS	10% (w/v) in ddH_2O
Borate buffer	Boric acid adjust pH to 8.4 with NaOH	25 mM
DAPI staining solution	DAPI	300 nM in PBS
DNA sample buffer (10x)	Tris-HCl, pH 7.6 Bromphenol blue Glycerol	50 mM 0.25% (w/v) 60%
gDNA isolation lysis buffer	Tris-HCl, pH 8.5 EDTA SDS NaCl	100 mM 5 mM 0.2% (w/v) 200 mM
Glucose stock solution	D(+)-Glucose 0.2 µm sterile-filtered	400 mg/ml
Iodoacetamide stock solution	Iodoacetamide	500 mM in ddH_2O
Mounting solution	Tris-HCl, pH 8.5	100 mM

	Glycerol	25%
	Mowiol	10%
	DABCO®	0.6%
PBS	NaCl	137 mM
	KCl	2.7 mM
	Na_2HPO_4	10.0 mM
	KH_2HPO_4	1.8 mM
Protein lysis buffer	Tris-HCl, pH 7.4	50 mM
	NaCl	150 mM
	SDS	0.2% (w/v)
	EDTA	25 mM
	Phosphatase inhibitor tablet	1 tablet / 10 ml
	Protease inhibitor tablet	1 tablet / 10 ml
SDS-PAGE sample buffer (6x)	Tris-HCl, pH 6.8	93.75 mM
	SDS	6%
	Glycerol	6%
	2-Mercaptoethanol	9%
	Bromphenol blue	0.25%
SDS stock solution	SDS	10 % (w/v) in ddH_2O
TAE (1x), agarose gel buffer	Tris, pH 8.0	200 mM
	EDTA	1 mM
	Glacial acetic acid	0.114%
TBS (10x)	Tris-HCl, pH 7.4	248 mM
	NaCl	1.37 M
	KCl	26.8 mM
TBST	TBS (10x)	10% (v/v)
	Tween® 20	0.1% (v/v)
Transfer buffer, western blotting	Tris-glycine buffer (10x)	10% (v/v)
	Methanol	20% (v/v)
	SDS	0.08% (v/v)
Tris-glycine buffer (10x)	Tris-HCl, pH 8.8	250 mM
	Glycine	1.92 M
Tris-HCl/SDS for polyacrylamide gels	Tris-HCl, pH 8.45	3 M
	SDS	0.3% (w/v)
Triton X-100 stock solution	Triton X-100	10% (v/v) in PBS

Tab. 15: Commercial buffers and solutions.

Buffer / Solution	**Manufacturer**	**Catalogue number**	**Registered office**
DNA polymerase buffer (10x)	Biozym	311611	Hessisch Oldendorf, Germany
Restriction buffer 2.1 (10x)	New England Bioloabs	B7202S	Ipswich, USA
T4 DNA ligase buffer (10x)	New England Bioloabs	B0202S	Ipswich, USA
TriFast™ peqGold	VWR	30-2010	Radnor, USA
Tris-Tricine-SDS buffer (10x)	Sigma-Aldrich	T1165-500ML	Darmstadt, Germany

5.3.2 Antibodies

Primary antibodies applied for immunocytochemistry (ICC) (Tab. 16) and western blotting (WB) (Tab. 18). If no clone number is given, the antibody was of polyclonal origin. Corresponding secondary antibodies are listed in Tab. 17 (ICC) and Tab. 19 (WB).

Tab. 16: Primary antibodies used for ICC.

Antibody (clone)	Host species	Dilution	Manufacturer	Catalogue number	Registered office
OCT3/4 (A-9)	mouse	1:500	Santa Cruz	Sc-365509	Santa Cruz, USA
MAP2	chicken	1:5000	BioLegend	822501	San Diego, USA
NeuN (D4G4O)	rabbit	1:200	Cell Signaling Technologies	24307S	Danvers, USA
PSD95	rabbit	1:200	Cell Signaling Technologies	2507S	Danvers, USA
PSD95 (K28/43)	mouse	1:200	BioLegend	810401	San Diego, USA
SOX2 (D6D9)	rabbit	1:400	Cell Signaling Technologies	3579S	Danvers, USA
SSEA4 (MC-813-70)	mouse	1:100	Developmental Studies Hybridoma Bank	MC-813-70	Iowa City, USA
Synapsin I/II/III (A17080A)	mouse	1:200	BioLegend	853701	San Diego, USA
Tau	guinea pig	1:200	Synaptic Systems	314004	Göttingen, Germany

Tab. 17: Secondary antibodies used for ICC.

Antibody (clone)	Host species	Dilution	Manufacturer	Catalogue number	Registered office
anti-chicken IgY Alexa Fluor-488	goat	1:1000	Thermo Fisher	A11039	Waltham, USA
anti-chicken IgY Alexa Fluor-633	goat	1:1000	Thermo Fisher	A21103	Waltham, USA
anti-guinea pig IgG Alexa Fluor-488	goat	1:1000	Thermo Fisher	A11073	Waltham, USA
anti-guinea pig IgG Alexa Fluor-568	goat	1:1000	Thermo Fisher	A11075	Waltham, USA
anti-mouse IgG Alexa Fluor-488	goat	1:1000	Thermo Fisher	A11001	Waltham, USA
anti-mouse IgG Alexa Fluor-568	goat	1:1000	Thermo Fisher	A11004	Waltham, USA
anti-rabbit IgG Alexa Fluor-488	goat	1:1000	Thermo Fisher	A11008	Waltham, USA
anti-rabbit IgG Alexa Fluor-555	goat	1:1000	Thermo Fisher	A21428	Waltham, USA
anti-rabbit IgG Alexa Fluor-647	goat	1:1000	Thermo Fisher	A21244	Waltham, USA

Tab. 18: Primary antibodies used for WB.

Antibody (clone)	Host species	Dilution	Manufacturer	Catalogue number	Registered office
Actin (8H10D10)	mouse	1:20,000	Cell Signaling Technologies	3700S	Danvers, USA
Actin (13E5)	rabbit	1:20,000	Cell Signaling Technologies	4970S	Danvers, USA
APAF-1 (D5C3)	rabbit	1:1000	Cell Signaling Technologies	8968S	Danvers, USA
ATF4 (D4B8)	rabbit	1:2000	Cell Signaling Technologies	11815S	Danvers, USA
BCL-2 (D55G8)	rabbit	1:1000	Cell Signaling Technologies	5023T	Danvers, USA
BAX (D2E11)	rabbit	1:1000	Cell Signaling Technologies	4223T	Danvers, USA
Caspase-3	rabbit	1:2000	Cell Signaling Technologies	9662S	Danvers, USA
Caspase-7 (D2Q3L)	rabbit	1:1000	Cell Signaling Technologies	12827S	Danvers, USA
Caspase-9 (C9)	mouse	1:1000	Cell Signaling Technologies	9508S	Danvers, USA
EIF2α (D7D3)	rabbit	1:1000	Cell Signaling Technologies	5324S	Danvers, USA
p-ElF2α (Ser51) (D9G8)	rabbit	1:1000	Cell Signaling Technologies	3398S	Danvers, USA
PARP-1	rabbit	1:1000	Cell Signaling Technologies	9542S	Danvers, USA
PERK (C33E100)	rabbit	1:1000	Cell Signaling Technologies	3192S	Danvers, USA
P-PERK (16F8)	rabbit	1:1000	Cell Signaling Technologies	3179S	Danvers, USA
SMAC/DIABLO (D5S3R)	rabbit	1:2000	Cell Signaling Technologies	15108S	Danvers, USA
XIAP (3B6)	rabbit	1:1000	Cell Signaling Technologies	2045S	Danvers, USA

Tab. 19: IR-dye conjugated secondary antibodies used for WB.
Antibodies were diluted 1:15,000 in TBST.

Antibody (clone)	Host species	Manufacturer	Catalogue number	Registered office
Anti-mouse DyLight™ 680	goat	Cell Signaling Technologies	5470S	Danvers, USA
Anti-mouse DyLight™ 800	goat	Cell Signaling Technologies	5257S	Danvers, USA
Anti-rabbit DyLight™ 680	goat	Cell Signaling Technologies	5366S	Danvers, USA
Anti-rabbit DyLight™ 800	goat	Cell Signaling Technologies	5151S	Danvers, USA

5.4 Chemicals and reagents

Tab. 20: Chemicals and reagents.

Chemical	Manufacturer	Catalogue number	Registered office
2-Mercaptoethanol	Merck Millipore	805740	Darmstadt, Germany
2-Propanol	Th. Geyer	1157-5L	Renningen, Germany
3-Methyladenine	VWR	CAYM13242-25	Radnor, USA
30% Bis/acrylamide	Roth	3029.1	Karlsruhe, Germany
A83-01	Biomol GmbH	Cay9001799-25	Hamburg, Germany
Agar (Bacto™)	BD Biosciences	214010	San Jose, USA
Agarose	Sigma-Aldrich	A9539-500G	Darmstadt, Germany
Ampicillin	Sigma-Aldrich	A9518-25G	Darmstadt, Germany
Ammonium persulfate	Sigma-Aldrich	A3678-25G	Darmstadt, Germany
Bafilomycin A1	VWR	J61835.MX	Radnor, USA
Boric acid	Life Technologies	15583-024	Carlsbad, USA
Bovine serum albumin (BSA)	Sigma-Aldrich	A3294-50G	Darmstadt, Germany
Bromphenol blue	Sigma-Aldrich	B8026-5G	Darmstadt, Germany
Bryostatin 1	Merck Millipore	203811-10UG	Darmstadt, Germany
Calcium chloride	Sigma-Aldrich	31307-1KG	Darmstadt, Germany
CHIR99021	Cell Guidance Systems	SM13-50	Cambridge, UK
Chloroform	Sigma-Aldrich	32211-1L	Darmstadt, Germany
Cyclopamine	Biomol GmbH	Cay11321-10	Hamburg, Germany
DAPCO®	Roth	0718.2	Karlsruhe, Germany
DAPI	BioLegend	422801	San Diego, USA
DAPT	Cell Guidance Systems	SM15-50	Cambridge, UK
DEPC	Roth	K028.1	Karlsruhe, Germany
D(+)-Glucose, cellpure	Roth	HN06.3	Karlsruhe, Germany
DMSO	Sigma-Aldrich	D5879-2.5L-M	Darmstadt, Germany
EDTA	Acros Organics	147850010	Fair Lawn, USA
EGTA	Sigma-Aldrich	E3889-10G	Darmstadt, Germany
Ethanol	Th. Geyer	2246.1000	Renningen, Germany
Fetal bovine serum (FBS)	Thermo Fisher	10270-106	Waltham, USA
Forskolin	Cell Guidance Systems	SM18-100	Cambridge, UK
FGF-2 (147)	Cell Guidance Systems	GFH28-1000	Cambridge, UK
FGF-2 (154)	Cell Guidance Systems	GFH146-1000	Cambridge, UK
γ-Aminobutyric acid (GABA)	Sigma-Aldrich	A5835-10G	Darmstadt, Germany
Glycerol	Sigma-Aldrich	15523-1L-M	Darmstadt, Germany
Glycine	Thermo Fisher	10070150	Waltham, USA
Hydrochloric acid	Th. Geyer	836.1000	Renningen, Germany
Insulin, human recombinant	Sigma-Aldrich	91077C-1G	Darmstadt, Germany
Iodoacetamide	Sigma-Aldrich	I1149-5G	Darmstadt, Germany
Laminin, murine	Sigma-Aldrich	L2020-1MG	Darmstadt, Germany
L-Ascorbic acid	Sigma-Aldrich	A4544-100G	Darmstadt, Germany
L-Ascorbic acid 2-phosphate (LAAP)	Sigma-Aldrich	A8960-5G	Darmstadt, Germany
LB broth	Roth	X968.4	Karlsruhe, Germany
LDN193189 hydrochloride	Stemcell Technologies	72148	Vancouver, Canada

LM22A	Sigma-Aldrich	SML0848-25MG	Darmstadt, Germany
LM22B	Tocris Bioscience	6037	Minneapolis, USA
Methanol	Roth	0082.1	Karlsruhe, Germany
MG132	Sigma-Aldrich	C2211-5MG	Darmstadt, Germany
Milk powder, blotting grade	Roth	T145.3	Karlsruhe, Germany
Mowiol®4-88	Roth	0713.1	Karlsruhe, Germany
N-acetyl-D-glucosamine	Sigma-Aldrich	A8625-5G	Darmstadt, Germany
Paraformaldehyde (PFA)	Sigma-Aldrich	16005	Darmstadt, Germany
Palbociclib (PD-0332991) HCl	Selleck Chemicals	S1116	Houston, USA
Phosphatase inhibitor mini tablets	Thermo Fisher	A32957	Waltham, USA
Poly-L-lysine hydrobromide (MW 30,000-70,000)	Sigma-Aldrich	P2636-100MG	Darmstadt, Germany
Progesterone	Sigma-Aldrich	P8783-1G	Darmstadt, Germany
Protease inhibitor mini tablets, EDTA-free	Thermo Fisher	A32955	Waltham, USA
Puromycin dihydrochloride	Merck Millipore	540222-25MG	Darmstadt, Germany
Putrescine	Sigma-Aldrich	51799-100MG	Darmstadt, Germany
ROCK inhibitor (Y-27632)	Cell Guidance Systems	SM02-100	Cambridge, UK
Rotenone	Sigma-Aldrich	8875-1G	Darmstadt, Germany
SDS, pellets	Roth	CN30.1	Karlsruhe, Germany
Sodium chloride, cell culture grade	Sigma-Aldrich	S5886-1KG	Darmstadt, Germany
Sodium hydroxide, pellets	Roth	6771.2	Karlsruhe, Germany
Sodium selenite	Sigma-Aldrich	S5261-10G	Darmstadt, Germany
Staurosporine	Enzo Life Sciences	LKT-S7600-M001	Farmingdale, USA
TEMED	Sigma-Aldrich	T9281-50ML	Darmstadt, Germany
TGF-β1	Cell Guidance Systems	GFH39-100	Cambridge, UK
TGF-β3	Cell Guidance Systems	GFH109	Cambridge, UK
Thapsigargin	Enzo Life Sciences	BML-PE180-0001	Farmingdale, USA
Transferrin, human recombinant	Sigma-Aldrich	T3705-5G	Darmstadt, Germany
TriFast™, peqGOLD	VWR	30-2010	Radnor, USA
TRIS	Roth	4855.2	Karlsruhe, Germany
Triton X-100	Merck Millipore	1.08603.1000	Darmstadt, Germany
Trypan blue	Lonza	17-942E	Basel, Switzerland
Tunicamycin	Merck Millipore	12819S-5MG	Darmstadt, Germany
Tween® 20	Sigma-Aldrich	P2287-100ML	Darmstadt, Germany
XAV939	Cell Guidance Systems	SM38-50	Cambridge, UK

5.5 Kits

Tab. 21: Commercial kits.

Kit	Manufacturer	Catalogue number	Registered office
BCA Protein Assay	Thermo Fisher	23228	Waltham, USA
Cell Line Nucleofector® Kit V	Lonza	VCA-1003	Basel, Switzerland
CellTiter-Glo® Luminescent Cell Viability Assay	Promega	G7572	Madison, USA
Chromium single cell 3' library & gel bead kit v2	10x Genomics	PN-120267	Pleasanton, USA
Gel extraction, peqGOLD	VWR	12-2501-01	Radnor, USA
iScript™ cDNA synthesis kit	Bio-Rad Laboratories	17088991BUN	Hercules, USA
Orangu™ cell counting solution	Cell Guidance Systems	OR01-500	Cambridge, UK
Plasmid midiprep kit, PureLink™ HiPure	Thermo Fisher	K210015	Waltham, USA
Plasmid miniprep kit, peqGOLD	VWR	732-2780	Radnor, USA
RNA 6000 Nano kit	Agilent Technologies	5067-1511	Santa Clara, USA

5.6 Cell culture, molecular biology and biochemistry consumables

Tab. 22: Consumables.

Consumable	Manufacturer	Catalogue number	Registered office
3.5 cm Ø TC dish, standard F	Sarstedt	83.3900	Nümbrecht, Germany
10 cm Ø TC dish, Cell+	Sarstedt	83.3902.300	Nümbrecht, Germany
6-well plate, TC standard F	Sarstedt	833.920.005	Nümbrecht, Germany
12-well plate, TC Cell+	Sarstedt	833.921.300	Nümbrecht, Germany
24-well plate, TC Cell+	Sarstedt	833.922.300	Nümbrecht, Germany
48-well plate, TC Cell+	Sarstedt	83.3923.300	Nümbrecht, Germany
96-well plate, black Nunc™ F96	Thermo Fisher	237108	Waltham, USA
96-well plate, TC standard F	Sarstedt	83.3924.005	Nümbrecht, Germany
Bottle top filter, 500 ml	Thermo Fisher	15983307	Waltham, USA
Bottle top filter, 1000 ml	Thermo Fisher	15993307	Waltham, USA
Cell Lifters (UltraCruz)	Santa Cruz	sc-395251	Heidelberg, Germany
Coverslip, 12 mm	VWR	631-1577	Radnor, USA
Coverslip, 15 mm	VWR	631-1579	Radnor, USA
Cryotubes, conical bottom, 1 ml	Greiner Bio-One	123280	Frickenhausen, Germany
Microscope slides, glass	Roth	H868.1	Karlsruhe, Germany
Nitrocellulose membrane Amersham Protran, 0.2 µm	Sigma-Aldrich	GE10600001	Darmstadt, Germany
Pasteur pipette, glass	Th. Geyer	7691061	Renningen, Germany
PCR strip tubes, 0.2 ml	Biozym	710971	Hessisch Oldendorf, Germany
Petri dish, 10 cm Ø	Greiner Bio-One	633180	Frickenhausen, Germany
Pipette tip, 10 µl	Sarstedt	70.1130	Nümbrecht, Germany

Pipette tip, 200 µl	Sarstedt	70.760.002	Nümbrecht, Germany
Pipette tip, 1250 µl	Sarstedt	701.186	Nümbrecht, Germany
Pipetting reservoir, 25 ml	Cole-Parmer GmbH	B3125-50	Wertheim, Germany
qPCR plate, 96-well	Steinbrenner Laborsysteme	4ti-0910/C	Wiesenbach, Germany
qPCR plate seal	Steinbrenner Laborsysteme	4ti-0500	Wiesenbach, Germany
Reaction tube, 0.2 ml	Sarstedt	72.737.002	Nümbrecht, Germany
Reaction tube, 0.5 ml	Sarstedt	72.699	Nümbrecht, Germany
Reaction tube, 1.5 ml	Sarstedt	72.690.001	Nümbrecht, Germany
Reaction tube, 2.0 ml	Sarstedt	72.695.200	Nümbrecht, Germany
Scalpel Cutfix®	Th. Geyer	9409814	Renningen, Germany
Screw cap tube, 15 ml	Sarstedt	62.554.502	Nümbrecht, Germany
Screw cap tube, 50 ml	Sarstedt	62.547.254	Nümbrecht, Germany
Serological pipettes, 5 ml	Sarstedt	861.253.001	Nümbrecht, Germany
Serological pipettes, 10 ml	Sarstedt	861.254.001	Nümbrecht, Germany
Serological pipettes, 25 ml	Sarstedt	861.685.001	Nümbrecht, Germany
Serological pipettes, 50 ml	Th. Geyer	7695555	Renningen, Germany
Syringe, 50 ml	Sarstedt	946.077.137	Nümbrecht, Germany
Syringe filter, 0.2 µm	Sarstedt	831.826.001	Nümbrecht, Germany
Western blot filter tissue	VWR	115-2166	Radnor, USA

5.7 Technical equipment

Tab. 23: Notable laboratory equipment.

Appliance	Name	Manufacturer	Registered office
Agarose gel imaging system	GeneFlash	Syngene	Bangalore, India
Analytical balance	BP121S	Sartorius	Göttingen, Germany
Centrifuge	Labofuge 400R	Thermo Fisher	Waltham, USA
Centrifuge	5415 D	Eppendorf	Hamburg, Germany
Centrifuge, coolable	Z216MK	Hermle	Gosheim, Germany
Centrifuge, plates	5810	Eppendorf	Hamburg, Germany
Electrophoresis RNA quality control	Bioanalyzer 2100	Agilent Technologies	Santa Clara, USA
Freezing container	Mr. Frosty™	Thermo Fisher	Waltham, USA
PCR cycler	PTC-200	Bio-Rad Laboratories	Hercules, USA
pH meter	ProfiLab pH597	Xylem Inc.	Rye Brook, USA
Microplate reader	Wallac Victor^2 1420	Perkin Elmer	Waltham, USA
Microplate reader	PowerWave™ XS	BioTek	Bad Friedrichshall, Germany
Microscope	Axioskop2 plus	Carl Zeiss	Wetzlar, Germany
Microscope	Celldiscoverer 7	Carl Zeiss	Wetzlar, Germany
Microscope	DM6 B	Leica	Wetzlar, Germany
Microscope, brightfield	DMIL LED	Leica	Wetzlar, Germany
Microscope, confocal	TCS SP5 II	Leica	Wetzlar, Germany
Nucleofector	Nucleofector II	Lonza	Basel, Switzerland
qPCR cycler	QuantStudio 7 Flex	Life Technologies	Carlsbad, USA
Sonication device	Branson Sonifier 250	Thermo Fisher	Waltham, USA
Spectrophotometer	NanoDrop™ 1000	Thermo Fisher	Waltham, USA

Thermomixer	Thermomixer comfort 5355	Eppendorf	Hamburg, Germany
Water purifier	Milli-Q® Integral 5	Merck Millipore	Darmstadt, Germany
Western blot imager	Odyssey IR imaging system	LI-COR Biosciences	Lincoln, USA
Western blot transfer system	Trans-Blot® Turbo™	Bio-Rad Laboratories	Hercules, USA

5.8 Software

Tab. 24: Computer software and other digital resources.

Computer program	**Supplier**
ApE – A plasmid editor	M. Wayne Davis
Biorender.com	BioRender
Excel 2019	Microsoft
Illustrator CS6	Adobe Inc.
ImageJ (FIJI)	National Institutes of Health (NIH), open source
Image studio v. 2.0	LI-COR
Mendeley reference manager	Mendeley Ltd.
PowerPoint 2019	Microsoft
Prism 6	GraphPad Software
QuantStudio qPCR software	Thermo Fisher
R Studio	RStudio PBC, open source
SnapGene® Viewer	GraphPad Software
Word 2019	Microsoft

6 Methods

6.1 Cell culture

All cell lines were kept in a humidified incubator at 37°C and an atmosphere containing 5% CO_2 and ambient O_2. Complete cell culture media are listed in Tab. 5.

6.1.1 Cultivation of human induced pluripotent stem cells (hiPSCs)

For maintenance of hiPSCs, tissue culture plates were coated at 4°C overnight with Geltrex™ diluted 1:100 in DMEM with GlutaMAX containing 1% penicillin/streptomycin (wash medium). Geltrex™ solution was stored at 4°C and re-used up to three times. HiPSCs were maintained in DMEM/F12 with glutamine and HEPES supplemented with 1% pen/strep, 14 ng/ml sodium selenite, 64 µg/ml LAAP, 20 µg/ml insulin, 2 ng/ml TGF-β1, 200 ng/ml FGF-2 (154) and 11 µg/ml transferrin.

For passaging, cells were washed once with 0.5 mM EDTA in PBS to remove bivalent Ca^{2+} and Mg^{2+} ions in order to weaken cell-cell interactions and attachment to the tissue plate. Cells were then incubated in EDTA solution for 3-5 min at room temperature (RT) until they started to detach. The EDTA solution was aspirated and cells were carefully resuspended in hiPSC medium containing 5 µM ROCK inhibitor (Y-27632). For routine propagation, cells were split every 4-6 days in a 1:5 – 1:10 ratio onto new tissue culture plates. HiPSC medium was exchanged every day.

6.1.2 Differentiation of neural progenitor cells (NPCs) from hiPSCs

For the generation of neuronal progenitor cells, n+1 wells of a 6-well plate of hiPSCs were grown to about 90% confluency. HiPSCs were separated into single cells by incubation with TrypLE™ for 5 min at 37°C. Subsequently, hiPSCs were collected in wash medium and centrifuged for 4 min at 1,000 rcf. The cell pellet was resuspended in hiPSC medium containing 5 µM ROCK inhibitor and split onto n wells of a 6-well plate coated with 1:50 Geltrex™. The next day, neural progenitor fate instruction of hiPSC monolayers was initiated by switching the culture medium to DMEM/F-12 supplemented with 1% pen/strep, 0.5% B27-supplement, 1% GlutaMAX, 800 µg/ml glucose, 500 nM A83-01, 200 nM LDN193189, 2 µM XAV939 and 1 mM cyclopamine. Cells were cultured for 8-11 days in this NPC induction medium and medium was exchanged every day.

This approach for the induction of neuroectoderm blocks development into the mesodermal or endodermal lineage by dual-smad inhibition of BMP and TGF-β signaling (Chambers *et al.*, 2009).

After the induction period, NPCs were detached by incubation with TrypLE™ for 8 min at 37°C. Single cells were taken up in wash medium and collected by centrifugation at 1,000 rcf for 4 min. NPCs were resuspended in NPC induction medium without cyclopamine but with 5 µM ROCK inhibitor and split

1:1.5-1:2 onto 6-well plates coated with 1:100 Geltrex™. NPCs were maintained in induction medium without cyclopamine. They were split every 5-8 days for a total of 2-3 passages of propagation before neuronal differentiation.

6.1.3 Differentiation and maturation of human forebrain neurons

Tissue culture plates for the cultivation of long-term neuronal cultures were coated with 0.1 mg/ml poly-L-lysine in 25 mM borate buffer (pH 8.4) at 4°C overnight. The next day, plates were washed twice with autoclaved ddH_2O and coated with 3.75 µg/ml laminin in PBS, also overnight at 4°C.

The protocol for neuronal differentiation from neural progenitor cells is based on work published by Kemp and Telezhkin *et al.* (Kemp *et al.*, 2016; Telezhkin *et al.*, 2016). The protocol consisted of four phases with varying media conditions (detailed media compositions are listed in Tab. 5). Phases 1 (3 days long) and 2 (8 days) promote a synchronized initiation of neuronal differentiation by inhibition of Notch signaling and forced cell-cycle exit of NPCs in the presence of elevated Ca^{2+} levels. Media for phases 3 (7 days) and 4 (long-term cultivation) activate TrkB and WNT signaling to enhance synaptogenesis and network formation (Fig. 7).

To initiate neuronal differentiation, medium on NPC monolayers was changed to phase 1 medium. This change of cell culture medium marked day 0 of differentiation. After three days, early neuronal cultures were dissociated into single cells by incubation with TrypLE™ for 5 min at 37°C. Detached neurons were resuspended in wash buffer and cells were collected by centrifugation at 1,000 rcf for 4 min. The cell pellet was resuspended in DMEM/F-12 neuronal base medium (1% pen/strep, 1% GlutaMAX, 800 µg/ml glucose, 0.5% B27-supplement, 0.5% N2-supplement) with 5 µM ROCK inhibitor. Neurons were either seeded in phase 2 medium with 5 µM ROCK inhibitor for long-term cultivation or in DMEM/F-12 neuronal base medium with ROCK inhibitor for experiments using immature neurons on day 5 of differentiation.

For immunocytochemistry, 150,000-200,000 cells/well were plated onto coverslips in 24-well plates and for cell viability assays, 50,000 cells/well were plated on 96-well plates.

Long-term neuronal cultures were kept in phase 2 medium until day 11, in phase 3 medium until day 18 and from then on in phase 4 medium. Half media changes were performed twice per week. Prior to experiments, culture medium was replaced with DMEM/F-12 neuronal base medium to avoid distorting effects of small molecules on cellular signal transduction pathways.

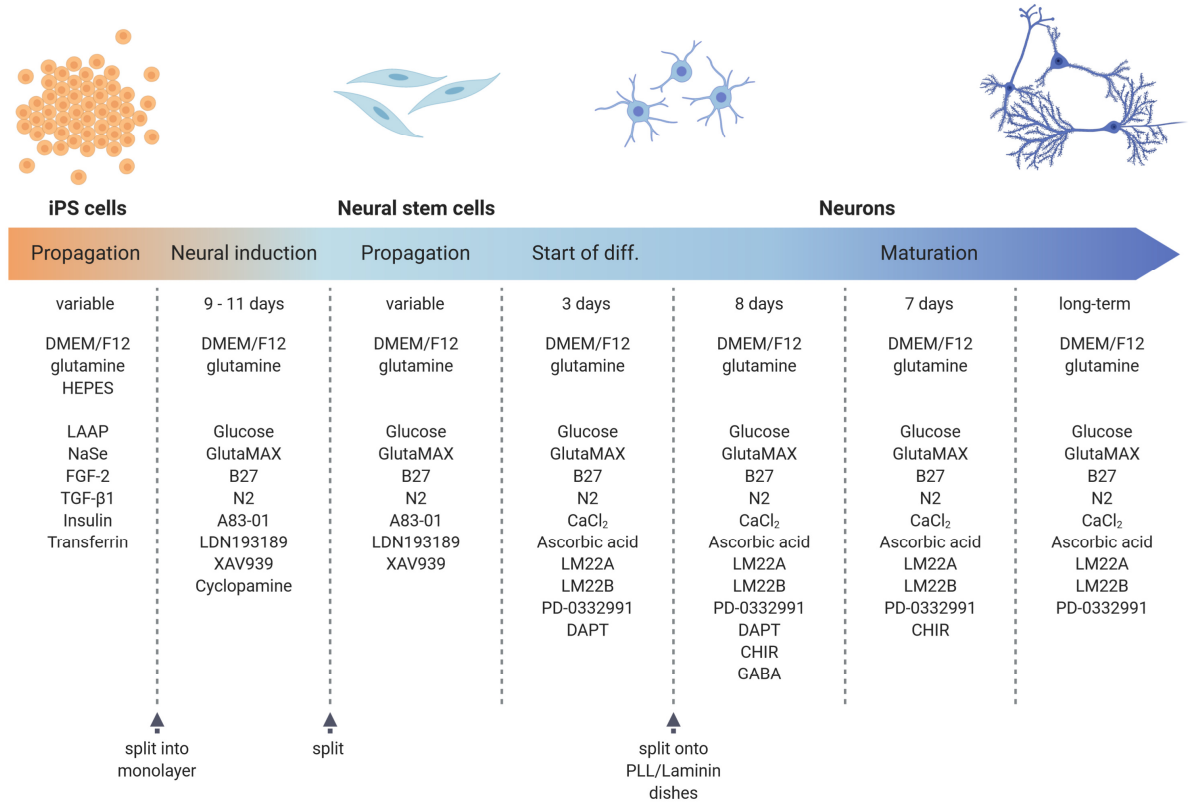

Fig. 7: Timeline for the generation of iPSC-derived forebrain neurons.

Schematic representation of the timeline for the generation of hiPSC-derived forebrain neurons and media components for the indicated culture periods. Please refer to main text for more detailed information (illustration created with BioRender.com).

6.1.4 Freezing and storage of cells

For freezing, hiPSCs were dissociated with EDTA as described in section 6.1.1. NPCs were detached by incubation with TrypLE™ for 5 min at 37°C. HiPSCs were centrifuged at 400 rcf, NPCs at 1,000 rcf. Cell pellets were resuspended in their respective culture media supplemented with 10% DMSO and 10 µM ROCK inhibitor and transferred to cryo vials. Cells were gradually cooled to -80°C in a Mr. Frosty™ freezing container (Thermo Fisher) and then transferred to -150°C for long-term storage.

6.1.5 Treatment of NPCs and neuronal cultures with cellular stressors

To assess viability of immature and mature neurons in the presence of different cellular stressors, 50,000 neurons were plated on 96-well plates coated with PLL/laminin as described above. Treatment of immature neuronal cultures was started on day 5 of differentiation, treatment of mature neuronal cultures at day 30. Starting two days prior to treatment, neuronal cultures were cultivated in DMEM/F-12 neuronal base medium (1% pen/strep, 1% GlutaMAX, 800 µg/ml glucose,

0.5% B27-supplement, 0.5% N2-supplement), but no further supplements to avoid artificial effects by small molecules on cellular signaling pathways.

NPCs were seeded on 96-well plates coated with 1:100 Geltrex™ at 30,000 cells/well. Neurons and NPCs were treated for up to 96 h in 50 µl DMEM/F-12 neuronal base medium containing the stressors indicated in Tab. 25.

Tab. 25: Stressors used for cell viability assays of immature and mature neuronal cultures.

Stressor	Function	Concentration
DMSO	control	1 µl/ml
Tunicamycin	Inhibition of protein N-glycosylation	0.05 – 1.5 µM
Thapsigargin	Disruption of Ca^{2+} homeostasis	0.5 – 1.0 µM
Staurosporine	Inhibition of kinases	50 nM
MG132	Inhibition of protein turnover	0.5 µM
Rotenone	Oxidative stress	2.5 µM
Bafilomycin A1 / 3-Methyladenine	Inhibition of autophagy	15 nM / 2 mM

6.2 CellTiter-Glo® cell viability assay

The CellTiter-Glo® cell viability assay (Promega) is based on the reaction of luciferin to oxyluciferin which is catalyzed by a luciferase and generates a luminescent signal (Fig. 8). The reaction requires ATP which is provided by metabolically active cells in the culture. The luminescent signal is proportional to the amount of ATP and is therefore a measure of cell viability.

Fig. 8: Luciferase reaction of the CellTiter-Glo® cell viability assay.

Recombinant luciferase catalyzes the oxidative decarboxylation of luciferin to oxyluciferin leading to the emittance of light (adapted from Promega CellTiter-Glo® manual).

On the day of the viability measurement, 50 µl of CellTiter-Glo® reagent were added to each well and plates were incubated for 20 min at room temperature on an orbital shaker to allow cell lysis and stabilization of the luminescence signal. Subsequently, the reaction mixture was transferred to a black flat-bottom 96-well plate. Luminescence intensity as a measure for cell viability was determined in a Wallac Victor^2 plate reader (Perkin Elmer). The integration time per well was set to 1 s.

6.3 Orangu™ cell viability assay

The Orangu™ assay is based on the reduction of WST-8 to a formazan dye which requires the activity of intracellular dehydrogenases of living cells (Fig. 9). The generated amount of orange formazan depends on the number of viable cells and the incubation period.

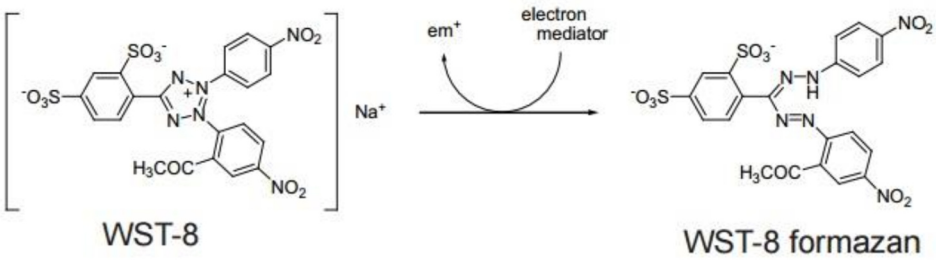

Fig. 9: Reduction of WST-8 to orange WST-8 formazan dye in the Orangu™ cell viability assay.
Dehydrogenases of viable cells transfer an electron to WST-8 which is reduced to a formazan dye whose quantity can be determined by an absorbance measurement at 450 nm (adapted from Orangu™ user guide by Cell Guidance Systems).

To determine the percentage of viable cells, 5 µl of Orangu™ cell counting solution were added to each well 2 h prior to the time point of measurement. Subsequently, cells were incubated as usual at 37°C to allow formazan production. After 2 h, generated formazan was quantified by measuring the absorbance at 450 nm in a PowerWave™ XS microplate reader (BioTek). Finally, dye-containing medium was aspirated and replaced with fresh medium containing the respective stressor to continue the exposure. This procedure was repeated every 12 h for up to 96 h.

6.4 Molecular Biology

6.4.1 Isolation of genomic DNA

For isolation of genomic DNA (gDNA), cells were washed twice with ice-cold PBS, scraped off and collected by centrifugation at 4°C and 3,000 rcf for 5 min. The cell pellet was resuspended in 150 µl lysis buffer (100 mM Tris-HCl (pH 8.5), 5 mM EDTA, 0.2% (w/v) SDS, 200 mM NaCl) supplemented with 1 µl proteinase K and incubated at 37°C and 500 rpm for 1 h. Proteinase K was inactivated at 95°C for 10 min. Subsequently, DNA was precipitated by addition of 105 µl isopropanol and incubation at RT for 30 min with vortexing every 10 min. Afterwards, DNA was collected by centrifugation at 12,000 rcf for 10 min at RT. The resulting pellet was washed twice by addition of 300 µl of 70% ethanol and subsequent centrifugation at RT and 12,000 rcf for 10 min. Finally, the pellet was air-dried at RT and then resuspended in 100-300 µl ddH_2O by incubation at 37°C and 400 rpm for 30 min. Solutions of gDNA were stored at -20°C.

6.4.2 Isolation of RNA

Cells were washed twice with and then scraped off into ice-cold PBS. Afterwards, cells were collected by centrifugation at 7,000 rcf at 4°C for 3 min. A pellet from one well in a 6-well plate was resuspended in 500 µl TriFast™ and lysed for 5 min at RT. Subsequently, 100 µl chloroform were added and samples were vortexed for 15 s. After mixing, samples were incubated for 10 min at RT followed by centrifugation at 12,000 rcf at RT for 5 min to allow phase separation. The upper aqueous phase which contained RNA and DNA was transferred to a new test tube. After addition of 250 µl isopropanol, samples were carefully mixed by repeated inversion and then incubated at -20°C overnight for nucleic acid precipitation. The next day, nucleic acids were collected by centrifugation at 12,000 rcf and 4°C for 15 min. The supernatant was removed and pellets were washed with 500 µl 75% ethanol in DEPC-treated H_2O. After another centrifugation at 12,000 rcf at 4°C for 10 min, the supernatant was removed and the pellet was washed a second time with 75% ethanol as before. Subsequently, pellets were left to air-dry and then resuspended in 20 µl DEPC-treated RNase-free H_2O. For complete resuspension, samples were incubated at 400 rpm and 37°C for 15 min in a thermomixer (Eppendorf).

To remove genomic DNA contamination, 2.5 µl DNase I and 2.5 µl 10x reaction buffer were added per sample. DNA was digested for 15 min at RT. The reaction was stopped by addition of 2.5 µl stop solution followed by heat inactivation of DNase I at 70°C for 10 min. The final RNA concentration was quantified with a NanoDrop™ 1000 spectrophotometer (Thermo Fisher).

6.4.3 Synthesis of complementary DNA (cDNA)

The iScript™ cDNA synthesis kit (Bio-Rad Laboratories) was used to reversely transcribe 1 µg of RNA into cDNA. Samples were incubated in a thermal cycler according to the protocol given in (Tab. 27). The resulting cDNA was diluted 1:5 in nuclease-free H_2O yielding a concentration of 10 ng/µl.

Tab. 26: Reaction mix for cDNA synthesis.

Component	Volume [µl]
5x iScript™ reaction mix	4
iScript™ reverse transcriptase	1
RNA template (1µg)	variable
Nuclease-free H_2O	variable
Total	**20**

Tab. 27: Cycling program for cDNA synthesis.

Step	Temperature [°C]	Duration [min]
Priming	25	5
Reverse transcription	46	20
Enzyme inactivation	95	1
Short-term storage	4	hold

6.4.4 Polymerase chain reaction (PCR)

Amplification of target amplicons from gDNA or cDNA was performed according to the cycling program given in Tab. 28. Annealing temperature and elongation time were adjusted based on the employed primers and the expected size of the amplicon.

Tab. 28: Composition of standard PCR reaction.

Component	Volume [µl]	Final concentration
10x Taq reaction buffer	2.5	1x
10 mM dNTP mix	0.5	200 µM
10 µM primer mix	1.0	400 nM
Taq DNA polymerase (5 U/µl)	0.125	0.625 U
Template DNA	variable	0.4 – 10 ng/µl
ddH_2O	variable	
Total	**25**	

Tab. 29: Standard PCR cycling program.

Step	Temperature [°C]	Duration	
Initial denaturation	95	2 min	
Denaturation	95	15 s	35 cycles
Annealing	60	20 s	
Elongation	72	15 s	
Final elongation	72	3 min	
Short-term storage	4	hold	

6.4.5 Mycoplasma PCR

As a measure for cell culture quality control, cells were regularly checked for the presence of mycoplasma contamination (Van Kuppeveld *et al.*, 1992; Ossewaarde *et al.*, 1996). To this end, cells were harvested and genomic DNA was isolated according to section 6.4.1. Whole genomic DNA was used as a template for PCR aimed at the amplification of the mycoplasma specific 16S rRNA gene. Sequences of primers used for mycoplasma detection are listed in Tab. 11. PCR products were analyzed by 1% agarose gel electrophoresis. If present, a mycoplasma contamination was detectable by a 270 bp band.

Tab. 30: PCR protocol for mycoplasma quality control.

Step	Temperature [°C]	Duration	
Initial denaturation	95	1 min	
Denaturation	95	15 s	
Annealing	50	15 s	35 cycles
Elongation	72	10 s	
Final elongation	72	3 min	
Short-term storage	4	hold	

6.4.6 Agarose gel electrophoresis and gel extraction of amplified DNA

Digested plasmids and PCR amplicons were mixed with 10x DNA sample buffer and separated by 1-2%-(w/v) agarose gel electrophoresis in TAE buffer. Gels contained 1:15,000 peqGREEN DNA detection reagent. A 100 bp or a 1 kbp DNA marker was included on gels as a reference for DNA fragment size. DNA was resolved for 50 min at 100 V and gels were imaged on a GeneFlash imaging system (Syngene).

If needed, amplified target DNA segments were excised and extracted from agarose gels using the peqGOLD gel extraction kit (VWR) according to the manufacturer's instructions. Isolated DNA was eluted in 30 µl ddH_2O and then used for cloning or analyzed by Sanger sequencing.

6.4.7 RNA quality control

6.4.7.1 RNA bulk samples

Prior to RNA sequencing, quality control of RNA bulk samples isolated by TriFast™-chloroform extraction was performed using the RNA 6000 Nano Kit (Agilent Technologies) according to the manufacturer's instructions. For each sample, 100-300 ng of RNA were analyzed on a Bioanalyzer 2100 (Agilent Technologies) to verify RNA concentration and to assess RNA integrity. For further procedure, refer to section 4.4.9.

6.4.7.2 Single-cell RNA samples

On the day of the experiment, neuronal cultures at days 6, 10, 17, 24, 31, 38, 45 and 52 of differentiation were dissociated into single cells by incubation in TryplE™. Cells were counted and an equal number of cells from cultures at each time point were mixed to yield a unified cell suspension which was further processed in the single-cell Open Lab (scOpenLab) at the German Cancer Research Center (DKFZ; Heidelberg, Germany). At the scOpenLab the cell suspension was filtered through a 30 µm cell strainer and counted again. Subsequently, 10,000 cells were used for single-cell cDNA library

preparation and quality control according to the 10x Genomics single cell user guide (v2 chemistry). The obtained cDNA library had a concentration of 22.2 ng/µl and an average fragment size of 505 bp.

6.4.8 RNA bulk sequencing

RNA extracted from biological triplicates (independent differentiations) of NPCs, d5, d25 and d45 neuronal cultures was adjusted to a concentration of 35 ng/µl. For each sample, 40 µl of RNA solution were sent to the High Throughput Sequencing Unit of the Genomics & Proteomics Core Facility at the DKFZ (Heidelberg, Germany) to be processed. Samples were run through in-house quality control and samples with an RNA integrity number (RIN) ≥ 7.5 were used for cDNA library preparation according to the TruSeq Stranded protocol (Illumina). Libraries were sequenced to 50 bp single reads on one lane on the Illumina HiSeq 4K platform.

Data was run through an RNAseq processing workflow by the Omics IT and Data Management Core Facility at the DKFZ. Total counts per feature were imported to R (R Core Team, 2020) and analyzed using DESeq2 (Love *et al.*, 2014). All features without any counts were removed, for differential testing with DESeq2 the formula "~timepoint" was used.

Euclidean distance between samples was calculated from rlog transformed counts using the stats (R Core Team, 2020) package. The sample distance plot was generated using the pheatmap package (Kolde, 2019) with the viridis plasma color scale (Garnier, 2018). Principal component analysis (PCA) was performed on rlog transformed counts with the top 500 variable features using prcomp (R Core Team, 2020).

The TCseq package (Wu & Gu, 2020) was used to perform time course sequencing analysis in which temporal patterns in gene expression are detected and genes with similar temporal expression patterns are grouped. For clustering, the cmeans algorithm was used with k=12. Features from specific gene clusters were used to perform gene ontology (GO) enrichment analysis using enrichGO from the clusterProfiler package (Yu *et al.*, 2012). The organism database used for this analysis is org.Hs.eg.db (Carlson, 2020). Heatmaps for RNAseq expression data show z-scaled DESeq2 normalized counts.

RNAseq data analysis was performed in collaboration with Dr. Anne Hoffrichter.

6.4.9 Single-cell RNA sequencing

The prepared single-cell cDNA library was sent to the High Throughput Sequencing Unit of the Genomics & Proteomics Core Facility at the DKFZ to be processed. The library was sequenced on one lane on the Illumina HiSeq 4K platform with a protocol specific for 10x scRNA libraries (paired-end 26+74). Fastq files were parsed to cellranger (10x Genomics) counts in order to generate a count matrix. FastQC was used for general sequencing quality control (Andrews *et al.*, 2015).

If not stated otherwise, data analysis was performed using the Seurat package in R (Stuart *et al.*, 2019). The count matrix was filtered with several parameters. Any feature that was expressed in less than three cells was removed from the analysis. Any cell with less than 2000 expressed features, more than 10% mitochondrial genes expressed, or less than 5000 total UMI counts was removed from further analysis. The data was normalized using sctransform. After initial quality control, 1,524 single cells remained for further analysis.

Differentially expressed genes (in total 2671) from RNAseq for time points NPC, d5, d25, d45, or d25&d45 were used as variable features for PCA. Further dimensional reduction was performed using UMAP with dims = 1:30. Shared nearest neighbor graph was constructed with dims = 1:50 and k.param = 30. Clusters were generated with resolution = 1.

Calculations for Neuron Maturity Index were performed using the neuMatIdx package (He & Yu, 2018) using normalized counts from the Seurat object. The pseudotime trajectory was calculated with the monocle3 package (Cao *et al.*, 2014; Trapnell *et al.*, 2014; Qiu *et al.*, 2017a, 2017b).

RNAseq data analysis was performed in collaboration with Dr. Anne Hoffrichter.

6.4.10 Transformation of chemically competent bacteria

To amplify plasmid DNA, a 50 µl aliquot of chemically competent *E. coli* DH5α was thawed on ice for 5 min. 50-500 ng of plasmid DNA were added to the bacterial suspension and the solution was mixed by carefully flicking the tube 2-3 times. Bacteria were incubated with DNA on ice for 40 min. Uptake of DNA into bacteria was triggered by heat shock at 42°C for 42 s. Afterwards, bacteria were left to recover on ice for 3 min. Subsequently, 300 µl of LB medium without antibiotics were added and bacteria were incubated for 1 h at 37°C and 400 rpm. Finally, the bacterial suspension was either plated on LB agar plates or used to inoculate midi cultures. Bacteria were grown at 37°C overnight in the presence of 100 µg/ml ampicillin for selection.

6.4.11 Isolation of plasmid DNA (mini and midi preparation)

Plasmid DNA from small and medium scale bacterial cultures was isolated either with the peqGOLD mini prep (VWR) or the PureLink™ HiPure midiprep kit (Thermo Fisher) according to the manufacturer's instructions. DNA from mini cultures was eluted in 30 µl ddH_2O, DNA from midi cultures in 100 µl. The DNA concentration was measured using a NanoDrop™ 1000 (Thermo Fisher).

6.5 CRISPR-Cas9 mediated generation of isogenic GFAT-1 G451E gain-of-function hiPSCs

To create hiPSCs with a GFAT-1 gain-of-function (gof) mutation as described by the group of Martin Denzel (Denzel *et al.*, 2014; Horn *et al.*, 2020; Ruegenberg *et al.*, 2020), the glycine residue at position 451 of the GFAT-1 protein had to be replaced by a glutamate. This required exchange of the last two nucleotides of the base triplet starting at position 1,405 of the open reading frame of the *GFPT1* gene (1,405-GGC > GAG).

6.5.1 Cloning of a *GFPT1*-targeting CRISPR-Cas9 plasmid

The px459 V2.0 plasmid published by the group of Feng Zhang was used for Cas9 gene editing. This plasmid encodes the *Streptococcus pyogenes* Cas9 enzyme fused to the puromycin N-acetyltransferase via a T2A sequence, a β-lactamase for ampicillin resistance and a restriction site for the insertion of a target specific guide RNA (gRNA) (Fig. 10).

To insert the *GFPT1*-targeting gRNA into the px459 V2.0 backbone, the plasmid backbone was linearized by digestion with *BbsI* for 1 h at 37°C. The reaction products were separated by 1% agarose gel electrophoresis. The linearized px459 backbone was isolated by gel extraction (section 6.4.6).

Tab. 31: Restriction digest of px459 V2.0.

Component	Volume
10x restriction buffer 2.1	2 µl
BbsI	1 µl
px459 V2.0 plasmid	1 µl (1µg)
ddH_2O	16 µl
Total	**20 µl**

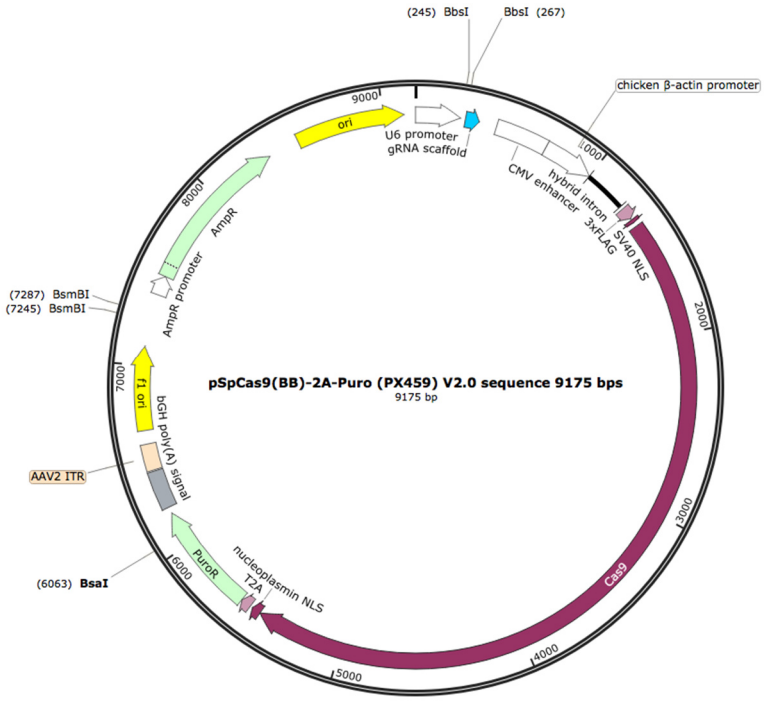

Fig. 10: Plasmid map of the px459 V2.0 backbone for CRISPR-Cas9 genome editing.

The px459 V2.0 plasmid contains a cloning site which enables integration of a desired gRNA via *BbsI*. The *Streptococcus pyogenes* Cas9 enzyme is expressed as a fusion with puromycin N-acetyltransferase via a T2A peptide (adapted from addgene.org).

The sequences of the *GFPT1* gRNA sense and anti-sense oligonucleotide are listed in Tab. 11. The pair of oligonucleotides was phosphorylated and annealed as described in the following two tables.

Tab. 32: Reaction mix for phosphorylation and annealing of oligonucleotides.

Component	Volume
sense oligo (100 µM)	1 µl
anti-sense oligo (100 µM)	1 µl
10x T4 ligation buffer	1 µl
T4 PNK	0.5 µl
ddH_2O	6.5 µl
Total	**10 µl**

Tab. 33: Thermocycler program for phosphorylation and annealing of oligonucleotides.

Step	Temperature [°C]	Duration
Phosphorylation	37	30 min
Annealing	95	5 min
	down to 25	5°C/min

Finally, the phosphorylated and annealed oligonucleotides for the gRNA were ligated into the linearized px459 V2.0 backbone. Ligation was performed for 1h at RT.

Tab. 34: Ligation reaction of gRNA and px459 V2.0.

Component	Volume
Linearized px459 backbone	variable (50 ng)
Phosphorylated, annealed gRNA oligos (1:200 dilution)	1 µl
10x T4 DNA ligase buffer	2 µl
T4 DNA ligase	1 µl
ddH_2O	variable
Total	**10 µl**

Ligation products were used for transformation of chemically competent *E. coli* DH5α which were plated on LB-agar plates containing 100 µg/ml ampicillin. Plasmid DNA isolated from resulting clones was analyzed by Sanger sequencing using the hU6-forward primer (Tab. 12) to validate correct insertion of the *GFPT1* gRNA.

6.5.2 Nucleofection of hiPSCs and clonal selection

For the CRISPR-Cas9-mediated generation of a GFAT-1 G451E gof cell line, hiPSCs of a healthy control subject were pre-incubated with 5 µM ROCK inhibitor overnight. The next day, hiPSCs were dissociated into single cells by incubation with TrypLE™ for 5 min at 37°C. For nucleofection, $1x10^6$ cells were centrifuged in a 2 ml test tube for 5 min at 400 rcf. In parallel, the DNA mix to be nucleofected was prepared by mixing 82 µl of Nucleofector® solution, 18 µl of Nucleofector® supplement (Cell Line Nucleofector® kit V), 2 µg of GFAT-1 gRNA targeting CRISPR-Cas9 px459 plasmid and 4 µg of single-stranded oligonucleotide repair template harboring the G451E mutation. Cells were carefully resuspended in DNA mix and transferred to a nucleofection cuvette. Program B-023 of the Lonza nucleofector II was used for DNA transfer into cells. Afterwards, cells were resuspended in hiPSC medium without pen/strep but with 5 µM ROCK inhibitor and distributed onto four wells of a 6-well plate at different densities (400,000, 300,000, 200,000 and 100,000 cells). Additionally, 400,000 untreated control cells were seeded on each of the two remaining wells to be used as selection controls.

After 24 h, the culture medium was changed to hiPSC medium without pen/strep supplemented with 5 µM ROCK inhibitor and 0.3 µg/ml puromycin to start transient selection of clones. The next day, clones received standard hiPSC medium containing ROCK inhibitor and puromycin as before. On the third day post nucleofection, puromycin and ROCK inhibitor were removed from the medium.

At this point, control cells had died from the selection. The remaining clones were propagated in standard hiPSC medium and screened for the genomic incorporation of the single-stranded repair oligonucleotide.

6.5.3 Screening of potential GFAT-1 G451E clones

HiPSCs of the generated GFAT-1 G451E clones were harvested for RNA isolation and cDNA synthesis. The cDNA was used to amplify an 837 bp sequence surrounding the desired point mutation by PCR. Primer sequences are listed in Tab. 11.

Tab. 35: PCR program for the screening of GFAT-1 gain-of-function clones.

Step	Temperature [°C]	Duration	
Initial denaturation	95	1 min	
Denaturation	95	15 s	
Annealing	60	15 s	40 cycles
Elongation	72	50 s	
Final elongation	72	3 min	
Short-term storage	4	hold	

Amplified PCR products were excised from agarose gels and DNA was extracted according to section 6.4.6. Amplicons were sequenced using the GFAT-1 forward primer listed in Tab. 12. Clones harboring the desired GGC > GAG nucleotide exchange but no further alterations in the sequenced DNA stretch were further propagated, the remaining clones were disposed.

6.6 Sanger Sequencing

Sequencing of plasmid DNA and PCR amplicons was performed by Microsynth Seqlab GmbH (Göttingen, Germany). For sequencing, 12 µl containing 100-500 ng of sample DNA were mixed with 3 µl of a 10 µM solution of the relevant sequencing primer in a 1.5 ml test tube. FASTA sequencing files were analyzed with the ApE plasmid editor and chromatograms were evaluated in SnapGene® Viewer to verify sequencing quality.

6.7 SNP analysis

Whole-genome sequencing and analysis of single nucleotide polymorphisms (SNPs) was performed by the Life & Brain GmbH (Bonn, Germany). 900 ng of gDNA at a concentration of 60 ng/µl were sent in

for genotyping using an Illumina Infinium® Global Screening Array – 24v1.0 BeadChip. Data were analyzed by Josef Frank at the department of genetic epidemiology at the Central Institute of Mental Health (Mannheim, Germany).

6.8 Biochemistry

6.8.1 Cover slip preparation and immunocytochemistry (ICC)

Glass coverslips were etched in concentrated hydrochloric acid for 1-2 h at RT with shaking. After three washing steps with ddH_2O, coverslips were washed once with 70% ethanol and subsequently one more time with ddH_2O. Eventually, coverslips were air-dried and then autoclaved. Sterile coverslips were placed in tissue culture plates and coated as needed for the cell type of interest.

Cells were washed once with PBS and then fixed in 4% PFA in PBS for 15 min at RT. Residual PFA was removed by three washing steps with PBS. If not indicated otherwise, cells were blocked and permeabilized in PBS containing 10% FBS and 0.3% Triton X-100 (blocking solution) for 1 h at RT. Primary antibodies were diluted in blocking solution and epitope tagging was performed at 4°C overnight in a wet chamber.

The next day, coverslips were washed three times with PBS and then incubated with fluorescently-labelled secondary antibodies in blocking solution for 1 h at room temperature. Unbound secondary antibodies were removed by washing twice with PBS. Cell nuclei were stained by intercalation of DAPI (300 nM in PBS) into genomic DNA for 3 min at RT. Subsequently, coverslips were washed two more times with PBS and once with ddH_2O. Coverslips were mounted on glass slides using Mowiol/DABCO solution and left to solidify at room temperature overnight.

Dilutions of individual primary and secondary antibodies are listed in Tab. 16 and Tab. 17.

6.8.2 Cell lysis and protein quantification

Cells were first washed twice with and then scraped off into ice cold PBS. Samples were centrifuged at 7,000 rcf for 4 min at 4°C. Depending on the collected number of cells, pellets were resuspended in 100-300 µl lysis buffer (Tab. 14) and incubated for 1 h on ice. Lysis buffer for the analysis of ubiquitinated proteins was supplemented with 50 µM iodoacetamide to inhibit deubiquitinating enzymes. Lysates were sonicated with 15 pulses (duty cycle 20%, output control 5.5) from a Branson Ultrasonics™ sonifier 250 (Thermo Fisher) to shear genomic DNA and reduce sample viscosity.

Cell debris was removed by centrifugation at 16,000 rcf for 15 min at 4°C and the supernatant was transferred to a new test tube.

A bicinchoninic acid (BCA) protein assay kit (Thermo Fisher) was used according to the manufacturer's instructions to quantify the total protein yield of cell lysates. The reaction relies on the reduction of Cu^{2+} to Cu^{+} ions in an alkaline solution in the presence of peptide bonds and functional groups of amino acid side chains. BCA chelates the arising Cu^{+} ions to form a complex which can be quantified by a spectrophotometric measurement and thus allows an estimation of the total protein content of a sample.

Samples were diluted 1:5 in ddH_2O in a 96-well plate and mixed with assay reagent. After incubation at 37°C for 30 min, the absorption at 562 nm was measured in a PowerWave™ XS (BioTek) microplate reader. The protein concentration of samples was calculated based on the included BSA standard dilution series.

6.8.3 SDS-PAGE and Western blotting

For analysis of protein contents, cell lysates were separated by SDS-polyacrylamide gel electrophoresis (SDS-PAGE). For each sample, 5-30 µg of total protein were mixed with 6x SDS sample buffer and boiled for 5 min at 95°C.
SDS gels were first run at 30 V for 20-30 min to allow stacking of proteins, followed by 1.5-2 h at 120 V to separate proteins according to molecular weight. Proteins were transferred onto nitrocellulose (NC) membranes with a pore size of 0.2 µm by semi-dry blotting in a Trans-Blot® Turbo™ transfer system (Bio-Rad Laboratories) for 45 min at 20 V and 1 A. Western blot filter tissue and NC membranes were soaked in transfer buffer. Subsequently, membranes were blocked either with 5% milk powder or 5% BSA in TBST for 1 h at room temperature. For detection of target proteins, membranes were incubated with primary antibody diluted in blocking buffer at 4°C overnight. Detailed information regarding specific primary antibodies is listed in Tab. 18.

The next day, membranes were washed three times with TBST for 10 min at RT. Primary antibodies were then labelled with infrared (IR)-dye conjugated secondary antibodies diluted 1:15,000 in TBST for 1 h at RT. After three additional washing steps as before, tagged proteins of interest were visualized on a Li-COR Odyssey IR western blot imaging system.

Tab. 36: Composition of resolving gels for use with Tris-tricine SDS-PAGE running buffer.

Component	Volume [ml] per gel mold volume of			
	10 ml	20 ml	30 ml	40 ml
10%				
ddH_2O	1.33	2.67	4.00	5.33
3M Tris-HCl/SDS (pH 8.45)	3.33	6.67	10.00	13.33
30% acrylamide mix	3.33	6.67	10.00	13.33
50% glycerol	2.00	4.00	6.00	8.00
10% ammonium persulfate	0.028	0.056	0.112	0.140
TEMED	0.009	0.019	0.037	0.047
14%				
ddH_2O	-	-	-	-
3M Tris-HCl/SDS (pH 8.45)	3.33	6.67	10.00	13.33
30% acrylamide mix	4.67	9.33	14.00	18.67
50% glycerol	2.00	4.00	6.00	8.00
10% ammonium persulfate	0.028	0.056	0.112	0.140
TEMED	0.009	0.019	0.037	0.047

Tab. 37: Composition of stacking gel for Tris-tricine SDS-PAGE.

Component	Volume [ml] per gel mold volume of			
	5 ml	10 ml	15 ml	20 ml
4%				
ddH_2O	3.12	6.24	9.36	12.48
3M Tris-HCl/SDS (pH 8.45)	1.24	2.48	3.72	4.96
30% acrylamide mix	0.64	1.28	1.92	2.56
10% ammonium persulfate	0.034	0.067	0.101	0.134
TEMED	0.011	0.022	0.033	0.044

6.9 Electrophysiological characterization of neurons

The degree of electrophysiological maturity of single neurons was analyzed by patch-clamp recordings by the group of PD Dr. Georg Köhr at the Central Institute of Mental Health. For this purpose, neurons were cultured on PLL/laminin coated glass cover slips. For whole-cell recordings, a cover slip was transferred to a recording chamber. During measurements, cells were continuously perfused with artificial cerebrospinal fluid (125 mM NaCl, 25 mM $NaHCO_3$, 2.5 mM KCl, 1.25 mM NaH_2PO_4, 10 mM D(+)-glucose, 2 mM $CaCl_2$, 1 mM $MgCl_2$; osmolarity 290 mOsm) bubbled with 5% CO_2 and 95% O_2 at RT. Pipettes were filled with intracellular solution (115 mM K-gluconate, 20 mM KCl, 10 mM-Na-phosphocreatine, 4 mM Mg-ATP, 0.3 mM GTP, 0.2 mM EGTA, 10 mM HEPES, pH 7.25; osmolarity 290 mOsm). To quantify elicited action potentials, current steps from -30 to 100 pA in increments of 10 pA were injected for 300 ms each. Recordings were obtained at a sampling rate of 20 kHz using an EPC9 patch clamp amplifier (HEKA Elektronik GmbH).

6.10 Statistical analysis

Unless indicated otherwise, data for quantitative analysis is based on at least three independent biological replicates. Results are displayed as means with standard deviation (SD) which were calculated using GraphPad Prism 6 statistical analysis software. Significance testing between two groups was performed by student's t-test. Comparisons of multiple groups influenced by a single variable were evaluated by one-way ANOVA, multiple groups influenced by two variables were evaluated by two-way ANOVA. Multiple group comparison correction was performed by Bonferroni post hoc significance testing. Significance levels against the respective controls are $*p < 0.05$, $**p < 0.01$, $***p < 0.001$ and $****p < 0.0001$.

7 Results

7.1 Generation of human forebrain neuronal cultures from iPSCs

To elucidate mechanisms underlying neuronal longevity, iPSCs of healthy control individuals were used to generate human forebrain neurons. The employed differentiation protocol started from iPSC monolayers which were guided into the ectodermal lineage by preventing mesodermal and endodermal specification via dual-smad inhibition (Chambers *et al.*, 2009). The resulting NPC monolayers were then differentiated into neurons by small molecules-driven cell cycle arrest and inhibition of notch signaling. Thereafter, transcriptional maturation and network formation of neuronal cultures continued for at least three weeks (Fig. 11A). This approach is based on work published by Kemp and Telezhkin (Kemp *et al.*, 2016; Telezhkin *et al.*, 2016) and yields highly pure and functional neuronal cultures by mimicking the milieu during embryonic development through temporary exposure to GABA and an increased concentration of $CaCl_2$.

Immunofluorescence microscopy of day 5 (d5) and day 35 (d35) neuronal cultures revealed an about 14-fold increase in the number of nuclei stained positive for the mature neuron marker NeuN (Fig. 11B, C). While only 6.25 ± 0.77% of neurons were $NeuN^+$ at d5, this fraction reached 86.61 ± 2.09% at d35. Within the same period, neurons displayed a cytoarchitectural reorganization illustrated by an advanced separation of MAP2 and Tau signals in immunofluorescence stainings (Fig. 11B). At d5, MAP2 and Tau distribution mostly overlapped but at d35 a distinct $MAP2^+$ dendritic arbor and a Tau^+ axonal compartment had been established. Both cellular subdomains are structurally distinct and the resulting cellular polarity is a precondition for proper neuronal functionality. Additionally, neurons at d35 possessed a significantly expanded network of neurites reaching 330.60 ± 67.30 µm per cell compared to 92.17 ± 13.28 µm at d5 (Fig. 11D). The neuronal maturation process was also apparent from immunofluorescence analysis showing a robust colocalization of the presynaptic protein Synapsin and the postsynaptic protein PSD95 at d35 (Fig. 11E). Signals for these two synaptic proteins were punctate and abundantly colocalized at d35. In contrast, at d5 the majority of Synapsin signal did not localize to distinct punctae but was diffusely distributed in the cytosol. These observations highlight the advanced synaptic network connectivity of neuronal cultures at d35.

Next, RT-PCR of NPCs and neuronal cultures at day 5, 15, 25, 35 and 45 of differentiation was used for a broader transcriptional characterization of the generated cell system. This approach revealed a time-dependent increase in the expression of the mature neuron marker *RBFOX3* (NeuN) which was only weakly detectable in immature neuronal cultures at d5 (Fig. 11F). However, mRNA levels of *RBFOX3* strongly increased from d15 onward.

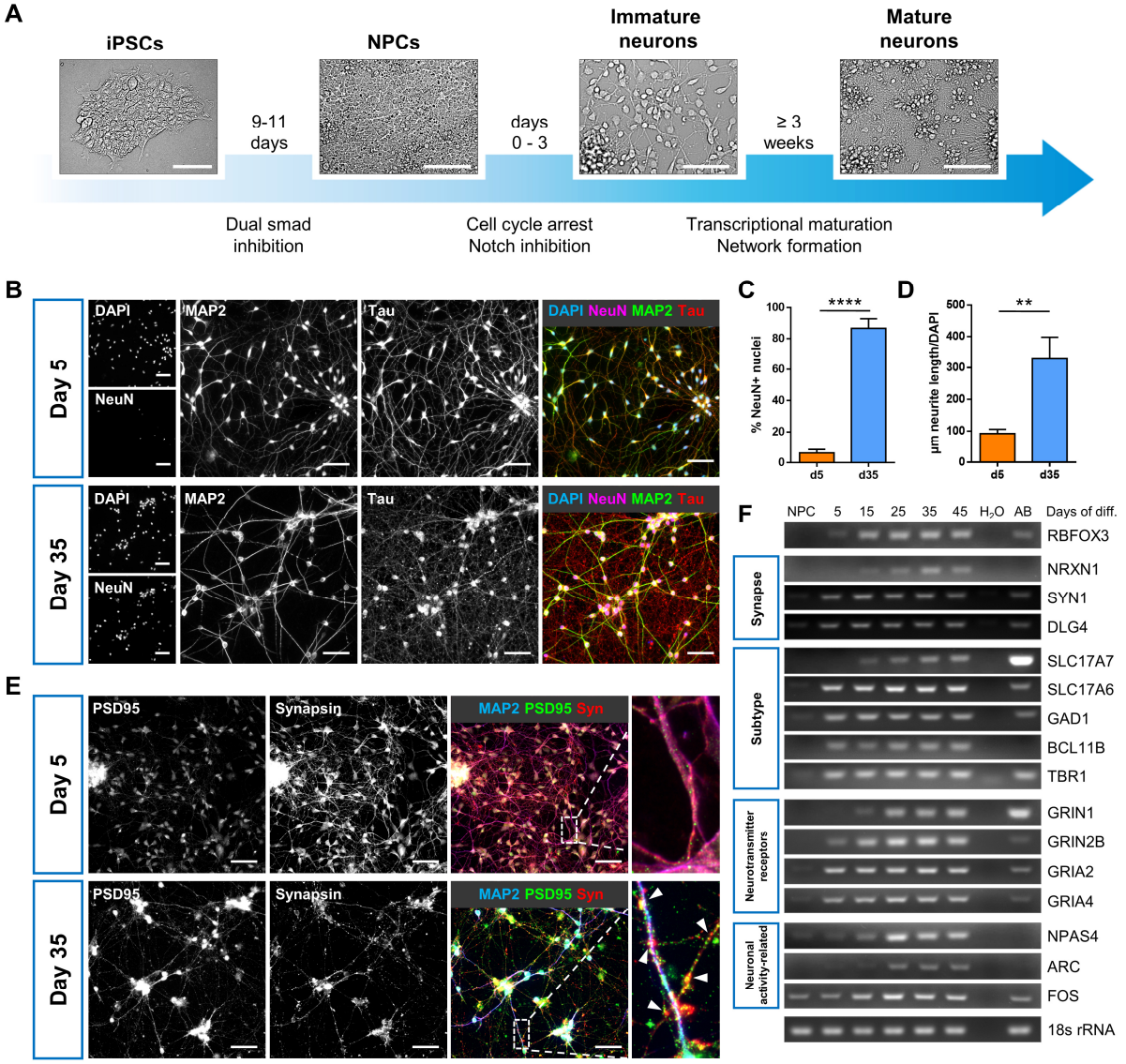

Fig. 11: Differentiation and maturation of hiPSC-derived forebrain neurons.

(**A**) Schematic representation highlighting the key steps within the timeline of the differentiation protocol to generate hiPSC-derived forebrain neurons. Exemplary brightfield images illustrate the different stages during maturation. Neuronal age is counted in days of differentiation starting from the day that NPC medium is exchanged for neuron differentiation medium (days 0 - 3). Neuronal cultures were left to mature for at least three weeks. Scale bars: 100 µm (**B**) Representative fluorescence microscopy images of immature neurons at day 5 (d5) and more mature neurons at d35 of differentiation. Scale bars: 50 µm (**C**) Quantification of the percentage of $NeuN^+$ nuclei in d5 and d35 neuronal cultures. With duration in culture the fraction of mature neurons expressing NeuN drastically increases. Bar graph shows mean with S.D., $P < 0.0001$, two-tailed t test. (**D**) Quantification of the total length of neurite expansion per cell in d5 and d35 neuronal cultures. Bar graph depicts mean with S.E.M., $P = 0.0031$, two-tailed t test. (**E**) Representative images illustrating the advancing synaptic connectivity of neuronal networks from d5 to d35 in culture based on increasing colocalization of the pre- and postsynaptic marker proteins Synapsin and PSD95 (highlighted by white arrowheads). Scale bars: 50 µm (**F**) RT-PCR analysis of canonical marker genes in NPCs and neuronal cultures at the indicated time points of differentiation. AB: adult brain.

This observation supported the findings from immunofluorescence experiments regarding the drastically increased number of $NeuN^+$ nuclei from d5 to d35. While expression of *SYN1* (Synapsin) and *DLG4* (PSD95) appeared constant at all stages of neuronal maturation, appreciable amounts of mRNA for the synaptic cell adhesion molecule *NRXN1* (neurexin-1) were only detectable starting at d15. Interestingly, expression of the neuronal activity-related immediate early genes *NPAS4* and *ARC* was strongly increased briefly after the onset of *NRXN1* expression. This suggests that synaptic connections were markedly advanced between d15 and d25 of differentiation. The generated cultures contained a mix of neuronal subtypes as illustrated by the expression of the GABAergic marker *GAD1* and the glutamatergic markers *SLC17A6* (vGlut2) and *SLC17A7* (vGlut1). Expression of *SLC17A7* was detectable from d15 onward whereas *SLC17A6* mRNA was present starting at d5. The forebrain identity of the generated neurons was confirmed by detection of *BCL11B* (Ctip2) and *TBR1* expression. The NMDA receptor subunit *GRIN1* was first detectable at d15, whereas *GRIN2B* was already expressed at d5. Expression of both subunits increased over time. Finally, neurons were also equipped with the AMPA receptor subunits *GRIN2* and *GRIN4*. These results highlight the regional identity of the generated neuronal cultures and document their progressive transcriptional maturation.

Apart from transcriptomic and cytoarchitectural changes, neuronal maturation should also be accompanied by modulation of electrophysiological properties. These characteristics were assessed using patch clamp recordings of single neurons (Fig. 12). During 300 ms of depolarization immature neurons (d4-5) elicited merely a single action potential (AP), if any at all. Conversely, more mature neurons (d25-28) responded with firing of repetitive trains of APs (Fig. 12A). Consequently, the average number of APs generated during 300 ms of depolarization was significantly higher in more mature neurons (8.083 ± 0.665) compared to immature neurons (0.900 ± 0.143) (Fig. 12B). However, once an AP was triggered, its amplitude did not differ significantly between immature (91.44 ± 3.08 mV) and mature neurons (96.02 ± 3.27 mV) (Fig. 12C). More mature neurons showed a trend towards a more negative resting membrane potential reaching -41.04 ± 1.92 mV compared to -37.85 ± 1.68 mV in immature neurons. Accordingly, the input resistance was significantly decreased in neurons at d25-28 of differentiation (1.054 ± 0.079 Ω) compared to neurons at d4-5 (1.305 ± 0.090 Ω). In addition, the cellular capacitance increased from 7.320 ± 0.505 pF at d4-5 to 9.825 ± 0.809 pF at d25-28 which is indicative of an increased cellular volume. Together, these data underline the advanced electrophysiological functionality of the generated iPSC-derived neurons after 3-4 weeks of cultivation.

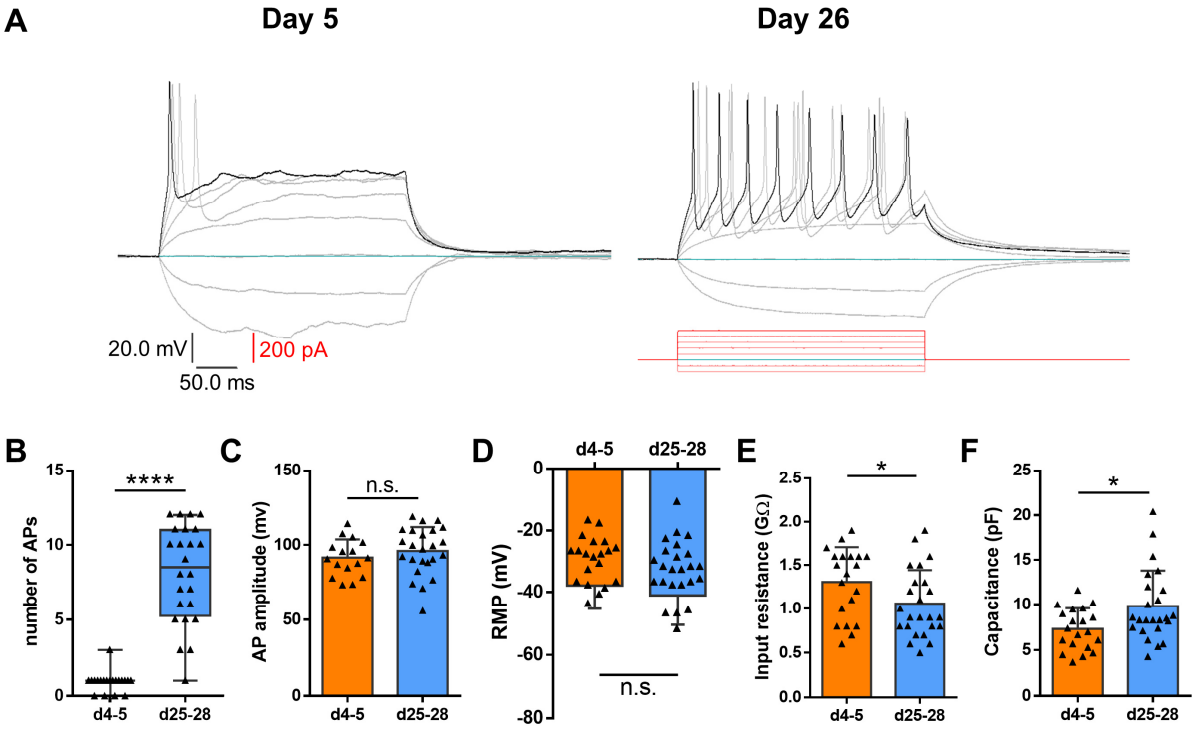

Fig. 12: Electrophysiological maturation of hiPSC-derived forebrain neurons.

(**A**) Representative action potential (AP) firing pattern of an immature neuron at d5 and a more mature neuron at d26 of differentiation during 300 ms of depolarization. (**B-F**) Electrophysiological properties of individual neurons at d4-5 (n = 20 cells) and d25-28 (n = 24 cells) of differentiation. Each data point represents a single neuron. Bar graphs show mean with S.D. (**B**) Box-plot of the number of APs fired during 300 ms of depolarization. More mature neurons elicit significantly more APs upon depolarization. Error bars are min-max values. $P < 0.0001$, two-tailed Mann-Whitney U test. (**C**) AP amplitudes of immature and mature neurons did not differ significantly. $P = 0.3393$, two tailed t test. (**D**) The resting membrane potential (RMP) of more mature neurons showed a trend toward a more negative potential. $P = 0.2268$, two-tailed t test. (**E**) The membrane resistance decreases during neuronal maturation. $P = 0.0414$, two-tailed unpaired t test. (**F**) Capacitance of neurons increases with duration of differentiation. $P = 0.0313$, two-tailed Mann-Whitney U test. Electrophysiology was performed in collaboration with the group of PD Dr. Georg Köhr.

7.2 Transcriptional hallmarks of neuronal maturation

For an in-depth analysis of the transcriptional changes taking place during neuronal maturation, whole transcriptome RNA bulk sequencing of NPCs and neuronal cultures at day 5, 25 and 45 of differentiation was performed (Fig. 13A). In addition, single-cell RNAseq of a mixture of neurons of different maturity ranging from day 6 to day 52 was used. This “maturity gradient” allowed a higher-resolution analysis of transcriptional adaptations at different stages of differentiation.

Similarity analysis of the samples used for RNA bulk sequencing revealed a high degree of overlap between transcriptomic signatures of biological replicates of the same stage of differentiation. With prolonged time in culture, differences between transcriptomes became more nuanced resulting in a lower Euclidean distance between d25 and d45 neuronal cultures (Fig. 13B).

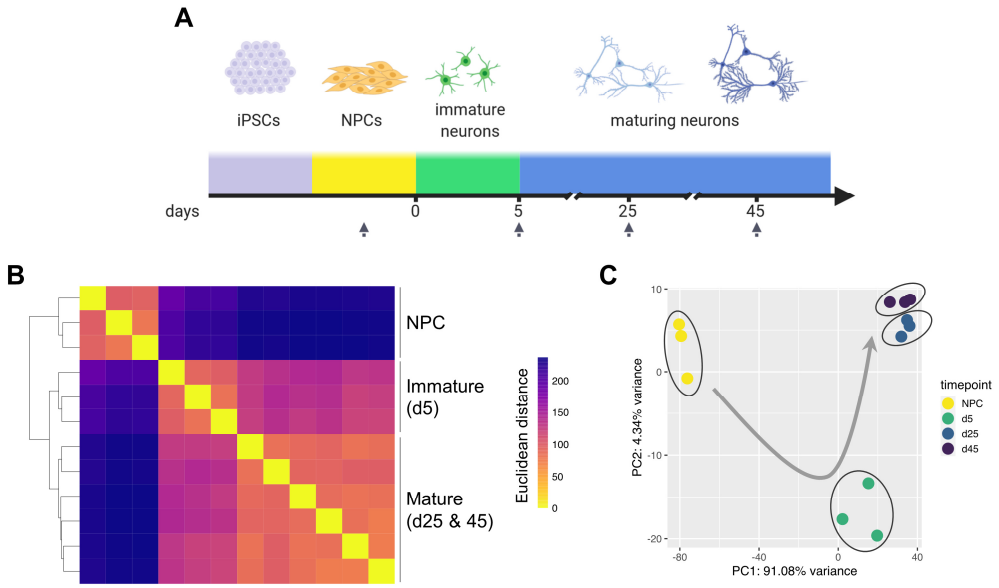

Fig. 13: RNA bulk sequencing of neuronal cultures at different stages of differentiation.

(**A**) Timeline of neuronal differentiation with grey arrowheads indicating time points of sample collection for RNAseq. For each time point (NPC, d5, d25, d45), three biological replicates of independent differentiations were analyzed. (**B**) Sample distance matrix with hierarchical clustering based on rlog normalized counts. Euclidean distance indicates sample similarity with dark purple corresponding to a high degree of differences between samples. (**C**) PCA biplot of PC1 and PC2 based on the 500 most variable features. Biological replicates group together (black ovals) but samples are separated based on time point of differentiation. Transcriptomic signatures of NPCs and d5 neuronal cultures are distinct. With prolonged time in culture, transcriptomic differences become more nuanced causing d25 and d45 neuronal cultures to cluster more closely together. Grey arrow highlights timeline of differentiation. PC: principal component. RNAseq data analysis was done in collaboration with Dr. Anne Hoffrichter.

In line with this observation, principal component (PC) analysis of PC1 vs PC2 showed clustering of NPC samples and samples of immature neuronal cultures at d5 most closely to one another and distinctly separated from the samples of all the other time points (Fig. 13C). Towards later stages of differentiation, the differences in the transcriptomic profiles of samples from d25 cultures to d45 were less pronounced. However, respective replicates still clustered most closely to one another. This highlights that the most profound transcriptional changes take place during the early phase of differentiation and that later stages are characterized by more fine-tuned adaptations. PC1 explained 91.08% and PC2 4.34% of variance between samples with PC3 consolidating only 1.94%. These data underline the homogeneity of the analyzed samples and are a sign for a high degree of reproducibility between independent differentiations.

Using time course (TC) clustering of genes with similar expression dynamics (Wu & Gu, 2020), gene ontology (GO) terms related to biological process (BP), molecular function (MF) and cellular compartment (CC) that are characteristic for the different stages of neuronal maturation were identified. In total, TCseq analysis resulted in 12 distinct clusters with different expression dynamics, four of which are presented in more detail below (Fig. 14).

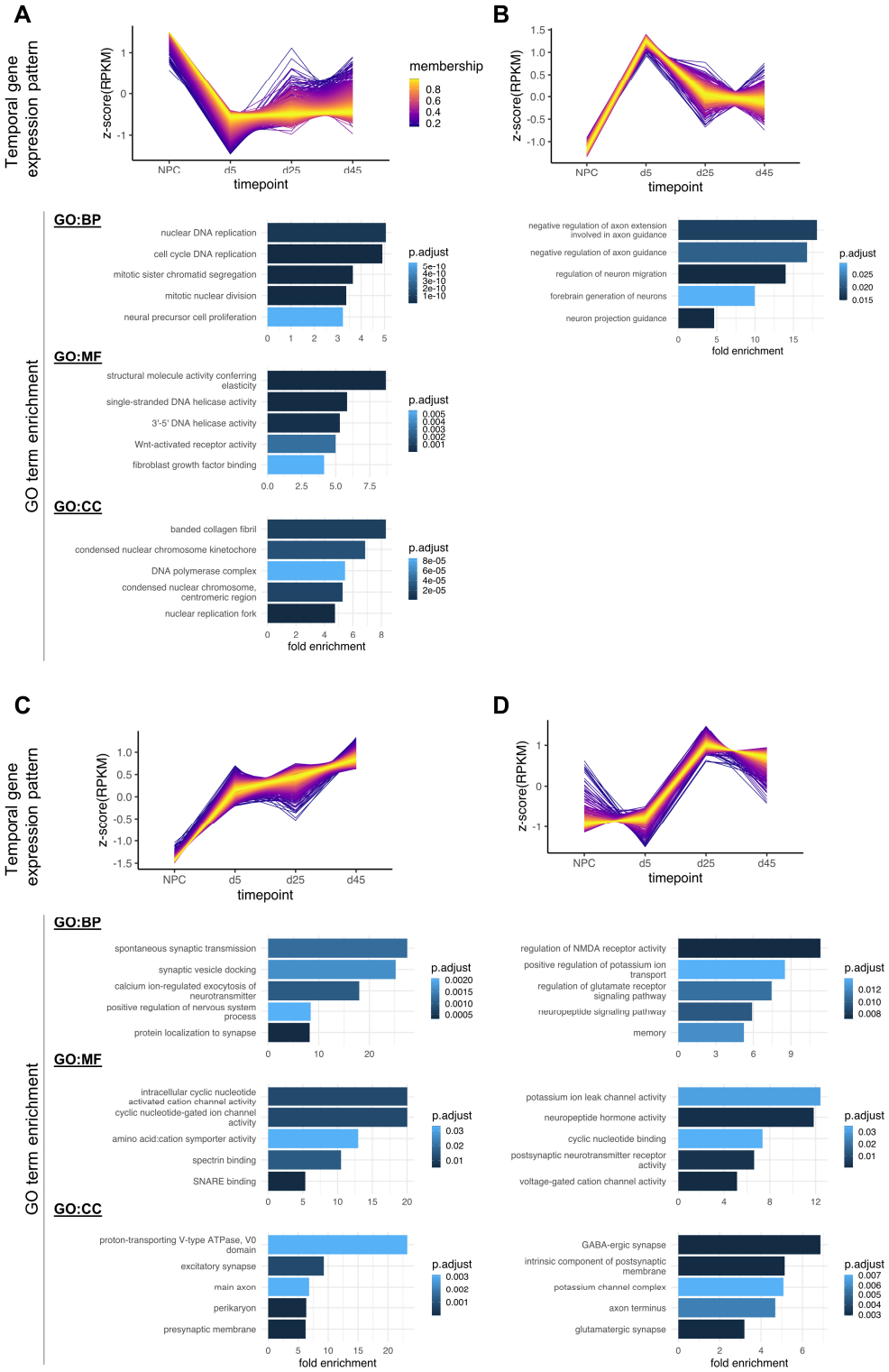

Fig. 14: TCseq clustering identifies phase-specific gene expression patterns.

(**A-D**) Time course (TC) soft clustering of genes based on temporal expression dynamics (z-scaled RPKM). The degree to which a specific gene fits to the respective cluster is indicated by its membership value. High membership values are represented in yellow. Four TCseq clusters with different temporal expression patterns are shown together with a GO term enrichment analysis based on the underlying cluster-specific genes. Terms are split into the three GO categories biological process (GO:BP), molecular function (GO:MF) and cellular compartment (GO:CC). (**A**) Genes that are highly expressed in NPCs but downregulated in neurons mainly relate to DNA replication and proliferation. (**B**) D5 neuronal cultures show a distinct suppression of axon growth while favoring genes involved in neuronal migration. No GO:MF or GO:CC were specifically enriched for this temporal expression pattern. (**C**) Genes progressively upregulated during neuronal maturation focus on synaptogenesis. (**D**) Genes that are specifically upregulated in more mature neuronal cultures (d25, d45) largely pertain to ion channel and neurotransmitter receptor activity. RNAseq data analysis was done in collaboration with Dr. Anne Hoffrichter.

TCseq analysis groups genes with similar temporal expression profiles together and thereby enables identification of broader transcriptional trends occurring over time. Genes that were strongly expressed in NPCs but downregulated in neurons at all stages of differentiation related predominantly to DNA replication, cell division and proliferation (Fig. 14A). This cluster contained GO terms like “mitotic sister chromatid segregation”, “single-stranded DNA helicase activity” and “fibroblast growth factor binding”. In contrast, d5 neuronal cultures showed a specific upregulation of genes involved in the generation of forebrain neurons and neuronal migration. However, the strongest enrichment at this stage of differentiation was observed for genes regulating the suppression of axon growth and guidance (Fig. 14B). This was in line with data from immunofluorescence imaging of d5 neuronal cultures showing that a distinct axonal compartment had not yet been formed (Fig. 11B). The third cluster contained genes that were not expressed in NPCs but which were progressively upregulated during neuronal maturation (Fig. 14C). These genes mainly related to processes involved in synaptogenesis and synaptic transmission with terms such as “synaptic vesicle docking”, “protein localization to synapse” and “excitatory synapse”. Lastly, genes which were specifically upregulated in d25 and d45 neuronal cultures played a role in neurotransmitter receptor signaling, regulation of ion channel activity and synapse refinement (Fig. 14D). Representative GO terms for this fourth cluster were, among others, “regulation of NMDA receptor activity”, “voltage-gated cation channel activity”, “GABAergic synapse” and “glutamatergic synapse”.

Relative gene expression analysis of individual canonical marker genes corroborated the developmental trajectories identified by TCseq clustering (Fig. 15A). NPC cultures expressed high levels of the proliferation marker *MKI67*, and the progenitor markers *SOX2*, *HES1 HES5* and *NES*. Immature neuronal cultures were enriched for the early neuron markers *TUBB3*, *FAT3* and *STMN1*. Immature neurons also expressed *DCX* which is involved in microtubule regulation and is required for directed neuronal migration during cortical development. Additionally, an on-set of expression of the

postsynaptic density protein *DLG4* (PSD95) and the ionotropic glutamate receptor (AMPA) subunits *GRIA1* and *GRIA2* were detectable at d5. Similarly, appreciable transcript levels of the neural cell adhesion molecule (*NCAM1*) and the axon initial segment (AIS) scaffolding component *ANK3* were present at this time point.

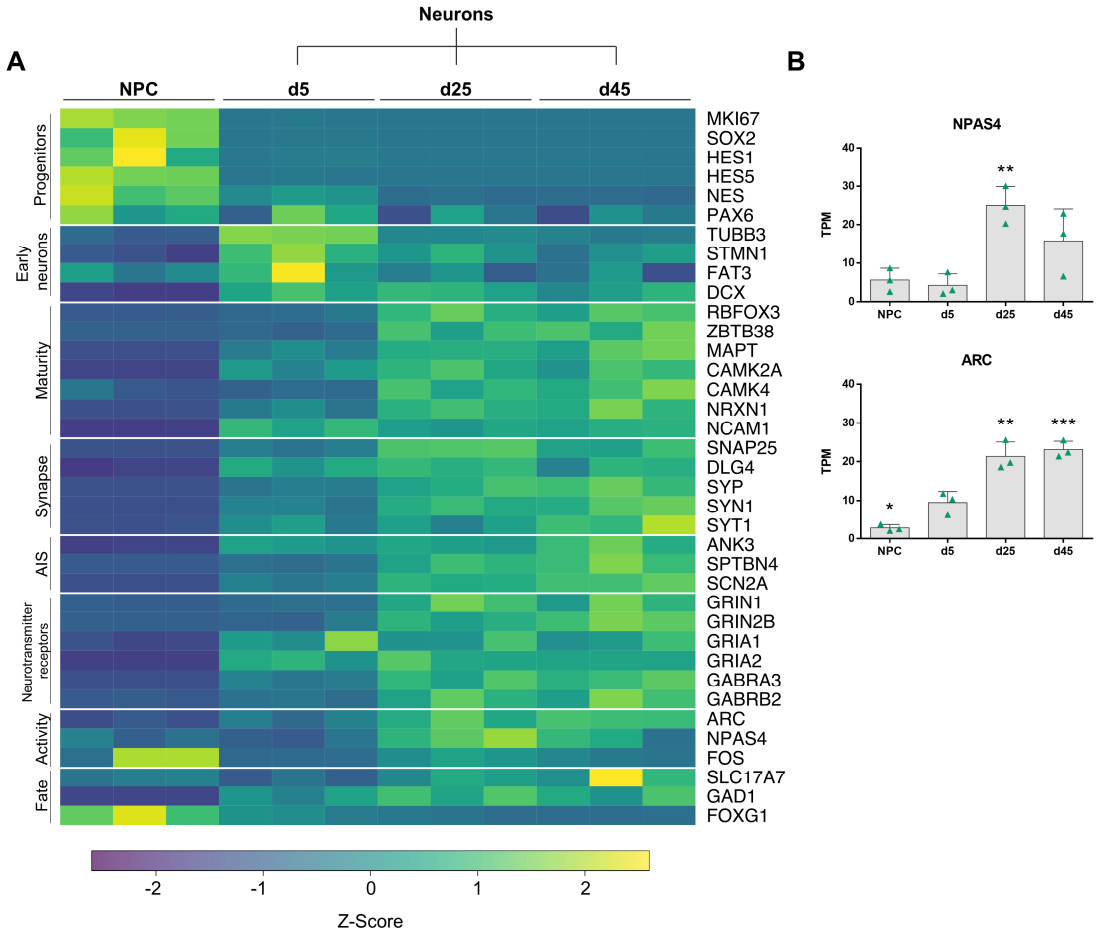

Fig. 15: Expression profiles of NPCs and neurons of different maturity.

(**A**) Heat map (z-scaled) showing expression of canonical marker genes for the analyzed time points during neuronal maturation. At d25 and d45 of differentiation, neuronal cultures display increased expression of synaptic proteins, components of the AIS and neurotransmitter receptors. Expression of *FOXG1* highlights the forebrain identity of the generated cultures. (**B**) Expression of the neuronal activity-related genes *NPAS4* and *ARC* is increased in more mature neuronal cultures (d25, d45). Bar graphs show mean of normalized expression in TPM (transcripts per kilobase million) with S.D., statistical significance calculated with d5 as reference, one-way ANOVA with Bonferroni correction. RNAseq data analysis was done in collaboration with Dr. Anne Hoffrichter.

Starting from day 25 of differentiation, neuronal cultures expressed higher levels of more mature neuron markers such as *RBFOX3* (NeuN), *CAMK2A* and *CAMK4*. Transcription of *MAPT* was strongly increased providing the building material to consolidate and expand the axonal compartment. Expression of central synaptic proteins like *NRXN1* and *SYN1* increased, accompanied by elevated levels of *SNAP25* which mediates synaptic vesicle fusion. The set of expressed neurotransmitter

receptors was widened by the addition of NMDA (*GRIN1*, *GRIN2B*) and GABA receptors (*GABRA3*, *GABRB2*). Furthermore, the expression of *ANK3*, the fundamental structural building block of the AIS was now accompanied by expression of its binding partner βIV Spectrin (*SPTBN4*) which is required for complete AIS assembly. The AIS also became equipped with the voltage-gated sodium channel Nav1.2 (*SCN2A*). The AIS lends neurons polarity and constitutes the central signaling hub for the generation of action potentials. Taken together, these changes are indicative of a more complex neuronal cytoarchitecture enabling increased neuronal activity. Accordingly, expression of the neuronal activity-related immediate early genes *ARC* and *NPAS4* was strongly increased in more mature neuronal cultures at day 25 and 45 compared to immature neurons at d5 in culture (Fig. 15B).

The generated neuronal cultures consisted of a mix of excitatory and inhibitory neuron subtypes as illustrated by the expression of the vesicular glutamate transporter-1 (*SLC17A7*) and glutamate decarboxylase-1 (*GAD1*), which are specific for glutamatergic and GABAergic neurons, respectively. The forebrain identity of these neurons was underlined by the prominent expression of *FOXG1* already at the NPC stage.

To analyze transcriptomes of individual neurons with varying degrees of maturity, single-cell RNAseq of a mix of neurons containing cells at different stages of differentiation from d6 to d52 was performed (Fig. 16A). Since not all neurons mature at the same rate *in vitro*, cultures at specific time points of differentiation always contain a mix of less and more mature cells even though the overall maturity of the culture advances with time. Consequently, d6 neuronal cultures may already contain a few more transcriptionally advanced neurons whereas at d52 a subpopulation of cells may be lacking behind in the maturation process. To adjust for this potential heterogeneity and optimally sort single neurons along a gradient based on increasing transcriptional maturity, data from the RNA bulk sequencing experiment was used for guided dimensional reduction of the single-cell transcriptomics data set. Subsequently, Seurat clustering resulted in six distinct subpopulations of single cells (Fig. 16B).

The different stages of neuronal differentiation and maturation from NPCs to mature neuronal cultures were recapitulated using monocle3 pseudotime analysis which produced two distinct paths (Fig. 16C). With cluster 1 at the origin of pseudotime, the first path included clusters 2-5 and the second path was formed by a branch consisting of cluster 6. GO term enrichment analysis for cluster 6 revealed that it contained cells unified by their activation of stress response pathways highlighted by GO terms relating to stress-induced transcription and proteasome activity as well as unfolded protein and heat shock protein binding (Fig. 16D). These stressed cells may be a result of the extended sample preparation procedure before the generation of cDNA libraries. Since the aim of the experiment was to investigate transcriptional changes during neuronal maturation, cluster 6 was excluded from further analyses.

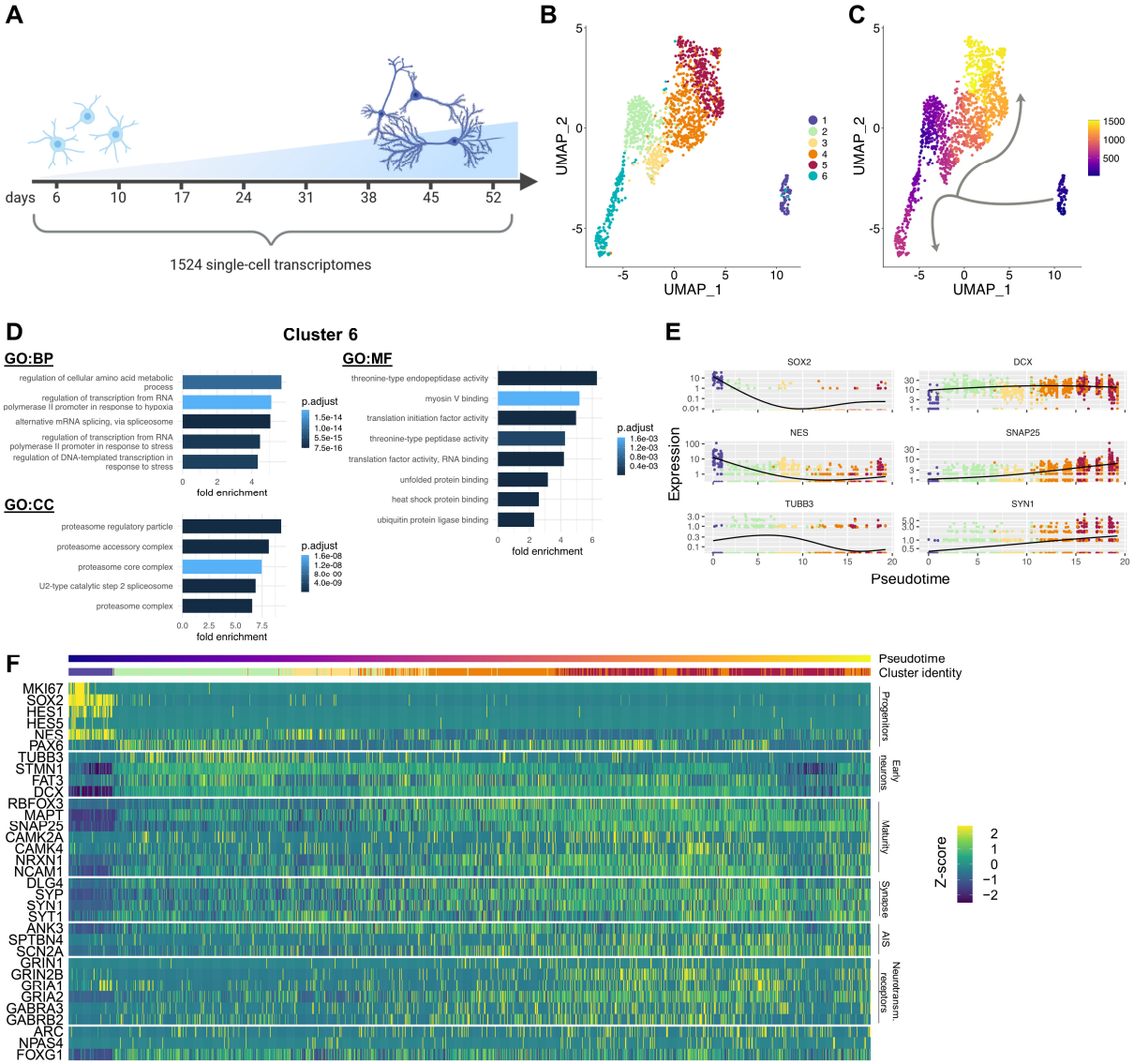

Fig. 16: Single-cell RNAseq dissects neuronal maturation dynamics.

(**A**) Schematic representation highlighting the days of differentiation at which different neuronal cultures were collected for scRNAseq. A total of 2259 cells were sequenced and after filtering and quality control 1524 cells were further analyzed. (**B**) Dimensional reduction plot in UMAP dimensions. Seurat clustering of single cell transcriptomes reveals six distinct subpopulations. Data from the bulk RNAseq experiment was used for guided dimensional reduction of the scRNAseq dataset. (**C**) Monocle3 pseudotime analysis based on the dimensional reduction from (B). Grey arrows indicate two paths for the progression of pseudotime. (**D**) GO term enrichment shows that cluster 6 consists of cells in a stressed condition. This cluster does not represent a path of neuronal development in pseudotime and was therefore excluded from further analyses. (**E**) Expression trajectories of canonical marker genes along the pseudotime axis based on normalized counts. These expression profiles highlight the neuronal identity of clusters 2-5. (**F**) Heat map (z-scaled) of marker gene expression in single cells ordered by pseudotime. Cells at the origin of pseudotime show a higher expression of NPC markers whereas cells at the end of pseudotime express more mature neuron markers like components of the AIS, neurotransmitter receptors and synaptic proteins. RNAseq data analysis was done in collaboration with Dr. Anne Hoffrichter.

Pseudotime expression trajectories of *SOX2* and *NES* showed decreasing expression from cluster 1 to cluster 5 (Fig. 16E). *TUBB3* expression peaked in clusters 2 and 3. For these two clusters, expression of *DCX* was also at a maximum and then began to decrease slightly in cells at the end of the pseudotime trajectory. Since *DCX* is involved in migration of neurons and is not required once a neuron has reached its final destination, a decrease in *DCX* expression likely is a sign of advanced neuronal maturity. Expression of the synaptic vesicle protein *SNAP25* increased along the pseudotime axis and peaked in cells of cluster 5. Similarly, the expression of the presynaptic protein Synapsin (*SYN1*) was most abundant towards the end of pseudotime. Cells in cluster 1 positioned at the origin of pseudotime also expressed genes like *MKI67*, *HES1* and *HES5* suggesting that these clusters are formed by non-neuronal cells (Fig. 16F). Clusters 2 and 3 were formed by more immature neurons illustrated by the expression of *TUBB3*, *FAT3*, *STMN1* and *DCX*. Cluster 4 represented an intermediate state of maturity and cluster 5 contained the most mature neurons with the highest expression of neurotransmitter receptors and the AIS components *SPTBN4* and *SCN2A*. Therefore, clusters 2-5 were formed by neurons whose transcriptomic maturity steadily increased from cluster 2 to 5.

Since the aim of this study was to elucidate neuron-specific phenomena, the RNAseq data was used to estimate the purity of the generated neuronal cultures by analyzing the abundance of canonical astrocyte marker genes (Fig. 17). TPM counts for *GFAP*, *SLC1A3*, *S100B* and *ALDH1L1* were either consistently low in neuronal cultures at d5, 25 and 45 or these genes were not expressed at all. This suggests that the investigated cultures almost exclusively contained neurons and that changes observed in their characteristics are attributable to neuron-specific adaptations and not astrocytic impurities.

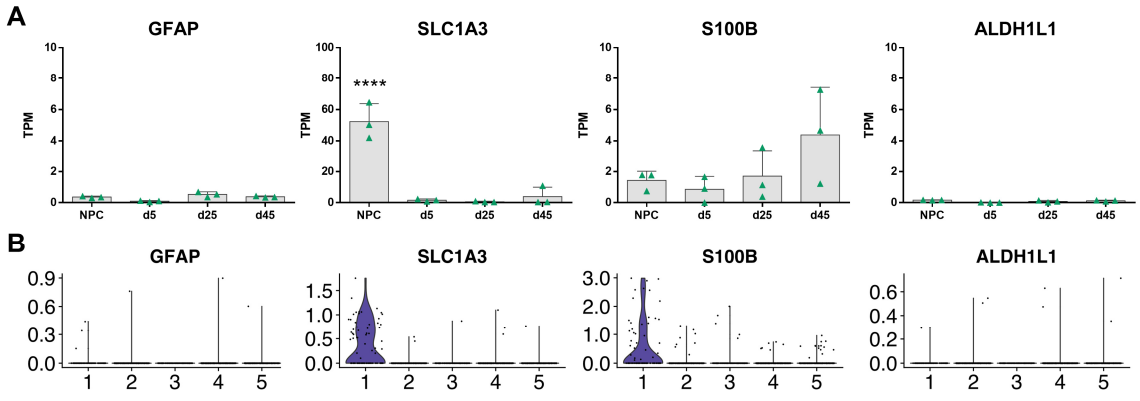

Fig. 17: The investigated neuronal cultures are highly pure.

(**A**) Bulk and (**B**) single-cell RNA seq data of canonical astrocyte marker genes highlight the high degree of purity of the generated neuronal cultures which are almost completely free of astrocytes. Note differing scales of y-axis. Bar graphs show mean with S.D., one-way ANOVA with Bonferroni's multiple comparison test. Violin plots indicate normalized counts.

In addition to the analysis of single canonical marker genes as a means to estimate the maturity state of neuronal cultures, it is also possible to quantify and score neuronal maturity in a manner suitable to permit comparison to other neuronal culture systems. For this purpose, the neuron maturity index (NMI) was calculated using the neuMatIdx R package published by He and Yu (He & Yu, 2018). This algorithm grades the maturity of neuronal cultures with a score from 0-1, with 1 being a perfect score. The algorithm was trained on the Reactome protein-protein interaction database and RNAseq data of fetal and adult human brain tissue. The "discriminating NMI" (dNMI) evaluates the status of transcriptional modules that were found to best account for the differences between immature and mature neurons. The neuron functionality index (NFI) only incorporates modules specifically enriched in mature neurons. Application of the NMI algorithms to the bulk and single-cell RNAseq data sets allowed scoring of the transcriptional maturity of the neurons generated within the scope of this study.

Based on the bulk RNAseq data set, d5 neuronal cultures reached a dNMI value of 0.6396 ± 0.0107, well above the threshold between immaturity and maturity of 0.5 as defined by He and Yu (Fig. 18A, C). This may suggest that the applied differentiation protocol strongly boosts neuronal maturation already in the initial phase. The progression of neuronal maturation from d5 onward was also reflected in the higher dNMI scores of d25 and d45 neuronal cultures which reached 0.7284 ± 0.0031 and 0.7380 ± 0.0122 respectively (Fig. 18A). The calculated NFI values were 0.7447 ± 0.0095 (d5), 0.8297 ± 0.0059 (d25) and 0.8506 ± 0.0026 (d45) which was in support of the expected trend of an increasing maturity with prolonged time in culture. NMI scores of the neuronal clusters 2-5 of the scRNAseq data set supported the assignment of the pseudotime axis as a trajectory of neuronal maturation. Clusters 2 and 3 scored the lowest dNMI and NFI whereas cluster 5 reached the highest scores (Fig. 18B). In general, RNA bulk samples obtained higher NMI scores than single-cell clusters. The dNMI values calculated for neuronal cultures in bulk and single-cell transcriptomics were comparable to scores of other published transcriptomics data sets (Fig. 18C).

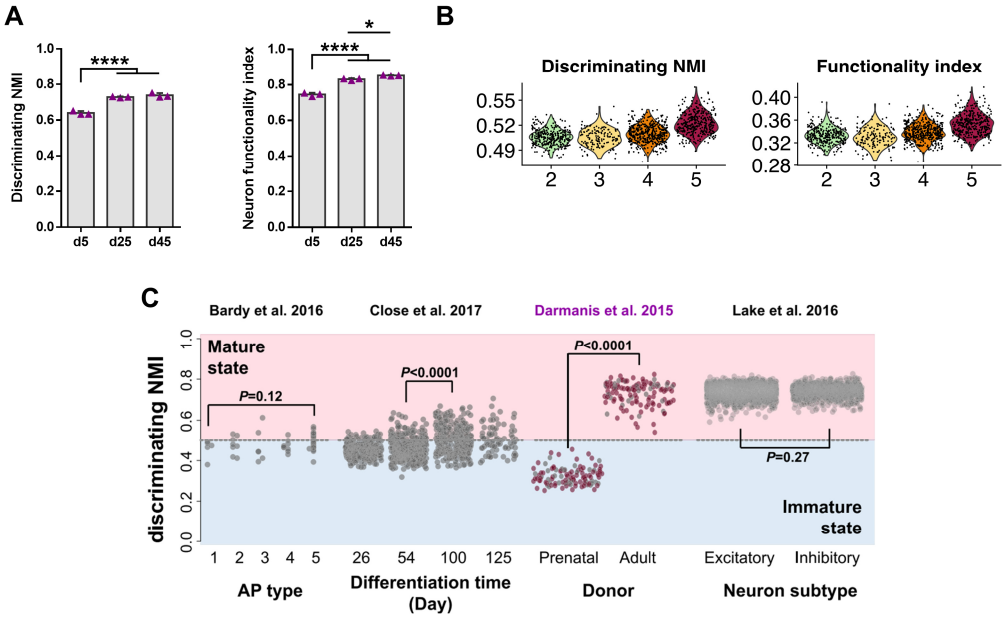

Fig. 18: Neuron maturity index (NMI) of neuronal cultures quantifies advancing maturity.

Calculation of the neuron maturity index based on (A) bulk neuronal cultures and (B) transcriptomes of single neurons using the neuMatIdx R package (He & Yu, 2018). The discriminating NMI is determined based on transcriptional modules most suitable to distinguish between immature and mature neurons whereas the neuron functionality index only takes into account modules specifically upregulated in mature neurons. (**A**) Transcriptional maturity of neuronal cultures increases significantly with prolonged time of cultivation. Bar graphs show mean with S.D., one-way ANOVA with Bonferroni correction. (**B**) Violin plots showing NMI scores for the neuronal clusters 2-5. Scores calculated for single cells are generally lower than scores of bulk neuronal cultures. This presumably results from a less complete transcript coverage per cell in the scRNAseq experiment. (**C**) Figure adopted from (He & Yu, 2018) indicating discriminating NMI-based distinction of immature and mature neurons calculated for various publicly available RNAseq data sets. RNAseq data analysis was done in collaboration with Dr. Anne Hoffrichter.

To conclude, RNA bulk and high-resolution single-cell transcriptomics of different time points throughout the applied neuronal differentiation protocol allowed to recapitulate changes in gene expression during neuronal maturation. Establishing a clear distinction between the transcriptional profiles of immature and mature neurons provided the basis for subsequent experiments.

7.3 Regulation of apoptosis pathways during neuronal maturation

7.3.1 Mature neurons restrict caspase availability and activation

During embryonic development, neurons are initially produced in excess numbers which are later reduced when the neuronal circuitry is refined. Once brain development has been concluded the remaining neurons have to persist for the whole lifetime of the individual. To guarantee their longevity, neurons are thus likely to rely on specific safety mechanisms to prevent their accidental loss. Using the detailed transcriptomic analysis of the established neuronal maturation trajectory, I first investigated the effect of neuronal maturation on the abundance of caspases, the classical key enzymes of the apoptotic machinery. Within the intrinsic apoptosis pathway, Caspase-9 acts as an initiator caspase for the activation of the effector Caspases-3 and -7. This activation requires the assembly of a protein complex called the apoptosome which consists of Apaf-1, Cytochrome c and Caspase-9 (Fig. 19A). APAF-1 protein was faintly detectable in NPCs and d5 neuronal cultures but became undetectable from d15 onward (Fig. 19B, C). Procaspase-9 protein levels peaked at d5 and decreased from there by about 50% until d45. Interestingly, protein levels of the two initiator Caspases-3 and -7 declined as well. Proaspase-3 protein levels reached a maximum at day 15 and then strongly decreased until day 45. Ablation of Procaspase-7 was even more drastic as it was abundant in NPCs and immature neurons but hardly detectable in Western blots after day 5.

RNA bulk analysis revealed a trend towards decreased *APAF1* expression in more mature neuronal cultures, but this trend did not reach statistical significance (Fig. 19D). Expression of the *CASP9* gene remained mostly unchanged throughout neuronal maturation and could therefore not explain the observed reduction in Procaspase-9 protein levels. In contrast, expression data for *CASP7* was in support of Western blotting results and showed a complete ablation in neuronal cultures at all time points. Loss of *CASP7* expression in immature neurons at d5 therefore preceded the loss of Procaspase-7 protein which was still detectable at this stage of maturation. Expression of *CASP3* reached a peak in d5 neuronal cultures and then slowly declined with time in culture.

On the single cell level, transcript counts of *APAF1*, *CASP9* and *CASP7* were too low, to make valid claims about possible trends in their expression (data not shown). However, a strong decrease in *CASP3* expression was observable in the most mature neuron cluster 5 compared to the immature neuron clusters 2 and 3 (Fig. 19E).

In addition to the major Caspases-3, -7 and -9, changes in the expression of other members of the caspase family of proteases were also investigated. Of note, a significant decrease in *CASP2* transcript levels was observable specifically in d25 and d45 neuronal cultures compared to d5 (Fig. 19D). This notion was also supported by the scRNAseq data (Fig. 19E).

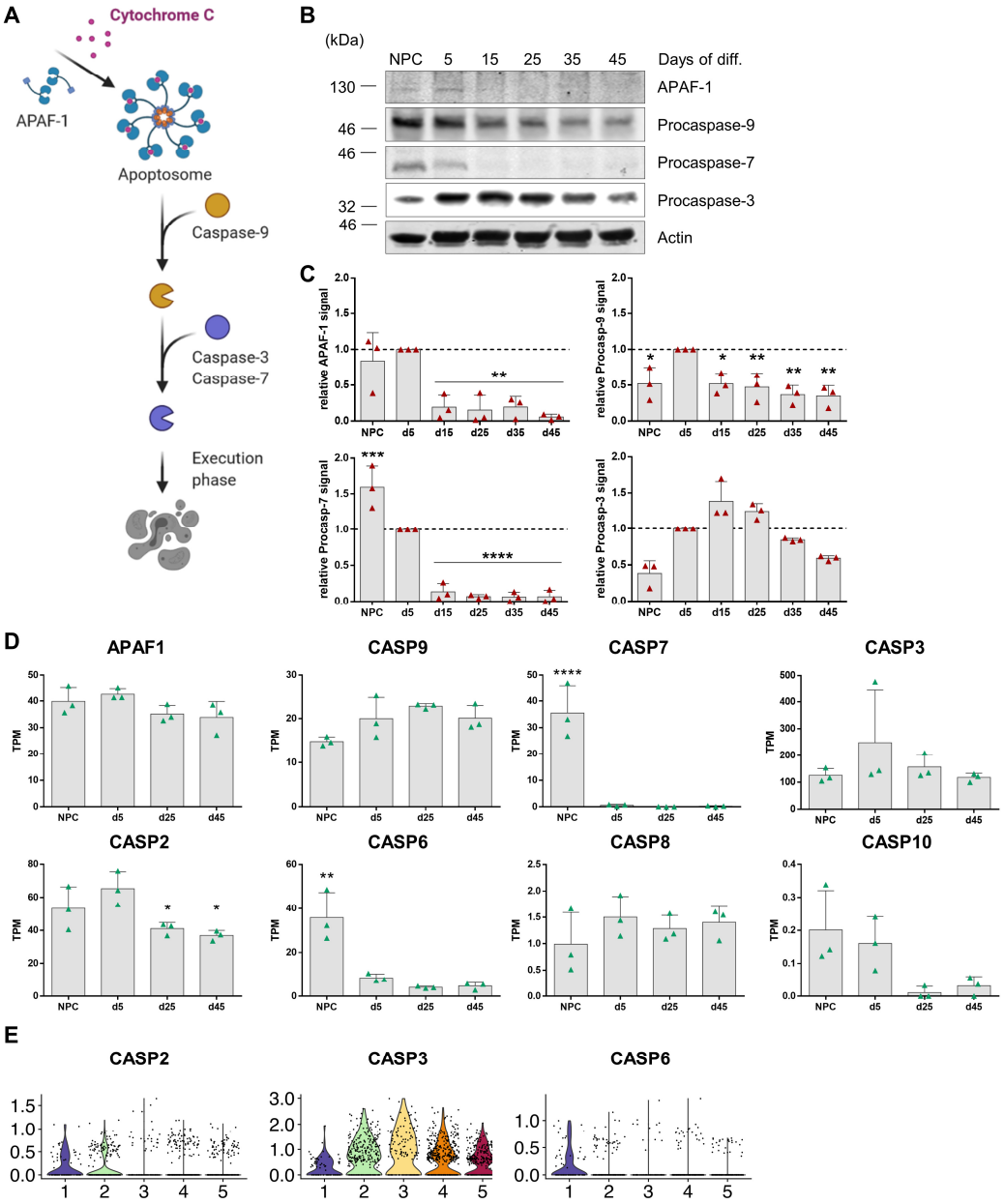

Fig. 19: Neuronal maturation is accompanied by a downregulation of caspases.

(**A**) Schematic representation of key events within the signaling cascade of the intrinsic apoptosis pathway. Apoptosome assembly requires release of Cytochrome c from mitochondria. The apoptosome enables activation of Caspase-9 which subsequently activates downstream effector caspases. The latter initiate the execution phase of apoptosis which entails DNA fragmentation and breakdown of the cellular architecture. (**B**) Representative Western blots of the indicated proteins of the intrinsic apoptosis pathway. (**C**) Quantification of relative protein signal intensities of the Western blots shown in (B) based on n = 3 biological replicates of independent differentiations. Signal intensities were first normalized to respective actin bands and then to the value of d5 immature neurons (dashed line) which also served as a reference point for statistical analysis. (**D**) Bulk RNAseq expression data for *APAF1* and major caspases of the intrinsic and extrinsic apoptosis pathway. Note different magnitudes of normalized expression (TPM) on y-axis. Expression of *CASP8* and *CASP10* was barely detectable. Bar graphs show mean with S.D., one-way ANOVA with Bonferroni correction. (**E**) Violin plots showing a maturation-dependent decrease in the expression of the indicated caspases. Violin plots indicate normalized counts.

Expression of *CASP6* was highest in NPCs and more broadly downregulated in neuronal cultures independently of maturation state (Fig. 19D, E). The two major caspases of the extrinsic apoptosis pathway, caspase-8 and -10, were expressed at very low levels in NPCs and neurons.

These findings corroborate that global changes in the availability of proapoptotic caspases take place during neuronal maturation. Even though changes on the transcript level were observed, altered gene expression is most likely not the only mechanism at play. For example, *CASP9* expression appeared to be largely unchanged whereas Procaspase-9 protein levels decreased significantly as neurons matured. This suggested an additional involvement of further regulatory mechanisms aside from transcriptional control. Regulation of the proapoptotic potential of APAF-1 and Caspase-9 can also be achieved by alternative splicing of the respective full-length mRNA transcripts. *APAF1* mRNA lacking exon 18 encodes an APAF-1 variant that is unable to oligomerize and to bind Caspase-9 (Benedict *et al.*, 2000). Exclusion of Exons 3-6 from *CASP9* mRNA produces a catalytically inactive variant called Caspase-9b (Seol & Billiar, 1999; Srinivasula *et al.*, 1999) (Fig. 20A). RT-PCR was used to examine possible changes in the splicing pattern of *APAF1* and *CASP9* mRNA. However, a significant switch in the distribution of splicing variants throughout neuronal maturation was not detectable (Fig. 20B). For both proteins, the full-length splicing variant remained prevalent.

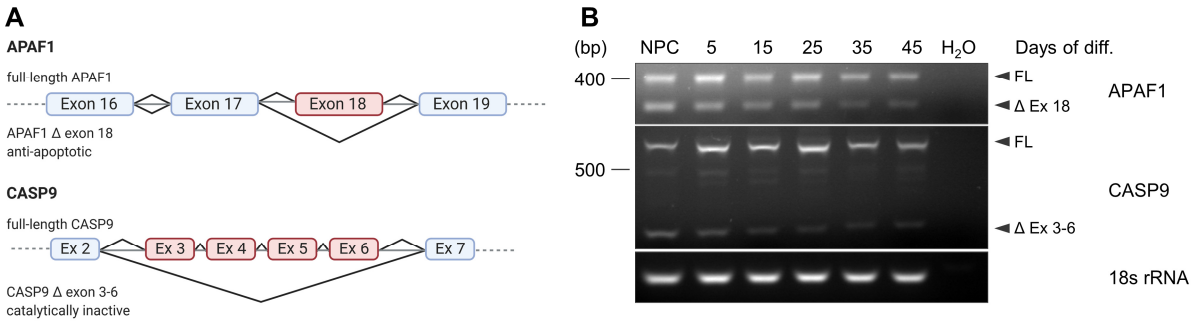

Fig. 20: *APAF1* and *CASP9* are not significantly regulated by alternative splicing during neuronal maturation.

(**A**) Schematic representation of *APAF1* and *CASP9* gene structure. Full-length variants of both proteins contain all indicated exons and possess proapoptotic potential. Alternative splice variants lacking exons marked in red are missing important structural components and are consequently unable to exert their apoptotic function. (**B**) Agarose gel of RT-PCR products evaluating alternative splicing of *APAF1* and *CASP9*. Neuronal maturation does not cause a major shift in the ratio of pro- and antiapoptotic splicing variants. Ex: exon, FL: full-length.

Interestingly, neuronal maturation was accompanied by a general upregulation of genes involved in the suppression of apoptosis while genes mediating the execution phase of apoptosis were downregulated (Fig. 21A, B). The execution phase of apoptosis is initiated following the activation of effector caspases. A prominent downstream target of Caspase-3 is PARP-1 which usually plays an

important role in DNA repair processes but is inactivated during the execution phase of apoptosis. PARP-1 protein levels were markedly decreased during neuronal maturation (Fig. 21C) and this trend was mirrored by bulk and single-cell RNA expression data (Fig. 21D).

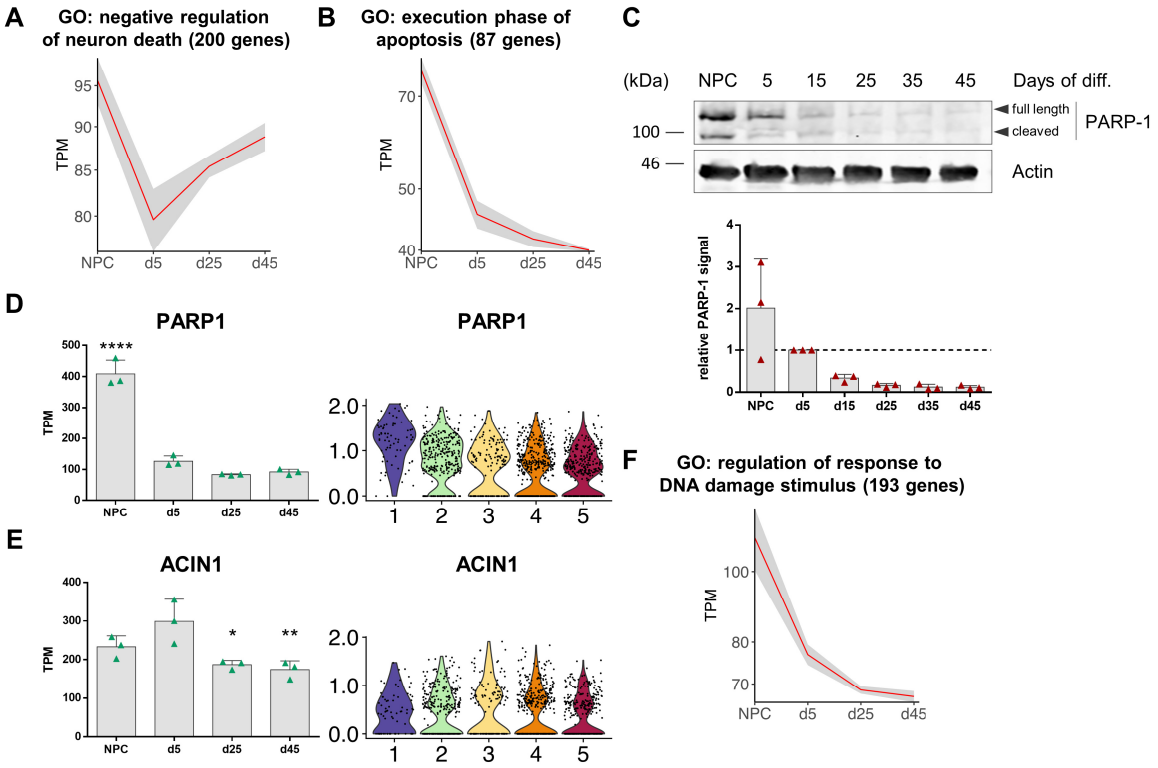

Fig. 21: Neuronal maturation leads to a downregulation of proteins involved in the execution phase of apoptosis.

(**A**, **B**, **F**) Show mean temporal expression pattern of genes belonging to the indicated GO terms based on TPM counts. Error bar shaded in grey indicates S.D. (**A**) Neuronal maturation is accompanied by a global upregulation of genes restricting neuron death and a (**B**) downregulation of genes orchestrating the execution phase of apoptosis. (**C**) Representative Western blot of the Caspase-3 downstream target PARP-1 and corresponding quantification of relative protein signal intensity of n = 3 independent experiments. Note: Statistical significance was not reached in one-way ANOVA with Bonferroni correction due to the high S.D. within the NPC triplicate. (**D**) Expression of *PARP1* is attenuated during neuronal maturation. Bar graph shows mean with S.D., one-way ANOVA with Bonferroni correction. (**E**) Expression of the Caspase-3 target apoptotic chromatin condensation inducer in the nucleus (*ACIN1*) also decreases during neuronal maturation. Bar graph indicates mean with S.D., one-way ANOVA with Bonferroni correction. (**F**) Neurons display a downregulation of genes involved in responses to DNA damage. RNAseq data analysis was done in collaboration with Dr. Anne Hoffrichter.

In parallel, more mature neurons displayed significantly lower expression of *ACIN1* (acinus), another Caspase-3 target (Fig. 21E). During apoptosis, acinus is cleaved by Caspase-3 and then triggers chromatin condensation in preparation for programmed cell death (Sahara *et al.*, 1999). Similar to

PARP-1, neuronal maturation also led to a downregulation of a broad range of further genes encoding factors involved in the response to DNA damage (Fig. 21F).

Taken together, these data highlight that neuronal maturation causes a restriction of the intrinsic apoptosis pathway at various levels of the signaling cascade. Apoptosome formation is inhibited by a decreased availability of APAF-1 and Caspase-9, increasing the threshold for activation of downstream effector caspases which are themselves downregulated as well. Finally, progression of apoptosis is hindered by a scarcity of proteins mediating the eventual breakdown of cellular integrity.

7.3.2 Neuronal maturation increases the threshold for mitochondrial outer membrane permeabilization

Upstream of apoptosome formation and effector caspase activation, mitochondria play a central role in the initiation of the intrinsic apoptosis pathway. Stress stimuli promote the oligomerization of the BCL-2 family proteins BAX and BAK enabling them to form pores in the outer mitochondrial membrane. This membrane permeabilization enables Cytochrome c and other mitochondrial proapoptotic constituents to enter the cytosol. However, pore formation may be prevented by the antagonistic action of the pro-survival protein BCL-2 (Fig. 22A). Thus, the balance between pro- and antiapoptotic BCL-2 family proteins is decisive for the apoptosis competence of cells. In the investigated neuronal cultures, protein levels of BAX were highest at d5 of differentiation and decreased by about 60% until d45 (Fig. 22B). Conversely, BCL-2 was barely detectable at d5 but had increased about 2.5-fold by the time neuronal cultures reached d45 of differentiation. This observation was supported by RNAseq data which showed a pronounced drop in the expression of *BCL2* from NPCs to d5 neuronal cultures followed by a strong rebound with advancing maturation. In parallel, *BAX* expression steadily declined. Even though the total transcript counts of *BAX* remained higher than counts for *BCL2* during the investigated time frame of maturation (Fig. 22C, D), these changes potently shifted the balance in favor of cell survival. This effect was even more enhanced by the simultaneous downregulation of *BAK1*, the second pore-forming BCL-2 protein (Fig. 22E, F). Of the pro-survival BCL-2 proteins Bcl-xL (*BCL2L1*) and Bcl-w (*BCL2L2*) were more strongly expressed in neurons at all stages than in NPCs, whereas *MCL1* seemed to be of special importance solely for the protection of NPCs and was attenuated during neuronal maturation (Fig. 22E). Expression of the proapoptotic BH3-only proteins encoded by *BCL2L11*, *PMAIP1* and *BMF* was highest in NPCs and significantly lower in neuronal cultures.

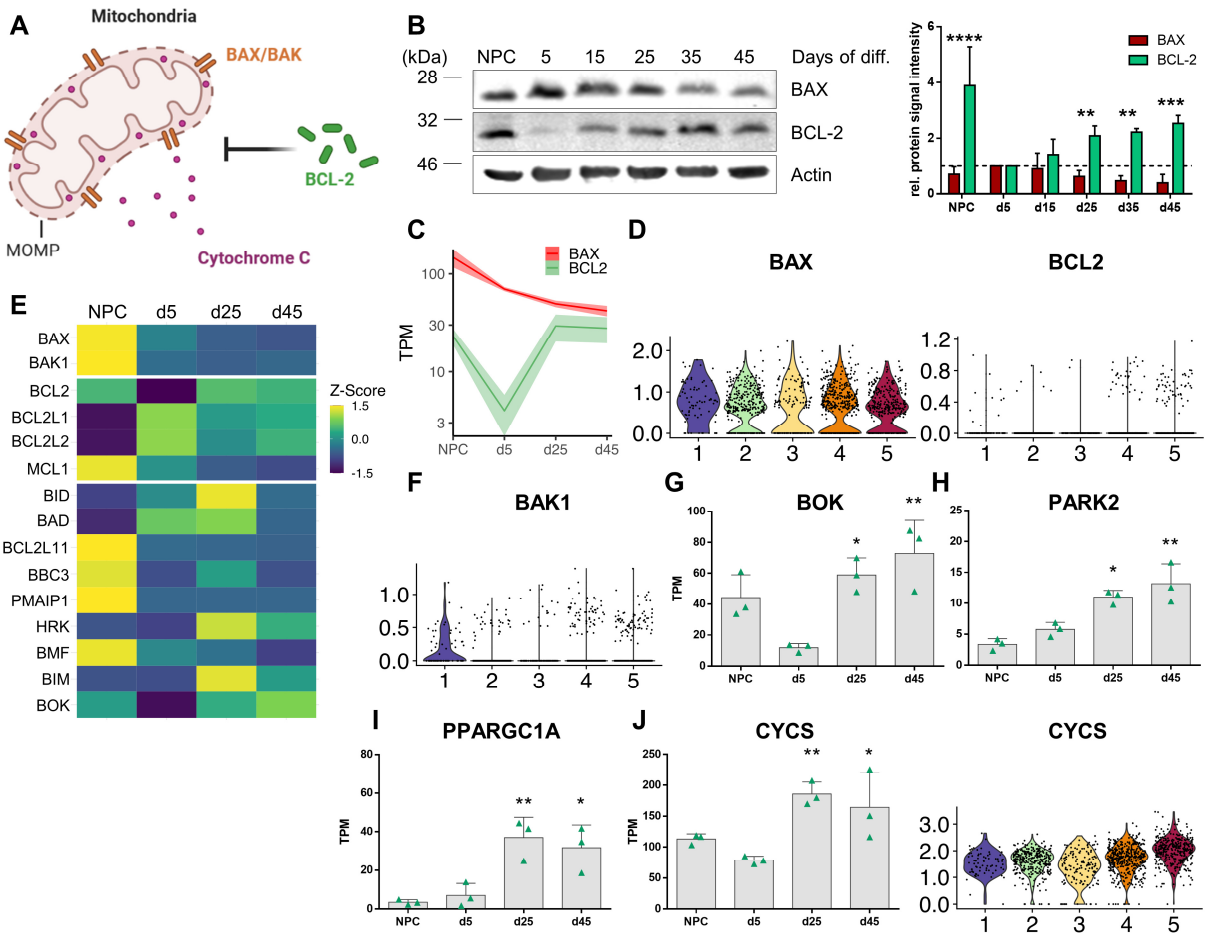

Fig. 22: Neuronal maturation increases the threshold for mitochondrial outer membrane permeabilization.

(**A**) The intrinsic apoptosis pathway is initiated by oligomerization and pore-formation of BAX and BAK in the outer mitochondrial membrane. This permeabilization allows release of Cytochrome c into the cytosol. Pore assembly may be prevented by antiapoptotic BCL-2. (**B**) Representative Western blots and corresponding quantification of relative protein signals (n = 3) showing changes in BAX and BCL-2 protein levels during neuronal maturation. Bar graph shows mean with S.D., one-way ANOVA with Bonferroni correction. (**C**) TPM-normalized mean temporal expression of *BAX* (red) and *BCL2* (green). Shaded error bar indicates S.D. (**D**) Violin plots showing cluster-specific expression of *BAX* and *BCL2* in scRNAseq. (**E**) Heat map (z-scaled) showing expression of pro- and antiapoptotic BCL-2 family members throughout neuronal maturation. (**F**) Violin plot highlighting downregulation of *BAK1* expression during neuronal maturation. (**G**) The BCL-2 protein BOK is tightly restricted in d5 neuronal cultures but strongly upregulated thereafter. (**H**) Expression of the mitochondrial ubiquitin E3 ligase Parkin (*PARK2*) is increased in more mature neuronal cultures. (**I**) Neuronal maturation is accompanied by a strongly elevated production of mitochondria. This is indicated by the increased expression of *PPARGC1A*, the master regulator of mitochondrial biogenesis. (**J**) Increased numbers of mitochondria lead to increased levels of Cytochrome c in more mature neurons. Bar graphs (G-J) show means with S.D., statistical comparison to d5 neurons using one-way ANOVA with Bonferroni's multiple comparison test. Violin plots indicate normalized counts. RNAseq data analysis was done in collaboration with Dr. Anne Hoffrichter.

Interestingly, expression of *BOK* was minimal in d5 neuronal cultures but significantly increased as neurons matured (Fig. 22E, G). The role of BOK in apoptosis is still subject to debate. Due to its structural similarity to BAX and BAK, it has been suggested as a third pore-forming proapoptotic BCL-2 protein (Fernández-Marrero *et al.*, 2017). However, it has been reported to fulfill cytoprotective functions in neurons (Orsi *et al.*, 2016). Of note, more mature neurons also expressed significantly higher levels of the mitochondrial E3 ubiquitin ligase parkin (*PARK2*) than immature neuronal cultures (Fig. 22H). Interestingly, parkin ubiquitinates both, BAX and BCL-2, but with opposing effects. Whereas ubiquitination of BAX by parkin causes degradation of BAX (Johnson *et al.*, 2012), steady-state levels of BCL-2 are increased after ubiquitination by parkin (Chen *et al.*, 2010). Potentially, increased *PARK2* expression is a side-effect of the strong increase in the number of mitochondria during neuronal maturation which is illustrated by a marked upregulation of *PPARGC1A*, the key regulator of mitochondrial biogenesis (Fig. 22I). Higher mitochondria count and the metabolic reliance on oxidative phosphorylation result in elevated levels of Cytochrome c in more mature neurons (Fig. 22J). This may be one of the reasons that necessitate a tight regulation of MOMP which is achieved in mature neurons by the observed beneficial changes in the balance of pro- and antiapoptotic BCL-2 proteins. An increased threshold for MOMP improves the survival competency of mature neurons by preventing a subsequent downstream activation of the intrinsic apoptosis pathway.

7.3.3 The protective potential of XIAP is enhanced in mature neurons

A prominent proapoptotic protein that does not belong to the BCL-2 protein family is SMAC/DIABLO. It acts as an antagonist of inhibitor of apoptosis proteins (IAPs) by binding them and thereby preventing them from inactivating their proapoptotic target proteins. SMAC/DIABLO localizes to mitochondria from which it is released together with Cytochrome c upon initiation of the intrinsic apoptosis pathway.

Surprisingly, Western blots revealed a strongly increased high molecular weight species detected by anti-SMAC antibody in lysates of neuronal cultures at multiple time points of differentiation (Fig. 23A). Usually, unmodified mature SMAC protein migrates at about 21 kDa. However, an additional band at about 48 kDa and a high molecular weight smear above it were observed, both of which increased in intensity as neurons matured. This pattern closely resembled previously published Western blot results from studies investigating the interaction partners involved in ubiquitination of SMAC (Macfarlane *et al.*, 2002; Hu & Yang, 2003; Morizane *et al.*, 2005; Ma *et al.*, 2006). Poly-ubiquitinated Smac was almost undetectable in immature neuronal cultures but was strongly increased in mature neurons. Accordingly, inhibition of protein degradation with the proteasome inhibitor MG132 tended to increase protein levels of Smac in mature but not in immature neuronal cultures (Fig. 23B).

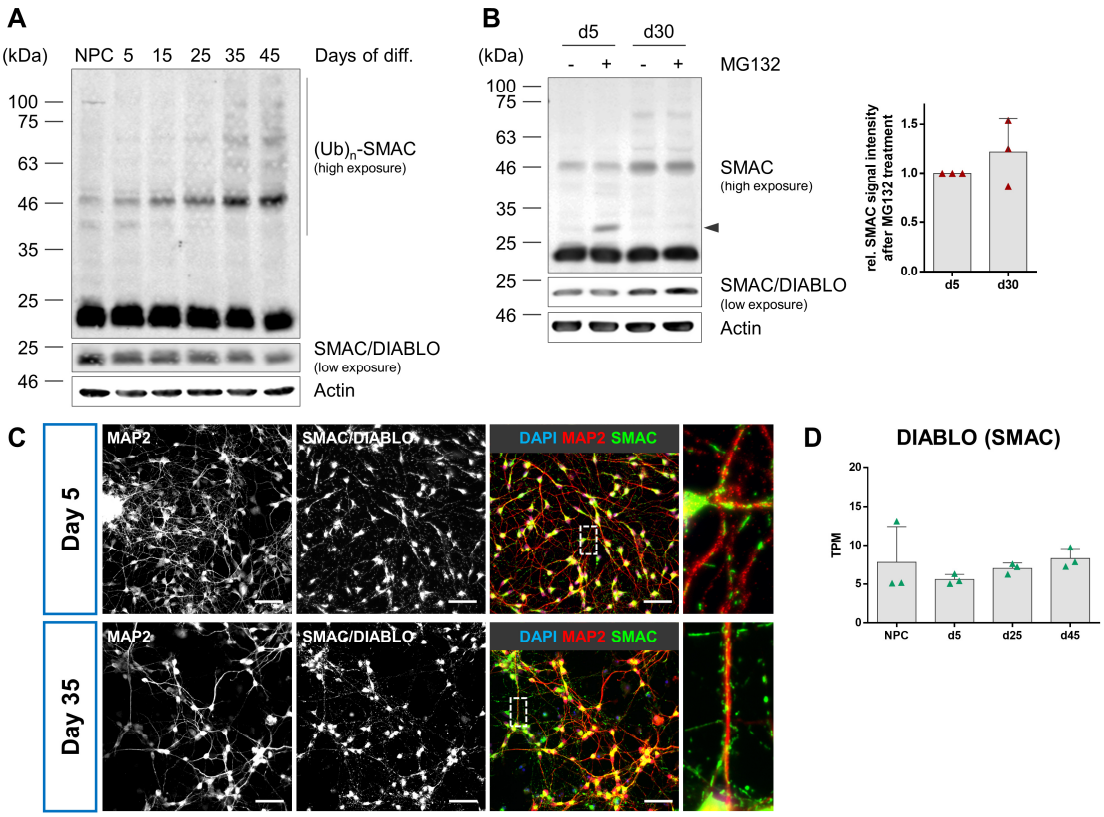

Fig. 23: The IAP antagonist SMAC/DIABLO is increasingly ubiquitinated during neuronal maturation.

(**A**) Representative Western blot of SMAC at different stages of neuronal maturation. Top panel shows complete image of the cropped middle panel with longer exposure time to reveal increasing ubiquitination of SMAC. (**B**) Western blot of neuronal cultures treated with 5 µM MG132 for 12 h at d5 and d30. Arrowhead indicates unprocessed precursor of SMAC. Bar graph shows mean with S.D. of n = 3 experiments. Not significant, two-tailed t test. (**C**) Representative immunofluorescence microscopy images of d5 and d35 neuronal cultures. SMAC was readily detectable at both stages and localized to elongated subcellular compartments, likely mitochondria. (**D**) Expression of *DIABLO* marginally increased as neurons matured, possibly a side-effect of higher mitochondrial biogenesis. Bar graph shows mean with S.D., no statistically significant differences detected by one-way ANOVA with Bonferroni correction.

Interestingly, exposure to MG132 also led to an accumulation of the unprocessed precursor of SMAC in immature but not in mature neurons. Immunofluorescence microscopy of neuronal cultures at d5 and d35 of differentiation did not show obvious differences in the intracellular distribution of SMAC which localized to slightly elongated subcellular structures in the soma and neurites (Fig. 23C). Presumably, these structures were mitochondria since SMAC is synthesized with an N-terminal mitochondrial targeting sequence and no other subcellular localization of SMAC has so far been reported. Expression of *DIABLO* increased slightly, yet not significantly, during neuronal maturation (Fig. 23D). Based on the strongly increased mitochondrial biogenesis in mature neurons, a proportionally higher expression of *DIABLO* could also have been expected.

To identify a potential source for the increased ubiquitination of SMAC/DIABLO, the expression levels of known SMAC E3 ubiquitin ligases were examined. Most of the candidate genes belong to the BIRC family of genes which encode IAPs. Expression of *BIRC3* (cIAP-2) and *BIRC7* (Livin) was neither detectable in bulk nor single-cell RNAseq (data not shown). *BIRC2* (cIAP1) was highly expressed at all stages of neuronal maturation but did not reveal any apparent trends (Fig. 24A, B). Notably, expression of *BIRC4* (XIAP) was elevated in bulk RNA of more mature neurons at d25 and d45. This effect was even more pronounced in scRNAseq analysis in which cluster 5 contained the most cells with *BIRC4* expression.

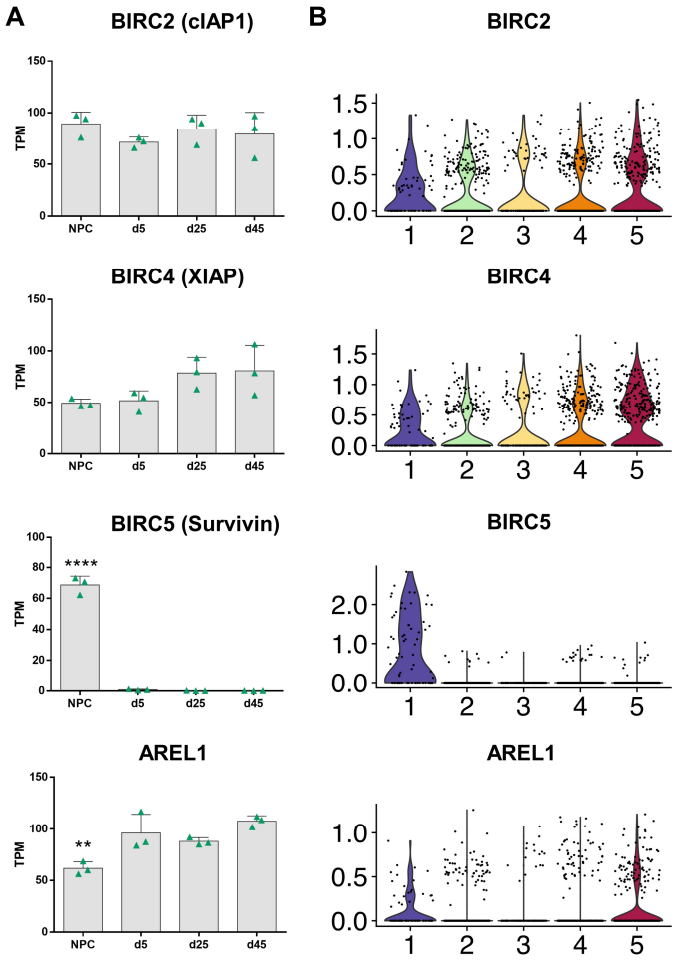

Fig. 24: Expression of potential SMAC/DIABLO ubiquitin E3 ligases during neuronal maturation.

(**A**) Bulk and (**B**) single-cell RNAseq expression data of reported SMAC/DIABLO ubiquitin E3 ligases during neuronal maturation. Expression of *BIRC4* (XIAP) was most clearly upregulated in bulk and single-cell RNAseq data of mature neurons. Bar graphs show mean with S.D., one-way ANOVA with Bonferroni correction. Violin plots indicate normalized counts.

Expression of BIRC5 (Survivin) was strong in NPCs but abrogated in neuronal cultures already at the beginning of maturation. The only known SMAC ubiquitin ligase outside of the IAP family is AREL1 (Kim *et al.*, 2013). Expression of *AREL1* was generally increased in bulk cultures of neurons compared to NPCs. Neuronal cultures at d45 reached the highest mean expression by a slight margin.

This difference was more obvious in the scRNAseq data in which the percentage of cells with detectable *AREL1* expression was highest in cluster 5 formed by the most mature neurons.

Since bulk and single-cell RNAseq results showed the strongest trends for XIAP as a promising candidate, its potential involvement in neuroprotection was subsequently further analyzed in more detail. XIAP is the only IAP that is known to directly bind and inhibit the activity of Caspases-3, -7 and -9. First, the levels of XIAP protein throughout neuronal maturation were examined by Western blotting (Fig. 25A). Interestingly, XIAP was not present in NPCs even though XIAP mRNA was readily detectable in bulk and single-cell transcriptomics. This discrepancy may hint at post-translationally regulated degradation of XIAP in NPCs. XIAP appeared in Western blots from d5 onward and increased about 4-fold until d45.

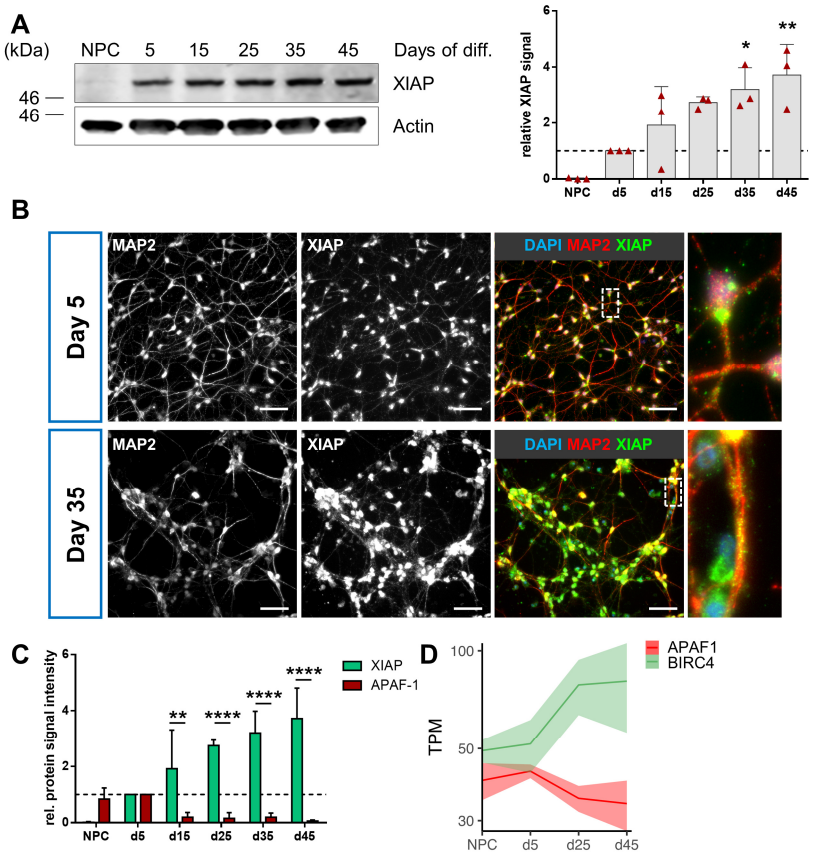

Fig. 25: Mature human forebrain neurons possess increased XIAP protein levels.

(**A**) Exemplary Western blot of XIAP protein level throughout neuronal maturation. More mature neurons display higher protein levels of XIAP. Quantification shows relative XIAP signal normalized to d5 cultures (dashed line). Bar graph shows mean with S.D., one-way ANOVA with Bonferroni correction. (**B**) Representative fluorescence microscopy images of d5 and d35 neuronal cultures. Note higher abundance of XIAP in neurites of neurons at d35. White dashed boxes highlight area of the zoom-in on the right. Scale bars: 50 µm. (**C**) Comparison of the development of APAF-1 and XIAP protein levels at different time points of neuronal maturation. (**D**) Mean temporal expression pattern of *APAF1* and *BIRC4* (XIAP) in TPM showing opposite trends of regulation. Shaded area indicates S.D.

In immunofluorescence stainings, XIAP was detectable in d5 and d35 neuronal cultures in the soma and neurites (Fig. 25B). These stainings supported the notion that the abundance of XIAP strongly increased during neuronal maturation. As a result of increased *BIRC4* levels and decreased *APAF1* expression, the XIAP to APAF-1 ratio is favorably altered in mature neurons (Fig. 25C, D). This ratio may serve as an indicator to estimate the relative threshold for the activation of caspases. Low availability of APAF-1 reduces the likelihood for apoptosome formation and thus initiation of the caspase cascade. Simultaneously, increased XIAP levels guarantee a fast inhibition of caspases in case they are activated anyhow.

Since mature neurons displayed a strong increase in XIAP levels, it was of interest to investigate whether expression of XIAP interaction partners was also altered. Thus, the expression of established XIAP antagonists was analyzed. These proteins are able to promote apoptosis indirectly by undermining XIAP pro-survival activity. Surprisingly, *XAF1* mRNA was almost completely absent from all of our samples in bulk and single-cell transcriptomics (Fig. 26A). XAF-1 (XIAP associated factor 1) is a proapoptotic protein that derives its name from its interaction with XIAP.

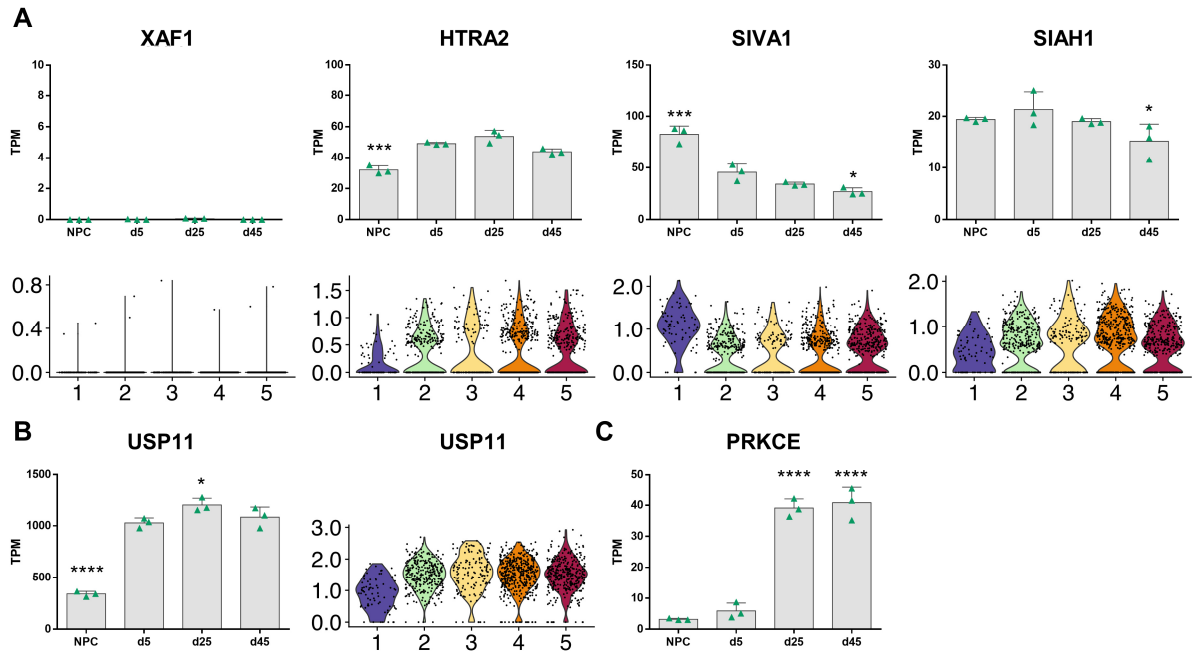

Fig. 26: Expression patterns of XIAP antagonists and stabilizers.

(**A**) Bulk and single-cell RNAseq expression data of known XIAP antagonists show a trend towards decreased expression in more mature neurons. (**B**) Expression of ubiquitin-specific protease 11 (*USP11*) is increased in neurons compared to NPCs. (**C**) Expression of *PRKCE* is strongly upregulated at later stages of neuronal maturation. USP11 and PKCε may stabilize steady-state levels of XIAP protein in mature neurons. All bar graphs display means with S.D., statistical significance calculated compared to d5, one-way ANOVA with Bonferroni correction. Violin plots indicate normalized counts. RNAseq data analysis was done in collaboration with Dr. Anne Hoffrichter.

Additionally, neuronal cultures at day 45 expressed lower levels of *HTRA2* than at day 5. HtrA2 is a mitochondrial serine protease with the ability to cleave XIAP to prevent it from interacting with caspases (Srinivasula *et al.*, 2003; Yang *et al.*, 2003). Like for *DIABLO*, the strongly increased mitochondrial biogenesis in mature neurons was not accompanied by a similarly large increase in the expression of *HTRA2*. Furthermore, mature neurons at d45 displayed significantly reduced levels of *SIVA1* transcripts compared to d5 neuronal cultures (Fig. 26A). SIVA-1 exerts its proapoptotic function by promoting XIAP ubiquitination and degradation (Coccia *et al.*, 2020). Another pathway for XIAP degradation requires the protein SIAH-1, an E3 ligase with the capability to directly ubiquitinate XIAP. Notably, cells lacking SIAH-1 have been shown to possess elevated steady-state levels of XIAP (Garrison *et al.*, 2011). In relation to d5 neuronal cultures, more mature cultures at d45 expressed significantly less *SIAH1*.

Aside from a beneficial modulation of XIAP antagonists, mature neurons may also profit from actively stabilizing XIAP protein. In this context two candidate genes seemed especially promising based on the obtained RNAseq data sets. As noted above, XIAP protein was only detectable in neuronal cultures but not in NPCs even though expression levels were almost identical in NPCs and d5 neuronal cultures (Fig. 24A, B). Interestingly, neuronal cultures displayed almost a 3-fold increase in the expression of the ubiquitin-specific protease 11 (USP11) (Fig. 26A). USPs catalytically remove ubiquitin chains from target proteins and are therefore able to prevent their degradation via the ubiquitin-proteasome system. Recently, USP11 has been shown to fulfill this role in the regulation of XIAP turnover (Zhou *et al.*, 2017). Consequently, elevated levels of USP11 may prevent degradation of XIAP in neurons but its reduced availability may XIAP removal in NPCs.

A second notable XIAP stabilizer is protein kinase C epsilon (PKCε), encoded by the *PRKCE* gene. PKCε maintains XIAP protein levels via phosphorylation (Kato *et al.*, 2011). It was more than 6-fold upregulated in mature compared to immature neurons, presumably due to its involvement in synapse formation and function (Fig. 26C). PKCε signaling may therefore offer an avenue for cytoprotection in mature neurons.

Together, these data reveal an increasingly tight regulation of proapoptotic SMAC and highlight the importance of XIAP in promoting survival of mature human neurons. Not only do levels of XIAP protein increase as neurons mature but also a number of known XIAP antagonists are concurrently downregulated. These adaptations synergize to cause a maturation-dependent increase in the protective potential of XIAP.

7.3.4 Neuronal maturation provides an increased protein folding capacity

Investigation of global transcriptomic trends during neuronal maturation revealed a time-dependent upregulation of genes involved in the regulation of protein stability and protein folding (Fig. 27A). Expression profiles of GRP78/BiP (*HSPA5*), HSP27 (*HSPB1*) and HSP90β (*HSPB90AB1*) showed similar trajectories (Fig. 27B). All three chaperones were most widely expressed in NPCs, strongly downregulated in immature neurons and finally re-expressed as neuronal maturation proceeded. An increased capability to maintain protein homeostasis may therefore be an additional survival advantage of mature over immature neurons.

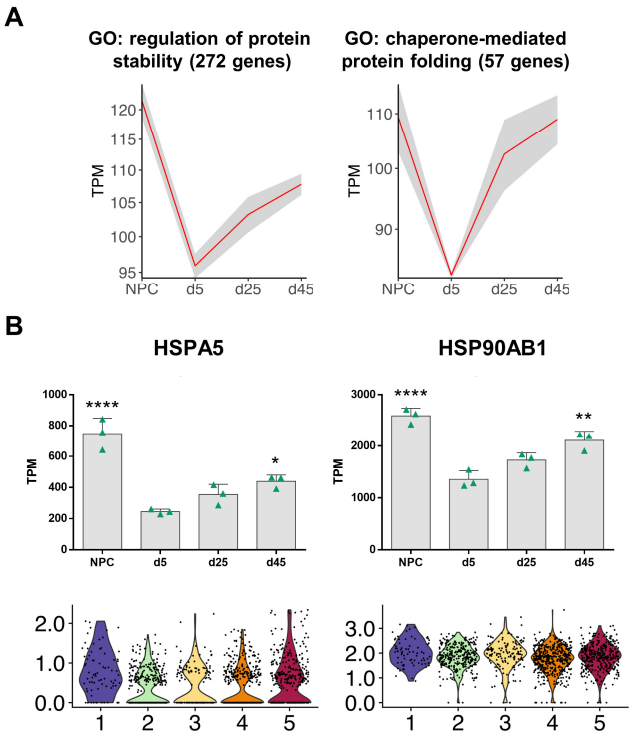

Fig. 27: Neuronal maturation increases the capacity for the maintenance of the cellular proteome.

(**A**) Temporal gene expression pattern of genes summarized under the indicated GO terms related to maintenance of proteostasis. Shaded error bar highlights S.D. (**B**) Bulk and single-cell RNAseq expression pattern of the indicated heat-shock proteins reveals a downregulation at initial stages of maturation and an upregulation at later time points. Mature neurons therefore possess an increased protein folding capacity. Bar graphs show mean with S.D., statistical significance in relation to d5, one-way ANOVA with Bonferroni correction. Violin plots indicate normalized counts. RNAseq data analysis was done in collaboration with Dr. Anne Hoffrichter.

7.3.5 Mature human neurons are highly resistant to a wide range of cellular insults

Based on the described range of pro-survival adaptations in mature neurons, they could be expected to display an increased resistance towards cellular stress compared to their immature counterparts. To test this hypothesis, immature and mature neuronal cultures were exposed to different stress stimuli and their viability was monitored for an extended period. Neurons were challenged by disruption of different cellular processes.

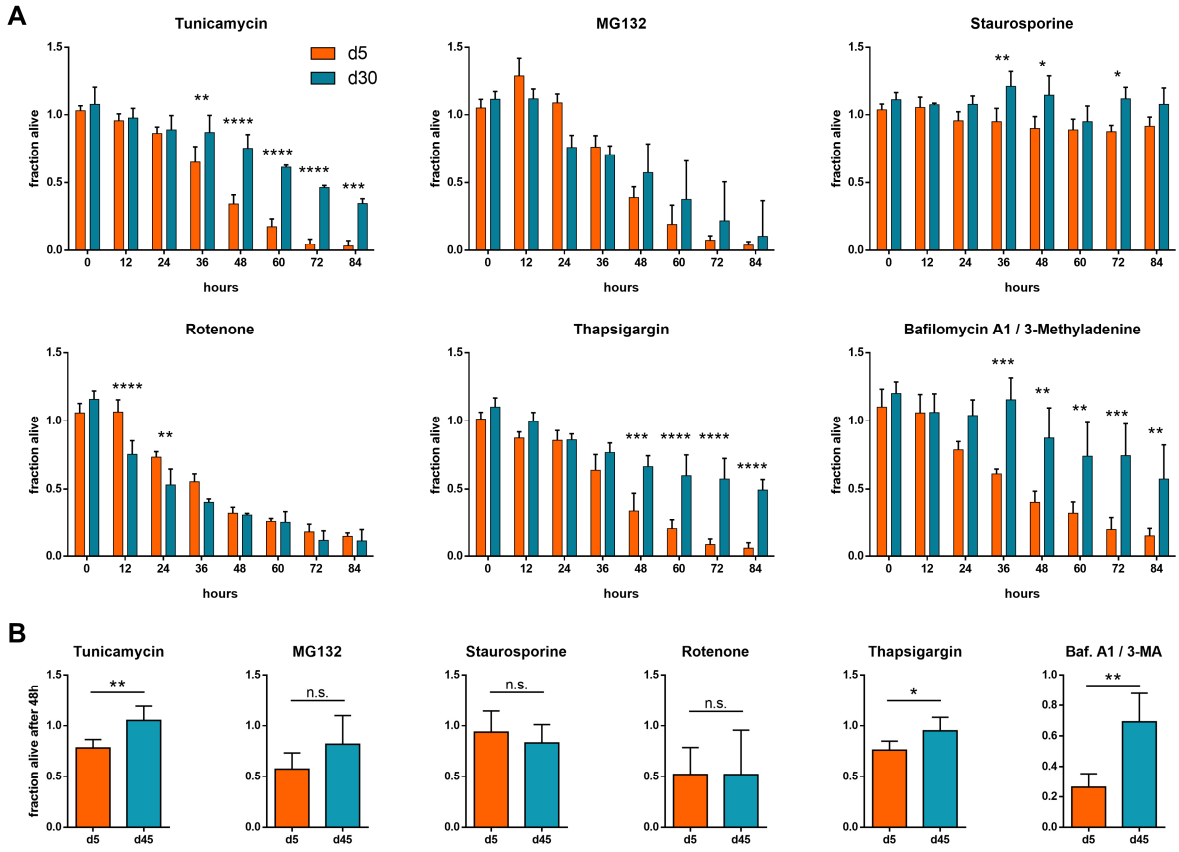

Fig. 28: Mature neurons possess an enhanced resistance against a wide range of cellular stressors.

(**A**) Orangu™ cell viability assay of d5 and d30 neuronal cultures exposed to the indicated stressor molecules for 84 h. In this assay, cell viability is determined based on activity of cellular dehydrogenases. Stressor concentrations were: TM 1.0 µM, MG132 0.5 µM, STS 50 nM, rotenone 2.5 µM, TG 1.0 µM, Baf. A1/3-MA 15 nM/2 mM. Bar graphs show mean with S.D. of the fraction of viable cells normalized to respective DMSO-treated control cells. n = 3 independent experiments. One-way ANOVA with Bonferroni correction. (**B**) CellTiter-Glo™ cell viability assay of d5 and d45 neuronal cultures treated for 48 h with the indicated stressors. Results from n ≥ 3 independent experiments. Stressor concentrations as above, except: TM and TG 0.5 µM. Bar graphs show mean with S.D., two-tailed t test. More mature neuronal cultures possess a higher survival competence than immature neuronal cultures under the tested conditions.

Tunicamycin (TM) was used to inhibit N-glycosylation of proteins, the proteasome inhibitor MG132 to prevent protein turnover, staurosporine (STS) to inhibit the activity of protein kinases, rotenone to interfere with the mitochondrial electron transport chain to cause oxidative stress, thapsigargin (TG) to disrupt the Ca^{2+} homeostasis of the ER and a combination of bafilomycin A1 (baf. A1) and 3-methyladenine (3-MA) to inhibit autophagic flux. Viability of mature (d30, d45) and immature neuronal cultures at d5 were determined using Orangu™ and CellTiter-Glo™ (CTG) assays (Fig. 28A, B). Orangu™ viability assays of d5 and d30 neuronal cultures were conducted over 84 hours with measurements in 12 h intervals. Viability of immature neuronal cultures in the presence of TM began to decrease significantly after 36 h. Survival of mature neuronal cultures was significantly higher with 46.3 ± 1.5% remaining after 72 h compared to 4.7 ± 3.8% in immature cultures. Similarly, d45 neuronal cultures persisted significantly better than d5 cultures in CTG assays after 48 h of exposure to TM (Fig. 28B). A similar trend was observable during treatment with MG132 but this effect was less pronounced and the differences in cell survival did not reach statistical significance. Additionally, neuronal cultures proved quite resistant to STS independent of their stage of maturation. Surprisingly, viability of mature and immature neurons was equally affected by rotenone. This was remarkable since rotenone disrupts mitochondria and the electron transport chain on which mature neurons rely much more heavily for oxidative phosphorylation. Consequently, mature neurons could have been expected to be more susceptible to rotenone exposure than immature neurons but this did not seem to be the case. Furthermore, TG caused a strong decline in the viability of immature neuronal cultures but the toxic effect was dampened in mature neurons. After 84 h, viability of d5 cultures had fallen to 6.0 ± 4.0% compared to 49.3 ± 7.6% in d30 neuronal cultures. Finally, mature neurons coped significantly better with an interruption of autophagic flux by baf. A1/3-MA. Viability of immature and mature neuronal cultures accumulated to 29.6 ± 6.5% vs 70.0 ± 20.6% after 48 h in CTG assays and 19.7 ± 8.7% vs 74.3 ± 23.5% after 72 h in Orangu™ assays.

These results highlight that neuronal maturation indeed confers a broadly increased stress resistance to prevent accidental loss of neurons in established networks. This is achieved by various regulatory switches described above that reinforce cell survival at multiple levels of cellular homeostasis.

7.4 Activation of the HBP in the human neural lineage

Aside from intrinsic safety breaks provided by neuronal maturation, it is desirable to discover further means of protecting the central nervous system cellular insults. Recent publications have proclaimed that increased output by the hexosamine biosynthetic pathway (HBP) via GFAT-1 gain-of-function mutations or supplementation of GlcNAc confers cytoprotection through activation of the integrated stress response (ISR). To date, these effects were only observed in the nematode *C. elegans*, murine neuroblastoma cells and keratinocytes (Denzel *et al.*, 2014; Horn *et al.*, 2020; Ruegenberg *et al.*, 2020). Therefore, I sought to investigate the potentially protective effects of HBP activation in the human neural lineage.

7.4.1 CRISPR-Cas9-mediated generation of GFAT-1 gain-of-function hiPSCs

As the rate-limiting enzyme of the hexosamine pathway, glucosamine-fructose-6-phosphate aminotransferase isomerizing-1 (GFAT-1) is central for the generation of UDP-GlcNAc, the precursor building block for N-glycosylation of proteins. The group by Martin Denzel described a GFAT-1 gain-of-function (gof) variant which increases base-line activation of the ISR and boosts resistance to tunicamycin-induced cell stress (Denzel *et al.*, 2014; Horn *et al.*, 2020; Ruegenberg *et al.*, 2020). Structurally, the glycine to glutamate (Gly > Glu) mutation underlying the GFAT-1 gof is located in the linker region between its two catalytic domains and renders the resulting GFAT-1 variant more resistant to negative feedback inhibition without major detrimental effects on the reaction rate (Ruegenberg *et al.*, 2020). The stretch of amino acids within the GFAT-1 protein containing the Gly > Glu gof mutation is a highly conserved consensus sequence. The relevant glycine residue is located at position 451 of the protein (Fig. 29A) and is encoded by a GGC triplet starting from position 1,405 of the *GFPT1* coding sequence.

To investigate potential effects of the GFAT-1 G451E gof in the human neural lineage, I used CRISPR-Cas9-guided genome editing to introduce the relevant mutation in the endogenous *GFPT1* locus of hiPSCs from a healthy control subject. This use of isogenic cell lines enables specific investigation of the effects of the GFAT-1 G451E mutation without having to take into account other potential genetic differences or artefacts resulting from exogenous overexpression.

The site of the desired mutation also constituted a suitable PAM sequence for Cas9 targeting (Fig. 29B). A 145 bp long single-stranded oligonucleotide (ssoligo) harboring the required GC > AG base pair exchange was used as a repair template after Cas9-mediated DNA strand cleavage at the target site.

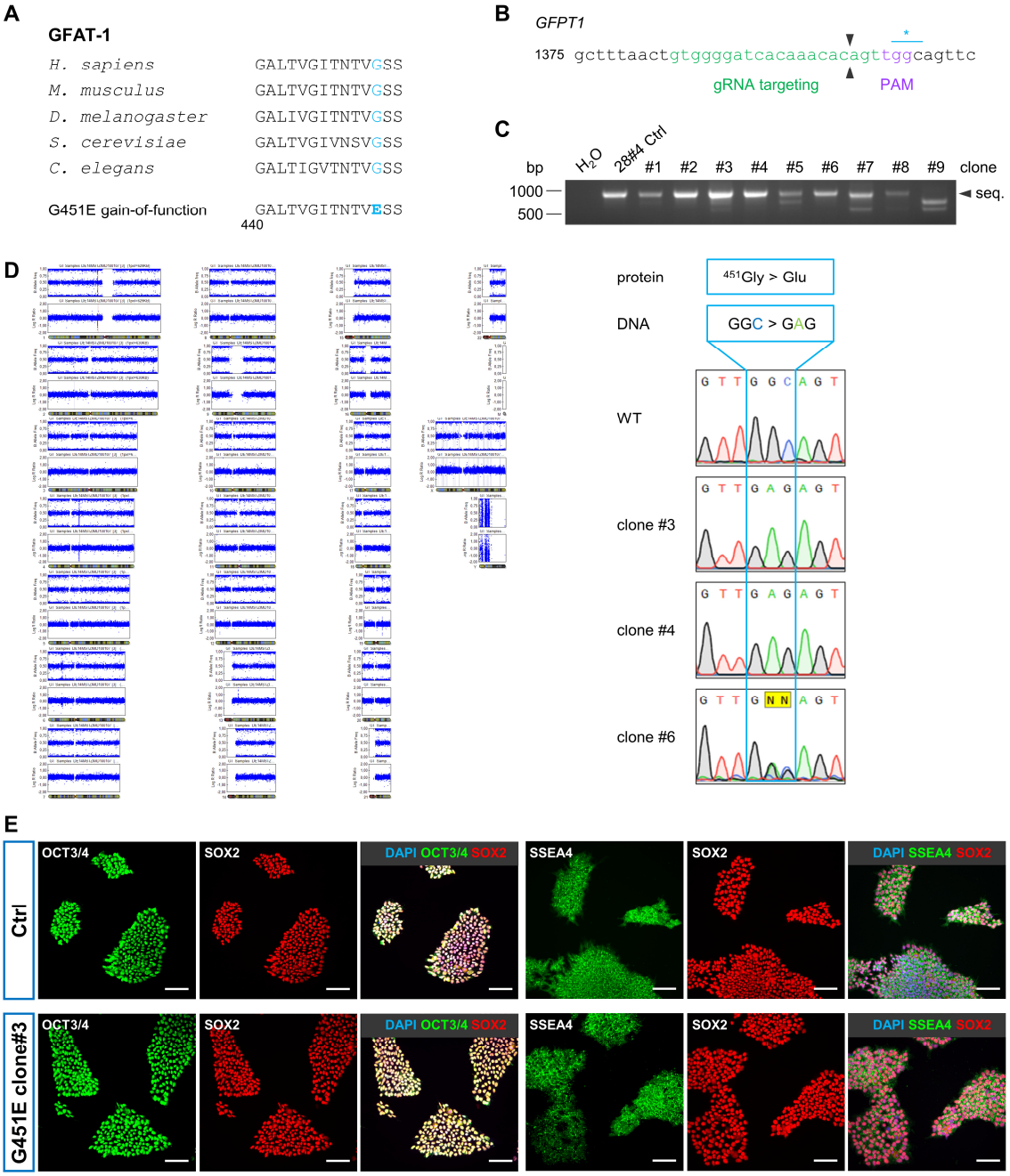

Fig. 29: Generation of hiPSCs with GFAT-1 G451E gain-of-function mutation.

(**A**) Excerpt from the alignment of the amino acid sequence of the GFAT-1 protein for the indicated species. The position of the amino acid exchange leading to the GFAT-1 gof variant is indicated in light blue. (**B**) DNA sequence within the *GFPT1* gene edited by CRISPR-Cas9 system. Cas9 gRNA recognition sequence ins indicated in green, the corresponding PAM sequence is highlighted in purple, blue line with star highlights the base triplet encoding glycine 451 in the GFAT-1 wild type protein. (**C**) RT-PCR for the identification of GFAT-1 G451E gof hiPSC clones. An 837 bp region surrounding the CRISPR-Cas9 target site was amplified. The band indicated by the black arrowhead was excised and analyzed by sanger sequencing. Chromatograms of sequences from clones #3, #4 and #6 revealed the desired mutation within the *GFPT1* gene. (**D**) Exemplary full genome SNP analysis of clone #3. The three validated hiPSC GFAT-1 gof clones did not display genomic alterations. (**E**) Representative fluorescence microscopy images of hiPSC cultures of the isogenic control and GFAT-1 G451E clone #3 highlighting the expression of the indicated canonical pluripotency markers. Scale bars: 100 µm.

Due to the GC > AG exchange, incorporation of the ssoligo removed the PAM sequence required for Cas9 binding and thus prevented repeated cleavage at the mutation site which increased the likelihood of a homozygous modification. As this approach was minimally invasive and did not involve a stable integration of a resistance gene, clones were transiently selected for 48 h with puromycin. After selection, a total of nine hiPSC clones remained. An 837 bp stretch of DNA surrounding the site of the desired GC > AG mutation was amplified from cDNA of all nine clones (Fig. 29C). The amplified DNA was extracted and analyzed by Sanger sequencing. Three of the nine clones harbored the desired nucleotide exchange without any further DNA alterations. The other six clones were either missing the GC > AG mutation or showed partial sequence deletions in the vicinity of the Cas9 targeting sequence.

Of the three positive clones, clones #3 and #4 possessed a homozygous mutation whereas clone #6 had one wildtype and one mutated allele. Alignment of the GFAT-1 protein sequence of isogenic controls and G451 mutants showed the desired Gly > Glu mutation but no additional amino acid exchanges (data not shown). To exclude unwanted off-target mutations introduced by the CRISPR-Cas9 system, all three clones were investigated for genomic and karyotypic integrity and analyzed for single nucleotide polymorphisms. None of the clones revealed marked genomic aberrations (Fig. 29D). To validate their normal developmental potential, hiPSCs of clones #3, #4 and #6 were stained for the pluripotency markers OCT3/4, SSEA4 and SOX2. Staining patterns for these markers in GFAT-1 G451E clones was identical to isogenic control cells (Fig. 29E). GFAT-1 G451E clones showed normal development when differentiated into NPCs and human forebrain neurons. Neuronal cultures matured as described before. They showed advanced separation of MAP2 and Tau as well as a nuclear signal for the mature neuron marker NeuN (Fig. 30A). *GFPT1* mRNA and GFAT-1 protein levels were not affected by the introduction of the G451E mutation (Fig. 30B, C).

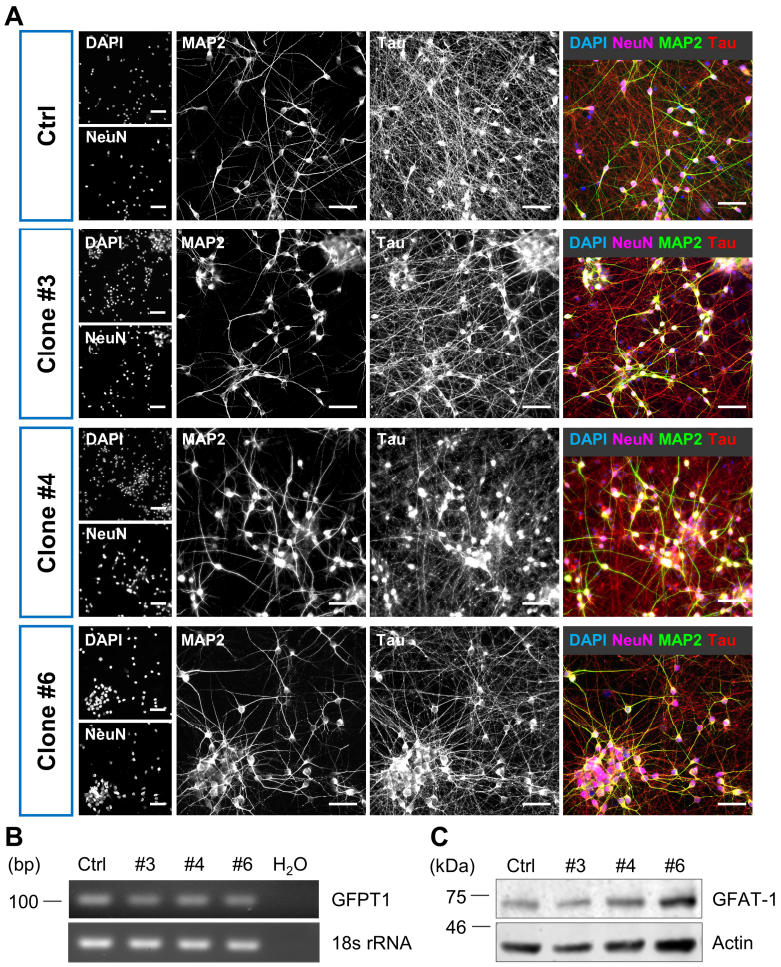

Fig. 30: Neuronal cultures generated from GFAT-1 gof hiPSCs.

(**A**) Representative fluorescence microscopy images of neuronal cultures generated from control cells and the three clones of hiPSCs harboring the GFAT-1 G451E gof mutation. The mutation introduced in the *GFPT1* gene did not have apparent effects on the generation of neuronal cultures. Scale bars: 50 µm (**B**) RT-PCR of *GFPT1* expression and (**C**) Western blot of GFAT-1 protein in d30 neuronal cultures of isogenic control cells and GFAT-1 G451E clones.

7.4.2 GFAT-1 gain-of-function and cellular stress resistance

Since Denzel *et al*. described N-acetylglucosamine (GlcNAc) or GFAT-1 gof to exert a protective effect against tunicamycin (TM)-induced cell stress in *C. elegans* and non-human mammalian cell lines, I wondered whether cells of the human neural lineage would also benefit under these conditions in a similar manner. Thus, the viability of NPCs and neuronal cultures generated from GFAT-1 gof and isogenic control hiPSCs was determined after cultivation in the presence of increasing concentrations of TM with and without 10 mM GlcNAc.

Supplementation of 10 mM GlcNAc effectively protected NPCs derived from control cells against TM-induced cell death (Fig. 31A). After 48 h in the presence of 0.05 µM TM, the percentage of viable cells

was more than double when 10 mM GlcNAc was added to the medium. The latter resulted in 73.1 ± 7.4% viable cells compared to 32.8 ± 4.7% in untreated controls. The relative improvement of cell survival was even higher at 0.10 µM TM for which GlcNAc supplementation led to a mean survival rate of 53.2 ± 9.7% compared to 17.4 ± 0.7%. At 0.50 µM TM GlcNAc still improved cell survival by about 50% reaching 12.7 ± 1.1% compared to 8.1 ± 1.3% in controls. However, the majority of NPCs had already died at this concentration of TM after 48 h.

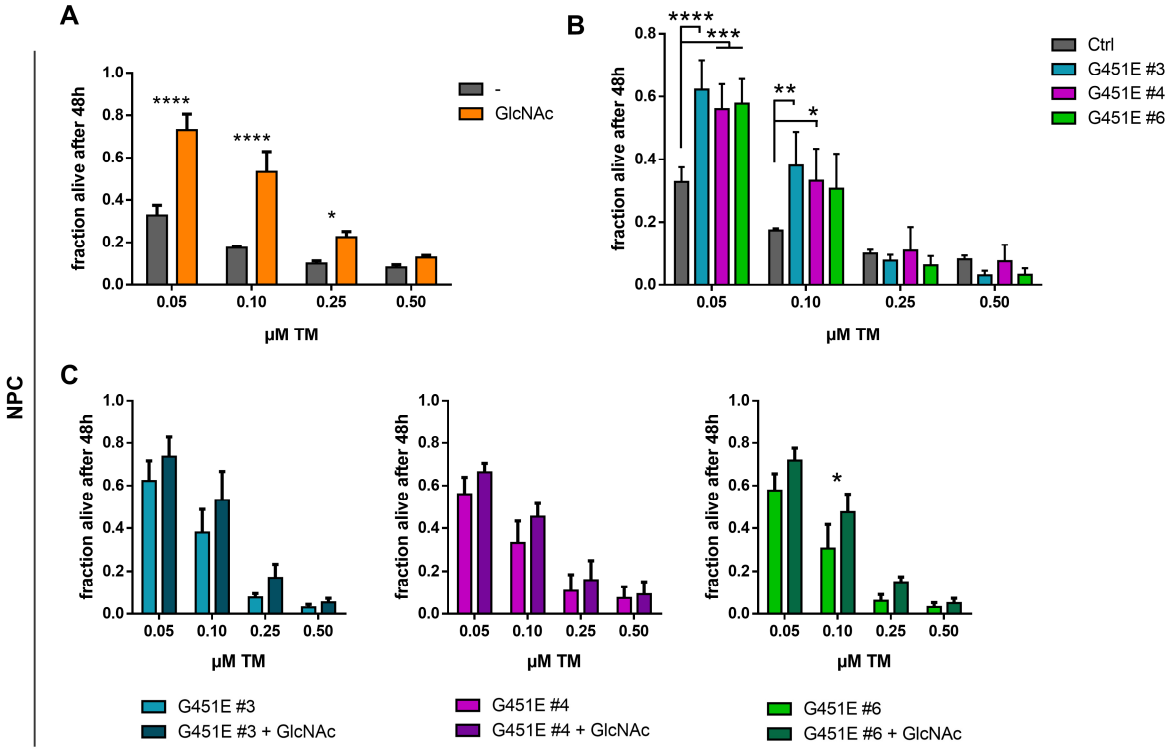

Fig. 31: GlcNAc supplementation and GFAT-1 gof provide a partial protection of NPCs from TM-induced cell death.

Viability of NPC cultures exposed to the indicated TM concentrations was determined by CellTiter-Glo™ assay after 48 h. Bar graphs show mean with S.D. of n = 3 independent experiments, two-way ANOVA with Bonferroni's multiple comparisons test. (**A**) Viability of NPC cultures of a control cell line exposed to TM in the presence or absence of 10 mM GlcNAc. GlcNAc is highly protective at lower TM concentrations. (**B**) Viability of isogenic control NPCs compared to NPCs with GFAT-1 gof highlights the survival promoting effect of GFAT-1 gof at lower concentrations of TM. (**C**) Effect of 10 mM GlcNAc on the viability of NPCs with GFAT-1 gof in the presence of the indicated concentrations of TM.

NPCs expressing the GFAT-1 G451E gof variant were significantly less susceptible to lower concentrations of TM (0.05, 0.10 µM) (Fig. 31B). At 0.05 µM TM, isogenic control NPCs were reduced to 32.8 ± 4.7% viable cells whereas GFAT-1 G451E clones #3, #4 and #6 displayed survival rates of 62.2 ± 9.4%, 56.0 ± 7.9% and 57.7 ± 7.9%, respectively. Doubling of TM to 0.10 µM resulted in

17.4 ± 0.7% viability of control NPCs and 38.0 ± 10.8%, 33.2 ± 10.2% and 30.6 ± 11.2% for the respective GFAT-1 gof clones. However, the protective effect of the GFAT-1 gof variant was negated at higher concentrations of TM (0.25, 0.50 µM). Supplementation of GFAT-1 gof NPCs with 10 mM GlcNAc tended to have an additive effect on cell survival but the observed differences did mostly not reach statistical significance (Fig. 31C).

As observed previously (section 7.3.5), immature neuronal cultures at d5 are susceptible to TM-induced ER-stress. Accordingly, cell viability was decreased by about 50% after 48 h in the presence of TM concentrations ranging from 0.25 to 1.5 µM (Fig. 32A). Parallel application of 10 mM GlcNAc in the culture medium did not enhance the survival rate of immature neurons. At day 30, neuronal cultures displayed an inherent resistance to TM at the applied concentrations. This effect was not augmented by GlcNAc supplementation (Fig. 32D). These experiments corroborate the phenomenon of increasing stress resistance of mature neurons but also show that, in contrast to NPCs, supplementation of GlcNAc does not confer a protective effect on neuronal cultures at day 5 and 30 of differentiation.

Next, the effect of the GFAT-1 G451E gof on neuronal survival under TM-induced stress was investigated. Remarkably, d5 neuronal cultures of all three GFAT-1 G451E clones displayed a higher survival rate than control cultures (Fig. 32B). At a concentration of 0.25 µM TM, viability of all three clones was mostly unaffected after 48 h reaching 103.8 ± 7.9%, 91.4 ± 25.2% and 95.4 ± 4.1% (clone #3, #4, #6). Conversely, the number of viable cells in control cultures had shrunk to 52.7 ± 1.8%. At the maximal TM concentration of 1.5 µM, control cells displayed 43.1 ± 17.2% viability whereas clones #3, #4 and #6 maintained 104.6 ± 37.2%, 75.5 ± 10.2% and 85.8 ± 12.8%, respectively.

As observed for the isogenic control cells, adding 10 mM GlcNAc to the culture medium of GFAT-1 G451E clones during the stress assay did not have an additive protective effect (Fig. 32C). At d30 of differentiation, there were no significant differences in the survival rate of control and GFAT-1 G451E gof neuronal cultures after 48 h in the presence of the applied concentrations of TM (Fig. 32E). Similar to results obtained for neuronal control cultures, survival of GFAT-1 gof neurons at d30 could not be further enhanced by supplementation with 10 mM GlcNAc (Fig. 32F).

To conclude, GlcNAc only exerted a cytoprotective effect against TM-induced cell death in NPCs but not in neuronal cultures at d5 and d30. Additionally, GFAT-1 G451E gof significantly improved survival of NPCs and d5 neuronal cultures. These data also further underline the inherent maturation-dependent stress resistance of more advanced neuronal cultures.

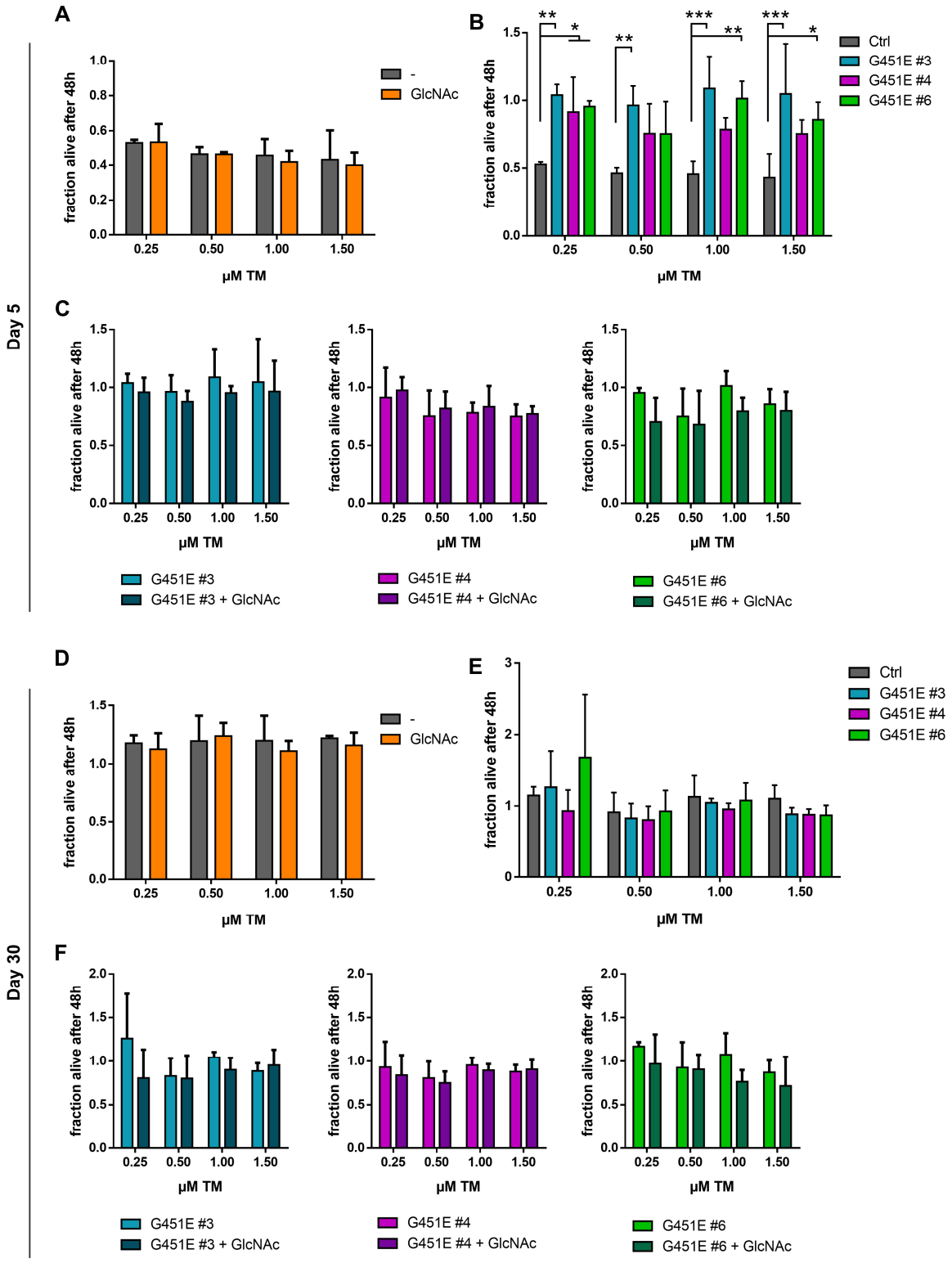

Fig. 32: GFAT-1 gof is beneficial for the survival of immature neuronal cultures exposed to TM-induced stress.

Results of CellTiter-Glo™ cell viability assays of immature d5 (**A-C**) and more mature d30 (**D-F**) neuronal cultures. Cells were treated with the indicated concentrations of TM for a period of 48 h. Bar graphs show mean with S.D. of n = 3 independent experiments, two-way ANOVA with Bonferroni correction. (**A**) Supplementation of 10 mM GlcNAc during TM exposure did not have a significant effect on the viability of immature neuronal cultures. (**B**) Comparison of the viability of immature neuronal cultures

of GFAT-1 gof and isogenic control cells highlighting a significant survival promoting effect of the GFAT-1 gof variant. (**C**) Combination of GFAT-1 gof and 10 mM GlcNAc does not yield difference in cell survival rates. (**D**) Supplementation of mature neuronal cultures of control cells with 10 mM GlcNAc. Mature neuronal cultures possess an inherent resistance to TM-induced stress and do not benefit from GlcNAc. (**E**) GFAT-1 gof does not improve viability of mature neuronal cultures in the presence of TM. (**F**) Viability of GFAT-1 gof cells supplemented with 10 mM GlcNAc.

7.4.3 The integrated stress response in human GFAT-1 gain-of-function neurons

In N2a cells, primary murine keratinocytes and *C. elegans* the protective effect of the GFAT-1 gof and GlcNAc have been attributed to the activation of the integrated stress response (ISR). The ISR is a signal transduction system for protein quality control that is highly conserved across species. One branch of ISR activation requires sequential phosphorylation of PERK and eIF2α which lead to activation of the transcription factor ATF4. Transcription of ATF4 target genes engages adaptive responses designed to cope with incoming stress stimuli.

To investigate a possible activation of the PERK branch of the ISR by GlcNAc supplementation or GFAT-1 gof in the human neural lineage, Western blot analysis of NPCs, immature and mature neuronal cultures was performed. As tunicamycin I is a known inducer of the PERK branch of the ISR and thus ATF4 (Oslowski & Urano, 2011), it was used as a positive control.

Exposure to TM robustly increased ATF4 protein levels in all cultures (Fig. 33). Surprisingly, this induction of ATF4 was not accompanied by appreciable elevation of PERK of EIF2α phosphorylation. PERK was readily detectable in NPCs and d5 neuronal cultures (Fig. 33A, B) but only faintly in neurons at d30 of differentiation (Fig. 33C). Phosphorylated PERK was barely detectable in d5 neuronal cultures but not in NPCs and d30 neuronal cultures. EIF2α and its phosphorylated form were detectable at all stages of differentiation. Unexpectedly, GFAT-1 gof or GlcNAc supplementation did neither lead to an apparent increase of PERK/EIF2α phosphorylation or ATF4 induction in NPCs nor in neurons. Consequently, these results call into question the universal applicability of the signaling mechanism behind protective overactivation of the HBP proposed by Horn *et al*. (Horn *et al.*, 2020).

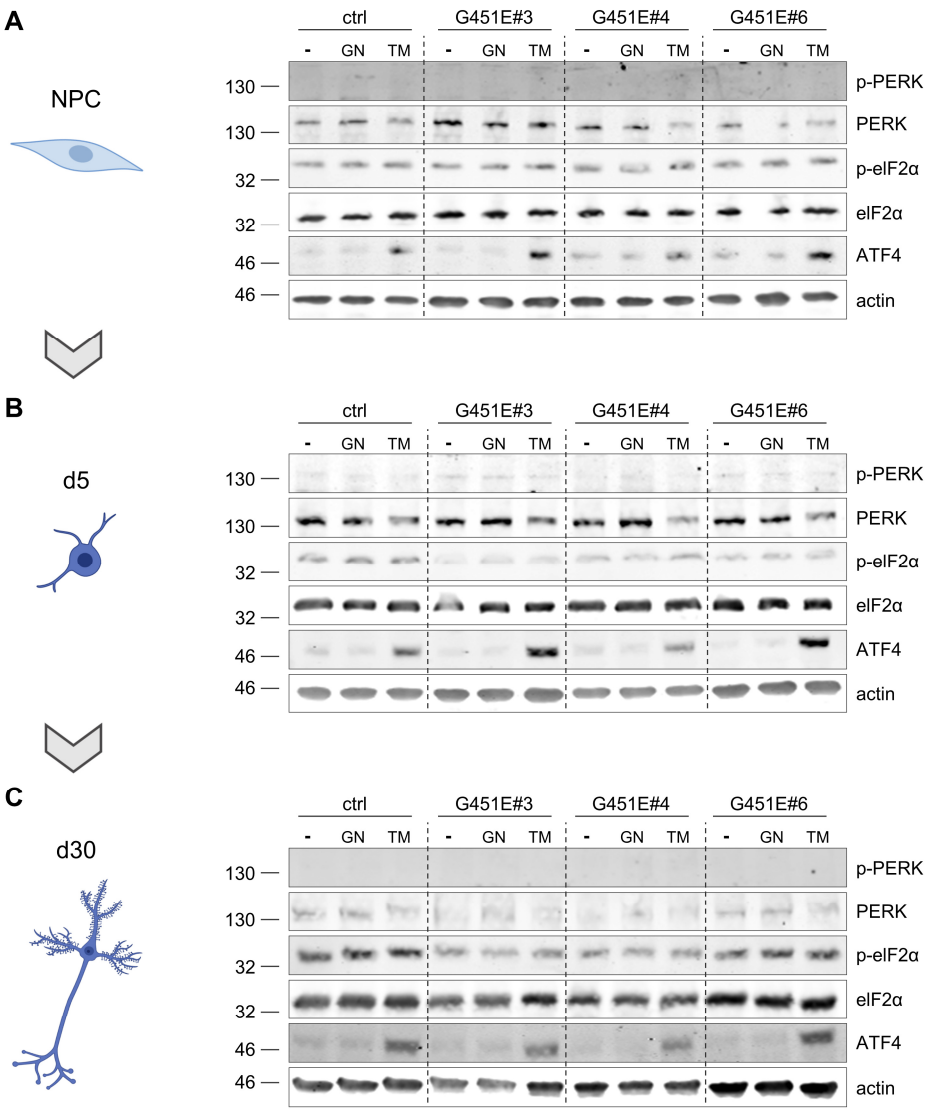

Fig. 33: GFAT-1 gof or GlcNAc supplementation do not cause appreciable activation of the PERK branch of the ISR in the human neural lineage.

Representative Western blots for components of the PERK signaling branch of the ISR in (**A**) NPCs, (**B**) d5 and (**C**) d30 neuronal cultures with GFAT-1 gof and/or 10 mM GlcNAc supplementation (16 h). NPCs were treated with 0.1 µM and neurons with 0.5 µM TM as a positive control for ATF4 induction. All samples of the individual subpanels were analyzed on the same gel, overlayed dashed lines merely serve as a visual aid.

7.4.4 Transcriptional regulation of the hexosamine biosynthetic pathway and the integrated stress response during neuronal maturation

The previously obtained bulk RNAseq data (section 7.2) provided the opportunity to examine the transcriptional regulation of the individual components of the HBP and the ISR during neuronal differentiation. Reactions within the HBP are catalyzed by four sequentially working enzymes and culminate in the production of UDP-GlcNAc (Fig. 34A).

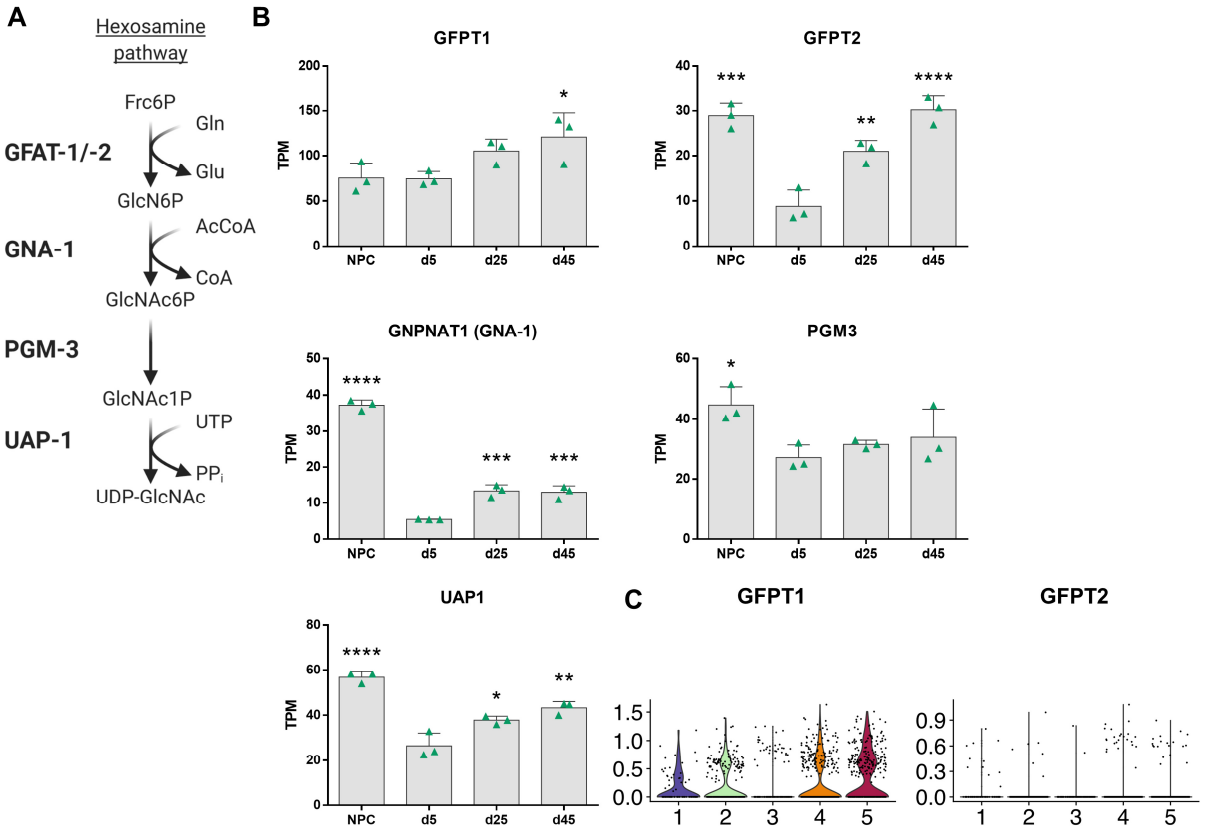

Fig. 34: Expression patterns of HBP enzymes during neuronal maturation.

(**A**) Schematic representation of the steps involved in the generation of UDP-GlcNAc via the HBP. Enzymes catalyzing the individual reactions are listed in bold on the left. (**B**) Normalized expression data (TPM) of the indicated HBP enzymes during neuronal maturation based on bulk RNAseq analysis of neuronal cultures from a control cell line. Note variable scale on y-axis, especially for *GFPT1*. Bar graphs show mean with S.D., statistical significance compared to d5 neuronal cultures based on one-way ANOVA with Bonferroni correction. Violin plots indicate normalized counts. RNAseq data analysis was done in collaboration with Dr. Anne Hoffrichter.

With the exception of *GFPT1*, expression of HBP enzymes was first downregulated during differentiation from NPCs to immature neurons and then tended to increase again during neuronal maturation (Fig. 34B). Expression of *PGM3* increased only mildly during neuronal maturation and not as significantly as the expression of the other HBP enzymes. Interestingly, *GFPT1* expression was almost identical in NPCs and d5 neuronal cultures. In contrast, expression of its paralogue *GFPT2* was

significantly decreased during this period. At all stages of differentiation, absolute expression of *GFPT1* was higher than expression of *GFPT2*. Even though expression of *GFPT2* increased about 4-fold from 8.82 ± 3.53 to 30.19 ± 3.08 TPM during neuronal maturation from d5 to d45, *GFPT1* expression was still more than 3-fold higher at d45 reaching 120.90 ± 26.67 TPM. This notion concerning the abundance of the two GFAT paralogues was supported by scRNAseq data in which transcript counts of *GFPT2* were very low but *GFPT1* was readily detectable (Fig. 34C). Together, these data indicate that HBP activity is transcriptionally elevated during neuronal maturation.

Of the four EIF2α kinases orchestrating the different branches of the ISR, only *EIF2AK4* (GCN2) showed a significant change in expression throughout neuronal maturation by doubling from 13.22 ± 1.61 TPM at d5 to 26.64 ± 1.30 TPM at d45 (Fig. 35A). *EIF2AK1* (HRI) was similarly expressed in neuronal cultures at all stages but it was the most abundantly expressed EIF2α kinase in neurons in absolute terms. Expression of *EIF2AK3* (PERK) showed a slight trend towards decreased levels at later stages of neuronal maturation but the observed differences did not reach statistical significance. Levels of *EIF2AK2* (PKR) were reduced by about 50% in neuronal cultures compared to NPCs. Expression of *EIF2S1* (EIF2α) and *ATF4* was highest in NPCs but while *EIF2S1* expression increased steadily during neuronal maturation, expression of *ATF4* remained mostly unchanged as neurons matured (Fig. 35B). Except for PERK, all of these ISR proteins were most abundantly expressed in NPCs and downregulated in neuronal cultures.

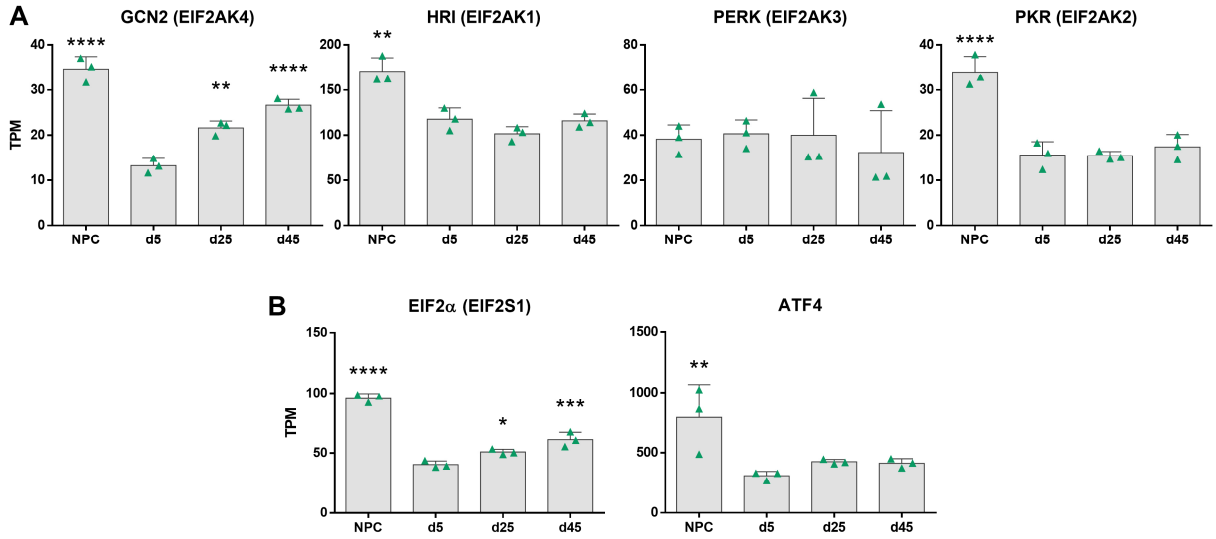

Fig. 35: Expression profiles of ISR components during neuronal maturation.

TPM-normalized expression data of (**A**) the four EIF2α kinases and (**B**) the two major ISR downstream effectors. Expression data is based on the previously described bulk RNAseq experiment (section 7.2). Note variable scale for TPM on y-axis. Bar graphs show mean with S.D., one-way ANOVA with Bonferroni correction.

8 Discussion

8.1 HiPSC-derived cultures for the study of neuronal maturation

Over the recent years, iPSC and transdifferentiation technology have provided the means to investigate human neurons *in vitro*. Many well-designed differentiation protocols have been established to generate neuronal cultures of desired regionality for the study of human neural development and disease. This thesis aimed to investigate neuron-specific phenomena associated with their maturation process. Thus, it required highly pure neuronal cultures to exclude potentially distorting effects from other cells like astrocytes which are often generated as a byproduct in the wake of neuronal differentiation in many protocols. To achieve this, we used a combination of small molecules to trigger cell-cycle exit of progenitor cells and promote the formation of neurons via the inhibition of Notch signaling (Kemp *et al.*, 2016; Telezhkin *et al.*, 2016). To guarantee suppression of potentially remaining proliferative cells in neuronal cultures, the cell cycle inhibitor PD-0332991 was also retained in media for long-term neuron cultivation. The resulting mature neuronal cultures contained minimal to no impurities by astrocytes which was illustrated by the very low expression levels of canonical astrocytic marker genes like *GFAP*, *SLC1A3*, *S100B* and *ALDH1L1*. The need for a high degree of purity comes with the caveat of eliminating many physiologically important interactions that take place between astrocytes and neurons *in vivo*. For example, astrocytes play an important role in formation and maintenance of synapses (Farhy-Tselnicker & Allen, 2018; Gonçalves *et al.*, 2018). However, even in the absence of astrocytes, our neuronal cultures showed robust synaptogenesis indicated by the increasing colocalization of the pre- and postsynaptic marker proteins Synapsin and PSD95. Thus, our approach enabled the dissection of transcriptomic changes during neuronal maturation and neuron-specific survival mechanisms using functionally relevant human neuronal networks.

Not all *in vitro* generated neurons are comparable. The data presented here on the difference between less and more mature neurons regarding their susceptibility towards molecular stressors highlights the importance of suitable, standardized model systems for the investigation of pharmacological interventions. Faithful recapitulation of neuronal physiology is a precondition for more realistic cell culture models and thus genuine transferability of research data to the human organism. Exemplarily, this is illustrated by the difference of the reported effect of GFAT-1 gof or GlcNAc supplementation on N2a cells compared to our neuronal cultures. Whereas these interventions caused an activation of PERK signaling and induction of ATF4 in N2a cells (Horn *et al.*, 2020), they did not affect signaling along this branch of the ISR in our hiPSC-derived forebrain neurons. Using N2a or SKNSH cells as a proxy for neural tissue in drug screening is therefore questionable since the applicability of the obtained insights to human neurons cannot be easily predicted. In every case, the chosen model system has to be

tailored to the disease context that is to be investigated. That is why transdifferentiation holds great promise as an approach to study age-related diseases as the resulting cells retain the epigenetic aging signatures of their respective donor (Mertens *et al.*, 2018; Traxler *et al.*, 2019). This epigenetic code is erased during the reprogramming procedure in the generation of iPSCs (Denoth-Lippuner & Jessberger, 2019). However, starting from such an epigenetically blank-slate may be advantageous when studying neurodevelopmental disorders or the effects off single mutations in monogenic diseases.

As stated above, this thesis provides ample evidence that with regards to neuronal cell culture models, their state of maturity may have a strong impact on the observed outcomes. As an effort to make research data obtained from different cultures more comparable and transferable, it would be desirable to have an objective basis for comparison regarding the maturity of the respective neurons. Here, we used the neuMatIdx (He & Yu, 2018) to score the transcriptional maturity of our neuronal cultures. When applied to a RNAseq data set, the algorithm will calculate an NMI independent of the actual underlying cell type. Therefore, only NMIs calculated based on data derived from neuronal samples should be compared. If this limitation is taken into account, the neuMatIdx reliably distinguishes between transcriptionally less and more mature neurons based on the relative activity of transcriptional modules pertaining to metabolism, cell-cell interactions and other cellular functions. Regarding the absolute NMI values, bulk RNAseq samples consistently achieved higher scores than scRNAseq samples. This results from the fact that transcript counts for a single cell are considerably lower than counts for a whole well of cells.

An algorithm like the neuMatIdx offers an opportunity to judge the transcriptional maturity of neurons. Ideally, this would be complemented by a set of metrics summarizing the functionality of the investigated cells. Together, these measures could improve transparency within the research field and improve the transferability of future results.

8.2 Restriction of MOMP and apoptosome assembly during neuronal maturation

Having established defined neuronal cultures with different well-characterized states of maturity, we sought to investigate maturation-dependent differences related to the regulation of the intrinsic apoptosis pathway. Signaling along this pathway is initiated upon mitochondrial outer membrane permeabilization (MOMP) by the pore-forming BCL-2 proteins BAK and BAX. The potential for MOMP is determined by the relative balance of pro- and antiapoptotic members of the BCL-2 protein family (Singh *et al.*, 2019a). Notably, we observed a significant, maturation-dependent decrease in the

expression of *BAX* and *BAK1* and a concomitant increase in the expression of their antagonist *BCL2*. Accordingly, the ratio of Bax to Bcl2 also inverted on the protein level. Developmental attenuation of *BAX* expression has been previously observed in PC12S neural cells (Polster *et al.*, 2003). Aside from direct transcriptional control, mature neurons may also rely on posttranslational regulation to fine-tune the abundance of BCL-2 proteins. For example, we observed a significant increase in the expression of the E3 ubiquitin ligase Parkin during neuronal maturation. Parkin is known to inhibit BAX and BAK (Johnson *et al.*, 2012; Bernardini *et al.*, 2019) while increasing steady-state levels of BCL-2 (Chen *et al.*, 2010). Loss of Parkin has been associated with accumulation of dysfunctional mitochondria and neurodegeneration (Bonifati *et al.*, 2002; Quinn *et al.*, 2020) but its overexpression may improve longevity (Rana *et al.*, 2013). Recently, differentiation of NPCs to neurons has been shown to be accompanied by a downregulation of the splicing regulator PTBP1 which enables a neuron-specific splicing mechanism of *BAK1* that leads to a decline in functional BAK protein and thus reduced apoptosis competence (Lin *et al.*, 2020). Our RNAseq data confirmed a strong decrease in *PTBP1* expression from NPCs to immature neurons and further throughout neuronal maturation (data not shown). However, our transcriptome data was not suitable to evaluate alternative splicing of individual mRNAs which would have required different approaches for sample preparation and sequencing.

The protein BOK is a less studied BCL-2 protein that has also been suggested to be able to form pores in the mitochondrial membrane (Inohara *et al.*, 1998; Einsele-Scholz *et al.*, 2016) but its functions seem to be wide-ranging and are still disputed. BOK is supposed to be regulated by ER-associated degradation and to cause MOMP independently of BAX and BAK (Llambi *et al.*, 2016). It was also found to be involved in uridine metabolism (Srivastava *et al.*, 2019), cell proliferation (Ray *et al.*, 2010) and the protection of neurons from excitotoxic stimuli (Orsi *et al.*, 2016). The diversity of functions reported for BOK suggests that its role might at least in part be cell type-specific. Of note, *BOK* expression was almost completely shut down in neurons at d5 but significantly upregulated at later stages of neuronal maturation. Either MOMP in mature neurons is more reliant on BOK instead of BAX and BAK or mature neurons benefit from the pro-survival effect of BOK on cellular Ca^{2+} homeostasis or from another so far unknown function. Taken together, the survival competence of more mature neurons is increased through a beneficial shift in the balance of major BCL-2 proteins which increases the threshold for MOMP.

If the outer mitochondrial membrane is permeabilized, the apoptotic signal is subsequently propagated by formation of the apoptosome. The latter is the central protein complex of the intrinsic apoptosis pathway required to initiate the downstream caspase cascade starting with Caspase-9 (Riedl & Salvesen, 2007; Bratton & Salvesen, 2010). Hence, controlling the assembly of the apoptosome

scaffold offers a powerful means to suppress apoptotic signaling events. A functional apoptosome is a multimeric complex formed by several units of mitochondrial Cytochrome c, APAF-1 and ATP. Cytochrome c is involved in the transfer of electrons within the electron transport chain of mitochondrial respiration. Neuronal maturation is accompanied by a metabolic shift towards increased reliance on this mitochondrial oxidative phosphorylation which produces high amounts of energy in the form of ATP (Zheng *et al.*, 2016). As a side effect of increased mitochondrial biogenesis, more mature neurons express significantly higher levels of Cytochrome c which was also apparent from our RNAseq analysis. This intracellular abundance of Cytochrome c makes tight control of MOMP and of APAF-1 in neurons especially important to prevent accidental apoptosome formation.

Expression of APAF-1 has been shown to be controlled by E2F1 and p53 (Fortin *et al.*, 2001). In addition, APAF-1 expression is restricted by chromatin remodeling during neuronal maturation (Wright *et al.*, 2007). Expression of E2F1 and p53 is linked to cell cycle progression and is thus highest in strongly proliferating cells. Both transcription factors are downregulated after cell cycle exit during differentiation into non-dividing cell types such as neurons which we could recapitulate during generation and maturation of our neuronal cultures. This opens a window for a potential therapeutic intervention in the treatment of brain tumors. Due to their low APAF-1 content, neurons are less vulnerable to externally applied Cytochrome c. In contrast, high levels of E2F1 and thus APAF-1 in glioblastoma or medullablastoma cells increase their susceptibility to cytochrome c exposure (Johnson *et al.*, 2007). Consequently, the differential propensity for activation of the apoptosome allows selective killing of tumor cells. In neurons, APAF-1 expression can be reestablished after acute injury leading to higher susceptibility for apoptosome-induced cell death (Yakovlev *et al.*, 2001; Chen *et al.*, 2014). This may serve as a mechanism to allow removal of disrupted neurons via the intrinsic apoptosis pathway while sparing the surrounding tissue from an inflammatory response. While we observed an ablation of APAF-1 protein in neurons after d5 of differentiation, *APAF1* expression declined less pronounced over time. This discrepancy may suggest an involvement of additional regulatory mechanisms aside from transcriptional control. Action of APAF-1 in apoptosome can be thwarted directly or indirectly in multiple ways (Bratton & Salvesen, 2010). For example, the heat shock protein HSP90β prevents APAF-1 oligomerization via a direct interaction with APAF-1 (Pandey *et al.*, 2000; Kurokawa *et al.*, 2008). Notably, expression of HSP90β increased significantly throughout neuronal maturation in our cultures and it may therefore contribute to the strict regulation of apoptosome assembly in mature neurons. Furthermore, Ca^{2+} directly interacts with APAF-1 to prevent nucleotide exchange of ADP for ATP which is a key step in formation of the apoptosome (Bao *et al.*, 2007). Hence, it is tempting to speculate that influx of Ca^{2+} resulting from neuronal activity acts as a pro-survival signal by inhibiting apoptosome activity. Together, these examples highlight the potential for tight

control of the apoptosome and thus downstream activation of caspases within the intrinsic apoptosis pathway in mature neurons.

8.3 Suppression of the caspase cascade and apoptosis execution as a consequence of neuronal maturation

The apoptosome serves as a platform for the activation of Caspase-9 which subsequently cleaves and activates downstream effector caspase. Remarkably, we noticed a 50% decrease of Caspase-9 protein levels from d5 to d45 of neuronal maturation. This change in Caspase-9 abundance could not be explained by a transcriptional downregulation as expression levels at d5 and d45 were almost identical. Neuronal maturation did not cause a change in the ratio of full-length and catalytically inactive splicing variants of Caspase-9. The transcript encoding full-length Caspase-9 remained predominant. Caspase-9 is a substrate of various protein kinases which regulate its activity via multiple phosphorylation sites (Li *et al.*, 2017b). We tried to investigate phosphorylation of Caspase-9 at Thr125 and Ser196 but our efforts were hampered by unreliable antibodies (data not shown). Therefore, possible changes in the phosphorylation of Caspase-9 throughout neuronal maturation remain to be elucidated. The discrepancy between the stable mRNA levels and the downregulation of Caspase-9 protein suggests a mechanism relying on an increasing post-translational regulation in maturing neurons which warrants further investigations.

Additionally, we observed a downregulation of the two major effector Caspases-3 and -7. While Caspase-7 protein was completely ablated after d5, Caspase-3 was still detectable even at d45 but its abundance was strongly reduced. *CASP7* mRNA was only detectable in NPCs. Transcript counts of *CASP3* reached a peak at d5 and then declined. Thus, transcription of these two effector caspases seems to be downregulated in a maturation-dependent manner. A similar observation has been made for *CASP3* expression in rat cortical neurons (Yakovlev *et al.*, 2001). In contrast, the abundance of Caspase-7 in the brain and its relevance in neuronal apoptosis is still controversially discussed (Juan *et al.*, 1997; Slee *et al.*, 2001; Henshall *et al.*, 2002; Le *et al.*, 2002). In addition to their involvement in cell death signaling, caspases also fulfill other important physiological functions in neurons like neurite outgrowth, arborization and synaptic plasticity (Hyman & Yuan, 2012; Hollville & Deshmukh, 2017; Espinosa-oliva *et al.*, 2019). Therefore, tight regulation of caspase activity may be necessary to prevent accidental apoptosis but their complete shutdown might not be desirable.

Aside from the effector caspases themselves, we also observed a global downregulation of genes associated with the execution phase of apoptosis. A prominent downstream target of Caspase-3 is PARP-1. Usually, PARP-1 is engaged in DNA repair, cellular bioenergetics and post-translational protein

modification (Gero *et al.*, 2012; Chaudhuri & Nussenzweig, 2017; Kamaletdinova *et al.*, 2019). However, following activation of Caspase-3, PARP-1 is cleaved and thereby degraded during apoptosis. We observed a steady decline in PARP-1 mRNA and protein levels over the time course of neuronal maturation. As maintenance of DNA repair should be highly beneficial to neurons, it is interesting to speculate which advantages are gained from a drastic decrease in PARP-1 abundance to make this trade-off worthwhile. To synthesize poly ADP-ribose, PARP-1 requires the oxidized form of nicotinamide adenine dinucleotide (NAD^+) as a donor for ADP-ribose moieties. NAD^+/NADH is an important acceptor or donor of electrons for a wide range of metabolic redox reactions. In mitochondria, NAD^+ is essential for the electron transport chain to produce ATP via oxidative phosphorylation. Consequently, consumption of NAD^+ by PARP-1 directly competes with energy production in cells with high metabolic activity like neurons. A higher number of mitochondria increases the risk for the generation of reactive oxygen species (ROS) and thus oxidative stress. ROS-induced DNA damage can trigger excessive PARP-1 activation causing a cellular energy crisis due to NAD^+ depletion. PARP-1 overactivation has been linked to neurodegeneration in Alzheimer's and Parkinson's disease (Martire *et al.*, 2015) and supplementation of NAD^+ is cytoprotective (Rajman *et al.*, 2018; Klimova & Kristian, 2019). Similar to our observation in neurons, a differentiation-dependent reduction in *PARP1* expression has also been observed during the formation of skeletal muscle in the development of myotubes from myoblasts (Oláh *et al.*, 2015). In this study, decreased levels of PARP-1 correlated with lower susceptibility to oxidative stress and improved mitochondrial bioenergetics due to higher NAD^+ availability. Conversely, these protective effects were eliminated upon ectopic overexpression of PARP-1. In the same manner, PARP-1-mediated NAD^+ depletion following oxidative stress has recently been reported to cause contractile dysfunction in cardiomyocytes (Zhang *et al.*, 2019a). Like myotubes and cardiomyocytes, neurons heavily rely on mitochondrial respiration for the generation of energy and might therefore benefit similarly from a suppression of PARP-1 activity. In this regard, it is also interesting that the BCL-2 protein BOK has been reported to protect mouse cortical neurons from PARP-1-dependent cell death (Orsi *et al.*, 2016). Here, we observed a significant increase of *BOK* expression during neuronal maturation which might serve as an additional safety brake to restrain activity of PARP-1. A downregulation of caspases and their potential downstream targets further attenuate the potential for the execution of the intrinsic apoptosis pathway in mature neurons.

8.4 Regulation of the IAP antagonist SMAC/DIABLO

Following MOMP, several proapoptotic proteins are released from mitochondria alongside cytochrome c to support in the execution of programmed cell death. One of these apoptosis-promoting factors is the IAP antagonist SMAC/DIABLO. It exerts its function by competing for the same binding sites that IAPs like XIAP use to bind caspases. Proteolytic processing of SMAC is required to enable its interaction with IAPs. Smac is synthesized in the ER as a precursor with an N-terminal sorting signal which is cleaved off upon arrival at mitochondria. Two mitochondrial proteases have been shown to mediate removal of the mitochondrial targeting sequence of the SMAC precursor: the inner mitochondrial membrane peptidase (IMP) and PARL (Burri *et al.*, 2005; Saita *et al.*, 2017). Of note, we observed a decreased expression of PARL in neurons compared to NPCs even though mitochondrial biogenesis was much more active in neurons (data not shown). Proteolytic processing of SMAC is necessary to reveal an N-terminal AVPI (Ala-Val-Pro-Ile) amino acid stretch which enables the interaction of SMAC with IAPs. Exposure to the proteasome inhibitor MG132 led to an accumulation of unprocessed SMAC precursor protein in immature but not in mature neuronal cultures. Conceivably, MG132 had already triggered apoptosis and a concomitant increase in SMAC expression in immature neuronal cultures whereas the mature neurons were not sufficiently affected after the chosen duration of treatment. However, we did not observe less viable cells in immature than in mature neuronal cultures after 24 h of exposure to MG132. An alternative explanation could be that the inhibition of protein degradation via the UPS by MG132 leads to an accumulation of unprocessed proteins in the ER of immature neurons. In support, MG132 induces expression of the ER stress response proteins GRP78 and CHOP (Bush *et al.*, 1997; Yoshida *et al.*, 2005). Additionally, we observed an increased baseline capacity for protein folding processes and maintenance of proteostasis in mature neuronal cultures. Mature neurons may therefore not be affected as quickly by MG132 treatment allowing protein processing at the ER to continue.

We noticed a slight, yet not significant, increase in the expression of *DIABLO* from d5 to d45. This was very likely a side-effect of the strongly increased mitochondrial biogenesis in mature neurons. In Western blots for SMAC at different time points during neuronal maturation, we observed a pattern of bands similar to previously reported ubiquitination patterns of SMAC (Morizane *et al.*, 2005; Ma *et al.*, 2006; Qin *et al.*, 2016; Guven *et al.*, 2019). Mature neurons robustly showed a high molecular weight smear indicating increasing ubiquitination of SMAC during neuronal maturation while levels of mature SMAC protein appeared to be largely unchanged. This suggests a dynamic turnover of SMAC via the ubiquitin-proteasome system. Indeed, blocking proteasome activity with MG132 tended to increase levels of mature SMAC protein in mature but not in immature neuronal cultures in our experiments.

Degradation of SMAC via the UPS can be mediated by multiple E3 ubiquitin ligases, most of which belong to the IAP family. Expression of *BIRC1* (NAIP), *BIRC3* (cIAP-2) and *BIRC7* (Livin) was very low or not detectable at all in NPC and neuronal cultures. Survivin (*BIRC5*) plays an important role during cell division in the separation of chromosomes and cytokinesis (Li *et al.*, 1999). Accordingly, we detected appreciable expression of *BIRC5* in NPCs but not in neuronal cultures at any stages of differentiation. This is also further evidence for the absence of dividing cells and thus the high degree of purity of the analyzed neuronal cultures. Lastly, expression of *BIRC4* (XIAP) increased in bulk and scRNAseq during neuronal maturation. XIAP is the most prominent IAP and its role in mature neurons is discussed in more detail in section 8.5.

A non-IAP E3 ligase with the potential to catalyze SMAC ubiquitination is apoptosis-resistant E3 ubiquitin protein ligase 1 (AREL1). Based on our RNAseq data, expression of *AREL1* was increased in neurons compared to NPCs but was highest in the most mature neuronal cultures. This was most apparent in the scRNAseq data set whereas the difference in expression between d5 and d45 in bulk RNAseq supported the trend bud did not reach statistical significance. Aside from SMAC, AREL1 also exerts antiapoptotic effects by promoting the degradation of the apoptotic proteins HtrA2 and ARTS (Kim *et al.*, 2013; Singh *et al.*, 2019b). To date, there is only one report of AREL1 connected to the nervous system (Rydbirk *et al.*, 2020). This study implicates AREL1 deregulation in multiple system atrophy. Additionally, the authors noted that within the prefrontal cortex in the human brain, AREL1 is predominantly expressed in neurons and markedly less in oligodendrocytes, astrocytes and microglia. With only 11 publications on the PubMed database as of January 2021, data about AREL1 is very limited making it an attractive target for future research.

It is of interest to consider in which cellular compartment the ubiquitination of SMAC that we observed takes place. After MOMP during apoptosis, cytosolic Smac is easily accessible by a variety of E3 ubiquitin ligases. However, under non-apoptotic conditions SMAC resides in the mitochondrial intermembrane space. The aforementioned E3 ligases are largely cytosolic proteins that oppose SMAC function during apoptosis but how they might interact with SMAC under non-apoptotic conditions is less clear. As there have been no reports about SMAC release into the cytosol under non-apoptotic conditions, it seems most likely that the increased ubiquitination of SMAC in mature neurons takes place inside of mitochondria. This could either occur via an as of yet undescribed interaction with a mitochondrial E3 ubiquitin ligase or a mechanism involving the translocation of a known SMAC ubiquitin ligase into mitochondria. At least for XIAP it has been reported that it can enter apoptotic mitochondria to reduce the apoptotic potential of SMAC by mediating its ubiquitin-dependent degradation (Flanagan *et al.*, 2010; Hamacher-Brady *et al.*, 2014).

8.5 XIAP is a central gatekeeper in safeguarding human forebrain neurons

XIAP is the only IAP protein with the ability to directly inhibit active Caspase-3, -7 and -9 and to ubiquitinate SMAC/DIABLO. In our experiments, expression of *BIRC4* (XIAP) was very similar in NPC and d5 neuronal cultures but elevated in d25 and d45 neuronal cultures. In scRNAseq analysis, cells belonging to the most mature neuron cluster displayed the highest expression of XIAP. Concurrently, protein levels of XIAP steadily increased until d45. However, we were surprised to be unable to detect appreciable amounts of XIAP protein in NPCs even though expression was almost identical to d5 neuronal cultures in which XIAP protein was readily detectable. This hints at a differential post-translational regulation of XIAP in NPCs and neurons. One major avenue to control the availability of proteins is their degradation via the UPS which requires tagging of target proteins with ubiquitin moieties. Existing ubiquitin modifications can be dynamically modulated by ubiquitin-specific proteases (USPs) and other deubiquitinating enzymes (DUBs) that remove them from their target proteins (Amerik & Hochstrasser, 2004; Mevissen & Komander, 2017). The ability to modulate the half-life of proteins makes USPs key players in the regulation of the cellular proteome. Not surprisingly, USPs are promising drug targets for the treatment of cancer and neurodegenerative diseases (Daviet & Colland, 2008; Lim *et al.*, 2020). Interestingly, expression of *USP11* was almost 3-fold upregulated in neurons compared to NPCs in our RNAseq data. *USP11* has been shown to catalyze deubiquitination of XIAP to prevent its degradation via the UPS (Zhou *et al.*, 2017). High expression of *USP11* might therefore help to protect XIAP from degradation in neurons whereas its decreased abundance in NPCs facilitates turnover of XIAP.

Protein stability of XIAP may also be enhanced via phosphorylation at Ser87 by protein kinase C (PKC)ε (Kato *et al.*, 2011). PKCε was about 3-fold upregulated in our d25 and d45 neuronal cultures compared to NPCs and d5 neuronal cultures. Several reports have documented the importance of PKCε in neurons where it is involved in neurite outgrowth (Fagerström *et al.*, 1996), synaptogenesis (Sen *et al.*, 2016), memory formation (Hongpaisan & Alkon, 2007), neuroprotection (Hongpaisan *et al.*, 2011; Sen *et al.*, 2018) and more (Chen & Tian, 2011). PKCε activity can be stimulated by bryostatin-1 (Szallasi *et al.*, 1994; Ekinci & Shea, 1997) which is currently investigated in a long-term phase 2 clinical trial with Alzheimer's disease patients by Neurotrope Inc. Potentially, neuroprotection conferred by bryostatin-1 and PKCε may thus also derive from a stabilization of XIAP protein levels, an intriguing hypothesis to be investigated in future experiments.

We also investigated potential differences in the subcellular localization of XIAP in immature and mature neuronal cultures. While XIAP was readily detectable in the soma of immature and mature neurons, it seemed to be less abundant in the neurites of immature neurons than in those of mature neurons. As an antagonist of Caspases-3, -7- and -9, XIAP likely increases the local threshold for caspase

activation in the soma already at earlier stages of maturation. In neurites and at more distant synapses, lower XIAP levels presumably permit more dynamic remodeling of the cytoarchitecture which, in part, relies on locally restricted caspase activity (D'Amelio *et al.*, 2010; Espinosa-oliva *et al.*, 2019). This may be especially important during the initial search for connections in the nascent neuronal network. Once a cell has established its position in the network, synaptic plasticity becomes even more localized and large-scale reorganization of neurites becomes less prevalent. Consequently, increased XIAP levels in neurites might from then on be favorable to protect interconnected cells from accidental cell death.

Aside from SMAC/DIABLO, several other endogenous inhibitors of XIAP have been discovered, namely XAF-1, HtrA2, SIAH-1 and SIVA-1. We investigated expression of these proteins to assess whether the increased abundance of XIAP in mature neurons was accompanied by an upregulation of its antagonists. Surprisingly, *XAF1* mRNA was completely absent from our cultures, also in NPCs. The proapoptotic function of XAF-1 is well studied (Liston *et al.*, 2001). Others have reported its presence in rat motor neurons in which it is downregulated during maturation (Perrelet *et al.*, 2004). Additionally, XAF-1 is upregulated in rat brain after ischemic injury (Siegelin *et al.*, 2005). XAF-1 is best studied for its role in cancer (Plenchette *et al.*, 2007; Pinto *et al.*, 2020) but data on its physiological role in human neurons remains scarce. Our observations suggest that XAF-1 is not expressed in human forebrain neurons under healthy physiological conditions.

HtrA2/Omi, like SMAC, is released from the mitochondrial intermembrane space during apoptosis. HtrA2 is a serine protease with the ability to cleave and inactivate XIAP to promote caspase activation (Suzuki *et al.*, 2001; Miguel Martins *et al.*, 2002). We noticed increased expression of HtrA2 in neurons compared to NPCs. However, d45 neuronal cultures expressed slightly less HtrA2 than d5 neuronal cultures. Considering that HtrA2 is a mitochondrial protein and that mitochondrial biogenesis is significantly higher in more mature neurons, this result was unexpected. It encourages to speculate that the total level of HtrA2 per mitochondrion might be lower in mature than in immature neurons. As HtrA2 is also involved in processing of mitochondrial proteins and is thus essential to maintain mitochondrial integrity, loss of HtrA2 leads to mitochondrial defects and neurodegeneration (Patterson *et al.*, 2014). Additionally, we observed a significant downregulation in the expression of the proapoptotic protein SIVA-1 over the time course of neuronal maturation. SIVA-1 is an interaction partner of XIAP with the ability to promote XIAP degradation although it is not clear whether it acts by causing XIAP autoubiquitination, serves as a ubiquitin ligase itself or as an adaptor to recruit another ubiquitin ligase (Wang *et al.*, 2013; Han *et al.*, 2014; Coccia *et al.*, 2020). High expression of SIVA-1 might be another explanation for the absence of appreciable amounts of XIAP protein in NPCs. An E3 ubiquitin ligase with the potential to directly mediate degradation of XIAP is SIAH-1. To interact with XIAP, SIAH-1 relies on the mitochondrial protein ARTS as an adaptor and the lack of either of these two

proteins leads to higher steady-state levels of XIAP (Garrison *et al.*, 2011). Based on our bulk RNAseq data, d45 neuronal cultures expressed significantly less Siah-1 than d5 cultures which might help to maintain higher XIAP protein levels in more mature neurons.

To conclude, our observations highlight that mature neurons not only become endowed with a strong increase in protective XIAP but that the potency of XIAP is additionally enhanced by adaptations that promote its protein stability and restrict its antagonists.

8.6 Maturation-dependent resistance of human forebrain neurons to apoptotic insults

During early phases of brain development, large numbers of neurons are generated but not all of them are maintained until the final stages. During the formation of mature neuronal networks, surplus neurons are removed by programmed cell death. Therefore, targeted apoptosis of neurons is very important in the developing brain but becomes a health threat in the adult individual which lacks the means to replace substantial neuronal loss. This is functionally illustrated by our data which highlights a maturation-dependent restriction of neuronal apoptosis signaling. Against this background, we surmised that mature neurons should display an increased survival competence when exposed to cellular stress. Thus, we challenged immature and mature neuronal cultures by disrupting different parts of the cellular machinery with molecular stressors and determined their respective viability.

Immature and mature neurons responded similarly to rotenone-induced oxidative stress. This was surprising because rotenone disrupts the electron transport chain in mitochondria which is far more important in mature than immature neurons due to the maturation-dependent metabolic shift towards oxidative phosphorylation. Mature neurons were significantly less affected by the inhibition of autophagic flux by bafilomycin A1/3-MA which suggest that they may possess a higher baseline activity of autophagy or possible compensatory mechanisms. As described before, we observed a significantly increased protein folding capacity in mature neurons which was exemplified by an upregulation of the heat shock protein genes *HSPB5* and *HSP90AB1*. In part, this may explain way mature neurons tended to display higher survivability when protein turnover was inhibited with MG132. Similarly, mature neurons survived significantly better when exposed to tunicamycin, which disrupts protein homeostasis by blocking N-glycosylation of proteins in the ER. The improved capacity of mature iPSC-derived neurons to cope with unphysiological protein aggregation may partially explain why overexpression of pathological, hyperphosphorylated Tau does not affect embryonic stem cell-derived neurons (Mertens *et al.*, 2013a) but is neurotoxic to less authentic cell systems like PC12 cells (Fath *et al.*, 2002).

Lastly, mature neurons were much better protected from cell death by exposure to thapsigargin which disrupts the cellular Ca^{2+} homeostasis. The mitochondrial protease PINK1 has been described to protect murine cortical neurons from insult by thapsigargin (Li & Hu, 2015) and we found *PINK1* expression to be significantly upregulated in our neuronal cultures during maturation (data not shown). Maintenance of Ca^{2+} homeostasis is especially important in neurons to prevent excitotoxicity-related cell death and it therefore seems likely that additional safety breaks provide mature neurons with protection from thapsigargin. Neuronal activity also offers a source for survival stimuli from which mature neurons within a network should profit more than immature neurons that may not yet have formed the required synaptic connections. In our cultures, we observed a strong increase in the expression of the neuronal activity-related immediate early genes *NPAS4* and *ARC* from d15 onward. This coincided with increased levels of components of the AIS, neurotransmitter receptors and synaptic proteins. Neurons around d25 of differentiation displayed higher electrophysiological responsiveness and elicited trains of action potentials upon stimulation which was not true for neurons at d5. Synaptic activity has been reported to protect murine cortical neurons from cellular stressors by suppressing the intrinsic apoptosis pathway (Léveillé *et al.*, 2010) and synaptic NMDA receptor activity supports antioxidant protection (Papadia *et al.*, 2008).

Considering the broad range of survival strategies that mature neurons become equipped with, one might not necessarily expect neurodegenerative diseases to be as prevalent as they are today. That is why the deterioration of neurons has been suggested to be connected to a reversion back to an immature phenotype which causes once highly-resistant cells to become more susceptible again (Kole *et al.*, 2013).

8.7 Regulation of the hexosamine biosynthetic pathway in human neurons

Despite its importance for the integration of multiple metabolic pathways and the provision of UDP-GlcNAc for glycosylation reactions, regulation of the hexosamine biosynthetic pathway (HBP) is not well studied in neurons. Of note, neurons themselves do not express glutamine synthetase (Norenberg, 1979; Norenberg & Martinez-Hernandez, 1979) and therefore lack the ability to produce glutamine which is required as a substrate for the amination of Frc-6P by GFAT. Consequently, HBP flux in neurons within the brain is reliant on glutamine externally supplied by astrocytes. In our cell culture model system, glutamine was provided in the culture medium. Using our RNAseq data we analyzed the expression of HBP enzymes during neuronal maturation.

Interestingly, our data does not support previous claims about the differential expression of GFAT-1 and -2 in the CNS. Initially, GFAT-2 was described as the prevalent GFAT in the CNS while GFAT-1 is

supposedly more abundant in pancreas, testis and other tissues (Oki *et al.*, 1999). In contrast, our expression data showed a 3-fold higher expression of GFAT-1 than GFAT-2 in our forebrain neuronal cultures at day 45 of maturation (section 7.4.4). Expression of both GFAT enzymes increased significantly as neurons matured. The discrepancy between our RNAseq data and the previous report may derive from a difference in the analyzed developmental stage. Even though our neuronal cultures display strong transcriptional, cytoarchitectural and functional maturation, the analyzed time frame of cultivation might not be sufficient to replicate the state of the adult human tissues analyzed by Oki *et al*. Potentially, the ratio between GFAT-1 and -2 reverses at even later stages of human brain development that might not be adequately modelled by our cell culture system at the investigated time point of cultivation. Alternatively, it is also possible that the two GFAT paralogues are preferentially expressed in different cell types within the brain such as neurons and astrocytes. Since the neuronal cultures used in this study were designed to analyze neuron-specific processes and were thus optimized for a high degree of purity, the underlying RNAseq data does not provide insights regarding other cell types. In contrast, Oki *et al*. used bulk tissue RNA representing a mixture of brain cells for their initial Northern blot experiments. Importantly, the functional consequences of a tissue specific prevalence of GFAT-1 or -2 have not yet been determined. Whether GFAT-1 and -2 fulfill other functions aside from their involvement in the HBP is not known. Even though both proteins catalyze the same reaction, they may be regulated differently. For example, GFAT-1 and -2 are both regulated via phosphorylation by protein kinase A but with opposing effects. While modulation by PKA decreases activity of GFAT-1 (Chang *et al.*, 2000), it boosts activity of GFAT-2 more than 2-fold (Hu *et al.*, 2004). Additionally, the two GFAT isoenzymes appear to possess a differing susceptibility to feedback inhibition by UDP-GlcNAc, the final product of the HBP. Interestingly, a surplus of UDP-GlcNAc was reported to reduce reaction rates of GFAT-1 by 51% (McKnight *et al.*, 1992) while GFAT-2 is only inhibited by 15% (Hu *et al.*, 2004). Functionally, this would make GFAT-2 similar to the GFAT-1 G451E gof variant which is rendered insensitive to this mode of feedback inhibition (Ruegenberg *et al.*, 2020). If GFAT-2 is indeed the prevalent GFAT variant in the CNS, this could mean that neurons might be able to amass more intracellular UDP-GlcNAc before HBP flux is downregulated providing a bigger leeway for related processes like protein glycosylation or O-GlcNAcylation. However, the differences in the potency of feedback inhibition cited above may also originate from differences in the experimental set-up. To date, no study has provided a direct comparison of the kinetics of GFAT-1 and -2 feedback inhibition by UDP-GlcNAc under the same experimental conditions.

We observed that aside from GFAT-1/-2, two of the three remaining enzymes of the HBP, GNA-1 and UAP-1, were also significantly upregulated during neuronal maturation. Simultaneously, our neuronal cultures showed significantly reduced expression of *GNPDA1* (data not shown), the gene encoding

glucosamine-6-phosphate isomerase-1 which counteracts GFAT by catalyzing the reverse reaction. These adaptations might provide neurons with an indirect way to boost HBP output.

The HBP consumes metabolites from all major types of macromolecules making it a nutrient-sensing metabolic hub. During differentiation, neurons undergo metabolic reprogramming from aerobic glycolysis to oxidative phosphorylation. Shutdown of aerobic glycolysis is mandatory to facilitate neuronal differentiation and failure to do so causes nascent neurons to undergo apoptosis (Zheng *et al.*, 2016). This rewiring of cellular metabolism to oxidative phosphorylation is necessary to meet the high energy demands imposed by neuronal activity (Laughlin *et al.*, 1998; Attwell & Laughlin, 2001). If such a wide-ranging reorganization is undertaken to ensure cellular energy supply, usage of Frc-6P may be even more skewed towards production of pyruvate for oxidative phosphorylation instead of the HBP in neurons than in other cell types.

8.8 HBP and the integrated stress response in cytoprotection

A connection between the HBP and cellular stress response pathways has been established in various cell culture systems, animal models and human diseases (Denzel & Antebi, 2015; Vasseur & Manié, 2015; Martinez *et al.*, 2017). Recently, gain-of-function mutations of the rate-limiting enzyme GFAT-1 have been described to cause cytoprotective activation of the integrated stress response (ISR) (Denzel *et al.*, 2014; Horn *et al.*, 2020; Ruegenberg *et al.*, 2020).

We sought to validate activation of the ISR by GFAT-1 gof in human NPCs and neurons. The CRISPR-Cas9-driven site-directed mutagenesis of the endogenous *GFPT1* locus for the generation of GFAT-1 G451E gof hiPSCs allowed a seamless modification of endogenously expressed GFAT-1. The use of isogenic cell lines has become the method of choice for the investigation of mutation-specific effects. This approach circumvents many of the potential pitfalls associated with random genomic integration of large viral expression constructs and eliminates the risk of analyzing biological artifacts resulting from unphysiological overexpression. Additionally, virally transduced hiPSCs tend to silence transgene expression by chromatin remodeling during prolonged differentiation processes (Ellis, 2005; Herbst *et al.*, 2012; Pfaff *et al.*, 2013).

Using the generated GFAT-1 gof hiPSCs and supplementation of GlcNAc, we investigated the effect of HBP activation on cell viability under TM-induced ER stress in NPCs and neurons. In NPCs, GlcNAc and GFAT-1 gof increased cell survival in the presence of TM. Interestingly, the excess of glucose contained in the culture media alone did not protect cells from TM-induced cell death even though elevated glucose levels should also boost HBP flux. It seems plausible that supplementation of GlcNAc is more

efficient at increasing intracellular levels of UDP-GlcNAc because it bypasses the first two reactions of the HBP and thus only requires two instead of four steps to yield the HBP end product. Circumventing the rate-limiting reaction catalyzed by GFAT-1 also prevents attenuation of HBP flux via UDP-GlcNAc-dependent feedback inhibition. In contrast to glucose, GlcNAc may thus short-circuit the HBP causing an outsized rise in UDP-GlcNAc levels. Interestingly, GlcNAc was only protective for NPCs but not neurons in our cell viability assays which may be a result of potentially differing uptake kinetics. In this context it is interesting to note that expression of *N*-acetyl-*D*-glucosamine kinase (NAGK) was more than 5-fold higher in neurons than NPCs in our RNAseq experiment (data not shown). NAGK catalyzes the phosphorylation of GlcNAc to GlcNAc-6-P which is a mandatory step before GlcNAc can be fed into the HBP. In neurons, NAGK plays a structural role involved in axonal outgrowth that does not require its kinase activity (Islam *et al.*, 2015). However, the abundance of NAGK should in theory enhance integration of GlcNAc into the HBP in neurons compared to NPCs.

GlcNAc supplementation was more potent in the protection of NPCs from TM-induced cell death than GFAT-1 gof as it was effective over a wider range of TM concentrations. In part, this could be due to the diminished feedback inhibition mentioned above. Likewise, the administered 10 mM GlcNAc also represent a bigger net supply than can presumably be provided enzymatically by GFAT-1 gof at endogenous expression levels. In immature neurons, GFAT-1 gof exerted protective effects but it did not further augment the strong inherent TM resistance of more mature neuronal cultures.

How exactly GlcNAc or UDP-GlcNAc protect against TM is unclear but they might act as competitive inhibitors of TM-binding, allosteric stabilizers of proteins or engage beneficial signaling pathways. It has been noted that glucosamine treatment is able to induce ER stress and PERK-mediated phosphorylation of eIF2α (Kline *et al.*, 2006; Qiu *et al.*, 2009; Lombardi *et al.*, 2012). Additionally, overexpression of UAP-1, the enzyme catalyzing the last step of the HBP, in prostate cancer has been reported to lead to elevated UDP-GlcNAc levels and protection from ER stress elicited by the inhibitors of N-glycosylation 2-deoxyglucose and TM (Itkonen *et al.*, 2015). In line with these observations, Horn *et al.* attributed the protective effect of HBP activation by GlcNAc supplementation or GFAT-1 gof against TM to a mild induction of the PERK branch of the ISR which is also part of the unfolded protein response in the ER. However, even though pharmacological and genetic activation of the HBP elicited protective effects in our experiments, we did not observe an activation of PERK by GFAT-1 gof in NPCs, immature or mature neurons. Similarly, the degree of ISR activation remained unchanged when cell culture media were supplemented with GlcNAc. In conclusion, our results suggest that GFAT-1 gof conferred cytoprotection in hiPSC-derived NPCs and neurons does not stem from a PERK-dependent engagement of the ISR. A potential mechanistic link between increased intracellular levels of UDP-GlcNAc and phosphorylation of PERK remains to be elucidated. Others have described induction of

GFAT-1 activity by XBP1s and ATF4 as a downstream response to cellular stress but not as the initial trigger (Wang *et al.*, 2014b; Chaveroux *et al.*, 2016). As a first step, pharmacological inhibition of PERK activity and eIF2α phosphorylation should reveal the role of the ISR in the cytoprotective effects associated with GFAT-1 gof and GlcNAc.

To date, the effects of GFAT-1 gof and supplementation of GlcNAc were predominantly examined in the nematode *C. elegans* and, with regards to mammalian cell systems, in highly proliferative cell populations of murine neuroblastoma (N2a) cells and murine primary keratinocytes. Biologically, these cell types resemble NPCs more than neurons. Although of neural origin, N2a cells do not offer a faithful recapitulation of neuronal biology and are often unsuitable to gauge the effects of pharmacological interventions in authentic human neurons (LePage *et al.*, 2005). In our experiments, genetic GFAT-1 gof or GlcNAc treatment conferred increased stress resistance in NPCs and immature neurons but not in mature neuronal cultures. It is therefore conceivable that the developmental and/or metabolic state of the impacted cell might play a role in the effectiveness of the provided protection.

When examining the expression of ISR components, we noticed a steady expression of PERK from NPCs to mature neurons. In contrast, the three other eIF2α kinases GCN2, HRI and PKR showed stronger expression in NPCs than neuronal cultures. This may indicate a higher sensitivity of NPCs in the responsiveness to stress stimuli. Among neuronal cultures, GCN2 was the only eIF2α kinase that was differentially expressed based on the degree of maturity displaying a significant upregulation as maturation proceeded. Since GCN2 senses the availability of amino acids, this may indicate their increasing importance for neuronal homeostasis. We were surprised to find HRI to be the most highly expressed eIF2α kinase in our neuronal cultures in absolute terms (TPM). HRI has mainly been studied in the erythroid lineage but its roles in other tissues are slowly emerging (Burwick & Aktas, 2017). In neurons, HRI has been implicated in synaptogenesis (Ill-Raga *et al.*, 2015) and restoration of proteostasis during proteasome malfunction (Alvarez-Castelao *et al.*, 2020) but a lot remains to be learned about its functions in the neural lineage. Lastly, the maturation-dependent increase in eIF2α expression that we observed likely reflects the general upregulation of protein synthesis needed to build and maintain the growing cell size.

Due to its involvement in the regulation of synapses and memory formation, the ISR plays a special role in neurons. Synaptic plasticity is the basis for memory formation and relies on fast, local protein synthesis in dendrites following neuronal activity (Sutton & Schuman, 2006; Buffington *et al.*, 2014). By regulating translation, the ISR impacts long-term potentiation and depression (Costa-Mattioli *et al.*, 2007; Panja *et al.*, 2009; Jiang *et al.*, 2010; Di Prisco *et al.*, 2014) and prolonged ISR activation has been shown to cause cognitive decline and memory deficits (Ma *et al.*, 2013a; Chou *et al.*, 2017). Under these circumstances, relieving ISR-mediated translational repression by treatment with the small

molecule inhibitor ISRIB (integrated stress response inhibitor) to block phosphorylation of eIF2α constitutes a neuroprotective remedy (Sidrauski *et al.*, 2013; Sharma *et al.*, 2018; Krukowski *et al.*, 2020). This special function of the ISR suggests that it may be more tightly controlled in neurons than in other cell types and that tinkering with its activation might be a double-edged sword.

In Western blot experiments analyzing the potential activation of the PERK branch by GFAT-1 gof and GlcNAc, we used TM as a positive control and were surprised to find robust ATF4 induction without a concomitant increase in levels of phosphorylated eIF2α. This warrants further investigation and could be examined by combining TM and ISRIB to check if protein levels of ATF4 are still increased in the absence of eIF2α phosphorylation.

Activation of the HBP due to genetic gof or supplementation of its metabolite substrates leads to increased production of its end product UDP-GlcNAc. The latter serves as the precursor molecule for glycosylation and O-GlcNAcylation of proteins. However, none of the previous studies investigating GFAT-1 gof have reported data related to these glycoside modifications but focused on more readily accessible signaling aspects. O-GlcNAc transferase (OGT), the enzyme catalyzing O-GlcNAcylation of proteins, is highly sensitive to changes in the intracellular concentration of UDP-GlcNAc (Kreppel & Hart, 1999; Boehmelt *et al.*, 2000). Therefore, it seems likely that potential beneficial effects of increased HBP flux at least in part stem from increased O-GlcNAcylation of certain, still unidentified, target proteins. Since O-GlcNAcylation is a wide-spread post-translational modification, identification of individual proteins differentially modified in a GFAT-1 gof background may be challenging. We tried to assess possible differences in the global abundance of O-GlcNAcylation in neuronal cultures due to GlcNAc supplementation or GFAT-1 gof but the relevant Western blot experiments remained unsuccessful owing to technical difficulties (data not shown). The elementary role of O-GlcNAcylation as a wide-ranging pro-survival response to various kinds of stress has been well described for many different cell types (Butkinaree *et al.*, 2011; Martinez *et al.*, 2017). Interestingly, Horn *et al*. claimed that knockdown of OGT in *C. elegans* did not attenuate the potency of HBP activation in alleviating the burden of cytotoxic protein aggregates (Horn *et al.*, 2020). In contrast, experiments with a cardiac ischemia/reperfusion model in mice found the UPR-dependent induction of GFAT-1 and the concomitant increase in O-GlcNAcylation to be essential for tissue protection (Wang *et al.*, 2014b). Similarly, human bronchial epithelial cells challenged by deprivation of glucose or amino acids relied on ATF4-driven upregulation of GFAT-1 to engage O-GlcNAcylation-based cytoprotection (Chaveroux *et al.*, 2016). Even though O-GlcNAcylation exists in *C. elegans*, its importance may be much more limited than in higher eukaryotes. In line with this notion, OGT knockout in mammals is embryonically lethal (Shafi *et al.*, 2000; O'Donnell *et al.*, 2004) whereas *C. elegans* OGT null animals are viable and fertile (Hanover *et al.*, 2005). Data reporting the effects of HBP activation in non-mammalian systems

may therefore be missing out on an important regulatory aspect. The same is true for sialic acids which also require UDP-GlcNAc for their biosynthesis and are very important in the biology of most vertebrates but are completely absent in *C. elegans* (Varki, 2008).

Detailed quantitative analysis of the abundance of O-GlcNAcylation in different tissues is still lacking but the importance of O-GlcNAc can be indirectly inferred from the expression of OGT and its counterpart OGA (O-GlcNAcase) whose tissue abundance has been thoroughly studied. OGT is most highly expressed in pancreas and brain (Kreppel *et al.*, 1997; Lubas *et al.*, 1997) and its activity is up to 10-fold higher in brain than in liver, heart, muscle or adipose tissue (Okuyama & Marshall, 2003). Similarly, OGA expression levels are highest in the brain (Gao *et al.*, 2001). Since O-GlcNAcylation often competes with phosphorylation for the same serine and threonine residues, increased O-GlcNAcylation may indirectly affect intracellular signaling by blocking phosphorylation target sites (Hart *et al.*, 2011; Laarse *et al.*, 2018). This interplay is exemplified by the decreased O-GlcNAcylation of Tau which opens the door for its aberrant hyperphosphorylation that is involved in the pathology of Alzheimer's disease (Gong *et al.*, 2016).

Usually, the brain accounts for about 20% of the body's energy consumption (Mink *et al.*, 1981; Attwell & Laughlin, 2001; Nortley & Attwell, 2017). A decline in glucose metabolism is a hallmark of the aging brain and it is even more pronounced in the brains of AD patients (Alexander *et al.*, 2002; Drzezga *et al.*, 2003). Aside from a resulting restriction of the cellular energy pool due to scarcity of ATP, impairment of glucose metabolism likely translates into reduced flux through the HBP and therefore less UDP-GlcNAc for protein glycosylation and O-GlcNAcylation. Extended fasting causes a strong ablation of O-GlcNAc levels in the cortex and hippocampus of mice and promotes aggregation of hyperphosphorylated Tau (Li *et al.*, 2006). Conversely, elevating O-GlcNAc levels increases the solubility of Tau and slows down neurodegeneration (Yuzwa *et al.*, 2012). This highlights the potential that genetic or pharmacological activation of the HBP might have for biochemical modulation of adult brain physiology by replenishing O-GlcNAc levels.

As a minimal PTM, O-GlcNAcylation is inherently difficult to study and not accessible by standard laboratory techniques. To date, experiments for a detailed mapping of O-GlcNAc modifications rely on metabolic labelling, intracellular click chemistry and sophisticated mass spectrometry approaches (Worth *et al.*, 2017; Chen *et al.*, 2019; Escobar *et al.*, 2020). Data explicitly focusing on the role and regulation of the HBP in human neurons is very limited and does currently not appear to be subject of major research projects. A few reports have highlighted deficiency of GFAT-1 in muscle to cause disruption of the neuromuscular junction and related neurotransmission in congenital myasthenic syndrome (Senderek *et al.*, 2011; Zoltowska *et al.*, 2013; Issop *et al.*, 2018). However, the involved motor neurons show normal *GFPT1* expression and their presynaptic compartments contributing to

the neuromuscular junction are only indirectly affected due to the functional deficiency of the postsynaptic site at the muscle. Consequently, elucidating the effects of GFAT-1 gof on global O-GlcNAcylation levels and identification of specifically affected proteins offers an interesting avenue for future research concerning the role of HBP activation and related therapeutic interventions in human neurons.

9 Abbreviations

Abbreviation	Full name
Ø	diameter
(v/v)	volume per volume
(w/v)	weight per volume
3-MA	3-methyladenine
AA	ascorbic acid
Ac-CoA	acetyl coenzyme A
ACIN1	
AD	Alzheimer's disease
AIS	axon initial segment
AMPA	α-amino-3-hydroxy-5-methyl-4-isoxazolepropionic acid
AMPK	adenosine monophosphate-activated kinase
AP	action potential
APAF-1	apoptotic protease activating factor-1
APP	amyloid precursor protein
APS	ammonium persulfate
AREL1	apoptosis-resistant E3 ubiquitin protein ligase 1
ARTS	apoptosis-related protein in TGF-β signaling pathway
ATF4	activating transcription factor 4
ATP	adenosine triphosphate
BAD	Bcl-2 associated agonist of cell death
Baf. A1	Bafilomycin A1
BCA	bicinchoninic acid
BDNF	brain-derived neurotrophic factor
BH	Bcl-2 homology
BID	BH-3 interacting domain death agonist
BiP	binding immunoglobulin protein
BIR	baculovirus IAP repeat
BIRC	BIR containing
BMP	bone morphogenetic protein
Bp	base pair
BrdU	bromodeoxyuridine
BSA	bovine serum albumin
CAD	caspase-activated DNase
CAM	cell adhesion molecule
CARD	caspase activation and recruitment domain
cDNA	complementary DNA
CDS	coding sequence
cIAP	cellular inhibitor of apoptosis protein
CNS	central nervous system
CP	cortical plate
CreP	constitutive repressor of eIF2α phosphorylation
CRISPR	Clustered regularly interspaced short palindromic repeats
CTG	CellTiter-Glo™
DAPI	4',6-diamidino-2-phenylindole
DAPT	N-[N-(3,5-Difluorophenacetyl-L-alanyl)]-(S)-phenylglycine t-butyl ester
DD	death domain
DEPC	diethyl pyrocarbonate
DIABLO	direct inhibitor of apoptosis-binding protein with low pI
DISC	death-inducing signal complex
DMSO	Dimethyl sulfoxide
DNA	deoxyribonucleic acid
dNTPs	deoxynucleoside triphosphate
ddH_2O	double-distilled water
DUB	deubiquitinating enzyme
ECM	extracellular matrix
EDTA	ethylenediaminetetraacetic acid
eIF2α	alpha subunit of eukaryotic translation initiation factor 2
EGTA	Ethylene glycol-bis(2-aminoethylether)-N,N,N,N-tetraacetic acid
ER	endoplasmic reticulum
ERAD	ER-associated degradation
ESC	embryonic stem cell
FADD	FAS-associated death domain
FasR	Fas receptor
FBS	fetal bovine serum
FGF2	fibroblast growth factor 2
GABA	γ-Aminobutyric acid
GADD34	growth arrest and DNA damage-inducible protein
GALE	UDP-galactose-4-epimerase

Abbreviation	Full name
GCN2	general control non-derepressible 2
gDNA	genomic DNA
GE	ganglionic eminence
GFAT	glutamine-fructose 6-phosphate aminotransferase
GlcNAc	N-acetyl-D-glucosamine
GNA-1	glucosamine-phosphate N-acetyltransferase
GO	gene ontology
gof	gain-of-function
gRNA	guide ribonucleic acid
GRP78	78-kDa glucose-regulated protein
HBP	hexosamine biosynthetic pathway
HDR	homology-directed repair
HEK	human embryonic kidney
hiPSCs	human induced pluripotent stem cells
HRI	heme-regulated eIF2α kinase
HSP	heat shock protein
HtrA2	high-temperature requirement A2
IAPs	inhibitor of apoptosis proteins
IBM	IAP binding motif
ICC	immunocytochemistry
IMP	inner mitochondrial membrane peptidase
iN	induced neuron
IPs	intermediate progenitors
IR	infrared
IRE-1	inositol-requiring enzyme-1
ISR	integrated stress response
ISRIB	Integrated stress response inhibitor
Kv	voltage-gated potassium channel
LAAP	L-ascobic acid 2-phosphate
LB	lysogeny broth
M	molar (mol/L)
MAP2	microtubule-associated protein 2
Met-tRNA$_i^{Met}$	methionyl-initiator tRNA
MOMP	mitochondrial outer membrane permeabilization
mOsm	milliosmole
MW	molecular weight
MZ	marginal zone
N2a cells	Neuro2a cells; murine neuroblastoma cells
NAD	nicotinamide adenine dinucleotide
NAGK	*N*-acetyl-*D*-glucosamine kinase
NAIP	NLR family apoptosis inhibitory protein
Nav	voltage-gated sodium channel
NC	nitrocellulose
NCAM	neural cell adhesion molecule
NEAA	non-essential amino acid
NEC	neuroepithelial cell
Neu5Ac	N-acetylneuraminic acid
NeuN	neuronal nuclei
NFI	neuron functionality index
NGF	nerve growth factor
NMDA	N-methyl-D-aspartate
NMI	neuron maturity index
NPC	neural progenitor cell
OGA	O-GlcNAcase
OGT	O-GlcNAc transferase
pA	picoampere
PAGE	polyacrylamide gel electrophoresis
PAM	protospacer adjacent motif
PARL	presenilins-associated rhomboid-like protein
PARP	poly (ADP-ribose) polymerase
PBS	phosphate-buffered saline
PC	principal component
PCA	principal component analysis
PCD	programmed cell death
PCR	polymerase chain reaction
PD	Parkinson's disease
Pen/Strep	Penicillin/Streptomycin
PERK	PKR-like ER kinase
pF	picofarad
PFA	paraformaldehyde
PGM-3	GlcNAc phosphomutase
PKA	protein kinase A
PKC	protein kinase C
PKR	double-stranded RNA-dependent protein kinase
PLL	poly-L-lysine hydrobromide
PNK	polynucleotide kinase

Abbreviation	Full name
PP	preplate
PP1	protein phosphatase 1
PSA	polysialic acid
PSD	postsynaptic density
PTM	post-translational modification
qPCR	quantitative polymerase chain reaction
RBFOX	RNA-binding protein FOX
RCF	relative centrifugal force
RGC	radial glial cell
RIN	RNA integrity number
RING	really interesting new gene
RMP	resting membrane potential
(m)RNA	(messenger) ribonucleic acid
ROCK1	rho-associated coiled-coil-containing protein kinase 1
ROCK inhibitor	Rho-associated protein kinase inhibitor
ROS	reactive oxygen species
RPKM	reads per kilobase million
RT	room temperature
RT-PCR	reverse transcription polymerase chain reaction
SALM	synaptic adhesion-like molecules
SP	subplate
SD	standard deviation
SDS	sodium dodecyl sulfate
SDS-PAGE	SDS-polyacrylamide gel electrophoresis
S.E.M.	standard error of mean
seq	sequencing
SLC	solute carrier
Smac	second mitochondria-derived activator of caspases
SNP	single nucleotide polymorphism
SOX2	sex determining region Y-box 2
ssoligo	single-stranded oligonucleotide
STS	staurosporine
SV2	synaptic vesicle protein 2
SVZ	subventricular zone
TBST	tris-buffered saline with Tween®20
TC	time course
TEMED	N, N, N‘, N‘ – tetramethylethylenediamine
TF	transcription factor
TG	thapsigargin
TGF-β	transforming growth factor beta
TM	tunicamycin
TNF	tumor necrosis factor
TPM	transcripts per kilobase million
TRADD	TNF receptor associated death domain
TRAIL	TNF-related apoptosis-inducing ligand receptor
tRNA	transfer RNA
TS-IAP	testis specific IAP
U	enzyme unit of catalytic activity (µmol/min)
UAP-1	UDP-N-acetylglucosamine pyrophosphorylase
Ub	ubiquitin
UBA	ubiquitin associated
UDP-GlcNAc	uridine diphosphate-N-acetylglucosamine
UMI	unique molecular identifier
uORF	upstream open reading frame
USP	ubiquitin-specific proteases
UTP	uridine triphosphate
UTR	untranslated region
vs	versus
VZ	ventricular zone
WB	Western blot
WT	wild type
XAF1	XIAP-associated factor 1
XBP1	X-box binding protein 1
XIAP	X-linked inhibitor of apoptosis protein

10 References

Adomavicius, T., Guaita, M., Zhou, Y., Jennings, M.D., Latif, Z., Roseman, A.M. & Pavitt, G.D. (2019). The structural basis of translational control by eIF2 phosphorylation. *Nat. Commun.* **10**, 2136.

Ahn, J., Jee, Y., Seo, I., Seung, Y.Y., Kim, D.H., Yoo, K.K. & Lee, H. (2008). Primary neurons become less susceptible to coxsackievirus B5 following maturation: The correlation with the decreased level of CAR expression on cell surface. *J. Med. Virol.* **80**, 434–440.

Akella, N.M., Ciraku, L. & Reginato, M.J. (2019). Fueling the fire: Emerging role of the hexosamine biosynthetic pathway in cancer. *BMC Biol.* **17**, 1–14.

Alexander, G.E., Chen, K., Pietrini, P., Rapoport, S.I. & Reiman, E.M. (2002). Longitudinal PET evaluation of cerebral metabolic decline in dementia: A potential outcome measure in Alzheimer's disease treatment studies. *Am. J. Psychiatry* **159**, 738–745.

Allen, N.J. & Barres, B.A. (2005). Signaling between glia and neurons: Focus on synaptic plasticity. *Curr. Opin. Neurobiol.* **15**, 542–548.

Altman, J. (1962). Are new neurons formed in the brains of adult mammals? *Science (80-.).* **135**, 1127–1128.

Altman, J. (1963). Autoradiographic investigation of cell proliferation in the brains of rats and cats. *Anat. Rec.* **145**, 573–591.

Altman, J. & Das, G.D. (1965). Autoradiographic and histological evidence of postnatal hippocampal neurogenesis in rats. *J. Comp. Neurol.* **124**, 319–335.

Alvarez-Buylla, A., Theelen, M. & Nottebohm, F. (1988). Birth of projection neurons in the higher vocal center of the canary forebrain before, during, and after song learning. *Proc. Natl. Acad. Sci. U. S. A.* **85**, 8722–8726.

Alvarez-Castelao, B., Dieck, S.T., Fusco, C.M., Donlin-Asp, P.G., Perez, J.D. & Schuman, E.M. (2020). The switch-like expression of heme-regulated kinase 1 mediates neuronal proteostasis following proteasome inhibition. *Elife* **9**.

Amerik, A.Y. & Hochstrasser, M. (2004). Mechanism and function of deubiquitinating enzymes. *Biochim. Biophys. Acta - Mol. Cell Res.* **1695**, 189–207.

Andrews, S., Krueger, F., Segonds-Pichon, A., Biggins, L., Krueger, C. & Wingett, S. (2015). FastQC: a quality control tool for high throughput sequence data.

Annis, R.P., Swahari, V., Nakamura, A., Xie, A.X. & Hammond, S.M. (2016). Mature neurons dynamically restrict apoptosis via redundant premitochondrial brakes **283**, 4569–4582.

Attwell, D. & Laughlin, S.B. (2001). An energy budget for signaling in the grey matter of the brain. *J. Cereb. Blood Flow Metab.* **21**, 1133–1145.

Azevedo, F.A.C., Carvalho, L.R.B., Grinberg, L.T., Farfel, J.M., Ferretti, R.E.L., Leite, R.E.P., Filho, W.J., *et al.* (2009). Equal numbers of neuronal and nonneuronal cells make the human brain an isometrically scaled-up primate brain. *J. Comp. Neurol.* **513**, 532–541.

Bao, Q., Lu, W., Rabinowitz, J.D. & Shi, Y. (2007). Calcium Blocks Formation of Apoptosome by Preventing Nucleotide Exchange in Apaf-1. *Mol. Cell* **25**, 181–192.

Bardy, C., Van Den Hurk, M., Kakaradov, B., Erwin, J.A., Jaeger, B.N., Hernandez, R. V., Eames, T., *et*

al. (2016). Predicting the functional states of human iPSC-derived neurons with single-cell RNA-seq and electrophysiology. *Mol. Psychiatry* **21**, 1573–1588.

Barker, R.A., Parmar, M., Studer, L. & Takahashi, J. (2017). Human Trials of Stem Cell-Derived Dopamine Neurons for Parkinson's Disease: Dawn of a New Era. *Cell Stem Cell* **21**, 569–573.

Benedict, M.A., Hu, Y., Inohara, N. & Nunez, G. (2000). Expression and Functional Analysis of Apaf-1 Isoforms **275**, 8461–8468.

Bennett, V. & Lorenzo, D.N. (2013). Spectrin- and Ankyrin-Based Membrane Domains and the Evolution of Vertebrates. In *Current Topics in Membranes*: 1–37. Academic Press Inc.

Bernardini, J.P., Brouwer, J.M., Tan, I.K., Sandow, J.J., Huang, S., Stafford, C.A., Bankovacki, A., *et al.* (2019). Parkin inhibits BAK and BAX apoptotic function by distinct mechanisms during mitophagy. *EMBO J.* **38**, 1–16.

Bertolotti, A., Zhang, Y., Hendershot, L.M., Harding, H.P. & Ron, D. (2000). Dynamic interaction of BiP and ER stress transducers in the unfolded-protein response. *Nat. Cell Biol.* **2**, 326–332.

Birnbaum, M.J., Clem, R.J. & Miller, L.K. (1994). An apoptosis-inhibiting gene from a nuclear polyhedrosis virus encoding a polypeptide with Cys/His sequence motifs. *J. Virol.* **68**, 2521–2528.

Biswas, D. & Jiang, P. (2016). Chemically induced reprogramming of somatic cells to pluripotent stem cells and neural cells. *Int. J. Mol. Sci.* **17**.

Blankenship, J.W., Varfolomeev, E., Goncharov, T., Fedorova, A. V., Kirkpatrick, D.S., Izrael-Tomasevic, A., Phu, L., *et al.* (2009). Ubiquitin binding modulates IAP antagonist-stimulated proteasomal degradation of c-IAP1 and c-IAP21. *Biochem. J.* **417**, 149–160.

Bobrovnikova-Marjon, E., Grigoriadou, C., Pytel, D., Zhang, F., Ye, J., Koumenis, C., Cavener, D., *et al.* (2010). PERK promotes cancer cell proliferation and tumor growth by limiting oxidative DNA damage. *Oncogene* **29**, 3881–3895.

Boehmelt, G., Wakeham, A., Elia, A., Sasaki, T., Plyte, S., Potter, J., Yang, Y., *et al.* (2000). Decreased UDP-GIcNAc levels abrogate proliferation control in EMeg32-deficient cells. *EMBO J.* **19**, 5092–5104.

Boldrini, M., Fulmore, C.A., Tartt, A.N., Simeon, L.R., Pavlova, I., Poposka, V., Rosoklija, G.B., *et al.* (2018). Human Hippocampal Neurogenesis Persists throughout Aging. *Cell Stem Cell* **22**, 589-599.e5.

Bonifati, V., Dekker, M.C.J., Vanacore, N., Fabbrini, G., Squitieri, F., Marconi, R., Antonini, A., *et al.* (2002). Autosomal recessive early onset parkinsonism is linked to three loci: PARK2, PARK6, and PARK7. *Neurol. Sci.* **23**.

Borck, G., Shin, B.S., Stiller, B., Mimouni-Bloch, A., Thiele, H., Kim, J.R., Thakur, M., *et al.* (2012). EIF2γ Mutation that Disrupts eIF2 Complex Integrity Links Intellectual Disability to Impaired Translation Initiation. *Mol. Cell* **48**, 641–646.

Bork, K., Horstkorte, R. & Weidemann, W. (2009). Increasing the sialylation of therapeutic glycoproteins: The potential of the sialic acid biosynthetic pathway. *J. Pharm. Sci.* **98**, 3499–3508.

Bratton, S.B. & Salvesen, G.S. (2010). Regulation of the Apaf-1-caspase-9 apoptosome. *J. Cell Sci.* **123**, 3209–3214.

Buffington, S.A., Huang, W. & Costa-Mattioli, M. (2014). Translational control in synaptic plasticity and cognitive dysfunction. *Annu. Rev. Neurosci.* **37**, 17–38.

Burke, E.E., Chenoweth, J.G., Shin, J.H., Collado-Torres, L., Kim, S.K., Micali, N., Wang, Y., *et al.* (2020). Dissecting transcriptomic signatures of neuronal differentiation and maturation using iPSCs. *Nat. Commun.* **11**, 1–14.

Burri, L., Strahm, Y., Hawkins, C.J., Gentle, I.E., Puryer, M.A., Verhagen, A., Callus, B., *et al.* (2005). Mature DIABLO/Smac Is Produced by the IMP Protease Complex on the Mitochondrial Inner Membrane. *Mol. Biol. Cell* **16**, 2926–2933.

Burwick, N. & Aktas, B.H. (2017). The eIF2-alpha kinase HRI: a potential target beyond the red blood cell. *Expert Opin Ther Targets* **176**, 139–148.

Bush, K.T., Goldberg, A.L. & Nigam, S.K. (1997). Proteasome Inhibition Leads to a Heat-shock Response, Induction of Endoplasmic Reticulum Chaperones, and Thermotolerance. *J Biol Chem* **272**, 9086–92.

Buss, R.R., Sun, W. & Oppenheim, R.W. (2006). Adaptive roles of programmed cell death during nervous system development. *Annu. Rev. Neurosci.* **29**, 1–35.

Butkinaree, C., Park, K. & Hart, G.W. (2011). Transcription in Response to Nutrients and Stress. *Biochim Biophys Acta.* **1800**, 1–23.

Cao, J., Spielmann, M., Qiu, X., Huang, X., Ibrahim, D.M., Hill, A.J., Zhang, F., *et al.* (2014). The dynamics and regulators of cell fate decisions are revealed by pseudo-temporal ordering of single cells. *Nat. Biotechnol.* **32**, 381–86.

Carlson, M. (2020). org.Hs.eg.db: Genome wide annotation for Human.

Chambers, S.M., Fasano, C.A., Papapetrou, E.P., Tomishima, M., Sadelain, M. & Studer, L. (2009). Highly efficient neural conversion of human ES and iPS cells by dual inhibition of SMAD signaling. *Nat. Biotechnol.* **27**, 275–280.

Chang, Q., Su, K., Baker, J.R., Yang, X., Paterson, A.J. & Kudlow, J.E. (2000). Phosphorylation of human glutamine:fructose-6-phosphate amidotransferase by cAMP-dependent protein kinase at serine 205 blocks the enzyme activity. *J. Biol. Chem.* **275**, 21981–21987.

Chang, R.C.C., Wong, A.K.Y., Ng, H.-K. & Hugon, J. (2002). Phosphorylation of eukaryotic initiation factor-2alpha (eIF2alpha) is associated with neuronal degeneration in Alzheimer's disease. *Neuroreport* **13**, 2429–2432.

Chaudhuri, A.R. & Nussenzweig, A. (2017). The multifaceted roles of PARP1 in DNA repair and chromatin remodelling. *Nat Rev Mol Cell Biol* **18**, 610–621.

Chaveroux, C., Sarcinelli, C., Barbet, V., Belfeki, S., Barthelaix, A., Ferraro-Peyret, C., Lebecque, S., *et al.* (2016). Nutrient shortage triggers the hexosamine biosynthetic pathway via the GCN2-ATF4 signalling pathway. *Sci. Rep.* **6**, 1–10.

Chen, A., Muzzio, I.A., Malleret, G., Bartsch, D., Verbitsky, M., Pavlidis, P., Yonan, A.L., *et al.* (2003). Inducible enhancement of memory storage and synaptic plasticity in transgenic mice expressing an inhibitor of ATF4 (CREB-2) and C/EBP proteins. *Neuron* **39**, 655–669.

Chen, D., Gao, F., Li, B., Wang, H., Xu, Y., Zhu, C. & Wang, G. (2010). Parkin Mono-ubiquitinates Bcl-2 and Regulates Autophagy. *J Biol Chem* **285**, 38214–38223.

Chen, H.H. & Tarn, W.Y. (2019). uORF-mediated translational control: recently elucidated mechanisms and implications in cancer. *RNA Biol.* **16**, 1327–1338.

Chen, I.P., Fukuda, K., Fusaki, N., Iida, A., Hasegawa, M., Lichtler, A. & Reichenberger, E.J. (2013). Induced pluripotent stem cell reprogramming by integration-free sendai virus vectors from peripheral blood of patients with craniometaphyseal dysplasia. *Cell. Reprogram.* **15**, 503–513.

Chen, M. & Wang, J. (2002). Initiator caspases in apoptosis signaling pathways. *Apoptosis* **7**, 313–319.

Chen, Q., Xu, J., Li, L., Li, H., Mao, S., Zhang, F., Zen, K., *et al.* (2014). MicroRNA-23a/b and microRNA-27a/b suppress Apaf-1 protein and alleviate hypoxia-induced neuronal apoptosis. *Cell Death Dis.* **5**, 1132.

Chen, Y. & Tian, Q. (2011). The role of protein kinase C epsilon in neural signal transduction and neurogenic diseases. *Front. Med. China* **5**, 70–76.

Chen, Z., Huang, J. & Li, L. (2019). Recent advances in mass spectrometry (MS)-based glycoproteomics in complex biological samples. *TrAC - Trends Anal. Chem.* **118**, 880–892.

Chiaradonna, F., Ricciardiello, F. & Palorini, R. (2018). The Nutrient-Sensing Hexosamine Biosynthetic Pathway as the Hub of Cancer Metabolic Rewiring. *Cells* **7**, 53.

Chou, A., Krukowski, K., Jopson, T., Zhu, P.J., Costa-Mattioli, M., Walter, P. & Rosi, S. (2017). Inhibition of the integrated stress response reverses cognitive deficits after traumatic brain injury. *Proc. Natl. Acad. Sci. U. S. A.* **114**, E6420–E6426.

Clark, B.D., Goldberg, E.M. & Rudy, B. (2009). Electrogenic tuning of the axon initial segment. *Neuroscientist* **15**, 651–668.

Cláudio, N., Dalet, A., Gatti, E. & Pierre, P. (2013). Mapping the crossroads of immune activation and cellular stress response pathways. *EMBO J.* **32**, 1214–1224.

Coccia, E., Planells-Ferrer, L., Badillos-Rodríguez, R., Pascual, M., Segura, M.F., Fernández-Hernández, R., López-Soriano, J., *et al.* (2020). SIVA-1 regulates apoptosis and synaptic function by modulating XIAP interaction with the death receptor antagonist FAIM-L. *Cell Death Dis.* **11**, 82.

Collins, M.O., Husi, H., Yu, L., Brandon, J.M., Anderson, C.N.G., Blackstock, W.P., Choudhary, J.S., *et al.* (2006). Molecular characterization and comparison of the components and multiprotein complexes in the postsynaptic proteome. *J. Neurochem.* **97 Suppl 1**, 16–23.

Corlew, R., Bosma, M.M. & Moody, W.J. (2004). Spontaneous, synchronous electrical activity in neonatal mouse cortical neurones. *J. Physiol.* **560**, 377–390.

Costa-Mattioli, M., Gobert, D., Stern, E., Gamache, K., Colina, R., Cuello, C., Sossin, W., *et al.* (2007). eIF2α Phosphorylation Bidirectionally Regulates the Switch from Short- to Long-Term Synaptic Plasticity and Memory. *Cell* **129**, 195–206.

Costa-Mattioli, M. & Walter, P. (2020). The integrated stress response: From mechanism to disease. *Science* **368**.

Creagh, E.M., Murphy, B.M., Duriez, P.J., Duckett, C.S. & Martin, S.J. (2004). Smac / Diablo Antagonizes Ubiquitin Ligase Activity of Inhibitor of Apoptosis Proteins. *J Biol Chem* **279**, 26906–26914.

Crook, N.E., Clem, R.J. & Miller, L.K. (1993). An apoptosis-inhibiting baculovirus gene with a zinc finger-like motif. *J. Virol.* **67**, 2168–2174.

D'Amelio, M., Cavallucci, V. & Cecconi, F. (2010). Neuronal caspase-3 signaling: Not only cell death. *Cell Death Differ.* **17**, 1104–1114.

D'Arcangelo, G., Miao, G.G., Chen, S.C., Scares, H.D., Morgan, J.I. & Curran, T. (1995). A protein related to extracellular matrix proteins deleted in the mouse mutant reeler. *Nature* **374**, 719–723.

D'Arcy, M.S. (2019). Cell death: a review of the major forms of apoptosis, necrosis and autophagy. *Cell Biol. Int.* **43**, 582–592.

D'Este, E., Kamin, D., Göttfert, F., El-Hady, A. & Hell, S.W. (2015). STED Nanoscopy Reveals the Ubiquity of Subcortical Cytoskeleton Periodicity in Living Neurons. *Cell Rep.* **10**, 1246–1251.

Daviet, L. & Colland, F. (2008). Targeting ubiquitin specific proteases for drug discovery. *Biochimie* **90**, 270–283.

Denisot, M.A., Goffic, F. Le & Badet, B. (1991). Glucosamine-6-phosphate synthase from Escherichia coli yields two proteins upon limited proteolysis: Identification of the glutamine amidohydrolase and 2R ketose/aldose isomerase-bearing domains based on their biochemical properties. *Arch. Biochem. Biophys.* **288**, 225–230.

Dennis, D., Picketts, D., Slack, R.S. & Schuurmans, C. (2017). Forebrain neurogenesis : From embryo to adult **9**, 77–90.

Denoth-Lippuner, A. & Jessberger, S. (2019). Mechanisms of cellular rejuvenation. *FEBS Lett.*

Denzel, M.S. & Antebi, A. (2015). Hexosamine pathway and (ER) protein quality control. *Curr. Opin. Cell Biol.* **33**, 14–18.

Denzel, M.S., Storm, N.J., Gutschmidt, A., Baddi, R., Hinze, Y., Jarosch, E., Sommer, T., *et al.* (2014). Hexosamine pathway metabolites enhance protein quality control and prolong life. *Cell* **156**, 1167–1178.

Dewson, G. & Kluck, R.M. (2009). Mechanisms by which Bak and Bax permeabilise mitochondria during apoptosis. *J. Cell Sci.* **122**, 2801–2808.

Dewson, G., Kratina, T., Sim, H.W., Puthalakath, H., Adams, J.M., Colman, P.M. & Kluck, R.M. (2008). To Trigger Apoptosis, Bak Exposes Its BH3 Domain and Homodimerizes via BH3:Groove Interactions. *Mol. Cell* **30**, 369–380.

Doi, D., Samata, B., Katsukawa, M., Kikuchi, T., Morizane, A., Ono, Y., Sekiguchi, K., *et al.* (2014). Isolation of human induced pluripotent stem cell-derived dopaminergic progenitors by cell sorting for successful transplantation. *Stem Cell Reports* **2**, 337–350.

Dong, T., Kang, X., Liu, Z., Zhao, S., Ma, W., Xuan, Q., Liu, H., *et al.* (2016). Altered glycometabolism affects both clinical features and prognosis of triple-negative and neoadjuvant chemotherapy-treated breast cancer. *Tumor Biol.* **37**, 8159–8168.

Drzezga, A., Lautenschlager, N., Siebner, H., Riemenschneider, M., Willoch, F., Minoshima, S., Schwaiger, M., *et al.* (2003). Cerebral metabolic changes accompanying conversion of mild cognitive impairment into alzheimer's disease: A PET follow-up study. *Eur. J. Nucl. Med. Mol. Imaging* **30**, 1104–1113.

Duan, F., Jia, D., Zhao, J., Wu, W., Min, L., Song, S., Wu, H., *et al.* (2016). Loss of GFAT1 promotes epithelial-to-mesenchymal transition and predicts unfavorable prognosis in gastric cancer. *Oncotarget* **7**, 38427–38439.

Dzhashiashvili, Y., Zhang, Y., Galinska, J., Lam, I., Grumet, M. & Salzer, J.L. (2007). Nodes of Ranvier and axon initial segments are ankyrin G-dependent domains that assemble by distinct mechanisms. *J. Cell Biol.* **177**, 857–870.

Easton, R.M., Deckwerth, T.L., Parsadanian, A.S. & Johnson, E.M. (1997). Analysis of the mechanism of loss of trophic factor dependence associated with neuronal maturation: A phenotype indistinguishable from Bax deletion. *J. Neurosci.* **17**, 9656–9666.

Edge, L., Sanes, J.R. & Zipursky, S.L. (2020). Synaptic Specificity , Recognition Molecules , and Assembly of Neural Circuits. *Cell* **181**, 536–556.

Eguchi, S., Oshiro, N., Miyamoto, T., Yoshino, K.I., Okamoto, S., Ono, T., Kikkawa, U., *et al.* (2009). AMP-activated protein kinase phosphorylates glutamine: Fructose-6-phosphate amidotransferase 1 at Ser243 to modulate its enzymatic activity. *Genes to Cells* **14**, 179–189.

Ehninger, D. & Kempermann, G. (2008). Neurogenesis in the adult hippocampus. *Cell Tissue Res.* **331**, 243–250.

Einsele-Scholz, S., Malmsheimer, S., Bertram, K., Stehle, D., Johänning, J., Manz, M., Daniel, P.T., *et al.* (2016). Bok is a genuine multi-BH-domain protein that triggers apoptosis in the absence of Bax and Bak. *J. Cell Sci.* **129**, 2213–2223.

Ekinci, F.J. & Shea, T.B. (1997). Selective activation by bryostatin-1 demonstrates unique roles for PKCε in neurite extension and tau phosphorylation. *Int. J. Dev. Neurosci.* **15**, 867–874.

Ellis, J. (2005). Silencing and variegation of gammaretrovirus and lentivirus vectors. *Hum. Gene Ther.* **16**, 1241–1246.

Elmore, S. (2007). Apoptosis: A Review of Programmed Cell Death. *Toxicol. Pathol.* **35**, 495–516.

Eriksson, P.S., Perfilieva, E., Björk-Eriksson, T., Alborn, A.M., Nordborg, C., Peterson, D.A. & Gage, F.H. (1998). Neurogenesis in the adult human hippocampus. *Nat. Med.* **4**, 1313–1317.

Escobar, E.E., King, D.T., Serrano-Negrón, J.E., Alteen, M.G., Vocadlo, D.J. & Brodbelt, J.S. (2020). Precision Mapping of O-Linked N-Acetylglucosamine Sites in Proteins Using Ultraviolet Photodissociation Mass Spectrometry. *J. Am. Chem. Soc.* **142**, 11569–11577.

Espinosa-oliva, A.M., García-revilla, J., Alonso-bellido, I.M., Burguillos, M.A., Campos-peña, V., Matias-guiu, J., Stupack, D.G., *et al.* (2019). Brainiac Caspases : Beyond the Wall of Apoptosis **13**, 1–9.

Estornes, Y. & Bertrand, M.J.M. (2015). IAPs, regulators of innate immunity and inflammation. *Semin. Cell Dev. Biol.* **39**, 106–114.

Fache, M.P., Moussif, A., Fernandes, F., Giraud, P., Garrido, J.J. & Dargent, B. (2004). Endocytotic elimination and domain-selective tethering constitute a potential mechanism of protein segregation at the axonal initial segment. *J. Cell Biol.* **166**, 571–578.

Fagerström, S., Påhlman, S., Gestblom, C. & Nånberg, E. (1996). Protein kinase C-ε is implicated in neurite outgrowth in differentiating human neuroblastoma cells. *Cell Growth Differ.* **7**, 775–785.

Farhy-Tselnicker, I. & Allen, N.J. (2018). Astrocytes, neurons, synapses: A tripartite view on cortical circuit development. *Neural Dev.* **13**, 1–12.

Farías, G.G., Guardia, C.M., Britt, D.J., Guo, X. & Bonifacino, J.S. (2015). Sorting of Dendritic and Axonal Vesicles at the Pre-axonal Exclusion Zone. *Cell Rep.* **13**, 1221–1232.

Farook, J.M., Shields, J., Tawfik, A., Markand, S., Sen, T., Smith, S.B., Brann, D., *et al.* (2013). GADD34 induces cell death through inactivation of Akt following traumatic brain injury. *Cell Death Dis.* **4**, e754.

Farooqui, T., Franklin, T., Pearl, D.K. & Yates, A.J. (1997). Ganglioside GM1 enhances induction by nerve growth factor of a putative dimer of TrkA. *J. Neurochem.* **68**, 2348–2355.

Fasano, C.A., Chambers, S.M., Lee, G., Tomishima, M.J. & Studer, L. (2010). Efficient Derivation of Functional Floor Plate Tissue from Human Embryonic Stem Cells. *Cell Stem Cell* **6**, 336–347.

Fath, T., Eidenmüller, J. & Brandt, R. (2002). Tau-mediated cytotoxicity in a pseudohyperphosphorylation model of Alzheimer's disease. *J. Neurosci.* **22**, 9733–9741.

Fernández-Marrero, Y., Bleicken, S., Das, K.K., Bachmann, D., Kaufmann, T. & Garcia-Saez, A.J. (2017). The membrane activity of BOK involves formation of large, stable toroidal pores and is promoted by cBID. *FEBS J.* **284**, 711–724.

Ferreira, C.G., Van der Valk, P., Span, S.W., Ludwig, I., Smit, E.F., Kruyt, F.A.E., Pinedo, H.M., *et al.* (2001). Expression of X-linked inhibitor of apoptosis as a novel prognostic marker in radically resected non-small cell lung cancer patients. *Clin. Cancer Res.* **7**, 2468–2474.

Fiock, K.L., Smalley, M.E., Crary, J.F., Pasca, A.M. & Hefti, M.M. (2020). Increased tau expression correlates with neuronal maturation in the developing human cerebral cortex. *eNeuro* **7**.

Flanagan, L., Sebastià, J., Tuffy, L.P., Spring, A., Lichawska, A., Devocelle, M., Prehn, J.H.M., *et al.* (2010). XIAP impairs Smac release from the mitochondria during apoptosis. *Cell Death Dis.* **1**, 1–13.

Fletcher, T.L., Cameron, P., De Camilli, P. & Banker, G. (1991). The distribution of synapsin I and synaptophysin in hippocampal neurons developing in culture. *J. Neurosci.* **11**, 1617–1626.

Flintegaard, T. V., Thygesen, P., Rahbek-Nielsen, H., Levery, S.B., Kristensen, C., Clausen, H. & Bolt, G. (2010). N-glycosylation increases the circulatory half-life of human growth hormone. *Endocrinology* **151**, 5326–5336.

Florio, M. & Huttner, W.B. (2014). Neural progenitors, neurogenesis and the evolution of the neocortex. *Dev.* **141**, 2182–2194.

Fortin, A., Cregan, S.P., MacLaurin, J.G., Kushwaha, N., Hickman, E.S., Thompson, C.S., Hakim, A., *et al.* (2001). APAF1 is a key transcriptional target for p53 in the regulation of neuronal cell death. *J. Cell Biol.* **155**, 207–216.

Frantz, C., Stewart, K.M. & Weaver, V.M. (2010). The extracellular matrix at a glance. *J. Cell Sci.* **123**, 4195–4200.

Fried, S.I., Lasker, A.C.W., Desai, N.J., Eddington, D.K. & Rizzo, J.F. (2009). Axonal sodium-channel bands shape the response to electric stimulation in retinal ganglion cells. *J. Neurophysiol.* **101**, 1972–1987.

Fuchs, Y. & Steller, H. (2011). Programmed cell death in animal development and disease. *Cell* **147**, 742–758.

Gage, F.H. (2000). Mammalian neural stem cells. *Science (80-.).* **287**, 1433–1438.

Gao, Y.-L., Wang, N., Sun, F.-R., Cao, X.-P., Zhang, W. & Yu, J.-T. (2018). Tau in neurodegenerative disease. *Ann. Transl. Med.* **6**, 175–175.

Gao, Y., Wells, L., Comer, F.I., Parker, G.J. & Hart, G.W. (2001). Dynamic O-glycosylation of nuclear and cytosolic proteins: Cloning and characterization of a neutral, cytosolic β-N-acetylglucosaminidase from human brain. *J. Biol. Chem.* **276**, 9838–9845.

García, M.A., Meurs, E.F. & Esteban, M. (2007). The dsRNA protein kinase PKR: Virus and cell control. *Biochimie* **89**, 799–811.

Garnier, S. (2018). viridis: Default Color Maps from “matplotlib.”

Garrison, J.B., Correa, R.G., Gerlic, M., Yip, K.W., Krieg, A., Tamble, C.M., Shi, R., *et al.* (2011). ARTS and Siah collaborate in a pathway for XIAP degradation. *Mol. Cell* **41**, 107–116.

George, N.M., Evans, J.J.D. & Luo, X. (2007). A three-helix homo-oligomerization domain containing BH3 and BH1 is responsible for the apoptotic activity of Bax. *Genes Dev.* **21**, 1937–1948.

Gero, D., Erde, K., Szoleczky, P., Dewitt, D., Szabo, C. & Mo, K. (2012). Cellular bioenergetics is regulated by PARP1 under resting conditions and during oxidative stress **83**, 633–643.

Ghose, P. & Shaham, S. (2020). Cell death in animal development. *Dev.* **147**.

Ghosh, S., Blumenthal, H.J., Davidson, E. & Roseman, S. (1960). Glucosamine metabolism. V. Enzymatic synthesis of glucosamine 6-phosphate. *J. Biol. Chem.* **235**, 1265–1273.

Goldman, S.A. & Nottebohm, F. (1983). Neuronal production, migration, and differentiation in a vocal control nucleus of the adult female canary brain. *Proc. Natl. Acad. Sci. U. S. A.* **80**, 2390–2394.

Gómez-Climent, M.Á., Guirado, R., Castillo-Gómez, E., Varea, E., Gutierrez-Mecinas, M., Gilabert-Juan, J., García-Mompó, C., *et al.* (2011). The polysialylated form of the neural cell adhesion molecule (PSA-NCAM) is expressed in a subpopulation of mature cortical interneurons characterized by reduced structural features and connectivity. *Cereb. Cortex* **21**, 1028–1041.

Gonçalves, C.A., Rodrigues, L., Bobermin, L.D., Zanotto, C., Vizuete, A., Quincozes-Santos, A., Souza, D.O., *et al.* (2018). Glycolysis-derived compounds from astrocytes that modulate synaptic communication. *Front. Neurosci.* **12**, 1–17.

Gong, C., Liu, F. & Iqbal, K. (2016). O-GlcNAcylation : A regulator of tau pathology and neurodegeneration **12**, 1078–1089.

Gordiyenko, Y., Llácer, J.L. & Ramakrishnan, V. (2019). Structural basis for the inhibition of translation through eIF2α phosphorylation. *Nat. Commun.* **10**, 2640.

Gould, E., Reeves, A.J., Graziano, M.S.A. & Gross, C.G. (1999). Neurogenesis in the neocortex of adult primates. *Science (80-.).* **286**, 548–552.

Griffith, L.S., Mathes, M. & Schmitz, B. (1995). β-Amyloid precursor protein is modified with O-linked N-acetylglucosamine. *J. Neurosci. Res.* **41**, 270–278.

Grubb, M.S. & Burrone, J. (2010). Activity-dependent relocation of the axon initial segment fine-tunes neuronal excitability. *Nature* **465**, 1070–1074.

Grzybowska-Izydorczyk, O., Cebula, B., Robak, T. & Smolewski, P. (2010). Expression and prognostic significance of the inhibitor of apoptosis protein (IAP) family and its antagonists in chronic lymphocytic leukaemia. *Eur. J. Cancer* **46**, 800–810.

Guerrero, A.D., Chen, M. & Wang, J. (2008). Delineation of the caspase-9 signaling cascade. *Apoptosis* **13**, 177–186.

Guirado, R., Perez-Rando, M., Sanchez-Matarredona, D., Castillo-Gómez, E., Liberia, T., Rovira-Esteban, L., Varea, E., *et al.* (2014). The dendritic spines of interneurons are dynamic structures influenced by PSA-NCAM expression. *Cereb. Cortex* **24**, 3014–3024.

Guo, Z., Zhang, L., Wu, Z., Chen, Y., Wang, F. & Chen, G. (2014). In vivo direct reprogramming of reactive glial cells into functional neurons after brain injury and in an Alzheimer's disease model. *Cell Stem Cell* **14**, 188–202.

Guven, A., Wu, W.S., Patil, S., Gokul, K., Tekumalla, P., Sharma, S., Diers, A., *et al.* (2019). Diablo ubiquitination analysis by sandwich immunoassay. *J. Pharm. Biomed. Anal.* **173**, 40–46.

Gyrd-Hansen, M., Darding, M., Miasari, M., Santoro, M.M., Zender, L., Xue, W., Tenev, T., *et al.* (2008). IAPs contain an evolutionarily conserved ubiquitin-binding domain that regulates NF-κB as well as cell survival and oncogenesis. *Nat. Cell Biol.* **10**, 1309–1317.

Haltiwanger, R.S., Holt, G.D. & Hart, G.W. (1990). Enzymatic additon of O-GlcNAc to nuclear and cytoplasmic proteins. Identification of a uridine diphospho-N-acetylglucosamine:peptide β-N-acetylglucosaminyltransferase. *J. Biol. Chem.* **265**, 2563–2568.

Hamacher-Brady, A., Choe, S.C., Krijnse-Locker, J. & Brady, N.R. (2014). Intramitochondrial recruitment of endolysosomes mediates Smac degradation and constitutes a novel intrinsic apoptosis antagonizing function of XIAP E3 ligase. *Cell Death Differ.* **21**, 1862–1876.

Han, J., Liu, T., Huen, M.S.Y., Hu, L., Chen, Z. & Huang, J. (2014). SIVA1 directs the E3 ubiquitin ligase RAD18 for PCNA monoubiquitination. *J. Cell Biol.* **205**, 811–827.

Han, K. & Kim, E. (2008). Synaptic adhesion molecules and PSD-95. *Prog. Neurobiol.* **84**, 263–283.

Hanahan, D. & Weinberg, R.A. (2011). Hallmarks of cancer: The next generation. *Cell* **144**, 646–674.

Hanover, J.A., Forsythe, M.E., Hennessey, P.T., Brodigan, T.M., Love, D.C., Ashwell, G. & Krause, M. (2005). A Caenorhabditis elegans model of insulin resistance: Altered macronutrient storage and dauer formation in an OGT-1 knockout. *Proc. Natl. Acad. Sci. U. S. A.* **102**, 11266–11271.

Hansen, D. V., Lui, J.H., Flandin, P., Yoshikawa, K., Rubenstein, J.L., Alvarez-Buylla, A. & Kriegstein, A.R. (2013). Non-epithelial stem cells and cortical interneuron production in the human ganglionic eminences. *Nat. Neurosci.* **16**, 1576–1587.

Hao, Y., Sekine, K., Kawabata, A., Nakamura, H., Ishioka, T., Ohata, H., Katayama, R., *et al.* (2004). Apollon ubiquitinates SMAC and caspase-9, and has an essential cytoprotection function. *Nat. Cell Biol.* **6**, 849–860.

Harding, H.P., Novoa, I., Zhang, Y., Zeng, H., Wek, R., Schapira, M. & Ron, D. (2000). Regulated translation initiation controls stress-induced gene expression in mammalian cells. *Mol. Cell* **6**, 1099–1108.

Harding, H.P., Zhang, Y. & Ron, D. (1999). Protein translation and folding are coupled by an endoplasmic- reticulum-resident kinase. *Nature* **397**, 271–274.

Harding, H.P., Zhang, Y., Zeng, H., Novoa, I., Lu, P.D., Calfon, M., Sadri, N., *et al.* (2003). An integrated stress response regulates amino acid metabolism and resistance to oxidative stress. *Mol. Cell* **11**, 619–633.

Hart, G.W., Slawson, C., Ramirez-Correa, G. & Lagerlof, O. (2011). Cross Talk between O-GlcNAcylation and phosphorylation: Roles in signaling, transcription, and chronic disease. *Annu. Rev. Biochem.* **80**, 825–858.

Hart, L.S., Cunningham, J.T., Datta, T., Dey, S., Tameire, F., Lehman, S.L., Qiu, B., *et al.* (2012). ER stress-mediated autophagy promotes Myc-dependent transformation and tumor growth. *J. Clin. Invest.* **122**, 4621–4634.

He, Z. & Yu, Q. (2018). Identification and characterization of functional modules reflecting transcriptome transition during human neuron maturation. *BMC Genomics* **19**, 1–11.

Hedstrom, K.L., Ogawa, Y. & Rasband, M.N. (2008). AnkyrinG is required for maintenance of the axon initial segment and neuronal polarity. *J. Cell Biol.* **183**, 635–640.

Henshall, D.C., Skradski, S.L., Meller, R., Araki, T., Minami, M., Schindler, C.K., Lan, J.Q., *et al.* (2002). Expression and differential processing of caspases 6 and 7 in relation to specific epileptiform EEG patterns following limbic seizures. *Neurobiol. Dis.* **10**, 71–87.

Herbst, F., Ball, C.R., Tuorto, F., Nowrouzi, A., Wang, W., Zavidij, O., Dieter, S.M., *et al.* (2012). Extensive methylation of promoter sequences silences lentiviral transgene expression during stem cell differentiation in vivo. *Mol. Ther.* **20**, 1014–1021.

Hetman, M. & Kharebava, G. (2006). Survival Signaling Pathways Activated by NMDA Receptors. *Curr. Top. Med. Chem.* **6**, 787–799.

Hinnebusch, A.G., Ivanov, I.P. & Sonenberg, N. (2016). Translational control by 5′-untranslated regions of eukaryotic mRNAs. *Science (80-.).* **352**, 1413–1416.

Holden, H.M., Rayment, I. & Thoden, J.B. (2003). Structure and Function of Enzymes of the Leloir Pathway for Galactose Metabolism. *J. Biol. Chem.* **278**, 43885–43888.

Hollville, E. & Deshmukh, M. (2017). Physiological functions of non-apoptotic caspase activity in the nervous system. *Semin Cell Dev Biol* **82**, 127–136.

Hollville, E., Romero, S.E. & Deshmukh, M. (2019). Apoptotic cell death regulation in neurons. *FEBS J.* **286**, 3276–3298.

Hongpaisan, J. & Alkon, D.L. (2007). A structural basis for enhancement of long-term associative memory in single dendritic spines regulated by PKC. *Proc. Natl. Acad. Sci. U. S. A.* **104**, 19571–19576.

Hongpaisan, J., Sun, M.K. & Alkon, D.L. (2011). PKC ε activation prevents synaptic loss, Aβ elevation, and cognitive deficits in alzheimer's disease transgenic mice. *J. Neurosci.* **31**, 630–643.

Horn, M., Denzel, I., Breuer, P., Antebi, A., Denzel, M.S., Horn, M., Denzel, S.I., *et al.* (2020). Hexosamine Pathway Activation Improves Protein Homeostasis through the Integrated Stress Response Hexosamine Pathway Activation Improves Protein Homeostasis through the Integrated Stress Response. *ISCIENCE* **23**, 100887.

Hornung, J.P. & De Tribolet, N. (1994). Distribution of GABA-containing neurons in human frontal cortex: a quantitative immunocytochemical study. *Anat. Embryol. (Berl).* **189**, 139–145.

Hrdinka, M. & Yabal, M. (2019). Inhibitor of apoptosis proteins in human health and disease. *Genes Immun.* **20**, 641–650.

Hu, S. & Yang, X. (2003). Cellular inhibitor of apoptosis 1 and 2 are ubiquitin ligases for the apoptosis inducer Smac/DIABLO. *J. Biol. Chem.* **278**, 10055–10060.

Hu, W., Qiu, B., Guan, W., Wang, Q., Wang, M., Li, W., Gao, L., *et al.* (2015). Direct Conversion of Normal and Alzheimer's Disease Human Fibroblasts into Neuronal Cells by Small Molecules. *Cell*

Stem Cell **17**, 204–212.

Hu, Y., Riesland, L., Paterson, A.J. & Kudlow, J.E. (2004). Phosphorylation of mouse glutamine-fructose-6-phosphate amidotransferase 2 (GFAT2) by cAMP-dependent protein kinase increases the enzyme activity. *J. Biol. Chem.* **279**, 29988–29993.

Huang, C.Y.M. & Rasband, M.N. (2018). Axon initial segments: structure, function, and disease. *Ann. N. Y. Acad. Sci.* **1420**, 46–61.

Hyman, B.T. & Yuan, J. (2012). Apoptotic and non-apoptotic roles of caspases in neuronal physiology and pathophysiology. *Nat. Rev. Neurosci.* **13**, 395–406.

Hynes, R.O. & Naba, A. (2012). Overview of the matrisome-An inventory of extracellular matrix constituents and functions. *Cold Spring Harb. Perspect. Biol.* **4**.

Ill-Raga, G., Tajes, M., Busquets-García, A., Ramos-Fernández, E., Vargas, L.M., Bosch-Morató, M., Guivernau, B., *et al.* (2015). Physiological control of nitric oxide in neuronal BACE1 translation by heme-regulated eIF2α kinase HRI induces synaptogenesis. *Antioxidants Redox Signal.* **22**, 1295–1307.

Inglis, A.J., Masson, G.R., Shao, S., Perisic, O., McLaughlin, S.H., Hegde, R.S. & Williams, R.L. (2019). Activation of GCN2 by the ribosomal P-stalk. *Proc. Natl. Acad. Sci. U. S. A.* **116**, 4946–4954.

Inohara, N., Ekhterae, D., Garcia, I., Carrio, R., Merino, J., Merry, A., Chen, S., *et al.* (1998). Mtd, a novel Bcl-2 family member activates apoptosis in the absence of heterodimerization with Bcl-2 and Bcl-X(L). *J. Biol. Chem.* **273**, 8705–8710.

Iqbal, K., Liu, F., Gong, C.X., del Alonso, A.C. & Grundke-Iqbal, I. (2009). Mechanisms of tau-induced neurodegeneration. *Acta Neuropathol.* **118**, 53–69.

Islam, M.A., Sharif, S.R., Lee, H. & Moon, I.S. (2015). N-acetyl-D-glucosamine kinase promotes the axonal growth of developing neurons. *Mol. Cells* **38**, 876–885.

Isomura, R., Kitajima, K. & Sato, C. (2011). Structural and functional impairments of polysialic acid by a mutated polysialyltransferase found in schizophrenia. *J. Biol. Chem.* **286**, 21535–21545.

Issop, Y., Hathazi, D., Khan, M.M., Weis, J., Spendiff, S., Slater, C.R. & Roos, A. (2018). GFPT1 deficiency in muscle leads to myasthenia and myopathy in mice. *Hum. Gene Ther.* **27**, 3218–3232.

Itkonen, H.M., Engedal, N., Babaie, E., Luhr, M., Guldvik, I.J., Minner, S., Hohloch, J., *et al.* (2015). UAP1 is overexpressed in prostate cancer and is protective against inhibitors of N-linked glycosylation. *Oncogene* **34**, 3744–3750.

Itoh, N. & Nagata, S. (1993). A novel protein domain required for apoptosis. Mutational analysis of human Fas antigen. *J. Biol. Chem.* **268**, 10932–10937.

Jacko, M., Weyn-Vanhentenryck, S.M., Smerdon, J.W., Yan, R., Feng, H., Williams, D.J., Pai, J., *et al.* (2018). Rbfox Splicing Factors Promote Neuronal Maturation and Axon Initial Segment Assembly. *Neuron* **97**, 853-868.e6.

Janowska, J., Gargas, J., Ziemka-Nalecz, M., Zalewska, T., Buzanska, L. & Sypecka, J. (2019). Directed glial differentiation and transdifferentiation for neural tissue regeneration. *Exp. Neurol.* **319**.

Jiang, Z., Belforte, J.E., Lu, Y., Yabe, Y., Pickel, J., Smith, C.B., Je, H.S., *et al.* (2010). eIF2α phosphorylation-dependent translation in CA1 pyramidal cells impairs hippocampal memory

consolidation without affecting general translation. *J. Neurosci.* **30**, 2582–2594.

Johnson, B.N., Berger, A.K., Cortese, G.P. & Lavoie, M.J. (2012). The ubiquitin E3 ligase parkin regulates the proapoptotic function of Bax **109**, 6283–6288.

Johnson, C.E., Huang, Y.Y., Parrish, A.B., Smith, M.I., Vaughn, A.E., Zhang, Q., Wright, K.M., *et al.* (2007). Differential Apaf-1 levels allow cytochrome c to induce apoptosis in brain tumors but not in normal neural tissues. *Proc. Natl. Acad. Sci. U. S. A.* **104**, 20820–5.

Jousse, C., Oyadomari, S., Novoa, I., Lu, P., Zhang, Y., Harding, H.P. & Ron, D. (2003). Inhibition of a constitutive translation initiation factor 2α phosphatase, CReP, promotes survival of stressed cells. *J. Cell Biol.* **163**, 767–775.

Juan, T.S.C., McNiece, I.K., Argento, J.M., Jenkins, N.A., Gilbert, D.J., Copeland, N.G. & Fletcher, F.A. (1997). Identification and mapping of Casp7, a cysteine protease resembling CPP32β, interleukin-1β converting enzyme, and CED-3. *Genomics* **40**, 86–93.

Kamaletdinova, T., Fanaei-kahrani, Z. & Wang, Z. (2019). The Enigmatic Function of PARP1: From PARylation Activity to PAR Readers. *Cells* **8**, 1625.

Kanato, Y., Kitajima, K. & Sato, C. (2008). Direct binding of polysialic acid to a brain-derived neurotrophic factor depends on the degree of polymerization. *Glycobiology* **18**, 1044–1053.

Kaplan, M.S. (1981). Neurogenesis in the 3-month-old rat visual cortex. *J. Comp. Neurol.* **195**, 323–338.

Kaplan, M.S. (1983). Proliferation of subependymal cells in the adult primate CNS: differential uptake of DNA labelled precursors. *J Hirnforsch.* **24**, 23–33.

Kato, K., Tanaka, T., Sadik, G., Baba, M., Maruyama, D., Yanagida, K., Kodama, T., *et al.* (2011). Protein kinase C stabilizes X-linked inhibitor of apoptosis protein (XIAP) through phosphorylation at Ser 87 to suppress apoptotic cell death. *Psychogeriatrics* **11**, 90–97.

Kaufmann, S.H., Desnoyers, S., Ottaviano, Y., Davidson, N.E. & Poirier, G.G. (1993). Specific Proteolytic Cleavage of Poly(ADP-ribose) Polymerase: An Early Marker of Chemotherapy-induced Apoptosis. *Cancer Res.* **53**.

Kemp, P.J., Rushton, D.J., Yarova, P.L., Schnell, C., Geater, C., Hancock, J.M., Wieland, A., *et al.* (2016). Improving and accelerating the differentiation and functional maturation of human stem cell-derived neurons: role of extracellular calcium and GABA. *J. Physiol.* **594**, 6583–6594.

Kenner, L.R., Anand, A.A., Nguyen, H.C., Myasnikov, A.G., Klose, C.J., McGeever, L.A., Tsai, J.C., *et al.* (2019). EIF2B-catalyzed nucleotide exchange and phosphoregulation by the integrated stress response. *Science (80-.).* **364**, 491–495.

Kernohan, K.D., Tétreault, M., Liwak-Muir, U., Geraghty, M.T., Qin, W., Venkateswaran, S., Davila, J., *et al.* (2015). Homozygous mutation in the eukaryotic translation initiation factor 2alpha phosphatase gene, PPP1R15B, is associated with severe microcephaly, short stature and intellectual disability. *Hum. Mol. Genet.* **24**, 6293–6300.

Khanna, S., Rink, C., Ghoorkhanian, R., Gnyawali, S., Heigel, M., Wijesinghe, D.S., Chalfant, C.E., *et al.* (2013). Loss of miR-29b following acute ischemic stroke contributes to neural cell death and infarct size. *J. Cereb. Blood Flow Metab.* **33**, 1197–1206.

Khazipov, R., Sirota, A., Leinekugel, X., Holmes, G.L., Ben-Ari, Y. & Buzsáki, G. (2004). Early motor activity drives spindle bursts in the developing somatosensory cortex. *Nature* **432**, 758–761.

Kikuchi, T., Morizane, A., Doi, D., Magotani, H., Onoe, H., Hayashi, T., Mizuma, H., *et al.* (2017). Human iPS cell-derived dopaminergic neurons function in a primate Parkinson's disease model. *Nature* **548**, 592–596.

Kilb, W., Kirischuk, S. & Luhmann, H.J. (2011). Electrical activity patterns and the functional maturation of the neocortex. *Eur. J. Neurosci.* **34**, 1677–1686.

Kim, J. Bin, Kim, S.Y., Kim, B.M., Lee, H., Kim, I., Yun, J., Jo, Y., *et al.* (2013). Identification of a novel anti-apoptotic E3 ubiquitin ligase that ubiquitinates antagonists of inhibitor of apoptosis proteins SMAC, HtrA2, and ARTS. *J. Biol. Chem.* **288**, 12014–12021.

Kim, K.K., Adelstein, R.S. & Kawamoto, S. (2009). Identification of neuronal nuclei (NeuN) as Fox-3, a new member of the Fox-1 gene family of splicing factors. *J. Biol. Chem.* **284**, 31052–31061.

Kirkeby, A., Grealish, S., Wolf, D.A., Nelander, J., Wood, J., Lundblad, M., Lindvall, O., *et al.* (2012). Generation of Regionally Specified Neural Progenitors and Functional Neurons from Human Embryonic Stem Cells under Defined Conditions. *Cell Rep.* **1**, 703–714.

Kirwan, P., Turner-Bridger, B., Peter, M., Momoh, A., Arambepola, D., Robinson, H.P.C. & Livesey, F.J. (2015). Development and function of human cerebral cortex neural networks from pluripotent stem cells in vitro. *Dev.* **142**, 3178–3187.

Kischkel, F.C., Hellbardt, S., Behrmann, I., Germer, M., Pawlita, M., Krammer, P.H. & Peter, M.E. (1995). Cytotoxicity-dependent APO-1 (Fas/CD95)-associated proteins form a death-inducing signaling complex (DISC) with the receptor. *EMBO J.* **14**, 5579–5588.

Klimova, N. & Kristian, T. (2019). Multi-targeted Effect of Nicotinamide Mononucleotide on Brain Bioenergetic Metabolism. *Neurochem. Res.* **44**, 2280–2287.

Kline, C.L.B., Schrufer, T.L., Jefferson, L.S. & Kimball, S.R. (2006). Glucosamine-induced phosphorylation of the α-subunit of eukaryotic initiation factor 2 is mediated by the protein kinase R-like endoplasmic-reticulum associated kinase. *Int. J. Biochem. Cell Biol.* **38**, 1004–1014.

Kobayashi, T., Storrie, B., Simons, K. & Dotti, C.G. (1992). A functional barrier to movement of lipids in polarized neurons. *Nature* **359**, 647–650.

Kola, I. & Landis, J. (2004). Can the pharmaceutical industry reduce attrition rates? *Nat. Rev. Drug Discov.* **3**, 711–715.

Kolde, R. (2019). pheatmap: Pretty Heatmaps.

Kole, A.J., Annis, R.P. & Deshmukh, M. (2013). Mature neurons: equipped for survival. *Cell Death Dis.* **4**, 1–8.

Kole, A.J., Swahari, V., Hammond, S.M. & Deshmukh, M. (2011). miR-29b is activated during neuronal maturation and targets BH3-only genes to restrict apoptosis. *Genes Dev.* **25**, 125–130.

Kole, M.H.P., Ilschner, S.U., Kampa, B.M., Williams, S.R., Ruben, P.C. & Stuart, G.J. (2008). Action potential generation requires a high sodium channel density in the axon initial segment. *Nat. Neurosci.* **11**, 178–186.

Kole, M.H.P. & Stuart, G.J. (2012). Signal Processing in the Axon Initial Segment. *Neuron* **73**, 235–247.

Komada, M. & Soriano, P. (2002). βIV-spectrin regulates sodium channel clustering through ankyrin-G at axon initial segments and nodes of Ranvier. *J. Cell Biol.* **156**, 337–348.

Kornack, D.R. & Rakic, P. (1999). Continuation of neurogenesis in the hippocampus of the adult

macaque monkey. *Proc. Natl. Acad. Sci. U. S. A.* **96**, 5768–5773.

Kornfeld, R. (1967). Studies on L-Glutamine D-Fructose 6-Phosphate Amidotransferase. *J. Biol. Chem.* **242**, 3135–41.

Krajewska, M., Krajewski, S., Banares, S., Huang, X., Turner, B., Bubendorf, L., Kallioniemi, O.P., *et al.* (2003). Elevated Expression of Inhibitor of Apoptosis Proteins in Prostate Cancer. *Clin. Cancer Res.* **9**, 4914–4925.

Kreppel, L.K., Blomberg, M.A. & Hart, G.W. (1997). Dynamic glycosylation of nuclear and cytosolic proteins: Cloning and characterization of a unique O-GlcNAc transferase with multiple tetratricopeptide repeats. *J. Biol. Chem.* **272**, 9308–9315.

Kreppel, L.K. & Hart, G.W. (1999). Regulation of a cytosolic and nuclear O-GlcNAc transferase. Role of the tetratricopeptide repeats. *J. Biol. Chem.* **274**, 32015–32022.

Kriks, S., Shim, J.W., Piao, J., Ganat, Y.M., Wakeman, D.R., Xie, Z., Carrillo-Reid, L., *et al.* (2011). Dopamine neurons derived from human ES cells efficiently engraft in animal models of Parkinson's disease. *Nature* **480**, 547–551.

Krukowski, K., Nolan, A., Frias, E.S., Boone, M., Ureta, G., Grue, K., Paladini, M.S., *et al.* (2020). Small molecule cognitive enhancer reverses age-related memory decline in mice. *Elife* **9**, 1–22.

Kuba, H. (2010). Plasticity at the axon initial segment. *Commun. Integr. Biol.* **3**, 597–598.

Kuijpers, M., van de Willige, D., Freal, A., Chazeau, A., Franker, M.A., Hofenk, J., Rodrigues, R.J.C., *et al.* (2016). Dynein Regulator NDEL1 Controls Polarized Cargo Transport at the Axon Initial Segment. *Neuron* **89**, 461–471.

Van Kuppeveld, F.J.M., Van der Logt, J.T.M., Angulo, A.F., Van Zoest, M.J., Quint, W.G.V., Niesters, H.G.M., Galama, J.M.D., *et al.* (1992). Genus- and species-specific identification of mycoplasmas by 16S rRNA amplification. *Appl. Environ. Microbiol.* **58**, 2606–2615.

Kurokawa, M., Zhao, C., Reya, T. & Kornbluth, S. (2008). Inhibition of Apoptosome Formation by Suppression of Hsp90β Phosphorylation in Tyrosine Kinase-Induced Leukemias. *Mol. Cell. Biol.* **28**, 5494–5506.

Laarse, S.A.M., Leney, A.C. & Heck, A.J.R. (2018). Crosstalk between phosphorylation and O-Glc <scp>NA</scp> cylation: friend or foe. *FEBS J.* **285**, 3152–3167.

Labrada, L., Liang, X.H., Zheng, W., Johnston, C. & Levine, B. (2002). Age-Dependent Resistance to Lethal Alphavirus Encephalitis in Mice: Analysis of Gene Expression in the Central Nervous System and Identification of a Novel Interferon-Inducible Protective Gene, Mouse ISG12. *J. Virol.* **76**, 11688–11703.

Ladewig, J., Koch, P. & Brüstle, O. (2013). Leveling Waddington: The emergence of direct programming and the loss of cell fate hierarchies. *Nat. Rev. Mol. Cell Biol.* **14**, 225–236.

Lal, D., Reinthaler, E.M., Altmüller, J., Toliat, M.R., Thiele, H., Nürnberg, P., Lerche, H., *et al.* (2013). RBFOX1 and RBFOX3 Mutations in Rolandic Epilepsy. *PLoS One* **8**.

Lalaoui, N. & Vaux, D.L. (2018). Recent advances in understanding inhibitor of apoptosis proteins. *F1000Research* **7**.

Larsen, B.D. & Sørensen, C.S. (2017). The caspase-activated DNase: apoptosis and beyond. *FEBS J.* **284**, 1160–1170.

Laughlin, S.B., De Ruyter Van Steveninck, R.R. & Anderson, J.C. (1998). The metabolic cost of neural information. *Nat. Neurosci.* **1**, 36–41.

Lazarus, K.J., Bradshaw, R.A., Wes, N.R. & Bunge, R.P. (1976). Adaptive survival of rat sympathetic neurons cultured without supporting cells or exogenous nerve growth factor. *Brain Res.* **113**, 159–164.

Le, D.A., Wu, Y., Huang, Z., Matsushita, K., Plesnila, N., Augustinack, J.C., Hyman, B.T., *et al.* (2002). Caspase activation and neuroprotection in caspase-3-deficient mice after in vivo cerebral ischemia and in vitro oxygen glucose deprivation. *Proc. Natl. Acad. Sci. U. S. A.* **99**, 15188–15193.

Lee, Y.Y., Cevallos, R.C. & Jan, E. (2009). An upstream open reading frame regulates translation of GADD34 during cellular stresses that induce eIF2phosphorylation. *J. Biol. Chem.* **284**, 6661–6673.

Leinekugel, X., Khazipov, R., Cannon, R., Hirase, H., Ben-Ari, Y. & Buzsáki, G. (2002). Correlated bursts of activity in the neonatal hippocampus in vivo. *Science (80-.).* **296**, 2049–2052.

Leloir, L.F. (1951). The enzymatic transformation of uridine diphosphate glucose into a galactose derivative. *Arch. Biochem. Biophys.* **33**, 186–190.

LePage, K.T., Dickey, R.W., Gerwick, W.H., Jester, E.L. & Murray, T.F. (2005). On the use of neuro-2a neuroblastoma cells versus intact neurons in primary culture for neurotoxicity studies. *Crit. Rev. Neurobiol.* **17**, 27–50.

Leterrier, C. (2016). The Axon Initial Segment, 50 Years Later: A Nexus for Neuronal Organization and Function. *Curr. Top. Membr.* **77**, 185–233.

Leterrier, C., Vacher, H., Fache, M.P., D'Ortoli, S.A., Castets, F., Autillo-Touat, A. & Dargent, B. (2011). End-binding proteins EB3 and EB1 link microtubules to ankyrin G in the axon initial segment. *Proc. Natl. Acad. Sci. U. S. A.* **108**, 8826–8831.

Léveillé, F., Papadia, S., Fricker, M., Bell, K.F.S., Soriano, F.X., Martel, M.A., Puddifoot, C., *et al.* (2010). Suppression of the intrinsic apoptosis pathway by synaptic activity. *J. Neurosci.* **30**, 2623–2635.

Li, F., Ackermann, E.J., Bennett, C.F., Rothermel, A.L., Plescia, J., Tognin, S., Villa, A., *et al.* (1999). Pleiotropic cell-division defects and apoptosis induced by interference with survivin function. *Nat. Cell Biol.* **1**, 461–466.

Li, L. & Hu, G.K. (2015). Pink1 protects cortical neurons from thapsigargin-induced oxidative stress and neuronal apoptosis. *Biosci. Rep.* **35**, 1–8.

Li, L., Shao, M., Peng, P., Yang, C., Song, S., Duan, F., Jia, D., *et al.* (2017a). High expression of GFAT1 predicts unfavorable prognosis in patients with hepatocellular carcinoma. *Oncotarget* **8**, 19205–19217.

Li, P., Zhou, L., Zhao, T., Liu, X., Zhang, P., Liu, Y., Zheng, X., *et al.* (2017b). Caspase-9: Structure, mechanisms and clinical application. *Oncotarget* **8**, 23996–24008.

Li, X., Lu, F., Wang, J.Z. & Gong, C.X. (2006). Concurrent alterations of O-GlcNAcylation and phosphorylation of tau in mouse brains during fasting. *Eur. J. Neurosci.* **23**, 2078–2086.

Li, X., Zuo, X., Jing, J., Ma, Y., Wang, J., Liu, D., Zhu, J., *et al.* (2015). Small-Molecule-Driven Direct Reprogramming of Mouse Fibroblasts into Functional Neurons. *Cell Stem Cell* **17**, 195–203.

Li, X.J., Zhang, X., Johnson, M.A., Wang, Z.B., LaVaute, T. & Zhang, S.C. (2009). Coordination of sonic hedgehog and Wnt signaling determines ventral and dorsal telencephalic neuron types from human embryonic stem cells. *Development* **136**, 4055–4063.

Li, Y., Roux, C., Lazereg, S., LeCaer, J.P., Laprévote, O., Badet, B. & Badet-Denisot, M.A. (2007). Identification of a novel serine phosphorylation site in human glutamine:fructose-6-phosphate amidotransferase isoform 1. *Biochemistry* **46**, 13163–13169.

Lie, E., Li, Y., Kim, R. & Kim, E. (2018). SALM/Lrfn family synaptic adhesion molecules. *Front. Mol. Neurosci.* **11**.

Lim, K.H., Joo, J.Y. & Baek, K.H. (2020). The potential roles of deubiquitinating enzymes in brain diseases. *Ageing Res. Rev.* **61**, 101088.

Lin, J. (2008). Applications and Limitations of Genetically Modified Mouse Models in Drug Discovery and Development. *Curr. Drug Metab.* **9**, 419–438.

Lin, L., Zhang, M., Stoilov, P., Chen, L., Zheng, S., Lin, L., Zhang, M., *et al.* (2020). Developmental Attenuation of Neuronal Apoptosis by Neural-Specific Splicing of Bak1 Microexon. *Neuron* **107**, 1180–96.

Lin, Y.S., Wang, H.Y., Huang, D.F., Hsieh, P.F., Lin, M.Y., Chou, C.H., Wu, I.J., *et al.* (2016). Neuronal splicing regulator RBFOX3 (NeuN) regulates adult hippocampal neurogenesis and synaptogenesis. *PLoS One* **11**.

Lindhout, T., Iqbal, U., Willis, L.M., Reid, A.N., Li, J., Liu, X., Moreno, M., *et al.* (2011). Site-specific enzymatic polysialylation of therapeutic proteins using bacterial enzymes. *Proc. Natl. Acad. Sci. U. S. A.* **108**, 7397–7402.

Liston, P., Fong, W.G., Kelly, N.L., Toji, S., Miyazaki, T., Conte, D., Tamai, K., *et al.* (2001). Identification of XAF1 as an antagonist of XIAP anti-caspase activity. *Nat. Cell Biol.* **3**, 128–133.

Liu, G., David, B.T., Trawczynski, M. & Fessler, R.G. (2020). Advances in Pluripotent Stem Cells: History, Mechanisms, Technologies, and Applications. *Stem Cell Rev. Reports* **16**, 3–32.

Liu, H. (2019). Synaptic organizers: synaptic adhesion-like molecules (SALMs). *Curr. Opin. Struct. Biol.* **54**, 59–67.

Liu, M.L., Zang, T., Zou, Y., Chang, J.C., Gibson, J.R., Huber, K.M. & Zhang, C.L. (2013). Small molecules enable neurogenin 2 to efficiently convert human fibroblasts into cholinergic neurons. *Nat. Commun.* **4**, 2183.

Liu, Y., Miao, Q., Yuan, J., Han, S., Zhang, P., Li, S., Rao, Z., *et al.* (2015). Ascl1 converts dorsal midbrain astrocytes into functional neurons In Vivo. *J. Neurosci.* **35**, 9336–9355.

Llambi, F., Wang, Y., Victor, B., Moldoveanu, T., Chen, T. & Green, D.R. (2016). BOK Is a Non-canonical BCL-2 Family Effector of Apoptosis Regulated by ER-Associated Degradation. *Cell* **165**, 421–433.

Lodato, S. & Arlotta, P. (2015). Generating Neuronal Diversity in the Mammalian Cerebral Cortex. *Annu. Rev. Cell Dev. Biol.* **31**, 699–720.

Lombardi, A., Ulianich, L., Treglia, A.S., Nigro, C., Parrillo, L., Lofrumento, D.D., Nicolardi, G., *et al.* (2012). Increased hexosamine biosynthetic pathway flux dedifferentiates INS-1E cells and murine islets by an extracellular signal-regulated kinase (ERK)1/2-mediated signal transmission pathway. *Diabetologia* **55**, 141–153.

Lorincz, A. & Nusser, Z. (2010). Molecular identity of dendritic voltage-gated sodium channels. *Science (80-.).* **328**, 906–909.

Love, M.I., Huber, W. & Anders, S. (2014). Moderated estimation of fold change and dispersion for RNA-seq data with DESeq2. *Genome Biol.* **15**, 550.

Lu, J., Zhong, X., Liu, H., Hao, L., Huang, C.T.L., Sherafat, M.A., Jones, J., *et al.* (2016). Generation of serotonin neurons from human pluripotent stem cells. *Nat. Biotechnol.* **34**, 89–94.

Lubas, W.A., Frank, D.W., Krause, M. & Hanover, J.A. (1997). O-linked GlcNAc transferase is a conserved nucleocytoplasmic protein containing tetratricopeptide repeats. *J. Biol. Chem.* **272**, 9316–9324.

Luhmann, H.J., Sinning, A., Yang, J.W., Reyes-Puerta, V., Stüttgen, M.C., Kirischuk, S. & Kilb, W. (2016). Spontaneous neuronal activity in developing neocortical networks: From single cells to large-scale interactions. *Front. Neural Circuits* **10**.

Ma, J. & Hart, G.W. (2014). O-GlcNAc profiling: From proteins to proteomes. *Clin. Proteomics* **11**, 8.

Ma, K., Vattem, K.M. & Wek, R.C. (2002). Dimerization and release of molecular chaperone inhibition facilitate activation of eukaryotic initiation factor-2 kinase in response to endoplasmic reticulum stress. *J. Biol. Chem.* **277**, 18728–18735.

Ma, L., Huang, Y., Song, Z., Feng, S., Tian, X., Du, W., Qiu, X., *et al.* (2006). Livin promotes Smac/DIABLO degradation by ubiquitin-proteasome pathway. *Cell Death Differ.* **13**, 2079–2088.

Ma, T., Trinh, M.A., Wexler, A.J., Bourbon, C., Gatti, E., Pierre, P., Cavener, D.R., *et al.* (2013a). Suppression of eIF2α kinases alleviates Alzheimer's disease-related plasticity and memory deficits. *Nat. Neurosci.* **16**, 1299–1305.

Ma, T., Wang, C., Wang, L., Zhou, X., Tian, M., Zhang, Q., Zhang, Y., *et al.* (2013b). Subcortical origins of human and monkey neocortical interneurons. *Nat. Neurosci.* **16**, 1588–1597.

Macfarlane, M., Merrison, W., Bratton, S.B. & Cohen, G.M. (2002). Proteasome-mediated Degradation of Smac during Apoptosis : XIAP Promotes Smac Ubiquitination in Vitro * **277**, 36611–36616.

Manning, G., Whyte, D.B., Martinez, R., Hunter, T. & Sudarsanam, S. (2002). The protein kinase complement of the human genome. *Science (80-.).* **298**, 1912–1934.

Marín-Padilla, M. (2015). Human cerebral cortex Cajal-Retzius neuron: Development, structure and function. A Golgi study. *Front. Neuroanat.* **9**.

Marín-Padilla, M. (1992). Ontogenesis of the pyramidal cell of the mammalian neocortex and developmental cytoarchitectonics: A unifying theory. *J. Comp. Neurol.* **321**, 223–240.

Marshall, S., Bacote, V. & Traxinger, R.R. (1991). Discovery of a metabolic pathway mediating glucose-induced desensitization of the glucose transport system: role of hexosamine in the induction of insulin resistance. *J. Biol. Chem.* **266**, 4706–4712.

Marshman, E., Booth, C. & Potten, C.S. (2002). The intestinal epithelial stem cell. *BioEssays* **24**, 91–98.

Martínez-Cerdeño, V. & Noctor, S.C. (2014). Cajal, Retzius, and Cajal-Retzius cells. *Front. Neuroanat.* **8**.

Martinez, M.R., Dias, T.B., Natov, P.S. & Zachara, N.E. (2017). Stress-induced O-GlcNAcylation: An

adaptive process of injured cells. *Biochem. Soc. Trans.*

Martire, S., Mosca, L. & Erme, M. (2015). PARP-1 involvement in neurodegeneration : A focus on Alzheimer ' s and Parkinson ' s diseases. *Mech. Ageing Dev.* **146**–**148**, 53–64.

McKnight, G.L., Mudri, S.L., Mathewes, S.L., Traxinger, R.R., Marshall, S., Sheppard, P.O. & O'Hara, P.J. (1992). Molecular cloning, cDNA sequence, and bacterial expression of human glutamine:fructose-6-phosphate amidotransferase. *J Biol Chem* **267**, 25208–25212.

Mertens, J., Reid, D., Lau, S., Kim, Y. & Gage, F.H. (2018). Aging in a dish: IPSC-derived and directly induced neurons for studying brain aging and age-related neurodegenerative diseases. *Annu. Rev. Genet.* **52**, 271–293.

Mertens, J., Stüber, K., Poppe, D., Doerr, J., Ladewig, J., Brüstle, O. & Koch, P. (2013a). Embryonic Stem Cell-Based Modeling of Tau Pathology in Human Neurons. *Am. J. Pathol.* **182**, 1769–1779.

Mertens, J., Stüber, K., Wunderlich, P., Ladewig, J., Kesavan, J.C., Vandenberghe, R., Vandenbulcke, M., *et al.* (2013b). APP processing in human pluripotent stem cell-derived neurons is resistant to NSAID-based γ-secretase modulation. *Stem Cell Reports* **1**, 491–498.

Mevissen, T.E.T. & Komander, D. (2017). Mechanisms of deubiquitinase specificity and regulation. *Annu. Rev. Biochem.* **86**, 159–192.

Miguel Martins, L., Iaccarino, I., Tenev, T., Gschmeissner, S., Totty, N.F., Lemoine, N.R., Savopoulos, J., *et al.* (2002). The serine protease Omi/HtrA2 regulates apoptosis by binding XIAP through a Reaper-like motif. *J. Biol. Chem.* **277**, 439–444.

Milewski, S., Kuszczak, D., Jędrzejczak, R., Smith, R.J., Brown, A.J.P. & Gooday, G.W. (1999). Oligomeric structure and regulation of Candida albicans glucosamine-6- phosphate synthase. *J. Biol. Chem.* **274**, 4000–4008.

Mink, J.W., Blumenschine, R.J. & Adams, D.B. (1981). Ratio of central nervous system to body metabolism in vertebrates: Its constancy and functional basis. *Am. J. Physiol. - Regul. Integr. Comp. Physiol.* **10**, 203–212.

Moloughney, J.G., Vega-Cotto, N.M., Liu, S., Patel, C., Kim, P.K., Wu, C.C., Albaciete, D., *et al.* (2018). MTORC2 modulates the amplitude and duration of GFAT1 Ser-243 phosphorylation to maintain flux through the hexosamine pathway during starvation. *J. Biol. Chem.* **293**, 16464–16478.

Molyneaux, B.J., Arlotta, P., Menezes, J.R.L. & Macklis, J.D. (2007). Neuronal subtype specification in the cerebral cortex. *Nat. Rev. Neurosci.* **8**, 427–437.

Moremen, K.W., Tiemeyer, M. & Nairn, A. V. (2012). Vertebrate protein glycosylation: Diversity, synthesis and function. *Nat. Rev. Mol. Cell Biol.* **13**, 448–462.

Moreno-Jiménez, E.P., Flor-García, M., Terreros-Roncal, J., Rábano, A., Cafini, F., Pallas-Bazarra, N., Ávila, J., *et al.* (2019). Adult hippocampal neurogenesis is abundant in neurologically healthy subjects and drops sharply in patients with Alzheimer's disease. *Nat. Med.* **25**, 554–560.

Morizane, Y., Honda, R., Fukami, K. & Yasuda, H. (2005). X-linked inhibitor of apoptosis functions as ubiquitin ligase toward mature caspase-9 and cytosolic Smac/DIABLO. *J. Biochem.* **137**, 125–132.

Morrish, E., Brumatti, G. & Silke, J. (2020). Future Therapeutic Directions for Smac-Mimetics. *Cells* **9**, 406.

Mouilleron, S., Badet-Denisot, M.A., Badet, B. & Golinelli-Pimpaneau, B. (2011). Dynamics of glucosamine-6-phosphate synthase catalysis. *Arch. Biochem. Biophys.* **505**, 1–12.

Mouilleron, S., Badet-Denisot, M.A. & Golinelli-Pimpaneau, B. (2006). Glutamine binding opens the ammonia channel and activates glucosamine-6P synthase. *J. Biol. Chem.* **281**, 4404–4412.

Moya, N., Cutts, J., Gaasterland, T., Willert, K. & Brafman, D.A. (2014). Endogenous WNT signaling regulates hPSC-derived neural progenitor cell heterogeneity and specifies their regional identity. *Stem Cell Reports* **3**, 1015–1028.

Mukhtar, T. & Taylor, V. (2018). Untangling Cortical Complexity During Development. *J. Exp. Neurosci.* **12**.

Mullen, R.J., Buck, C.R. & Smith, A.M. (1992). NeuN, a neuronal specific nuclear protein in vertebrates. *Development* **116**, 201–211.

Nagata, S. (2018). Apoptosis and Clearance of Apoptotic Cells. *Annu. Rev. Immunol.* **36**, 489–517.

Nakada, C., Ritchie, K., Oba, Y., Nakamura, M., Hotta, Y., Iino, R., Kasai, R.S., *et al.* (2003). Accumulation of anchored proteins forms membrane diffusion barriers during neuronal polarization. *Nat. Cell Biol.* **5**, 626–632.

Nichols, A.J. & Olson, E.C. (2010). Reelin promotes neuronal orientation and dendritogenesis during preplate splitting. *Cereb. Cortex* **20**, 2213–2223.

Nie, H. & Yi, W. (2019). O-GlcNAcylation, a sweet link to the pathology of diseases. *J. Zhejiang Univ. Sci. B* **20**, 437–448.

Nirschl, J.J., Ghiretti, A.E. & Holzbaur, E.L.F. (2017). The impact of cytoskeletal organization on the local regulation of neuronal transport. *Nat. Rev. Neurosci.* **18**, 585–597.

Norenberg, M.D. (1979). The distribution of glutamine synthetase in the rat central nervous system. *J. Histochem. Cytochem.* **27**, 756–762.

Norenberg, M.D. & Martinez-Hernandez, A. (1979). Fine structural localization of glutamine synthetase in astrocytes of rat brain. *Brain Res.* **161**, 303–310.

Nortley, R. & Attwell, D. (2017). Control of brain energy supply by astrocytes. *Curr. Opin. Neurobiol.* **47**, 80–85.

Novoa, I., Zeng, H., Harding, H.P. & Ron, D. (2001). Feedback inhibition of the unfolded protein response by GADD34-mediated dephosphorylation of eIF2α. *J. Cell Biol.* **153**, 1011–1021.

O'Donnell, N., Zachara, N.E., Hart, G.W. & Marth, J.D. (2004). Ogt-Dependent X-Chromosome-Linked Protein Glycosylation Is a Requisite Modification in Somatic Cell Function and Embryo Viability. *Mol. Cell. Biol.* **24**, 1680–1690.

Oki, T., Yamazaki, K., Kuromitsu, J., Okada, M. & Tanaka, I. (1999). cDNA cloning and mapping of a novel subtype of glutamine:fructose-6- phosphate amidotransferase (GFAT2) in human and mouse. *Genomics* **57**, 227–234.

Okuyama, R. & Marshall, S. (2003). UDP-N-acetylglucosaminyl transferase (OGT) in brain tissue: Temperature sensitivity and subcellular distribution of cytosolic and nuclear enzyme. *J. Neurochem.* **86**, 1271–1280.

Oláh, G., Szczesny, B., Brunyánszki, A. & López-garcía, I.A. (2015). Differentiation-Associated Downregulation of Poly (ADP-Ribose) Polymerase-1 Expression in Myoblasts Serves to Increase

Their Resistance to Oxidative Stress. *PLoS One* **10**.

Oppenheim, R.W. (1991). Cell death during development of the nervous system. *Annu. Rev. Neurosci.* **14**, 453–501.

Orsi, B.D., Engel, T., Pfeiffer, X.S., Nandi, X.S., Kaufmann, T., Henshall, D.C. & Prehn, X.J.H.M. (2016). Bok Is Not Pro-Apoptotic But Suppresses Poly ADP-Ribose Polymerase-Dependent Cell Death Pathways and Protects against Excitotoxic and Seizure-Induced Neuronal Injury **36**, 4564–4578.

Oslowski, C.M. & Urano, F. (2011). Measuring ER stress and the unfolded protein response using mammalian tissue culture system. In *Methods in Enzymology*: 71–92. Academic Press Inc.

Ossewaarde, J.M., De Vries, A., Bestebroer, T. & Angulo, A.F. (1996). Application of a Mycoplasma group-specific PCR for monitoring decontamination of Mycoplasma -infected Chlamydia sp. strains. *Appl. Environ. Microbiol.* **62**, 328–331.

Pakos-Zebrucka, K., Koryga, I., Mnich, K., Ljujic, M., Samali, A. & Gorman, A.M. (2016). The integrated stress response. *EMBO Rep.* **17**, 1374–1395.

Palam, L.R., Baird, T.D. & Wek, R.C. (2011). Phosphorylation of eIF2 facilitates ribosomal bypass of an inhibitory upstream ORF to enhance CHOP translation. *J. Biol. Chem.* **286**, 10939–10949.

Pandey, P., Saleh, A., Nakazawa, A., Kumar, S., Srinivasula, S.M., Kumar, V., Weichselbaum, R., *et al.* (2000). Negative regulation of cytochrome c-mediated oligomerization of Apaf-1 and activation of procaspase-9 by heat shock protein 90. *EMBO J.* **19**, 4310–4322.

Pang, Z.P., Yang, N., Vierbuchen, T., Ostermeier, A., Fuentes, D.R., Yang, T.Q., Citri, A., *et al.* (2011). Induction of human neuronal cells by defined transcription factors. *Nature*.

Panja, D., Dagyte, G., Bidinosti, M., Wibrand, K., Kristiansen, Å.M., Sonenberg, N. & Bramham, C.R. (2009). Novel translational control in arc-dependent long term potentiation consolidation in Vivo. *J. Biol. Chem.* **284**, 31498–31511.

Papadia, S., Soriano, F.X., Léveillé, F., Martel, M.A., Dakin, K.A., Hansen, H.H., Kaindl, A., *et al.* (2008). Synaptic NMDA receptor activity boosts intrinsic antioxidant defenses. *Nat. Neurosci.* **11**, 476–487.

Paridaen, J.T. & Huttner, W.B. (2014). Neurogenesis during development of the vertebrate central nervous system. *EMBO Rep.* **15**, 351–364.

Parrish, A.B., Freel, C.D. & Kornbluth, S. (2013). Cellular mechanisms controlling caspase activation and function. *Cold Spring Harb. Perspect. Biol.* **5**, a008672.

Paşca, S.P., Portmann, T., Voineagu, I., Yazawa, M., Shcheglovitov, A., Paşca, A.M., Cord, B., *et al.* (2011). Using iPSC-derived neurons to uncover cellular phenotypes associated with Timothy syndrome. *Nat. Med.* **17**, 1657–1662.

Patterson, V.L., Zullo, A.J., Koenig, C., Stoessel, S., Jo, H., Liu, X., Han, J., *et al.* (2014). Neural-Specific Deletion of Htra2 Causes Cerebellar Neurodegeneration and Defective Processing of Mitochondrial OPA1. *PLoS One* **9**, e115789.

Perkinton, M.S., Ip, J.K., Wood, G.L., Crossthwaite, A.J. & Williams, R.J. (2002). Phosphatidylinositol 3-kinase is a central mediator of NMDA receptor signalling to MAP kinase (Erkl/2), Akt/PKB and CREB in striatal neurones. *J. Neurochem.* **80**, 239–254.

Perrelet, D., Perrin, F.E., Liston, P., Korneluk, R.G., MacKenzie, A., Ferrer-Alcon, M. & Kato, A.C.

(2004). Motoneuron Resistance to Apoptotic Cell Death In Vivo Correlates with the Ratio between X-Linked Inhibitor of Apoptosis Proteins (XIAPs) and Its Inhibitor, XIAP-Associated Factor 1. *J. Neurosci.* **24**, 3777–3785.

Pfaff, N., Lachmann, N., Ackermann, M., Kohlscheen, S., Brendel, C., Maetzig, T., Niemann, H., *et al.* (2013). A ubiquitous chromatin opening element prevents transgene silencing in pluripotent stem cells and their differentiated progeny. *Stem Cells* **31**, 488–499.

Pinto, E.M., Figueiredo, B.C., Chen, W., Galvao, H.C.R., Formiga, M.N., Fragoso, M.C.B.V., Ashton-Prolla, P., *et al.* (2020). XAF1 as a modifier of p53 function and cancer susceptibility. *Sci. Adv.* **6**, eaba3231.

Plenchette, S., Cheung, H.H., Fong, W.G., LaCasse, E. & Korneluk, R.G. (2007). The role of XAF1 in cancer. *Curr. Opin. Investig. Drugs* **8**, 469–476.

Polster, B.M., Robertson, C.L., Bucci, C.J., Suzuki, M. & Fiskum, G. (2003). Postnatal brain development and neural cell differentiation modulate mitochondrial Bax and BH3 peptide-induced cytochrome c release. *Cell Death Differ.* **10**, 365–370.

Prendergast, J., Umanah, G.K.E., Yoo, S.W., Lagerlöf, O., Motari, M.G., Cole, R.N., Huganir, R.L., *et al.* (2014). Ganglioside regulation of AMPA receptor trafficking. *J. Neurosci.* **34**, 13246–13258.

Di Prisco, G.V., Huang, W., Buffington, S.A., Hsu, C.C., Bonnen, P.E., Placzek, A.N., Sidrauski, C., *et al.* (2014). Translational control of mGluR-dependent long-term depression and object-place learning by eIF2α. *Nat. Neurosci.* **17**, 1073–1082.

Qi, Y., Zhang, M., Li, H., Frank, J.A., Dai, L., Liu, H. & Chen, G. (2014). MicroRNA-29b regulates ethanol-induced neuronal apoptosis in the developing cerebellum through SP1/RAX/PKR Cascade. *J. Biol. Chem.* **289**, 10201–10210.

Qin, S., Yang, C., Zhang, B., Li, X., Sun, X., Li, G., Zhang, J., *et al.* (2016). XIAP inhibits mature Smac-induced apoptosis by degrading it through ubiquitination in NSCLC. *Int. J. Oncol.* **49**, 1289–1296.

Qiu, W., Su, Q., Rutledge, A.C., Zhang, J. & Adeli, K. (2009). Glucosamine-induced endoplasmic reticulum stress attenuates apolipoprotein B100 synthesis via PERK signaling. *J. Lipid Res.* **50**, 1814–1823.

Qiu, X., Hill, A., Packer, J., Lin, D., Ma, Y.-A. & Trapnell, C. (2017a). Single-cell mRNA quantification and differential analysis with Census. *Nat. Methods* **14**, 309–15.

Qiu, X., Mao, Q., Tang, Y., Wang, L., Chawla, R., Pliner, H. & Trapnell, C. (2017b). Reverse graph embedding resolves complex single-cell developmental trajectories. *Nat. Methods* **14**, 979–82.

Quinn, P.M.J., Moreira, P.I., Ambrósio, A.F. & Alves, C.H. (2020). PINK1/PARKIN signalling in neurodegeneration and neuroinflammation. *Acta Neuropathol. Commun.* **8**, 189.

R Core Team. (2020). R: A Language and Environment for Statistical Computing.

Raczynska, J., Olchowy, J., Konariev, P. V., Svergun, D.I., Milewski, S. & Rypniewski, W. (2007). The Crystal and Solution Studies of Glucosamine-6-phosphate Synthase from Candida albicans. *J. Mol. Biol.* **372**, 672–688.

Rajman, L., Chwalek, K. & Sinclair, D.A. (2018). Review Therapeutic Potential of NAD-Boosting Molecules : The In Vivo Evidence. *Cell Metab.* **27**, 529–547.

Rana, A., Rera, M. & Walker, D.W. (2013). Parkin overexpression during aging reduces proteotoxicity,

alters mitochondrial dynamics, and extends lifespan. *Proc. Natl. Acad. Sci. U. S. A.* **110**, 8638–8643.

Rao, A., Kim, E., Sheng, M. & Craig, A.M. (1998). Heterogeneity in the molecular composition of excitatory postsynaptic sites during development of hippocampal neurons in culture. *J. Neurosci.* **18**, 1217–1229.

Ray, J.E., Garcia, J., Jurisicova, A. & Caniggia, I. (2010). Mtd/Bok takes a swing: Proapoptotic Mtd/Bok regulates trophoblast cell proliferation during human placental development and in preeclampsia. *Cell Death Differ.* **17**, 846–859.

Rehm, M., Düßmann, H. & Prehn, J.H.M. (2003). Real-time single cell analysis of Smac / DIABLO release during apoptosis **162**, 1031–1043.

Richez, C., Boetzel, J., Floquet, N., Koteshwar, K., Stevens, J., Badet, B. & Badet-Denisot, M.A. (2007). Expression and purification of active human internal His6-tagged l-glutamine: d-Fructose-6P amidotransferase I. *Protein Expr. Purif.* **54**, 45–53.

Riedl, S.J. & Salvesen, G.S. (2007). The apoptosome: Signalling platform of cell death. *Nat. Rev. Mol. Cell Biol.* **8**, 405–413.

Rubin, L.L. (2008). Stem Cells and Drug Discovery: The Beginning of a New Era? *Cell* **132**, 549–552.

Ruegenberg, S., Horn, M., Pichlo, C., Allmeroth, K., Baumann, U. & Denzel, M.S. (2020). Loss of GFAT-1 feedback regulation activates the hexosamine pathway that modulates protein homeostasis. *Nat. Commun.* **11**, 1–16.

Rydbirk, R., Folke, J., Busato, F., Roché, E., Chauhan, A.S., Løkkegaard, A., Hejl, A.M., *et al.* (2020). Epigenetic modulation of AREL1 and increased HLA expression in brains of multiple system atrophy patients. *Acta Neuropathol. Commun.* **8**, 29.

Sahara, S., Aoto, M., Eguchi, Y., Imamoto, N., Yoneda, Y. & Tsujimoto, Y. (1999). Acinus is a caspase-3-activated protein required for apoptotic chromatin condensation. *Nature* **401**, 168–173.

Sahara, S., Yanagawa, Y., O'Leary, D.D.M. & Stevens, C.F. (2012). The fraction of cortical GABAergic neurons is constant from near the start of cortical neurogenesis to adulthood. *J. Neurosci.* **32**, 4755–4761.

Saita, S., Nolte, H., Fiedler, K.U., Kashkar, H., Saskia, A.V., Zahedi, R.P., Krüger, M., *et al.* (2017). PARL mediates Smac proteolytic maturation in mitochondria to promote apoptosis. *Nat. Cell Biol.* **19**, 318–328.

Saito, A., Hayashi, T., Okuno, S., Ferrand-Drake, M. & Chan, P.H. (2003). Interaction between XIAP and Smac/DIABLO in the mouse brain after transient focal cerebral ischemia. *J. Cereb. Blood Flow Metab.* **23**, 1010–1019.

Schile, A.J., García-fernández, M. & Steller, H. (2008). Regulation of apoptosis by XIAP ubiquitin-ligase activity. *Genes Dev.* **22**, 2256–2266.

Schnaar, R.L. (2010). Brain gangliosides in axon-myelin stability and axon regeneration. *FEBS Lett.* **584**, 1741–1747.

Schnaar, R.L. (2016). Gangliosides of the Vertebrate Nervous System. *J. Mol. Biol.*

Schnaar, R.L., Gerardy-Schahn, R. & Hildebrandt, H. (2014). Sialic acids in the brain: Gangliosides and polysialic acid in nervous system development, stability, disease, and regeneration. *Physiol. Rev.*

94, 461–518.

Schnaar, R.L. & Lopez, P.H.H. (2009). Myelin-associated glycoprotein and its axonal receptors. *J. Neurosci. Res.* **87**, 3267–3276.

Scott, F.L., Denault, J.B., Riedl, S.J., Shin, H., Renatus, M. & Salvesen, G.S. (2005). XIAP inhibits caspase-3 and -7 using two binding sites: Evolutionary conserved mechanism of IAPs. *EMBO J.* **24**, 645–655.

Sebbagh, M., Renvoizé, C., Hamelin, J., Riché, N., Bertoglio, J. & Bréard, J. (2001). Caspase-3-mediated cleavage of ROCK I induces MLC phosphorylation and apoptotic membrane blebbing. *Nat. Cell Biol.* **3**, 346–352.

Sen, A., Hongpaisan, J., Wang, D., Nelson, T.J. & Alkon, D.L. (2016). Protein Kinase Cε (PKCε) promotes synaptogenesis through membrane accumulation of the postsynaptic density protein PSD-95. *J. Biol. Chem.* **291**, 16462–16476.

Sen, A., Nelson, T.J., Alkon, D.L. & Hongpaisan, J. (2018). Loss in PKC Epsilon Causes Downregulation of MnSOD and BDNF Expression in Neurons of Alzheimer's Disease Hippocampus. *J. Alzheimer's Dis.* **63**, 1173–1189.

Senderek, J., Müller, J.S., Dusl, M., Strom, T.M., Guergueltcheva, V., Diepolder, I., Laval, S.H., *et al.* (2011). Hexosamine biosynthetic pathway mutations cause neuromuscular transmission defect. *Am. J. Hum. Genet.* **88**, 162–172.

Seol, D. & Billiar, T.R. (1999). A Caspase-9 Variant Missing the Catalytic Site Is an Endogenous Inhibitor of Apoptosis. *J Biol Chem* **274**, 2072–2076.

Sessler, T., Healy, S., Samali, A. & Szegezdi, E. (2013). Structural determinants of DISC function: New insights into death receptor-mediated apoptosis signalling. *Pharmacol. Ther.* **140**, 186–199.

Shafi, R., Iyer, S.P.N., Ellies, L.G., O'Donnell, N., Marek, K.W., Chui, D., Hart, G.W., *et al.* (2000). The O-GlcNAc transferase gene resides on the X chromosome and is essential for embryonic stem cell viability and mouse ontogeny. *Proc. Natl. Acad. Sci. U. S. A.* **97**, 5735–5739.

Sharma, V., Ounallah-Saad, H., Chakraborty, D., Hleihil, M., Sood, R., Barrera, I., Edry, E., *et al.* (2018). Local inhibition of PERK enhances memory and reverses age-related deterioration of cognitive and neuronal properties. *J. Neurosci.* **38**, 648–658.

Shi, Y., Kirwan, P. & Livesey, F.J. (2012). Directed differentiation of human pluripotent stem cells to cerebral cortex neurons and neural networks. *Nat. Protoc.* **7**, 1836–1846.

Shin, H., Renatus, M., Eckelman, B.P., Nunes, V.A., Sampaio, C.A.M. & Salvesen, G.S. (2005). The BIR domain of IAP-like protein 2 is conformationally unstable: Implications for caspase inhibition. *Biochem. J.* **385**, 1–10.

Shiozaki, E.N., Chai, J., Rigotti, D.J., Riedl, S.J., Li, P., Srinivasula, S.M., Alnemri, E.S., *et al.* (2003). Mechanism of XIAP-mediated inhibition of caspase-9. *Mol. Cell* **11**, 519–527.

Sidrauski, C., Acosta-Alvear, D., Khoutorsky, A., Vedantham, P., Hearn, B.R., Li, H., Gamache, K., *et al.* (2013). Pharmacological brake-release of mRNA translation enhances cognitive memory. *Elife* **2013**.

Siegelin, M., Touzani, O., Toutain, J., Liston, P. & Rami, A. (2005). Induction and redistribution of XAF1, a new antagonist of XIAP in the rat brain after transient focal ischemia. *Neurobiol. Dis.* **20**, 509–518.

Da Silva, J.S., Hasegawa, T., Miyagi, T., Dotti, C.G. & Abad-Rodriguez, J. (2005). Asymmetric membrane ganglioside sialidase activity specifies axonal fate. *Nat. Neurosci.* **8**, 606–615.

Singh, R., Letai, A. & Sarosiek, K. (2019a). Regulation of apoptosis in health and disease: the balancing act of BCL-2 family proteins. *Nat. Rev. Mol. Cell Biol.* **20**, 175–193.

Singh, S., Ng, J., Nayak, D. & Sivaraman, J. (2019b). Structural insights into a HECT-type E3 ligase AREL1 and its ubiquitination activities in vitro. *J. Biol. Chem.* **294**, 19934–19949.

Slee, E.A., Adrain, C. & Martin, S.J. (2001). Executioner Caspase-3, -6, and -7 Perform Distinct, Non-redundant Roles during the Demolition Phase of Apoptosis. *J. Biol. Chem.* **276**, 7320–7326.

Slee, E.A., Harte, M.T., Kluck, R.M., Wolf, B.B., Casiano, C.A., Newmeyer, D.D., Wang, H.G., *et al.* (1999). Ordering the cytochrome c-initiated caspase cascade: Hierarchical activation of caspases-2,-3,-6,-7,-8, and -10 in a caspase-9-dependent manner. *J. Cell Biol.* **144**, 281–292.

Smith, H.L. & Mallucci, G.R. (2016). The unfolded protein response: Mechanisms and therapy of neurodegeneration. *Brain* **139**, 2113–2121.

Sobotzik, J.M., Sie, J.M., Politi, C., Del Turco, D., Bennett, V., Deller, T. & Schultz, C. (2009). AnkyrinG is required to maintain axo-dendritic polarity in vivo. *Proc. Natl. Acad. Sci. U. S. A.* **106**, 17564–17569.

Soldani, C. & Scovassi, A.I. (2002). Poly(ADP-ribose) polymerase-1 cleavage during apoptosis: An update. *Apoptosis* **7**, 321–328.

Son, E.Y., Ichida, J.K., Wainger, B.J., Toma, J.S., Rafuse, V.F., Woolf, C.J. & Eggan, K. (2011). Conversion of mouse and human fibroblasts into functional spinal motor neurons. *Cell Stem Cell* **9**, 205–218.

Sorrells, S.F., Paredes, M.F., Cebrian-Silla, A., Sandoval, K., Qi, D., Kelley, K.W., James, D., *et al.* (2018). Human hippocampal neurogenesis drops sharply in children to undetectable levels in adults. *Nature* **555**, 377–381.

Spalding, K.L., Bhardwaj, R.D., Buchholz, B.A., Druid, H. & Frisén, J. (2005). Retrospective birth dating of cells in humans. *Cell* **122**, 133–143.

Srinivasula, S.M., Ahmad, M., Guo, Y., Zhan, Y., Lazebnik, Y., Fernandes-alnemri, T. & Alnemri, E.S. (1999). Identification of an Endogenous Dominant-Negative Short Isoform of Caspase-9 That Can Regulate Apoptosis 1. *Cancer Res.* **59**, 999–1002.

Srinivasula, S.M., Gupta, S., Datta, P., Zhang, Z.J., Hegde, R., Cheong, N.E., Fernandes-Alnemri, T., *et al.* (2003). Inhibitor of apoptosis proteins are substrates for the mitochondrial serine protease Omi/HtrA2. *J. Biol. Chem.* **278**, 31469–31472.

Srivastava, R., Cao, Z., Nedeva, C., Naim, S., Bachmann, D., Rabachini, T., Gangoda, L., *et al.* (2019). BCL-2 family protein BOK is a positive regulator of uridine metabolism in mammals. *Proc. Natl. Acad. Sci. U. S. A.* **116**, 15469–15474.

Stiles, J. & Jernigan, T.L. (2010). The basics of brain development. *Neuropsychol. Rev.* **20**, 327–348.

Stuart, T., Butler, A., Hoffman, P., Hafemeister, C., Papalexi, E., III, W.M.M., Hao, Y., *et al.* (2019). Comprehensive Integration of Single-Cell Data. *Cell* **177**, 1888–1902.

Südhof, T.C. (2018). Towards an Understanding of Synapse Formation. *Neuron* **100**, 276–293.

Sutton, G. & Chandler, L.J. (2002). Activity-dependent NMDA receptor-mediated activation of protein

kinase B/Akt in cortical neuronal cultures. *J. Neurochem.* **82**, 1097–1105.

Sutton, M.A. & Schuman, E.M. (2006). Dendritic Protein Synthesis, Synaptic Plasticity, and Memory. *Cell* **127**, 49–58.

Suzuki, Y., Imai, Y., Nakayama, H., Takahashi, K., Takio, K. & Takahashi, R. (2001). A serine protease, HtrA2, is released from the mitochondria and interacts with XIAP, inducing cell death. *Mol. Cell* **8**, 613–621.

Szallasi, Z., Smith, C.B., Pettit, G.R. & Blumberg, P.M. (1994). Differential regulation of protein kinase C isozymes by bryostatin 1 and phorbol 12-myristate 13-acetate in NIH 3T3 fibroblasts. *J. Biol. Chem.* **269**, 2118–2124.

Tait, S.W.G. & Green, D.R. (2010). Mitochondria and cell death: Outer membrane permeabilization and beyond. *Nat. Rev. Mol. Cell Biol.* **11**, 621–632.

Tak, T., Tesselaar, K., Pillay, J., Borghans, J.A.M. & Koenderman, L. (2013). What's your age again? Determination of human neutrophil half-lives revisited. *J. Leukoc. Biol.* **94**, 595–601.

Takahashi, K., Tanabe, K., Ohnuki, M., Narita, M., Ichisaka, T., Tomoda, K. & Yamanaka, S. (2007). Induction of Pluripotent Stem Cells from Adult Human Fibroblasts by Defined Factors. *Cell* **131**, 861–872.

Takahashi, K. & Yamanaka, S. (2006). Induction of Pluripotent Stem Cells from Mouse Embryonic and Adult Fibroblast Cultures by Defined Factors. *Cell* **126**, 663–676.

Takeda, Y., Harada, Y., Yoshikawa, T. & Dai, P. (2018). Chemical compound-based direct reprogramming for future clinical applications. *Biosci. Rep.* **38**, 20171650.

Tao, Y. & Zhang, S.C. (2016). Neural Subtype Specification from Human Pluripotent Stem Cells. *Cell Stem Cell* **19**, 573–586.

Telezhkin, V., Schnell, C., Yarova, P., Yung, S., Cope, E., Hughes, A., Thompson, B.A., *et al.* (2016). Forced cell cycle exit and modulation of GABAA, CREB, and GSK3β signaling promote functional maturation of induced pluripotent stem cell-derived neurons. *Am. J. Physiol. - Cell Physiol.* **310**, C520–C541.

Thoden, J.B., Wohlers, T.M., Fridovich-Keil, J.L. & Holden, H.M. (2001). Human UDP-galactose 4-epimerase. Accommodation of UDP-N-acetylglucosamine within the active site. *J. Biol. Chem.* **276**, 15131–15136.

Trapnell, C., Cacchiarelli, D., Grimsby, J., Pokharel, P., Li, S., Morse, M., Lennon, N.J., *et al.* (2014). The dynamics and regulators of cell fate decisions are revealed by pseudo-temporal ordering of single cells. *Nat. Biotechnol.* **32**, 381–86.

Trauth, B.C., Klas, C., Peters, A.M.J., Matzku, S., Möller, P., Falk, W., Debatin, K.M., *et al.* (1989). Monoclonal antibody-mediated tumor regression by induction of apoptosis. *Science (80-.).* **245**, 301–305.

Traxler, L., Edenhofer, F. & Mertens, J. (2019). Next-generation disease modeling with direct conversion: a new path to old neurons. *FEBS Lett.*

Trujillo, C.A., Gao, R., Negraes, P.D., Gu, J., Buchanan, J., Preissl, S., Wang, A., *et al.* (2019). Complex Oscillatory Waves Emerging from Cortical Organoids Model Early Human Brain Network Development. *Cell Stem Cell* **25**, 558-569.e7.

Utami, K.H., Hillmer, A.M., Aksoy, I., Chew, E.G.Y., Teo, A.S.M., Zhang, Z., Lee, C.W.H., *et al.* (2014). Detection of chromosomal breakpoints in patients with developmental delay and speech disorders. *PLoS One* **9**.

Varki, A. (2008). Sialic acids in human health and disease. *Trends Mol. Med.* **14**, 351–360.

Varki, A. (2011). Evolutionary forces shaping the Golgi glycosylation machinery: Why cell surface glycans are universal to living cells. *Cold Spring Harb. Perspect. Biol.* **3**, 1–14.

Varki, A. (2017). Biological roles of glycans. *Glycobiology* **27**, 3–49.

Vasseur, S. & Manié, S.N. (2015). ER stress and hexosamine pathway during tumourigenesis: A pas de deux? *Semin. Cancer Biol.* **33**, 34–39.

Vattem, K.M. & Wek, R.C. (2004). Reinitiation involving upstream ORFs regulates ATF4 mRNA translation in mammalian cells. *Proc. Natl. Acad. Sci. U. S. A.* **101**, 11269–11274.

Victor, M.B., Richner, M., Hermanstyne, T.O., Ransdell, J.L., Sobieski, C., Deng, P.Y., Klyachko, V.A., *et al.* (2014). Generation of Human Striatal Neurons by MicroRNA-Dependent Direct Conversion of Fibroblasts. *Neuron* **84**, 311–323.

Vierbuchen, T., Ostermeier, A., Pang, Z.P., Kokubu, Y., Südhof, T.C. & Wernig, M. (2010). Direct conversion of fibroblasts to functional neurons by defined factors. *Nature* **463**, 1035–1041.

Vucic, D. (2018). XIAP at the crossroads of cell death and inflammation. *Oncotarget* **9**, 27319–27320.

Vucic, D., Deshayes, K., Ackerly, H., Pisabarro, M.T., Kadkhodayan, S., Fairbrother, W.J. & Dixit, V.M. (2002). SMAC negatively regulates the anti-apoptotic activity of melanoma inhibitor of apoptosis (ML-IAP). *J. Biol. Chem.* **277**, 12275–12279.

Wajant, H. (2003). Death receptors. *Essays Biochem.* **39**, 53–71.

Walker, R.A., O'Brien, E.T., Pryer, N.K., Soboeiro, M.F., Voter, W.A., Erickson, H.P. & Salmon, E.D. (1988). Dynamic instability of individual microtubules analyzed by video light microscopy: rate constants and transition frequencies. *J. Cell Biol.* **107**, 1437–1448.

Wang, B. (2012). Molecular mechanism underlying sialic acid as an essential nutrient for brain development and cognition. *Adv. Nutr.* **3**, 465–72.

Wang, B., Miller, J.B., McNeil, Y. & McVeagh, P. (1998). Sialic acid concentration of brain gangliosides: Variation among eight mammalian species. *Comp. Biochem. Physiol. - A Mol. Integr. Physiol.* **119**, 435–439.

Wang, C., Wei, Z., Chen, K., Ye, F., Yu, C., Bennett, V. & Zhang, M. (2014a). Structural basis of diverse membrane target recognitions by ankyrins. *Elife* **3**, 1–22.

Wang, H.Y., Hsieh, P.F., Huang, D.F., Chin, P.S., Chou, C.H., Tung, C.C., Chen, S.Y., *et al.* (2015). RBFOX3/NeuN is Required for Hippocampal Circuit Balance and Function. *Sci. Rep.* **5**.

Wang, P., Li, J., Tao, J. & Sha, B. (2018). The luminal domain of the ER stress sensor protein PERK binds misfolded proteins and thereby triggers PERK oligomerization. *J. Biol. Chem.* **293**, 4110–4121.

Wang, X., Zha, M., Zhao, X., Jiang, P., Du, W., Tam, A.Y.H., Mei, Y., *et al.* (2013). Siva1 inhibits p53 function by acting as an ARF E3 ubiquitin ligase. *Nat. Commun.* **4**, 1551.

Wang, Z. V., Deng, Y., Gao, N., Pedrozo, Z., Li, D.L., Morales, C.R., Criollo, A., *et al.* (2014b). Spliced X-

box binding protein 1 couples the unfolded protein response to hexosamine biosynthetic pathway. *Cell* **156**, 1179–1192.

Wani, W.Y., Chatham, J.C., Darley-Usmar, V., McMahon, L.L. & Zhang, J. (2017). O-GlcNAcylation and neurodegeneration. *Brain Res. Bull.* **133**, 80–87.

Wei, M.C., Zong, W.X., Cheng, E.H.Y., Lindsten, T., Panoutsakopoulou, V., Ross, A.J., Roth, K.A., *et al.* (2001). Proapoptotic BAX and BAK: A requisite gateway to mitochondrial dysfunction and death. *Science (80-.).* **292**, 727–730.

Weisenberg, R.C. (1972). Microtubule formation in vitro in solutions containing low calcium concentrations. *Science (80-.).* **177**, 1104–1105.

Wek, R.C. (2018). Role of eIF2α kinases in translational control and adaptation to cellular stress. *Cold Spring Harb. Perspect. Biol.* **10**, a032870.

Wek, S.A., Zhu, S. & Wek, R.C. (1995). The histidyl-tRNA synthetase-related sequence in the eIF-2 alpha protein kinase GCN2 interacts with tRNA and is required for activation in response to starvation for different amino acids. *Mol. Cell. Biol.* **15**, 4497–4506.

Weyer, A. & Schilling, K. (2003). Developmental and cell type-specific expression of the neuronal marker NeuN in the murine cerebellum. *J. Neurosci. Res.* **73**, 400–409.

Wobus, A.M. & Boheler, K.R. (2005). Embryonic stem cells: Prospects for developmental biology and cell therapy. *Physiol. Rev.* **85**, 635–678.

Wonders, C.P. & Anderson, S.A. (2006). The origin and specification of cortical interneurons. *Nat. Rev. Neurosci.* **7**, 687–696.

Worth, M., Li, H. & Jiang, J. (2017). Deciphering the Functions of Protein O-GlcNAcylation with Chemistry. *ACS Chem. Biol.* **12**, 326–335.

Wright, K.M., Smith, M.I., Farrag, L. & Deshmukh, M. (2007). Chromatin modification of Apaf-1 restricts the apoptotic pathway in mature neurons **179**, 825–832.

Wu, M. & Gu, L. (2020). TCseq: Time course sequencing data analysis.

Xiang, G., Wen, X., Wang, H., Chen, K. & Liu, H. (2009). Expression of X-linked inhibitor of apoptosis protein in human colorectal cancer and its correlation with prognosis. *J. Surg. Oncol.* **100**, 708–712.

Xu, K., Zhong, G. & Zhuang, X. (2013). Actin, spectrin, and associated proteins form a periodic cytoskeletal structure in axons. *Science (80-.).* **339**, 452–456.

Xue, Y., Ouyang, K., Huang, J., Zhou, Y., Ouyang, H., Li, H., Wang, G., *et al.* (2013). Direct conversion of fibroblasts to neurons by reprogramming PTB-regulated MicroRNA circuits. *Cell* **152**, 82–96.

Yakovlev, A.G., Ota, K., Wang, G., Movsesyan, V., Bao, W.-L., Yoshihara, K. & Faden, A.I. (2001). Differential Expression of Apoptotic Protease-Activating Factor-1 and Caspase-3 Genes and Susceptibility to Apoptosis during Brain Development and after Traumatic Brain Injury. *J. Neurosci.* **21**, 7439–7446.

Yang, C., Peng, P., Li, L., Shao, M., Zhao, J., Wang, L., Duan, F., *et al.* (2016). High expression of GFAT1 predicts poor prognosis in patients with pancreatic cancer. *Sci. Rep.* **6**, 39044.

Yang, L.J.S., Zeller, C.B., Shaper, N.L., Kiso, M., Hasegawa, A., Shapiro, R.E. & Schnaar, R.L. (1996). Gangliosides are neuronal ligands for myelin-associated glycoprotein. *Proc. Natl. Acad. Sci. U. S.*

A. **93**, 814–818.

Yang, Q.H., Church-Hajduk, R., Ren, J., Newton, M.L. & Du, C. (2003). Omi/HtrA2 catalytic cleavage of inhibitor of apoptosis (IAP) irreversibly inactivates IAPs and facilitates caspase activity in apoptosis. *Genes Dev.* **17**, 1487–1496.

Yang, X. & Qian, K. (2017). Protein O - GlcNAcylation : emerging mechanisms and functions. *Nat. Publ. Gr.* **18**, 452–465.

Yang, Y., Ogawa, Y., Hedstrom, K.L. & Rasband, M.N. (2007). βIV spectrin is recruited to axon initial segments and nodes of Ranvier by ankyrinG. *J. Cell Biol.* **176**, 509–519.

Yoshida, T., Shiraishi, T., Nakata, S., Horinaka, M., Wakada, M., Mizutani, Y., Miki, T., *et al.* (2005). Proteasome Inhibitor MG132 Induces Death Receptor 5 through CCAAT/Enhancer-Binding Protein Homologous Protein. *Cancer Res.* **65**, 5662–7.

Yu, G., Wang, L.-G., Han, Y. & He, Q.-Y. (2012). clusterProfiler: an R package for comparing biological themes among gene clusters. *Omi. A J. Integr. Biol.* **16**, 284–287.

Yuzwa, S.A., Shan, X., MacAuley, M.S., Clark, T., Skorobogatko, Y., Vosseller, K. & Vocadlo, D.J. (2012). Increasing O-GlcNAc slows neurodegeneration and stabilizes tau against aggregation. *Nat. Chem. Biol.* **8**, 393–399.

Yuzwa, S.A. & Vocadlo, D.J. (2014). O -GlcNAc and neurodegeneration : biochemical mechanisms and potential roles in Alzheimer ' s disease and beyond. *Chem. Soc. Rev.* **43**, 6839–6858.

Zhang, D., Hu, X., Li, J., Liu, J., Baks-te Bulte, L., Wiersma, M., Malik, N. ul A., *et al.* (2019a). DNA damage-induced PARP1 activation confers cardiomyocyte dysfunction through NAD + depletion in experimental atrial fibrillation. *Nat. Commun.* **10**, 1307.

Zhang, S., Macias-Garcia, A., Ulirsch, J.C., Velazquez, J., Butty, V.L., Levine, S.S., Sankaran, V.G., *et al.* (2019b). HRI coordinates translation necessary for protein homeostasis and mitochondrial function in erythropoiesis. *Elife* **8**, e46976.

Zhang, W., Feng, D., Li, Y., Iida, K., McGrath, B. & Cavener, D.R. (2006). PERK EIF2AK3 control of pancreatic β cell differentiation and proliferation is required for postnatal glucose homeostasis. *Cell Metab.* **4**, 491–497.

Zheng, X., Boyer, L., Jin, M., Mertens, J., Kim, Y., Ma, L., Ma, L., *et al.* (2016). Metabolic reprogramming during neuronal differentiation from aerobic glycolysis to neuronal oxidative phosphorylation. *Elife* **5**, 1–25.

Zhou, J., Huynh, Q.K., Hoffman, R.T., Crook, E.D., Daniels, M.C., Gulve, E.A. & McClain, D.A. (1998). Regulation of glutamine: Fructose-6-phosphate amidotransferase by cAMP- dependent protein kinase. *Diabetes* **47**, 1836–1840.

Zhou, Z., Luo, A., Shrivastava, I., He, M., Huang, Y., Bahar, I., Liu, Z., *et al.* (2017). Regulation of XIAP Turnover Reveals a Role for USP11 in Promotion of Tumorigenesis. *EBioMedicine* **15**, 48–61.

Zibrova, D., Vandermoere, F., Göransson, O., Peggie, M., Mariño, K. V., Knierim, A., Spengler, K., *et al.* (2017). GFAT1 phosphorylation by AMPK promotes VEGF-induced angiogenesis. *Biochem. J.* **474**, 983–1001.

Zoltowska, K., Webster, R., Finlayson, S., Maxwell, S., Cossins, J., Müller, J., Lochmüller, H., *et al.* (2013). Mutations in GFPT1 that underlie limb-girdle congenital myasthenic syndrome result in reduced cell-surface expression of muscle AChR. *Hum. Mol. Genet.* **22**, 2905–2913.

Zou, H., Henzel, W.J., Liu, X., Lutschg, A. & Wang, X. (1997). Apaf-1, a human protein homologous to C. elegans CED-4, participates in cytochrome c-dependent activation of caspase-3. *Cell* **90**, 405–413.

11 Contributions

Aside from all the helpful discussions that I had with my colleagues I want to highlight a few particularly important contributions for which I am very grateful:

Dr. Anne Hoffrichter performed quality control, processing and visualization of RNAseq data. She provided custom-made R applications allowing me to spend my time on detailed data analysis.

Bettina Bohl helped with scRNAseq sample preparation.

PD Dr. Georg Köhr, together with his master's students Carolin Fischer and Nadja Lehmann, measured electrophysiological properties of neuronal cultures that I provided.

12 Acknowledgements

I am thankful to Prof. Dr. Philipp Koch for his guidance, patience and scientific inspiration. Thank you for having an open door and ear whenever needed.

I thank Prof. Dr. Jörg Höhfeld for making the time and having the interest to take over the responsibility of second reviewer to my thesis.

My thanks also go to Prof. Dr. Gerhard von der Emde and Prof. Dr. Pavel Kroupa for volunteering as members of my disputation committee.

I was lucky to have had great colleagues, both, at the Institute of Reconstructive Neurobiology as well as at the Hector Institute for Translational Brain Research. Thanks to Bettina Bohl, Ammar Jabali, Jasmin Jatho-Gröger, Kevin Weynans, Fabio Marsoner, Karolina Kleinsimlinghaus, Anne Hoffrichter, Isabell Moskal, Marco Siekmann, Andrea Rossetti, Karen Schmitt, Klara Rehder, Malin Schmidt, Julia Wangemann, Elena Muñoz, Raquel Pérez Fernández, Annasara Artioli, Dana Fleischhauer, Carolin Fischer and Lea Wagner for helpful discussions and lots of laughs. I will always remember brainstorming technologically enhanced raccoons and related or unrelated business ventures. Keep tugging at the anchor of sanity from time to time. You are all beautiful people.

I want to thank Gina Tillmann and Helene Schamber for their great technical support. PD Dr. Georg Köhr, Dr. Thorsten Lau and Dr. Sandra Horschitz provided helpful advice whenever necessary – thank you!

I want to thank my long-standing friends, my sister and my parents for their moral support and a refreshing “outsiders” view on my scientific work and the related journey. Thank you for your trust, you are awesome human beings. Finally, I am grateful for the support and patience by my wife Rike. Thank you for your laughs and your calm encouragement. You know best what it took to get this done. Thank you!

13 Publications

- Poppe D, …, **Wilkens R**, et al., *Genome editing in neuroepithelial stem cells to generate human neurons with high adenosine-releasing capacity.* Stem Cells Transl. Med., 2018. DOI: 10.1002/sctm.16-0272
- Iefremova V, …, **Wilkens R**, et al., *An organoid-based model of cortical development identifies non-cell-autonomous defects in Wnt signaling contributing to Miller-Dieker-Syndrome*. Cell Rep, 2017. DOI: 10.1016/j.celrep.2017.03.047
- Schmidt-Arras D, …, **Wilkens R,** et al., *Oncogenic deletion mutants of gp130 signal from intracellular compartments*. J Cell Sci, 2014. DOI: 10.1242/jcs.130294